Fluorescent Probes for the Labelling of Cardiomyocyte and Mitochondrial Proteins.

A thesis submitted in partial fulfilment of the requirements for the degree of Doctor of Philosophy.

By

Thomas D. Z. Pearson

2017

School of Science and Technology

Nottingham Trent University

Clifton Lane

Nottingham

NG11 8NS

United Kingdom

Declaration

I hereby certify that the work embodied in this thesis is the result of my own investigations except

where reference has been made to published literature.

Abstract

Organophosphates are a known danger to human health with an array of biochemical targets and complex toxic effects. Phenyl saligenin phosphate (PSP) is an organophosphate and related phenoxy substituted organophosphates irreversibly bind to a variety of important enzymes causing the condition known as organophosphate induced delayed neuropathy (OPIDN). These compounds also potentially cause cardiac muscle damage but little is known about how this class of compounds effect cardiomyocytes. The identification of proteins targeted by these toxins is of interest.

This study investigates the synthesis and application of novel fluorescently labelled organophosphates to investigate organophosphate interaction with H9c2 cardiomyoblasts. The synthesis of probes with BODIPY, pyrene and rhodamine fluorescent component is explored with success in preparation of pyrene and rhodamine probes. The fluorescent behaviour of three rhodamine labelled phenyl saligenin phosphates probes with alkyl and PEG linkers is examined and the cytotoxicity of the probes assessed by monitoring MTT reduction, and LDH release from exposed H9c2 cardiomyoblasts. All three analogues showed cytotoxicity (4 h exposure; 100 μM). These probes were found to bind to proteins within mitochondria and spots from 2D-gel electrophoresis experiments, visualised at 532 nm, which are undergoing MS analysis.

This project also describes progress towards a photoreactive-fluorescent probe to identify the site of action of the potassium channel opener, diazoxide, which activates cardioprotective pathways. The drug is believed to target mitochondrial K_{ATP} channels, but the protein structure of these channels has yet to be elucidated. The fluorescence labelling of whole cardiac cells with a dansyl fluorescent - benzophnone-photoreactoive diazoxide probe has been demonstrated and the progress toward a rhodamine fluorescent analogue is presented.

Acknowledgements

List of Acronyms, Abbreviations and Symbols

Acronym, Abbreviation or Symbol	Name
ABC	ATP-binding cassette
Ac	Acetyl
ACh	Acetylcholine
AChE	Acetylcholinesterase
ADP	Adenosine diphosphate
ANT	Adenine nucleotide translocator
aq.	Aqueous
Ar	Aryl / heteroaryl
ATP	Adenosine triphosphate
BAPTA	1,2-bis(o-aminophenoxy)ethane-N,N,N,N-tetraacetic acid
br	Broad
BSA	Bovine serum albumin
CBDP	Cresyl saligenin phosphate
CDI	Carbonyldimidazole
d	Doublet
DCE	Dichloroethane
DCM	Dichloromethane
dd	Doublet of doublets
DiAM	Dialkynylimidazole
DMAP	4-dimethylaminopyridine
DMF	N, N-dimethylformamide
DMSO	Dimethylsulfoxide
ε	Extinction coefficient
eNOS	Endothelial nitric oxide synthase
eq.	Equivalents
Et	Ethyl
FBS	Foetal bovine serum
h	Hour
H_2O_2	Hydrogen peroxide
HMQC	Heteronuclear multiple quantum coherence
HRMS	High resolution mass spectrum
HSP	Heat shock proteins
I/R	Ischaemia/reperfusion
IMS	Intermediate syndrome
iNOS	inducible nitric oxide synthase
IPC	Ischaemia preconditioning
Kca	Calcium-activated potassium channel
Kir	Inwardly rectifying potassium channel subunit
m	multiplet
M1 /M2	Transmembrane unit
m. /min.	Minutes
mABC	Mitochondrial ATP-binding cassette
MAPK	Mitogen-activated protein kinases
Me	Methyl
MitoK$_{ATP}$	Mitochondrial ATP-activated potassium channel
MnSOD	mitochondrial antioxidant enzyme superoxide dismutase
mol	Mole
μM	Micromolar
Mp	Melting point
MS	Mass spectrometry
NADP	nicotinamide adenine dinucleotide
NBD	Nucleotide binding domain
NEt$_3$ / TEA	Triethylamine

NF-κB	transcriptional nuclear factor κB
NMR	Nuclear magnetic resonance
NTE	Neuropathy target esterase
Nu	Nucleophile
o	Ortho
OPIDN	Organophosphate induced delayed neuropathy
PAGE	Polyacrylamide gel electrophoresis
PAL	Photoaffinity labelling
PEG	Polyethyl glycol
Ph	Phenyl
PIC	Mitochondrial phosphate carrier
PKC	Protein kinase C
PPC	Pharmacological preconditioning
ppm	Parts per million
PSP	Phenylsaligenin phosphate
φ	Quantum yield
q	Quartet
Quin	quintet
Rf	Retention factor
Rho	Rhodamine B
ROMK	renal outer medullary potassium channel
ROS	Reactive oxygen species
s	Singlet
Structure and Reactivty	SAR
SCOTP	Saligenin cyclic *ortho*-tolylphosphate
SDH	Succinate dehydrogenase
SDS	Sodium dodecyl sulphate
SOD	superoxide dismutases
SUR	Sulfonylurea receptor
t	Triplet
T3P	tripropylphosphinic anhydride
tBu	*Tert*-butyl
TGase	Transglutaminase
THF	Tetrahydrofuran
TK	Tyrosine kinase
TLC	Thin layer chromatography
TMD	Transmembrane domain
TOCP	Tri-*ortho*-cresyl phosphate
UV	Ultra-violet

Contents

1 Introduction

1.2 Proteomics

The understanding of protein profiles and interactions is fundamental to understanding biochemistry. Whilst great advances have been made in genetics and gene sequencing,[1] the detailed study of all proteins within an organism is in its infancy. The study of these proteins and their interactions is called Proteomics.

1.3 Functional Probes

Functional methodology has developed to a point where biological systems can be probed through various techniques to gather information on protein functions. Chemically reactive fluorescent probes can profile enzymes and determine catalytic activity. Intact cells can be investigated and, using microscopy, the fluorescent probes can be visualised to identify where they have bound to receptors or enzymes. In addition to this, small molecules that may be selective inhibitors within enzyme families can be screened in, intact cells or crude lysates, and can then lead to new drug discoveries.[2]

Mitochondrial-targeted fluorescent probes are a salient example of this approach. Mitochondria are the powerhouses of cells, and synthesise adenine triphosphate (ATP) the chemical energy for cellular processes. These organelles consume a large amount of oxygen in aerobic organisms, and produce cellular reactive oxygen species (ROS). Cancer, diabetes and heart disease have all shown links to elevated ROS. Although ROS are important for normal cellular functions, mismanagement and over-release causes oxidative stress.[3] The inner membrane of the mitochondrion[4] is substantially more negatively charged than that of any other organelle in the cell by a factor of ten.[5] This charge, combined with the universally negative charge on emitted radical species, means that probes with a positive charge congregate along the outside of the mitochondrial membrane. The most common way of staining mitochondria is through rhodamine-based dyes as these carry a permanent positive charge.[6]

Hydrogen peroxide (H_2O_2) is produced when incomplete reduction of O_2 to H_2O occurs during electron transport. This species can be beneficial to metabolic function when specific ligand-receptor interactions are in control, but random fluctuations in H_2O_2 release can incite undesirable apoptosis.[7] Lipophilic moieties have been incorporated into the design of a cationic probe which detects H_2O_2 *in vivo.* MitoPY1 is a highly selective probe for H_2O_2 and features an aliphatic cationic triphenylphosphine group to target mitochondrial membrane (Figure 1).[8] In this probe the peroxide induced loss of the boronate the rhodamine/fluorescein hybrid molecule switches from the non-fluorescent closed form to the open form which is highly fluorescent.
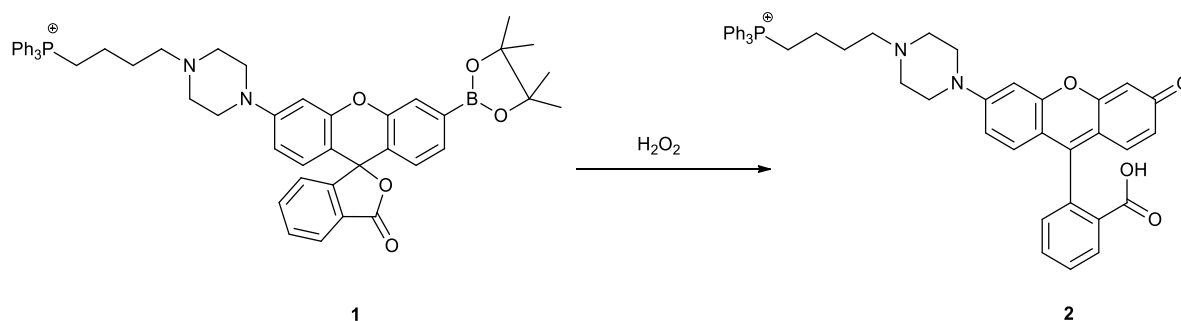
Figure 1. MitoPY1 – TPP targeting H_2O_2 probe featuring boronate hybrid rhodamine/fluorescein for activatable fluorescence.

Halo fusion proteins are another powerful tool in probing particular intracellular compartments.[9] The HaloTag is a modified haloalkane dehalogenase, which covalently binds to synthetic ligands. Genetically transfecting cRNA into a cell allows for expression of a Halo fusion protein. When the HaloTag synthetic ligand is added, a response can be measured depending on the nature of the ligand. One example featuring this technique detects calcium ions (Ca^{2+}). The ligand for the probe contains a 1,2-bis(O-aminophenoxy)ethane-N,N,N,N-tetraacetic acid (BAPTA) chelator with a rhodamine based TMR fluorophore. The ligand is only weakly fluorescent before chelation to a Ca^{2+} ion, when the fluorescence increases over 200-fold with the quantum yield rising to 0.29.[10]
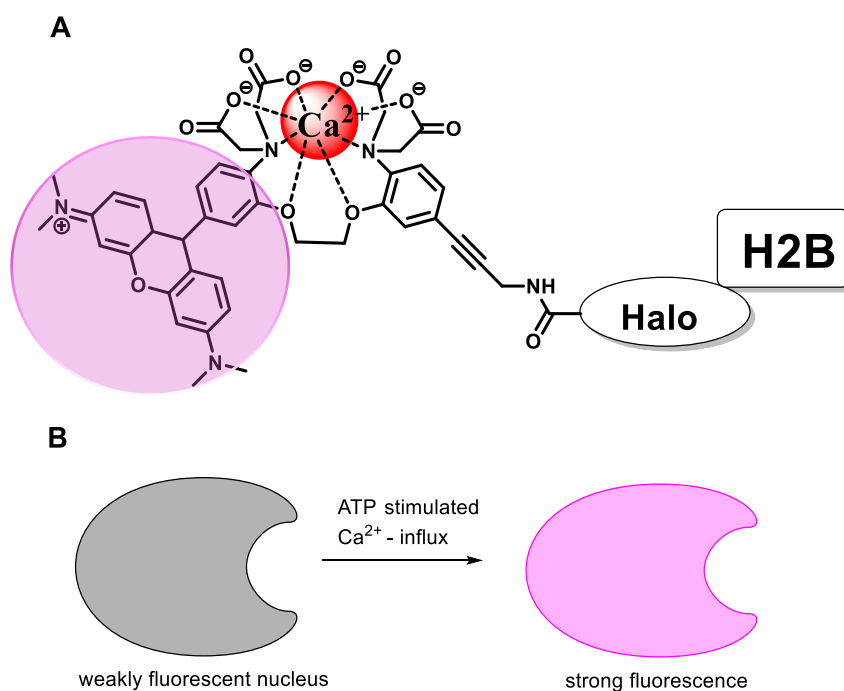
Figure 2. Illustration of HaloTag calcium sensor taken from reference 6. (A) The Halo-H2B fusion protein expressed in cells is labelled with the calcium sensitive probe RhoCa-Halo. This probe measures the concentration of calcium ions found in the nucleus. The fluorescence emitted by this probe is significant when calcium ions are drawn into the nucleus by adenine triphosphate (ATP), stimulation. (B) Structure of the RhoCa-Halo probe once chelated around calcium.

Fluorescent tagging by covalent bond formation is a useful tool for retrieving desired proteins. The covalent bond is a permanent chemical connection and allows biological techniques such as gel electrophoresis, or protein chromatography to separate probed proteins from the unwanted, unlabelled proteins.[11]

Mitogen-activated protein kinases (MAPKs) are enzymes that play a role in signalling cascades for normal cellular activity. Cancer cell survival pathways also make use of this protein and development of inhibitors could lead to new treatments for this disease.[12] Currently, the inhibitors trialled regrettably target other bystander proteins with a similar or greater potency. [13] A team at the University of Texas has developed a probe for selectively tagging and inhibiting the p38α region of a MAPK. The inhibitor covalently binds to the Cys119 residue and avoids non-covalent interactions at the ATP-binding site. While not inherently fluorescent, a dialkynylimidazole (DiAm 1) has one N-alkyne that binds to the free thiol of a cysteine residue, the other alkyne can then be used in azide-alkyne Huisgen cycloaddition click chemistry with an Alexa fluorophore (Figure 3).[14]

Evidence of DiAm 1 binding to p38α was found *in vivo*, when cells were treated with 1 µM, 5 µM and 50 µM of DiAm 1 and tagged via click reaction with 50 µM of Alexa 594. This gave a dark band on a gel produced by SDS-PAGE gel electrophoresis, and was compared with isolated p38α that had been tagged by click reaction with 50 µM of DiAm 1 *in vitro*. Validation of identity was determined by comparison of the protein bands between these two gels, followed by further confirmation via other assaying techniques, demonstrating the power a covalent fluorescent probe can have in proteomics.
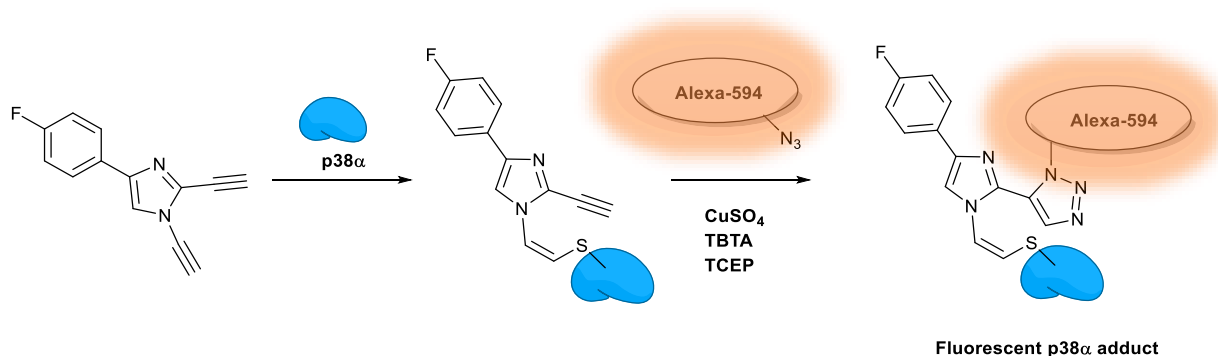
Figure 3. Mechanism of covalent tagging from DiAm1 onto p38α, followed by click-chemistry to attach fluorophore Alexa 594.

Use of the fluorophore in this example allowed visualisation of the fluorescent protein bands found within a gel under a red-light source in a gel imager. In addition to identifying known proteins or detecting small molecules *in vivo*, fluorescent tagging may be useful in identifying novel targets of drugs and toxins. A fluorescent tag on a covalently binding toxin bound to a protein target is a new development in proteomic study. One family of toxins which are of interest are organophosphates.

1.4 Organophosphates

Organophosphates (OPs) have been widely used as pesticides, but also have other industrial uses. Many of these compounds target acetylcholinesterase (AChE) activity in the nervous tissue and there is concern about OPs widespread use due to the toxicity in humans, with numerous reports linking some OPs to various forms of delayed neuropathy.[15]

VX nerve agent (**3**) is a particularly toxic organophosphate that was synthesised by British chemists working for ICI in 1952. It is the deadliest synthetic toxin known to man and was synthesised while

attempting to make a new type of pesticides. Research on compounds in this class ceased in the UK

in 1955 when the extreme lethal potency to humans was discovered. VX is toxic enough that only

10-µg of the oil on the skin, or inhaled as a vapour, is enough to kill within hours.[16]
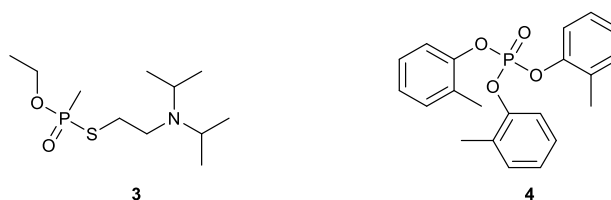
Figure 4. The chemical structures of VX gas, **3**, and TOCP, **4**.

The Chemical Weapons Convention classifies VX gas as a weapon of mass destruction, and bans any

use or storage beyond that of research.[17] Tragic instances of use include the Halabja chemical attack

in 1988 where Iraqi military, under Saddam Hussein, used VX gas against the Kurds. Thousands of

civilians were killed and approximately 10 000 people were injured.[18] Recently, the half-brother of

the North Korean leader Kim Jong-un was assassinated using VX.[19]

There are other, less dramatic, examples of organophosphate toxicity. In 1930s America, under the

prohibition laws, an alcohol containing Jamaica Ginger based remedy known by the slang name

"Jake"[20] gave rise to nervous system damage. The drink, which was adulterated with tri-ortho-cresyl

phosphate (TOCP) (Figure 4), was offered by bootleggers as an alcohol substitute. Although thought

to be non-toxic, many who regularly ingested the drink lost the use of their hands and feet. This gave

rise to a peculiar walk known as "Jake leg", as the toes bent upward and calves softened and

atrophied.[21]

Aerotoxic syndrome is another disease which has been accredited to organophosphate exposure.[22]

The organophosphate TOCP is also used as a lubricant in jet fuel. Cabin crew and frequent fliers can

be at risk from air contaminated with engine fumes, which can leak into the pressurised cabin air.[23]

The issue of poisoning is contentious, however there are many reports of crew ill health and

premature deaths linked to TOCP. Official studies are yet to conclude if this is a genuine condition

caused by the engineering of the plane. Reports issued by both the House of Lords (2007),[24] and a US Congress Committee on Air Quality in Passenger Cabins of Commercial Aircraft (2002), stated that evidence is inconclusive.[25] The latter reference even states the dangers of a "nocebo effect leading to serious health problems". However, many pilots and cabin crew believe there is a definite issue and, although the investigations are failing to detect even safe levels of engine fumes in the cabins, coroner Stanhope Payne has issued a report saying that a pilot's death in 2012 was likely caused by a build-up of toxic organophosphates. [26]

1.5 Mechanism of Toxicity

Organophosphates are known to cause three distinct toxic effects: cholinergic syndrome, intermediate syndrome and organophosphate induced delayed neuropathy. The first, cholinergic syndrome, in which acetylcholinesterase, an enzyme responsible for the breakdown and reuptake of acetylcholine, is inhibited. This leads to a build-up of acetylcholine at nerve endings.

The normal nerve impulse occurs in four stages (Figure 5 A). Acetylcholine travels across the synaptic cleft binding to a receptor (either a nicotinic acetylcholine receptor, or muscarinic acetylcholine receptor). An action potential travels down the axon to the terminal end. Release of acetylcholine into the next synaptic cleft, then causes a response to occur.

This response can be a muscular response, as illustrated, or neuronal. The type of response is dependent on the type of nervous system where the action is occurring. Generally nicotinic receptors are ligand-ion gated channels and muscarinic receptors function as G protein-coupled receptors that are ultimately used in cellular communication.[27]

In a patient suffering cholinergic syndrome, the resultant excess of neurotransmitters causes involuntary and unmediated nerve impulse and responses (Figure 5 B). The physiological symptoms are numerous; seizures, coma and respiratory failure which may often lead to death upon acute exposure.[28] This is the mode of toxicity associated with VX.
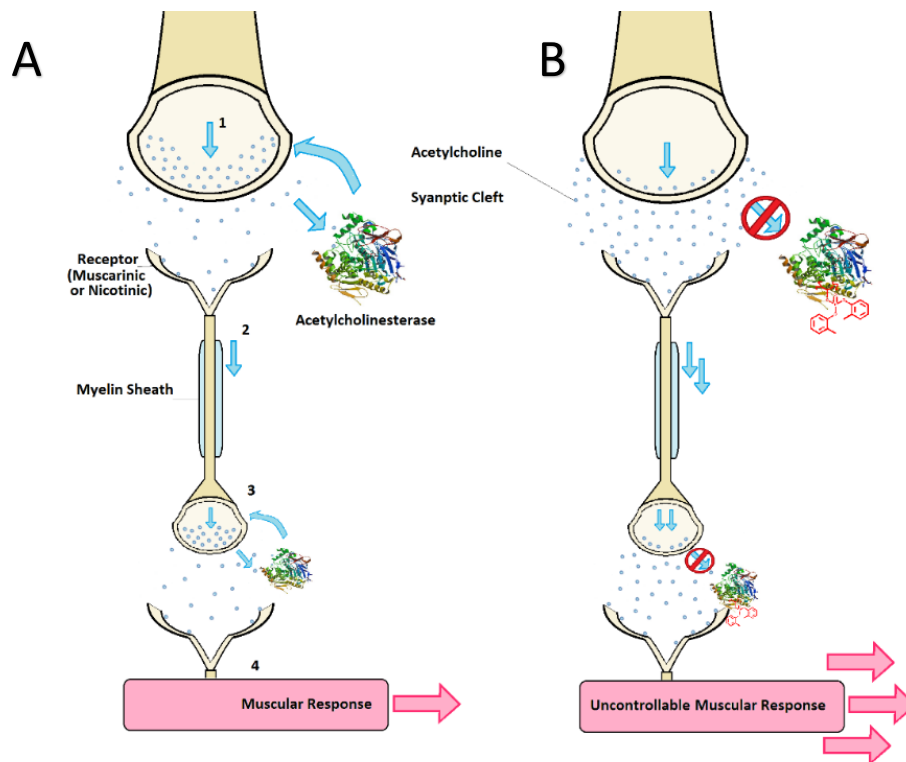
Figure 5. Mechanism of acetylcholinesterase inhibition by OP during an action potential. (A), normal nerve function. (B), nerve function featuring organophosphate interaction with acetylcholinesterase.

Intermediate syndrome (IMS) is the second effect that may occur after cholinergic crisis and can commence approximately 24-96 hours after exposure.[29] It is characterised by an acute ventilator insufficiency caused by paralysis or weakness of respiratory muscles. Patients normally require assisted ventilation at the onset of the syndrome, but after 5-18 days, full recovery is generally expected. This syndrome is biochemically understood and has exhibited two distinct types, clinically characterised by patient response to atropine. Type 1 responds to atropine treatment and is due to activation of muscarinic receptors, whereas type 2 does not respond to atropine and indicates an affliction of nicotinic receptors pathways.[30]

The third effect, which is less biochemically characterised, is termed Organophosphorus-Induced

Delayed Neuropathy (OPIDN). The disease is associated with chronic organophosphate poisoning,

and can be diagnosed by symptoms appearing 7-21 days after a single exposure.[31] These symptoms

include paralysis, ataxia and loss of function of motor axons, and damage to the central nervous

system. Degeneration of myelin sheaths, cerebrospinal axons swelling, the disappearance of

muscular tissue and even morphology changes in mitochondria have also been observed. OPIDN is

the effect that was experienced by the drinkers of Ginger Jake in the 1930s.[32]

1.6 Organophosphates' Mechanism of Covalent Binding

Several organophosphates are known to cause OPIDN in mammals. These include the

aforementioned tri-ortho-cresyl phosphate **4** (TOCP) currently used as a fuel additive,[33] the

structurally related saligenin cyclic ortho-tolylphosphate **5** (SCOTP), and phenyl saligenin phosphate

7 (PSP) (Figure 6). One pesticide known as chlorpyrifos **6**, induces OPIDN effects but not IMS.[34] TOCP

is interestingly also a poor inhibitor of AChE. Many organophosphates that induce OPIDN are poor

inhibitors of AChE and instead strongly inhibit the enzyme Neuropathy Target Esterase (NTE).[35]
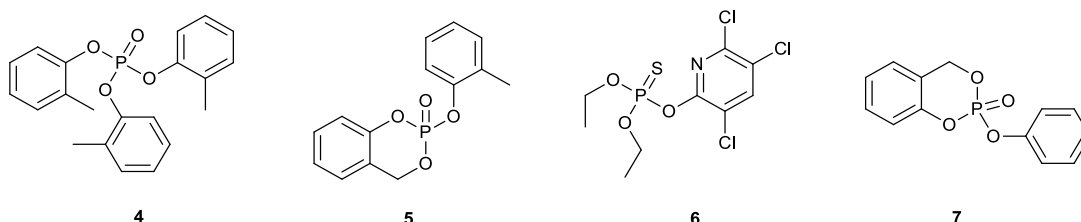
Figure 6. Commonly found organophosphates known to induce OPIDN. Tri-ortho-cresyl phosphate (TOCP) **4**, saligenin cyclic ortho-tolylphosphate **5** (SCOTP), chlorpyrifos **6**, and phenyl saligenin phosphate **7** (PSP).

There are many organophosphates, from the severely toxic nerve agents (VX and Sarin), to

compounds that have therapeutic uses, and even include the phosphate esters necessary for life,

biomolecules such as DNA, RNA and ATP. This study focusses on the TOCP toxin and related

compounds which can cause acute and prolonged toxic effects. [36]

Phenyl saligenin phosphate (PSP) is an organophosphate neurotoxin which is not a strong inhibitor

of acetylcholinesterase. NTE has been identified as a primary toxicity target.[37] In addition, SCOTP

was discovered to be a highly active metabolite of the neurotoxin, TOCP, which is actively converted *in vivo* via specific cytochrome P450 enzymes.[38] Structurally PSP is analogous to SCOTP, and Hargreaves *et al* have shown that it inhibits neurite growth of mouse neuroblastoma in accordance with strong inhibition of NTE.[39]

All these compounds feature a pentavalent phosphorous centre, with three substituent groups attached via a relatively weak P-O bond. Each has a phenol substituent which can be displaced during reaction with nucleophilic species, this allows the organophosphate to covalently bind to a protein target. Inhibition via this route is potentially chemically reversible, with treatments for acute organophosphate poisoning employing non-enzymatic reagents for the reactivation of enzymatic activity.[40]

1.7 Hydrolysis Products (Aging)

Following the initial reaction of the organophosphate with its targeted protein, further reactions can take place, in a process termed aging. For example, an OP covalently binds in the active site of an enzyme by organophosphorylation of the serine oxygen. This causes enzyme deactivation; which in the case of acetylcholinesterase, leads to extreme muscle contractions to the point of paralysis and convulsions.[41] Further to this, spontaneous cleavage of the auxiliary groups around the phosphate centre, generates a phosphate group permanently attached to the residues of the protein complex. This spontaneous dealkylation can occur any time from 2 minutes up to 16 hours post initial reaction, and can be observed with the partial loss of only one R-group. This is the case for many organophosphates, or can result in the complete loss of the R groups leaving phosphate moiety bound to a residue as seen with PSP (Figure 7).[42]

Although, when partial hydrolysis occurs, studies have shown that an enzyme can spontaneously reactivate, regaining lost functionality.[43]
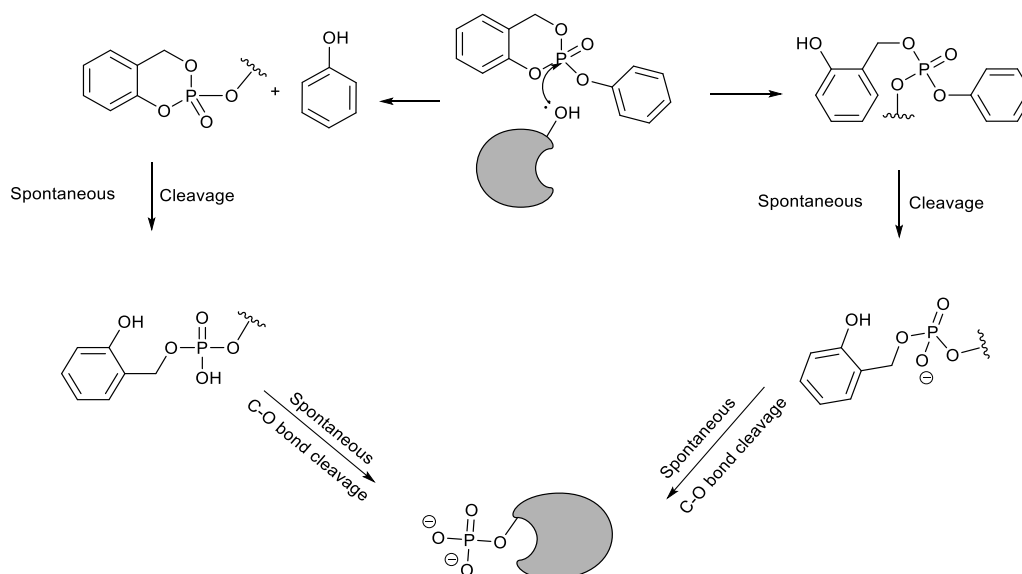
Figure 7. PSP aging to leave a permanent phosphate group in active site of enzyme. [44, 45]

1.8 Interesting Targets for Organophosphates

Chronic illness related to organophosphates binding to targets beyond the normal serine found in AChE can happen at low exposures.[46] There is also evidence that organophosphates bind to exposed nucleophilic residues of tyrosine, lysine and histidine at high concentrations.[35] This reactivity implies that organophosphates may interfere with a wide range of potential targets which have not yet been fully investigated with implications for the understanding of OPIDN. There is need to determine more information on the other targets involved in OPIDN through proteomic probing.

One of the early established targets of organophosphates, other than AChE, is NTE, an integral part of neurons (except glia). NTE is a membrane protein regulating membrane traffic and hydrolysis of lipids. This enzyme has the most direct involvement with OPIDN. The active site consists of a serine, SER^{966} and two aspartate residues, ASP^{960} and ASP^{1086}. Deacylation of endoplasmic reticulum-membrane bound phosphatidylcholine to fatty acids and glycerophosphocholine is catalysed by NTE. The deactivation of this enzyme by structural changes caused by organophosphate binding, results in a build-up of phosphatidylcholine. [47] This build-up ultimately results in cell death due to abnormal membrane structure, influencing the disruption and interactions of axons.[48] It is worth noting however, that organophosphate inhibitors of NTE that do not age, do not cause OPIDN, suggesting some non-classical enzymic role for NTE.[49]
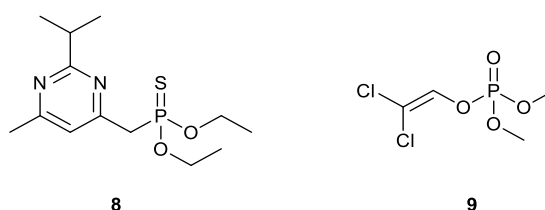
Figure 8. Two commonly occurring organophosphorus insecticides, diazinon and dichlorvos.

In detailed mass spectroscopic studies, histidine and lysine residues have also been found to react with organophosphates. TOCP metabolite SCOTP, forms a stable o-hydroxybenzyl adduct with histidine and lysine residues found in albumin. [50] This study examined a forensic application which

can benefit from the measurement of OP-modified albumin as it does not undergo aging. Many nerve agents bind also to tyrosine residues found in albumin, and the mass spectroscopic analyses of albumin from suicidal patients who had ingested either just dichlorvos **9** (Figure 8),[51] just chlorpyrifos **6** (Figure 6) or both chlorpyrifos and diazinon **8** have all found phosphate analogues of the toxins bound to tyrosine residues.[52] However, there is little capacity for diagnostic use of albumin in cases of unknown OP poisoning, due to large volume of plasma required and comparatively slow binding rates.

Figure 9 illustrates the reactive sites for cresyl saligenin phosphate (CBDP) on albumin. Tyrosine residues attack the phosphorous centre, displacing saligenin and are organophosphorylated. More nucleophilic histidine and lysine residues can be alkylated by attacking the benzylic carbon and displacing the O-cresyl phosphoryl moiety, as reported by Liyasova *et al*.[53]
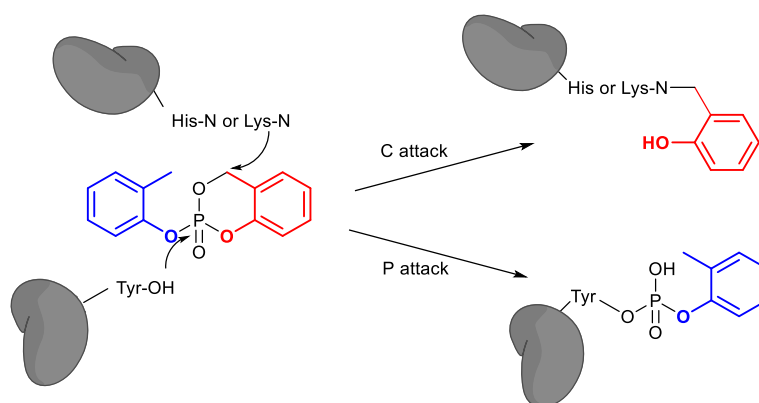
Figure 9. Binding route CBDP can take with albumin residues.

The quite promiscuous reactivity of organophosphates with nucleophilic residues suggests that the target proteins for organophosphates are numerous and found in a range of different tissue types. Studying tissue that responds to acetylcholine via nicotinic receptors would be indicative as a target for organophosphates. Due to an interest in developing a probe for cardiovascular disease (Section 2), cardiac muscle tissue is appropriate for this investigation into organophosphate toxicity.

1.9 Focus of Study – Myocardial Cells

Cardiac muscle tissue and its interactions with organophosphates, have not been much explored and are the focus of part 1 of this study. Several studies have shown that occupational exposure to organophosphates has links to cardiac complications,[54] and 35 patients died of fatal arrhythmias after ingesting Diazole in mass a suicide attempt in 1970.[55]

The exact cause of cardiac arrhythmias is difficult to determine, but three stages are observed. Initially brief, and intense, tachycardia, followed by parasympathetic disturbances which can lead to ventricular fibrillation. Finally, the third stage is characterised by a variety of fluctuating tachycardia and may even result in sudden death.[56,57] This last phase can be delayed for up to several days after the initial intoxication period, and parallels OPIDN in that sickness and death appear to be dependent on complex chemical pathways. [58] Myocardial cells express NTE in membranes, and this protein may be the target for organophosphates causing tachycardia, or other heart complaints.[59] However, it is likely that the target protein could be some other novel target and the processes that underpin these mechanisms are undiscovered. Mitochondria that have been exposed to organophosphates have reportedly received damage of some significant enzymes, notably succinate dehydrogenase, NADH dehydrogenase and cytochrome oxidase.[60] Damage to the key respiratory components of a cell can cause apoptosis and tissue degradation.[61] Targeting mitochondria may reveal the answers to organophosphate toxicity in cardiac tissue. Therefore, the focus of this study was to investigate potential new protein targets found within differentiated rat cardiomyoblasts (H9c2).

H9c2 cells

The cardiomyocyte rodent cell line has widely been used as an *in vitro* model that displays similar physiological, morphological and biochemical properties to human cardiac myocytes.[62] Derived from embryonic rat heart tissue, H9c2 cells have been used in the mitotic form in a number of studies as they express nicotinic acetylcholine receptors and possess a skeletal muscle-like phenotype.[63] H9c2 cells are able to differentiate into a cardiomyocyte-like phenotype. The phenotype is expressed when the culture medium has low levels of foetal bovine serum (FBS) and is supplemented with 10 nM retinoic acid. These conditions encourage the H9c2 cells to undergo the physiological changes found in cardiac tissue.[64] These changes include the physiological morphology, biochemical signalling and responses to stress not found expressed in the skeletal muscle-like phenotype. The morphological changes observed include the formation of elongated multinucleated myotubes, with branched fibres and characteristic actin filaments. Thus, studies looking at cardiomyocyte cytotoxicity often use this differentiated cell line as an *in vitro* model.[65]

1.10 The Potential Use of an Organophosphate Probe in Protein Identification

1.10.1 Previous Work

The objective of work presented in this thesis was to design a fluorescent organophosphate probe that could pick out target proteins in organophosphate poisoning and, in doing so, help to elucidate the mechanisms involved. In previous work, Smida *et al* prepared analogue dansylaminohexanol saligenin phosphate (DSP-**10**), an organophosphate fluorescently modified with dansyl amide (Figure 10).[66, 67]
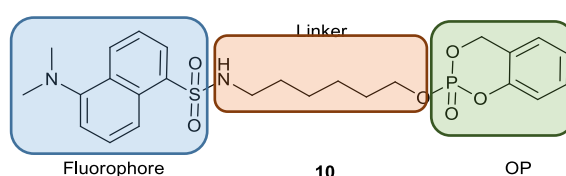
Figure 10. Dansylated saligenin phosphate.

The active saligenin phosphate centre here is linked via a primary alkoxy group. This moiety is a poorer leaving group than phenoxy, so there are only two likely hydrolysis products. It should have a similar mechanism and binding affinity with the organophosphates of interest (Figure 11).
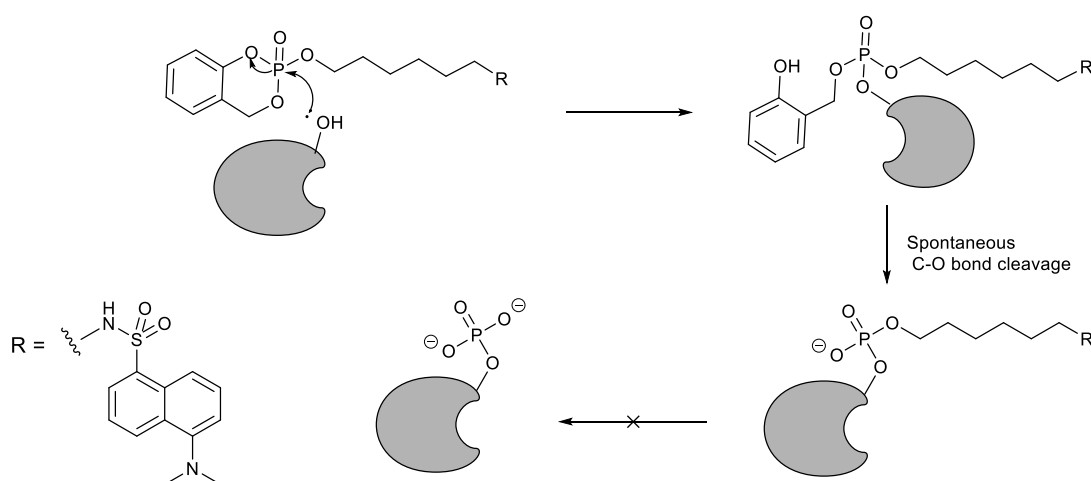
Figure 11. Proposed binding mechanism for alkoxy-fluorophore modified PSP on a serine residue, where R is a fluorophore.

One of the problems found with this probe during the initial experiments performed was that the solubility of the DSP-**10** in an aqueous environment was lower than desired. Clinically,

concentrations of 100 µM are irrelevant, however at this concentrations and above, the probe starts

aggregating and then precipitating. This indicates that solubility is an issue when wishing to study

their behaviour within certain experiments where concentrations of probe may be as high as 200

µM.

A proof of concept experiment was performed to ascertain if the DSP probe binds to known

organophosphate protein targets.[67] The probe was incubated with both trypsin and chymotrypsin,

two enzymes that contain active site serine residues,[68] which are an established target of PSP. These

enzymes were then subjected to one dimensional gel-electrophoresis and visualized using UV light

from a transilluminator. The results showed fluorescent bands at 25 kDa, corresponding to

covalently labelled protease (Figure 12). The fluorescence of the bands containing chymotrypsin was

greater than that of trypsin. This result suggested that the binding to chymotrypsin may be greater,

and that the protein may contain more residues available for phosphorylation. However, the

coomassie stained gel had much darker bands indicating that there was more protein occupying this

band then with the corresponding trypsin band.
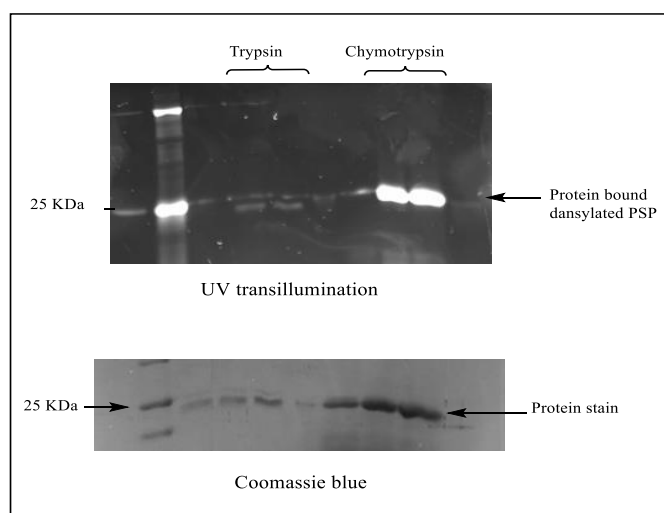
Figure 12. Incubation of dansylated saligenin phosphate with trypsin and chymotrypsin. Chymotrypsin is a more potent substrate for PSP then trypsin, although, increased fluorescence could also be partly due to error in loading chymotrypsin wells with more protein then with trypsin wells.

A second problem with the dansyl amide fluorophore is that it has a low extinction coefficient and quantum yield, (ε =4300 Φ =0.66,),[69,70] and a brighter fluorophore than dansyl amide is desirable to explore PSP interactions with low concentration of proteins. Using a fluorophore which is photostable with a high extinction coefficient and quantum yield, should increase the sensitivity of the probe in gel electrophoresis experiments and confocal microscopy, ideally revealing protein targets of low abundance.

Additionally, a third issue associated with using a dansyl fluorophore is one of interference from autofluorescence of the proteins. Certain tissues and proteins containing large amounts of fluorescently active amino acid residues, such as tryptophan, tyrosine and phenylalanine, can all be active over the same wavelength range as dansyl amide.[71] To resolve this issue it is better to use probes which are excited and emit at wavelengths beyond green light (>490 nm).

The inhibitory effect of PSP on trypsin and chymotrypsin enzymatic activity was demonstrated in competition reactions with two substrates, benzyl-L-arginine 4-nitroaniline hydrochloride (L-BAPNA), and N-Succinyl-Gly-Gly-Phe-p-nitroanilide (Suc-GGF-pNA).[67] These substrates are peptides with fluorescent para-nitroaniline components that, when cleaved by either trypsin or chymotrypsin respectively, fluoresce in light at 415 nm. Inhibition of the protease by the OP probe was seen in the greatly reduced emission of light. The success of this work demonstrates the capability of the probe both in covalently binding to a protein target, but also in deactivation of the enzyme by the probe, it has also set benchmarks for biological activity for newly synthesised PSP probes.

1.10.2 The Synthetic Route of an Organophosphate Probe

The aim of the project was to fabricate an effective cardiac protein probe using organophosphates and a connected fluorophore. Whilst the previous probe is useful, labelling of low abundance targets in cell incubation experiments would benefit from a brighter fluorescent component than a dansyl group. The probe design starts with examining the simple components that are commercially available. A new fluorophore is needed along with a suitable moiety for linking the two. Linking units

can be aliphatic carbon chains with reactive groups on either end, or polar chains. Brief analysis of the literature identified three potential classes of brighter fluorophores appropriate for the purposes of the project: rhodamines, BODIPY dyes and pyrenes.[72,73] This was based on the three identified problems: solubility, brightness, and selectivity.

Selectivity

Many studies have shown that toxicity is dependent on interactions with multiple targets, and the mechanisms of chemical hydrolysis are dependent on R group structure.[74,42] Changing the nature of the R groups will change the toxicity of the compound, the high potency of VX **3** is due to the *N,N*-diisopropylaminoethylthiol R group present. Phenyl saligenin phosphate **7** (PSP), was chosen as the organophosphate component of the probe. It is an acetylcholine esterase inhibitor with numerous other known targets.[75] The primary R group in the compound PSP is a phenol, and it is worth noting that changing the secondary R group to a linker-fluorophore will either increase or decrease toxicity comparatively to PSP. There are three mechanisms to the hydrolytic product and as previously mentioned are dependent on aging, and will be influenced by R group change.

Solubility

Currently, aminohexanol **11**, is incorporated into DSP-**10**. To increase the solubility of the probe, linkers featuring polar groups can be utilised. Two categories of linkers were chosen, polyethylene glycol (PEG) **12**, and polyglycine **13**.
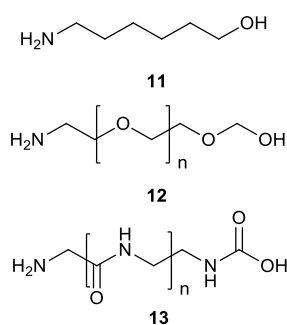
Figure 13. 6-aminohexan-1-ol, PEG, and polyglycine, three chains to linker fluorophore to OP.

Brightness

Rhodamine dyes are cheap and can be used directly in coupling reactions. If commercial rhodamines couple effectively but do not function well as a fluorophore in biological testing, there is considerable scope to customize this skeleton and modify its properties. Rhodamine B **14** is bright with high extinction coefficients and quantum yield (ε =140,000 Φ =0.8). This fluorophore also has a high level of photostability, and absorbs and emits around 554 and 627 nm respectively; far beyond the autofluorescence limitations below green light. [76] These values highlight that the probe will be more selective for low abundance targets compared to a probe with lower brightness and quantum yield.

14
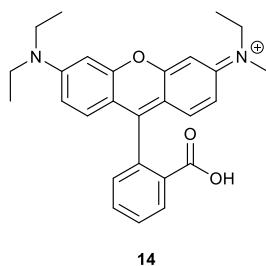
Figure 14. Structure of rhodamine B in fluorescent cationic open form.

Components **11**, **12** and **13** could be coupled to **14** via peptide coupling agents to form an amide bond, linking the linker to the fluorophore (Figure 15).

15   16   17
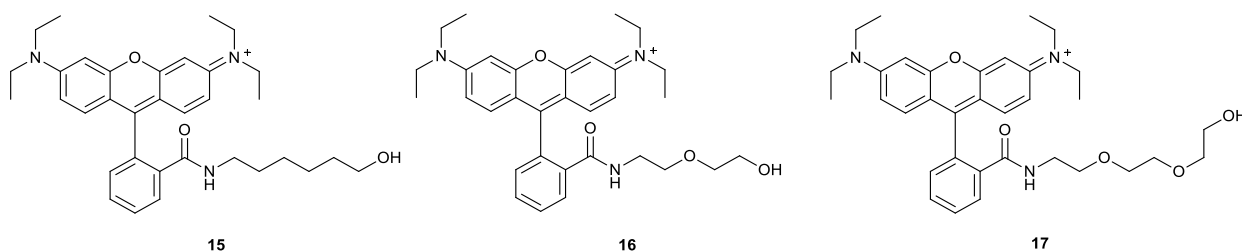
Figure 15. Rhodamine B coupled to three different linkers, 6-aminohexanol, 2(2-aminoethoxy)ethanol, 2(2[2-aminoethoxy]ethoxy)ethanol.

With a fluorophore connected to a linker, saligenin chlorophosphate can then be added to the alcohol end of compounds **15**, **16** and **17**, (Figure 16). This then completes the synthesis of a novel organophosphate probe. With cardiac myocytes being of interest to this research group, the rhodamine organophosphate probe will be useful in discovering protein targets of PSP.

18
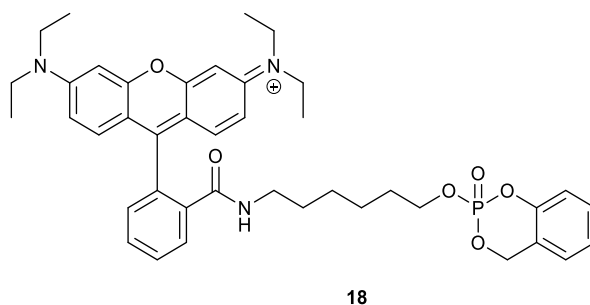
Figure 16. Rhodamine B amidohexanol saligenin phosphate, a rhodamine B PSP probe.

After synthesis of these organophosphate probes, biological testing can be performed. Assays to include cell proliferation, enzyme activity assays, and one or two-dimensional gel electrophoresis. These assays determine the efficacy of the probe when binding to organophosphate targets and inducing a biological response; measuring whether it is similar to the other organophosphates of interest e.g. PSP by using it as a positive control. The final step in analysis of the probes usefulness, is to extract a target protein via 2-dimesional gel electrophoresis and to carry out identification with mass spectrometry.

2 Cardiovascular Disease

2.1 Background

Cardiovascular disease kills more than 17.3 million people yearly, approximately one third of all worldwide deaths.[77] In 2013, 8.2 million people died due to ischaemic heart disease,[78] and the disease accounted for 17.8% of deaths of men aged 50 to 64 in England and Wales during 2015 (Figure 17).[79] Ischaemia is the restriction of blood supply to tissues, causing oxygen starvation of cells, which causes a cascade of problems, due to shortage of nutrients as well as a failure to

adequately remove metabolic waste. Restoring blood flow can cause further damage called

reperfusion injury, through rapid production of free radicals ($\cdot O_2^{-2}$, $\cdot O_2^-$ and $\cdot OH$), and reactive oxygen

species (ROS) such as H_2O_2.[80] These free radicals lead to cell death via uncontrolled oxidation of

cellular components and as a result, ischaemia and cardioprotection are very important areas of

research.

Top 5 causes of death for 50 to 64 year olds, 2015
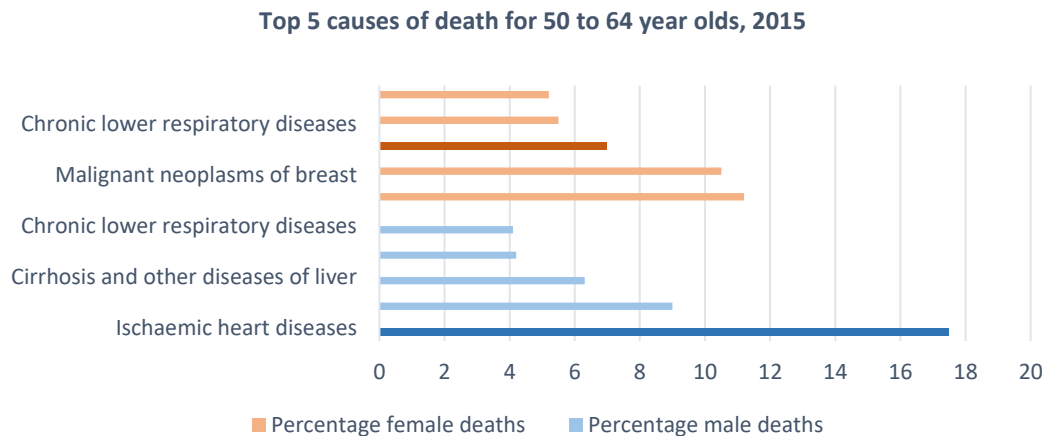
Figure 17. Leading causes of death during 2015 for men and women in England and Wales from adapted from British government statistical data published by the Office for National Statistics in the online bulletin.[79]

2.2 Ischaemia-Reperfusion Injury

Ischaemia-reperfusion injury can affect any tissue type, and not just myocardial cells. Vascular

endothelial cells are however more susceptible to injury.[81] These cells regulate perfusion and

reperfusion, leukocytes, platelet function and the control of inflammation and thrombosis during

myocardial events.

2.3 Preconditioning

Strategies that aim to reduce the effects caused by ischaemia are given the term cardioprotective.

Normally the goal of cardioprotectrive techniques is to activate pathways that endogenously reduce

the damage caused by myocardial ischaemia-reperfusion injury. Ischaemic preconditioning (IPC)

refers to the observation that brief periods of ischaemia in a tissue or organ can activate

mechanisms of resistance which protect the cell when a subsequently damaging period of ischaemia

arises (Figure 18).[82] The role of this technique is clearly limited as it directly interferes with coronary

blood flow, potentially giving rise to lethal ischaemia or plaque rupture. The evidence that this technique clinically reduces myocardial infarction damage or mortality rates is also in doubt.[83]
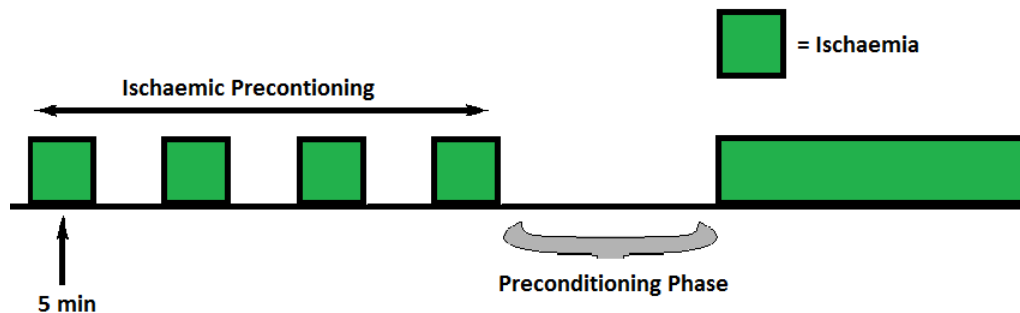
Figure 18. Block diagram highlighting IP. Four sequential periods of 5 minutes of ischaemia followed by 40 minutes of prolonged ischaemia were shown to decrease infarct size in anaesthetised dogs. The early preconditioning phase is up to 2 hours. A second window protection can be seen when this phase is increased to 24-72 hours before administering ischaemia and is called delayed preconditioning. Adapted from Murry et al.[84]

The exact biochemistry of IPC and the processes that give rise to this phenomenon are not well elucidated. It has been suggested that early and delayed protection of cardiomyocytes are generated by cascades of intracellular signalling. A preconditioning stimulus, for example ischaemic insult, triggers IPC via endogenous activation of membrane receptors, protein kinase C (PKC), tyrosine kinase (TK), and mitogen activated protein kinase (MAPK) pathways.[85] K_{ATP} channels in either or both the sarcolemma, and mitochondria can be opened, allowing potassium ions to leave the cell or organelle, hyperpolarising the membrane causing local cardiac muscle relaxation. Alternatively, release of the transcriptional nuclear factor κB (NF-κB) may also result in the synthesis of protective proteins such as heat shock proteins (HSPs), and the mitochondrial antioxidant enzyme superoxide dismutase (MnSOD). Release of nitric oxide (NO) and the two nitric oxide synthases, endothelial (eNOS) and inducible (iNOS), has also been shown to give both early and delayed cardioprotection (Figure 19).
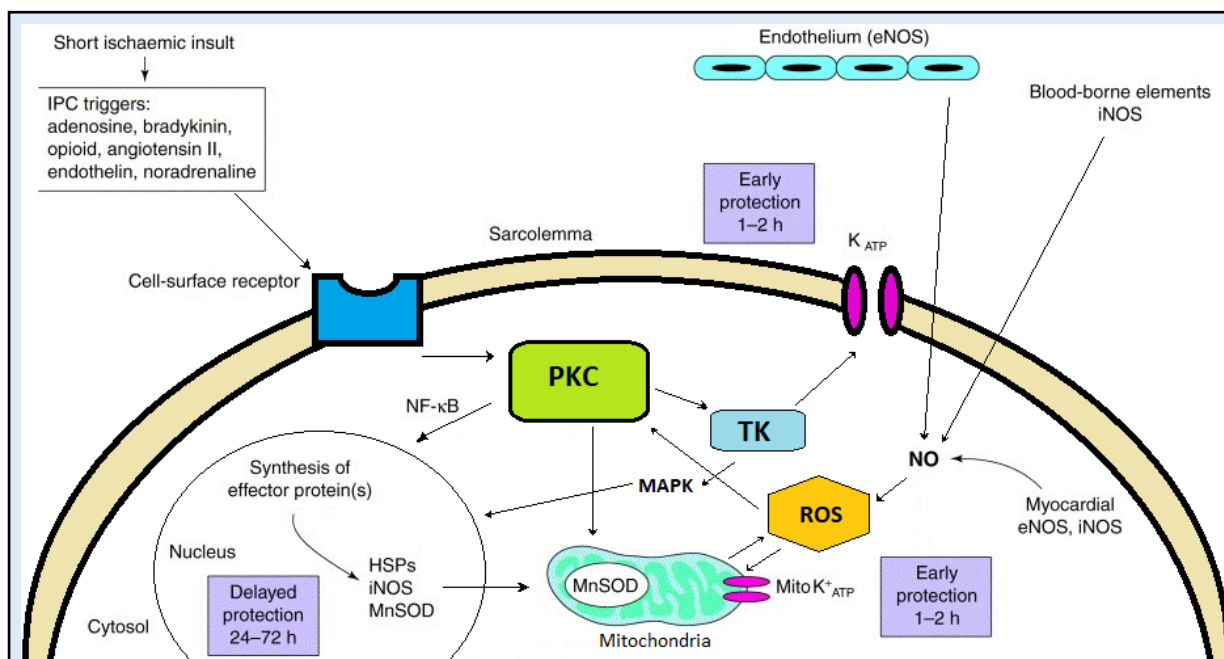
Figure 19. Diagram illustrating potential mechanisms of ischaemic preconditioning. Intracellular signalling cascades that lead to both early and delayed protection of cardiomyocytes. Ischaemic insult induces endogenous triggers to be released ultimately ending with ischaemic preconditioning (IPC). The interaction of these triggers with specific membrane receptors leads to protein kinase C (PKC), tyrosine kinase (TK) and mitogen activated protein kinase (MAPK) pathways being activated. This can result in several potential options: 1. K_{ATP} channels open within the sarcolemma, mitochondria, or both. 2. The increase in expression of genes leading to synthesis of effector proteins such as transcriptional nuclear factor kB (NF-kB) and protective heat shock proteins (HSPs) and mitochondrial antioxidant superoxide dismutase (MnSOD), which are then transported to the nucleus. 3. Nitric oxide (NO) is synthesised and released under the regulation of two forms of nitric oxide synthase, the endothelial (eNOS) and inducible (iNOS) forms. This also contributes to early and delayed cardioprotection.[85]

2.4 Diazoxide – Pharmacological Preconditioning

Diazoxide is a drug that has been known for many years as Proglycem[86], and was originally prescribed as a hypotensive agent (Figure 20). Currently it is marketed to treat diabetes as it causes inhibition of insulin secretion. This is achieved by hyperpolarising the pancreatic tissue. In normal insulin release, increased levels of blood glucose in the β-cells causes a cascade of processes resulting in an increase in the ATP: ADP ratio. This increase in ATP causes K_{ATP} channels to close.[87] The membrane then steadily depolarises until voltage-gated Ca^{2+} channels open, allowing calcium ions to enter and insulin to be secreted. With a hyperpolarised tissue, the surface membrane is more negatively charged and therefore less sensitive to elevated glucose levels, inhibiting the release of insulin.[88]

This study is interested in diazoxide as it has shown cardioprotective qualities, as well as pancreatic, anti-diuretic benefits, and even synaptic enhancement. Unsurprisingly, with such a wide and varied pharmacological activity, it has been utilised as a lead compound in many drug discovery programs for over 50 years, and has led to the development of some promising analogues.

19
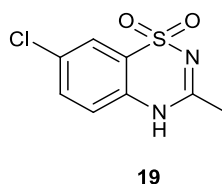
Figure 20. Structure of diazoxide (Proglycem).

The biological effect of this drug on rat aortic rings has been shown to delay stimulated contractions. Diazoxide depolarises cardiac membrane tissue and produces an effect similar to a period of ischaemic preconditioning. This leads to temporary changes in cell biochemistry that can be protective if substantial ischaemia occurs.[89]

Given the recognised mode of action in pancreatic β cells,[87] activating potassium channels found in cardiomyocytes would also hyperpolarize the cell membrane, delaying action potential and preserving residual energy. Alternatively, diazoxide may hyperpolarise the mitochondrial membrane, causing increased release of ROS into the cytosol.[90] The increase of ROS may then stimulate other beneficial signalling pathways.

It has been established that ROS scavengers administered before treatment with diazoxide can block the beneficial effects of protection upon ischaemic insult. This blocking effect suggests a link between diazoxide and ROS.[91] However, the binding sites of diazoxide within the cell and the exact drivers of the cellular processes leading to cardioprotection are not known. Figure 21 illustrates the two potential mechanisms for protection mentioned above.
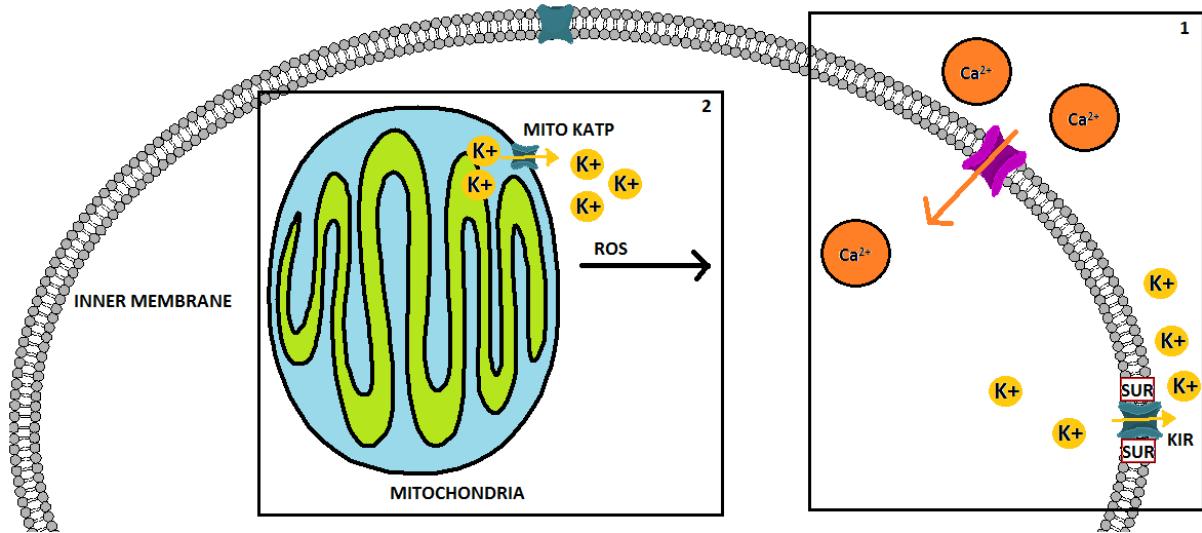
Figure 21. Diazoxide action, 1. Sarcolemma K^+ channels induce a delayed action potential through activation of a K_{ca} channel, allowing Ca^{2+} ions in. 2. Hyperpolarisation of mitochondrial membrane, as a result of which potassium channels release ROS into the cell.

Identification of the protein targets for diazoxide, and establishment of the cellular location, will clarify whether diazoxide acts via a sarcolemma potassium channel or a mitochondrial channel activation, or indeed, via other unforeseen pathways.

2.5 Potassium Channels

2.5.1 Types of Potassium Channel

Potassium ion channels are one of the most abundant ion channels found in cell biology, located not only on the plasma membrane but also on the membranes of intracellular components like mitochondria. These channels are involved in the modulation of a wide variety of processes and are integral to membrane transport, muscle contraction and neurotransmission.

In general, transmembrane channels mediate the movement of ions across membranes and the K^+ ions play a central role in many biological processes. The principal functions of potassium channels differ depending on the speciality of the tissue in which they are located. Nevertheless, all K^+ channels regulate charge control across a membrane; either sarcolemma or located on an organelle.[92] Membrane polarisation controls other functions beyond action potentials. For instance,

production of ROS in mitochondria is influenced by K^+ ions hyperpolarising the inner membrane. However, the functions are multifarious and, as previously mentioned with insulin secreting tissue, these channels play a role in the management and secretion of hormones and proteins. [93]

There are four general types of K^+ channels: Calcium-activated, , tandem pore domain, voltage-gated, and inwardly rectifying. Each of these four classes of potassium channels can be differentiated further into subclasses.[94]

Calcium-activated potassium channel (K_{Ca}) are a type of K^+ channel, comprising of eight different family members normally activated by Ca^{2+}. Although some are further moderated by Na^+ and Cl^-, and the $K_{Ca}1$ channel is both voltage-gated and Ca^{2+} activated.

Tandem pore domain potassium channels are part of the leak pathways, these are active at rest, and stabilize the membrane polarisation found in mammalian cells. Voltage-gated potassium channels manage the level of extracellular K^+ during an action potential.[95]

Inwardly rectifying potassium channels (K_{ir}) form a family of seven K^+ channels that are responsible for allowing positive charge to enter the cell during the refractory period.[96] The pumping in of K^+ ions helps establish the resting potential of neurons and is the target for many toxins. The roles of inwardly rectifying channels vary in accordance with the location. For example, the channels found on cardiac myocytes close on depolarisation causing a more prolonged cardiac action potential by slowing repolarisation. Whereas K_{ir} channels found in the kidneys, act to remove surplus potassium and store it, either for excretion or to return to the system later. This is in contrast with typical neuronal potassium channels which are responsible for repolarising the cell after action potential. These allow K^+ to leave the cell as opposed to entering it. The associated proteins of these types of channel are of interest due to an acknowledged role in cardioprotection.

2.5.2 Sarcolemma K_{ATP} Structure

One further subtype of potassium channel is the ATP nucleotide gated channel. This can be found in the sarcolemma, mitochondria and the nucleus. The sarcolemma K_{ATP} channels are a complex formed from inwardly rectifying (K_{ir}) channel subunits. The $K_{ir}6.2$ subunits which are pore-forming and tetrameric in structure. The subunits are connected to two transmembrane units (M1 and M2), a form of ATPase, and sulfonylurea (SUR) receptors, all located within the sub-membrane space.[97] The connection to SUR is via transmembrane protein used to anchor the K_{IR} unit.[98] There are four variants of SUR receptor in these complexes: SUR1, SUR2A, SUR2B and SUR2C.[99] The SUR2A receptor is present as a subunit in cardiac myocytes. Interestingly, overexpression of this subunit generates a resistance to ischaemia as seen in modified mice.[100] The SUR2A makes up the ATP- binding cassette (ABC), and is octameric in structure. Consisting of three transmembrane domains (TMD), and a nucleotide binding domain (NBD), selective for ATP (Figure 22).[101]
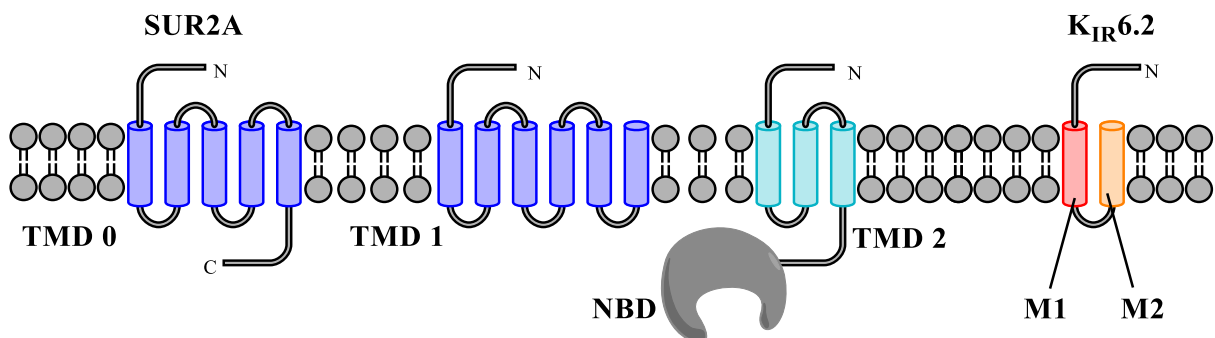
Figure 22. Schematic of K_{ATP} channel found on the sarcolemma. Sulfonyl urea (SUR2A) consists of three transmembrane domains (TMD), and nucleotide binding domains (NBD). Potassium inwardly rectifying subunits ($K_{IR}6.2$) also contain two transmembrane domains, M1 and M2.

2.5.3 Mitochondrial K_{ATP} Structure

The structure of mitochondrial K_{ATP} (mitoK$_{ATP}$), has not yet been fully elucidated, but mitoK$_{ATP}$ channels are thought to have $K_{ir}6.1$ and a type of SUR2 receptor.[102] Early research by Ardehali *et al*, found that whilst investigating mitochondrial lysates via co-immunoprecipitation studies, components of mitoK$_{ATP}$ channels were found alongside succinate dehydrogenase (SDH).[103] This implies that SDH interacts with other mitochondrial proteins including: mitochondrial ATP-binding cassette protein-1 (mABC1), adenine nucleotide translocator (ANT), mitochondrial phosphate carrier (PIC) and ATPase (Figure 23). The complexes that these proteins make were partially purified and, after fusion with planar lipid bilayers, K^+ currents were recorded. This activity was increased by diazoxide, and inhibited by ATP, 5-HD and glibenclamide, (5-HD, a postulated specific mitoK$^+$ channel inhibitor, glibenclamide is in a class of sulfonylureas and inhibits K_{ATP} channels).[104]

Diazoxide has also shown an affinity for SDH, which brings into question whether it directly influences mitoK$_{ATP}$ or acts via a more indirect mechanism which features SDH. What is clear is that that there is a definite link between SDH, mitoK$_{ATP}$ and diazoxide.[105]
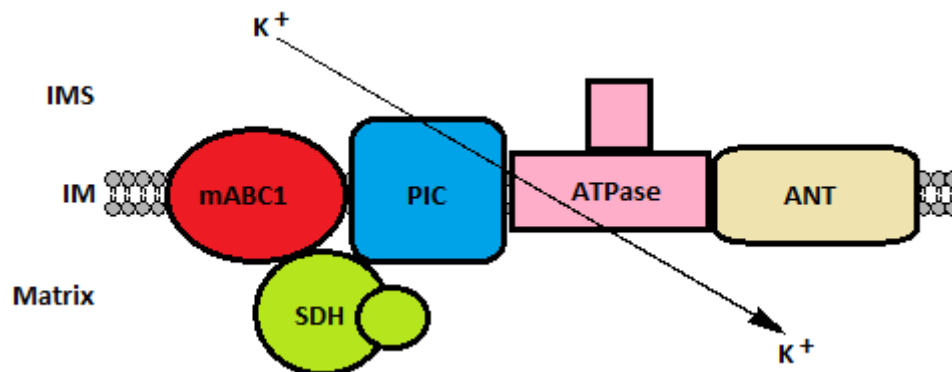
Figure 23. Schematic diagram of the diazoxide-sensitive complex containing SDH-PIC-mABC1-ATPase-ANT, the proteins associated with mitoKATP activity. K^+ ions are capable of being transported with characteristics similar to those of mitoK$_{ATP}$. IMS, intermembrane space; Mito IM, mitochondrial inner membrane. Adapted from reference O'Rourke.[103]

More recent studies suggest however that $K_{ir}6.1$ units are not foumd in the mitochondrial inner membrane, and instead the membrane contains a renal outer medullary potassium channel or ROMK unit (Figure 24).[106] Conversely, Lacza et al have suggested that mitoK$_{ATP}$ contain structures

both like Kir6.1 and Kir6.2 subunits, but neither SUR1 nor SUR2, although there is the potential for some smaller light weight SUR2-like protein.[107]

To date, the precise nature of the subunits found on mitoK$_{ATP}$ channels and the interaction with diazoxide are unknown. Furthermore, the involvement of ROS in the mechanism for ischaemic preconditioning (IPC) is not clear.
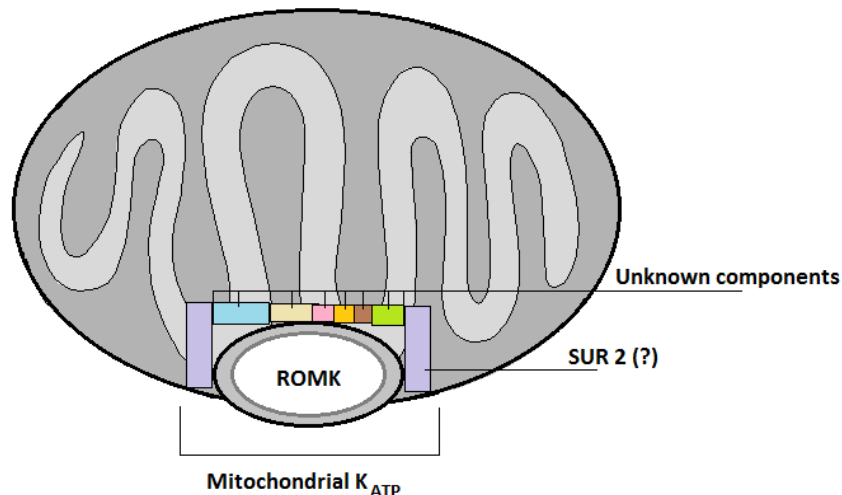
Figure 24. Structure of mitochondrial K$_{ATP}$ channel on inner membrane. Glibencamide sensitivity highlights the likelihood of a short SUR2 type of subunit. Tertiapin Q is an established inhibitor of renal outer medullary potassium channel (ROMK) and has been shown to effect K$^+$ levels indicative of decrease in activity of a mitoK$_{ATP}$ channel. Adapted from reference 105.

2.6 Mitochondrial Role in Cardiovascular Disease

Mitochondria produce ATP, the stored chemical energy the body uses as fuel (Section 1.3), in a series of redox reactions that occur in the inner membrane of mitochondria. In this process, an electron is moved from a donor molecule such as nicotinamide adenine dinucleotide (NADH), to an electron acceptor (O$_2$). The O$_2$ is then reduced to produce a primary ROS, superoxide radical (O$_2^{\cdot-}$), which is reasonably reactive and is subsequently transformed into H$_2$O$_2$, a more stable compound through the activity of Mn, Cu and Zn superoxide dismutases (SOD). H$_2$O$_2$ may be metabolized by the mitochondria, however, in the event where it is not metabolized and the antioxidant systems have failed, H$_2$O$_2$ will degenerate into a hydroxyl radical HO·, which is extremely reactive.[108]

Intracellular Ca^{2+} ions control much of the bioenergetics of a mitochondrion and play an important role in the citric acid cycle, activation of pyruvate dehydrogenase, NADH formation and ROS release. Mitochondrial membrane potential can decrease following uptake of Ca^{2+}, which can decrease ROS formation. However, excessive accumulation of Ca^{2+} is associated with mitochondrial stress and may lead to increased levels of ROS species. The mechanisms for ROS release via Ca^{2+} can be related to enhanced NADH formation which activates glycerol phosphate and α-ketoglutarate dehydrogenase two ROS-generating enzymes. [109]

2.7 Structure and Reactivity of Diazoxide

Given the historical interest as a drug lead, diazoxide has been subject to a great number of structure-activity relationship (SAR) studies. One aim of this project is to incorporate diazoxide into a probe. There are several positions for substitution around the diazoxide pharmacophore where the probe could feasibly be coupled (Figure 25). Adding groups to positions 3, 5 and 7, notably increase or decrease potency toward $mitoK_{ATP}$ channels. With the knowledge gained from the variation of substitution, selectivity for channel subtypes such as Kir6.2 and SUR1 can be fashioned. Furthermore, incorporating diazoxide into any larger probe system may unfavourably change the reactivity of the diazoxide. Structural changes around the molecule need to be made in a position that bares no decrease in biological activity. An understanding of the structure and reactivity of diazoxide is essential for the current study.
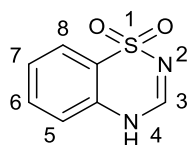
Figure 25. Diazoxide core structure with numbered locations for substituent change.

2.7.1 Cardioprotective Derivatives

In the 1970s, John Topliss and Milton Yudis synthesised numerous derivatives of diazoxide. They measured the ability of the drug to block norepinephrine-induced contractions of rat aortic rings.[110] Using Hanschs' structure-activity analysis, equations were applied to determine the biological

efficacy after a substituent change, and then compared against observed values measured as an ED$_{50}$. The ED$_{50}$ (µl/ml) value vs. norepinephrine may be viewed as an *in vitro* measure of antihypertensive activity in this series of compounds. Stimulation of aorta causes contractions of the aortic rings which indicate membrane potential activity and regulation, and is indicative of diazoxides antihypertensive activity.[111] The equations used in tandem with biological responses are a good indicator of how substituent change will affect efficacy of drug modifications.

The results of substituent change, represented in arbitrary units, with higher values illustrating a greater decrease in norepinephrine-induced aortic ring contractions, suggests that both electronic and steric effects of substituents at position 3 have very little influence on biological activity. It also suggests that increasing lipophilicity of this position beyond an optimum value leads to reduced activity (Figure 26).
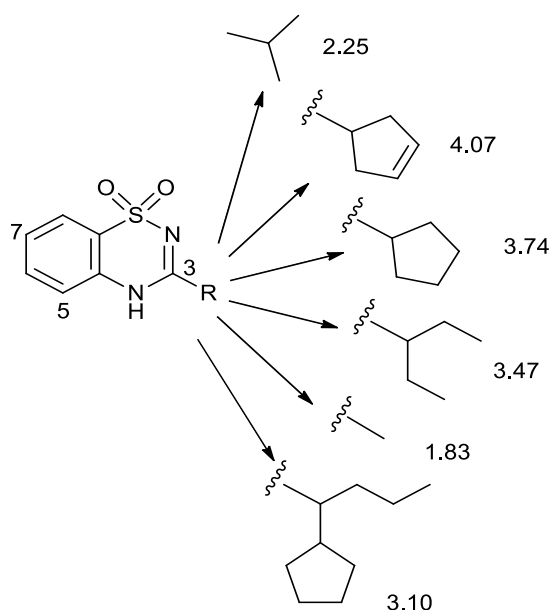
Figure 26. Diazoxide analogues, with an R3 substituent change (values in arbitrary units), derived from equations calculating structure-reactivity changes on efficacy are compared with activity of observed values.

In addition to this trend, Topliss *et al* go on to illustrate that there is an increase in activity for substitution of H for either a halogen, small ether, nitro, amine, trifluoromethyl or small alkyl chain about the 5,6,7 or 8 positions.[109] Singly substituting chlorine in these positions achieves the largest increase in activity for mono substituted derivatives, with chlorine in the 7 position the highest.

Disubstitution of positions 6 and 7 with chlorines gives the second highest activity, whereas

disubstitution in either positions 6 and 8 or 7 and 8 does not give as high an activity increase as

mono-substituted chlorine at 7. Tri-substitution of 6,7, and 8 with chlorine grants the fourth largest

increase in activity. However, 6,7-dichloro substitution and 6-CF$_3$, 7-Cl produce the most potent

derivatives (Figure 27).

Detailed analysis of their results suggests that the activity is affected by both steric and electronic

effects, and in the 6 position steric effects take priority. In the 7 position, F or Br substituents raise

the activity significantly less than Cl does, indicating that group size has some influence. Whilst

replacing position 7 with a CH$_3$ only gives a modest rise in activity, this suggests that electronic

effects are also important.
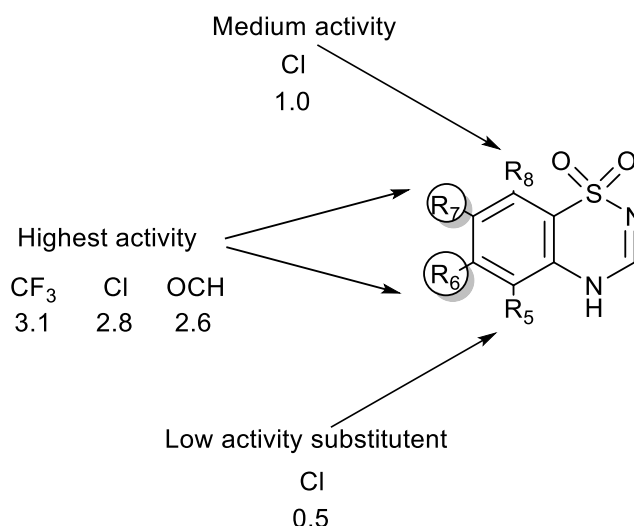
Figure 27. Activity of diazoxide analogues calculated by Topliss *et al* in arbitrary units containing substituents at the R5, 6, 7 and 8 positions, where equations calculating structure-reactivity changes on efficacy are compared with observed values.[109]

It was calculated from this study that the most potent analogue theoretically was 7-chloro-3-(cyclopent-3-en-1-yl)-6-(trifluoromethyl)-4H-benzo[e][1,2,4]thiadiazine 1,1-dioxide **20**. With disubstitution at positions 6 and 7 and a Δ^3-cyclopentenyl system at the 3 position(Figure 28).
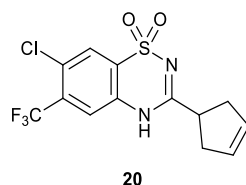
Figure 28. Highest theoretical activity diazoxide analogue from the Topliss studies.[109]

Analogues **21** and **22** of diazoxide, bearing amines or sulphonyl ureas on positions 5 and 7 were synthesised by Smail Khelili *et al*. in 2003.[112] These derivatives in comparison with diazoxide and the K_{ATP} channel opener cromakalim, were less effective at inducing vasodilation. However, when the sulphonylurea was attached via an SO_2 group at the 7 position the potency increased greatly (Figure 29).
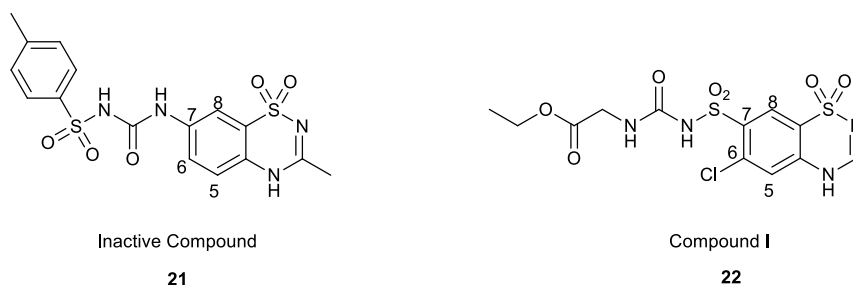
Figure 29. Sulphonyl urea based diazoxide as selective K_{ATP} channel openers.

2.7.2 Derivatives with Cognitive Effects

One group of diazoxide derivatives has shown effects on glutamate receptors in the brain. In 1994, Jimonet *et al*. were comparing 2H-1,2,4-benzothiadiazine-1,1-dioxide-3-carboxylic acid derivatives for their potency as antagonists against the NMDA (N-methyl-D-aspartate) glutamate receptor, and found that introduction of chlorine atom(s) to positions 5 and 7 enhanced binding affinity with the glycine active site.[113]

Glutamate is a neurotransmitter which is associated with learning and memory, and the receptors mediate synaptic plasticity.[114] These receptors can be split into ionotropic and metabotropic types. Ionotropic glutamate receptors are ligand-gated cation channels which are non-specific, allowing K^+, Na^+, and Ca^{2+} ions to flow across the membrane. Both AMPA[1] and KA[2] receptors desensitise rapidly following glutamate exposure, and repolarisation of AMPA receptors is thought to be a mechanism for cognitive enhancement.[115,116] AMPA, NMDA[3] as well as the KA receptors are three ionotropic glutamate receptors and are responsible for different tasks. AMDA and NMDA stimulate fast and slow synaptic responses whilst the KA receptor physiological function is currently debated. [117]

In another study that looked at cyclothiazide is one of the most potent AMPA re-sensitisers and a potential synaptic enhancer, but it does not cross the blood-brain barrier. G. Puia *et al* from the University of Modena developed diazoxides analogues IDRA 21 (**24**) and IDRA 5 (**25**) that can travel across the blood-brain barrier and target AMPA receptors. (Figure 30).

Cyclothiazide
23
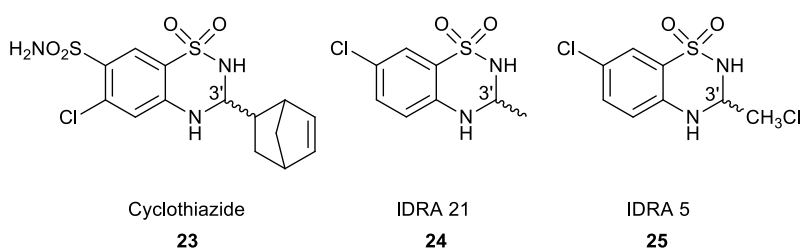
IDRA 21
24

IDRA 5
25

Figure 30. Diazoxide analogues with AMPA biological effects; cyclothiazide and blood-brain barrier crossing analogues, IDRA 21 a sensitiser and IDRA 5 a desensitiser.[118]

IDRA 21 shows an effective increase in conductivity of KA-receptors and positively modulates AMPA receptors. Although, the latter not as effectively as cylothiazide. IDRA 5 however, has shown the opposite effects on both KA and AMPA receptors.[119] Interestingly, removal of the double bond between the 3' position and the sulphonamide helps this drug target glutamate receptors. Replacement of a hydrogen with a chloride, as in IDRA 5, completely changes the effect of the

---

[1] α-amino-3-hydroxy-5-methyl-4-isoxazolepropionic acid is the agonist for this receptor, and mimics glutamate.
[2] Kainate receptor, responds to glutamate.
[3] N-Methyl-D-aspartate is the agonist for this receptor, and mimics glutamate.

compound on its two targets. Pierre Francotte has more recently synthesised seven analogues which positively modulate AMPA receptors each with the fully saturated 3' carbon.[120]

2.7.3 Pancreatic β Cells Stimulation

In-depth analysis of many isomers of the benzothiadiazine 1,1-dioxides can be found in the work of Pascal de Tullio *et al.*[121] In this study, the secretion of insulin from rat pancreatic islet cells was measured in addition to the induction of contractile activity by K^+ in depolarised rat aorta rings. They studied compounds, with the addition of a 3 position side chain hydroxy group, creating a stereogenic centre on the R group. For their derivatives, the *R* enantiomers are generally more potent at inhibiting insulin release than the *S* enantiomers. The three most potent inhibitors (**26**, **27** and **28**) all inhibited at concentrations below the micromolar range (Figure 31).
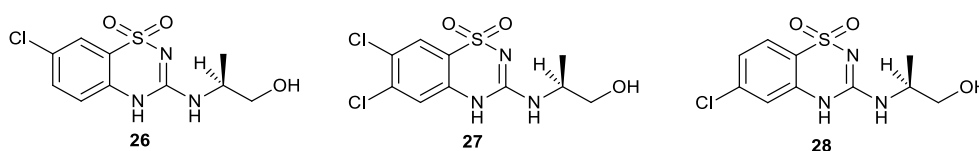
Figure 31. The most efficacious diazoxide analogues at stimulating pancreatic β-cells.

The myorelaxant activity of each compound was given an EC_{50} value; the drug concentration giving 50% relaxation of the 30 mM KCl-induced contraction of the rat aortic rings. The introduction of the amino chain on position 3 decreases the vasorelaxant effect of the hydroxylated derivatives in comparison with the non-hydroxylated. The 6,7-dichloro, non-hydroxylated derivative **27** was the most potent ultimately. The findings concluded that the stereochemistry of these side chains only had a weak effect on the pharmacological role.

M. Dabrowski *et al* developed NNC 55-09216 (**30**) as a diabetes treatment. This compound and BPDZ 44 (**29**) developed by B. Pirrotte *et al* are other potent insulin secretion inhibiting derivatives. NNC 55-09216 is a selective opener of Kir6.2/SUR1 channels.[122] BPDZ 44 is in a class of pyridothiadiazine analogues which use a pyridine ring instead of a phenyl ring with the N sitting at the 7 position

(Figure 32).[123] Like other potential diabetes medications, they hyperpolarise the pancreatic β-cell, meaning inward Ca^{2+} ion transport is delayed, inhibiting insulin secretion.
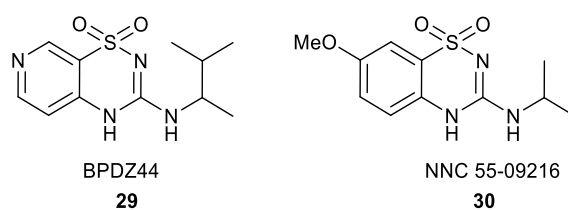
Figure 32. Insulin secretion inhibiting analogues of diazoxide.

Notably across all these studies, structural changes that yield the largest differences in activity come from the chlorine positioned on the phenyl ring. Of any derivative of diazoxide in any role or location, chlorines are optimally positioned at the 6 or 7 position, with substitution at 5 or 8 reducing potency.[124] It is therefore the best course of actions to substitute at the 3 position to couple diazoxide to a probe.

2.8 Non-Covalent Binding of Diazoxide to Protein Targets

The targets of diazoxide are reported to be MitoK$_{ATP}$, the SUR, K$_{ir}$ and ROMK subunits, as well as sarcolemmal K$_{ATP}$. The documented effects of the compound are as a hyperglycaemic, hypotensive, anti-diuretic and insulin secretion inhibitor.[125, 126] Unlike the organophosphates discussed earlier, diazoxide has no reactive central moiety with which to irreversibly bind to amino acid residues. Whatever the target of diazoxide may be, it is not covalently bound and therefore is difficult to identify in cell and tissue extracts. Many non-covalent drug-receptor interactions are characterised by up and down regulation of the genes that code for the target, or via introduction of competing inhibitors. It would seem simpler to determine protein targets by some means of labelling via a covalent bond. One way to induce covalent binding is through the use of photo affinity probes.

2.9 Photoaffinity Probes

In the 1970s, Arnold Ruoho *et al*. at the University of California published a paper detailing a technique of permanent covalent binding of proteins via a photoaffinity label. [127] This technique follows on from Westheimer and co-workers' original diazocarbonyl derivatives published in 1962, and utilises a photolytic reaction with a labelling component that converts to a reactive carbene intermediate.[128] During a reversible binding of a ligand to an active site on a protein, the carbene irreversibly binds to the protein target. The rest of the ligand may now disassociate but will be covalently tagged onto the target protein.

In a recent review, Yutaka Sadakane and Yasumaru Hatanaka discuss three carbene-generating reactive probes (Figure 33).[129] The first, a nitrene based label, has the advantage of being easily synthesised and commercially available. The azide **31** is also small and represents minimal structural change biologically. A nitrene is more reactive than a carbene and can form more labile products. This could create undesirable non-specific crosslinking with other proteins and incorrect labelling. The second example is a carbene forming phenyldiazirine **33**. The phenyldiazirine label has none of the non-specific crosslinking issues of the phenylazide and photolyses at 360 nm, a wavelength that is less damaging to biomacromolecules compared to the 300 nm of phenylazide. Previous work by the Garner group had prepared phenyldiazirine photo reactive probe but it required considerable synthetic effort.

The current study shall focus on the third example, benzophenone **35**. This photoreactive component is commercially available, highly selective and creates a stable carbonyl group as a product of finding a C-H bond capable of being activated. The excited triplet state then inserts between a C-H bond, assuming correct geometry of attack. Excitation at 360 nm is favourable and the excited state can regenerate the ground state if no suitable bonds are available to react with.

Phenylazide
31

Phenylnitrene
32

Phenyldiazirine
33

Phenylcarbene
34

Benzophenone
35

Excited benzophenone
36
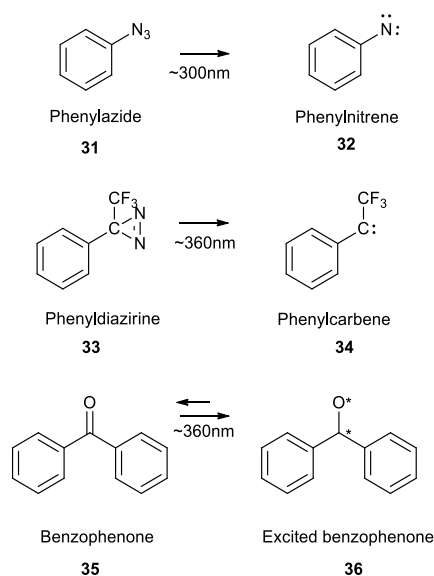
Figure 33. Three photoreactive labels and their excited intermediates.

In the current study, the photoaffinity labels were used in conjunction with a fluorophore and the reversibly binding K^+ channel activator diazoxide, the label covalently tagging the sub-unit target of diazoxide.

2.10 The Potential Use of Labelled Diazoxide Probe

Diazoxide and its analogues are generally accepted to reversibly act on ATP sensitive, inwardly rectifying potassium channels. This study was interested with the mechanism of ischaemic preconditioning associated with the drug, and therefore the binding locations found within mitochondria, or the sarcolemma. There is debate, as discussed previously, as to which potassium channels (or their sub-unit types) the diazoxide interacts with; mitochondrial K_{ATP} or sarcolemma K_{ATP}. Therefore, a way of permanently binding diazoxide to either of these channels, extracting the

related proteins and then determining where it has bound, would increase the body of useful information related to the IPC debate.

Due to drugs binding through temporary electronic and steric effects to proteins (with factors based on tertiary structure and size), an activated photoaffinity label was used to tag those proteins permanently through covalent cross-linking.

The plan for probing the potassium channel structure was to create and test diazoxide analogues for biological efficacy. Suitable analogues were then used to construct a probe featuring a photo affinity barb, and a fluorophore linked to the biologically effective analogues to facilitate identification of the targeted proteins.

2.11 Aims

1. Design and build new PSP probes, featuring bright, water soluble fluorophores.

2. Test the efficacy of the PSP probes and determine whether they are suitably designed as a tool in proteomic identification of PSP-binding proteins.

3. Probe cardiac myocytes for protein-PSP interactions using gel-electrophoresis and mass spectrometry.

4. Incubate novel diazoxide analogue **109**, with mitochondria and using gel-electrophoresis and mass spectrometry, identify protein targets that may provide information for mitoK$_{ATP}$ channel structure.

5. Build a fluorescently bright, selective diazoxide probe and test that with mitochondrial tissue samples.

3 Experimental Results

The exploration of protein targets found in cardiomyocytes begins with considering organophosphate (OP) toxicity with respect to the myocytes. With biological and analytical techniques, such as proliferation assays and mass spectrometry, a probe can be built and used to identify targeted proteins.

Based on the previously proposed mode of action in section 1.6, the covalent interactions OP's have with exposed residues, no photoaffinity component will be needed. Construction of this probe would also shed light on an effective construction for the diazoxide probe. The purported design shown in Figure **121** and comprised of diazoxide coupled via an alkyl linker to a photoreactive benzophenone, and a rhodamine group. This is similar to Smida design[67] but incorporating improved fluorescent component.

3.1 Synthesis of Rhodamine B with 6 Carbon Alkyl Linker

The starting point for the synthesis of an improved probe was the coupling of rhodamine B to the simplest alkyl linker 6-aminohexanol. A myriad of coupling agents were available, but initially DCC was explored as a standard reagent for this coupling.

3.1.1 DCC Coupling

N,N-dicyclohexylcarbodiimide can activate the carboxylic acid of rhodamine B. The N-terminus of the 6-aminohexanol can then attack the carbonyl centre, displacing dicyclohexylurea (DCU) which is insoluble in DCM (Scheme 1).
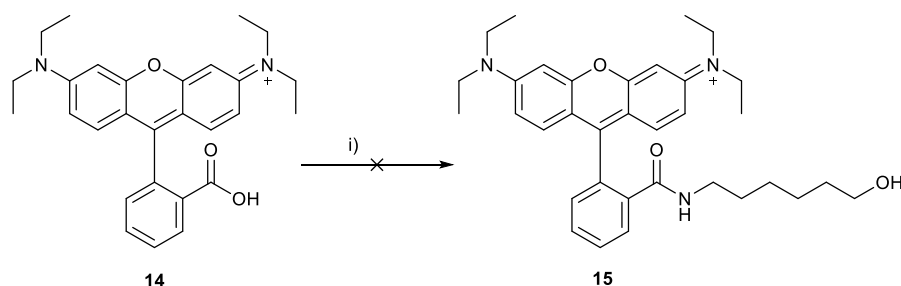
Scheme 1. Rhodamine B coupling, (i). DCC, TEA, DCM, 6-aminohexanol

Treatment of rhodamine B with DCC in dry DCM was followed by addition of 6-aminohexanol. After 12h the solution was filtered, and following aqueous work-up, the solvent was then removed and, analysis by ^{1}H NMR spectroscopy revealed an intractable mess of peaks, with no evidence of the coupled material in the mixture and TLC gave a pink smear.

3.1.2 Benzoic Acid Trial Coupling

This then led to a series of trial coupling reactions using benzoic acid and 6-aminohexanol and four different coupling reagents (Scheme 2). Firstly, investigations to see if the two would react with DCC in the presence of triethylamine. Dissolved in dry DCM and treated the same way as in the first attempted rhodamine B coupling, the ^{1}H NMR again returned a spectrum with no coupling product.

37   **38**
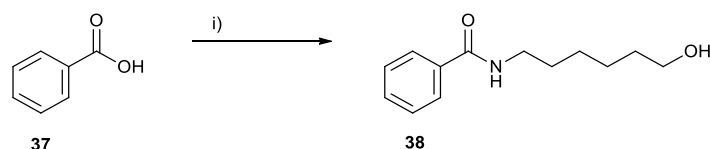
Scheme 2. Benzoic acid coupling trial reaction. (i). DCC, TEA, DCM, 0 $^{\circ}$C, 12 h. Or, (ii). TsCl, Pyr, DCM, 0 $^{\circ}$C, 8 h. Or, (iii). CDI, TEA, DCM, 0 $^{\circ}$C, 12 h. Or, (iv). T3P, TEA, DCM, 0 $^{\circ}$C, 12 h.

Tosyl chloride was then explored as an activating agent for the benzoic acid. This acid was mixed with pyridine in dry DCM at 0 $^{\circ}$C then had 6-aminohexan-1-ol added before being allowed to warm to room temperature over three hours. Analysis of ^{1}H NMR gave no evidence of the desired amide product.

The two water soluble reagents: 1,1-carbonyldiimidazole (CDI) and tripropylphosphinic anhydride (T3P)were then examined.[130] These reagents underwent a variety of trial reactions with variation of base and reagent equivalents to determine if the water-soluble coupling reagents were effective.

The by-products of using CDI are carbon dioxide and imidazole, both are easily removed from the reaction mixture by aqueous work-up. T3P activates the carboxylic acid oxygen turning it into a good leaving group. The amino alcohol can then attack displacing 1,5-dioxido-1,3,5-trioxo-1,3,5-tripropyltriphosphoxane, a by-product that gets easily removed by aqueous work-up.

Experiment series				1	2
Linker mg	Acid mg	DMAP %	TEA equivalents	T3P equivalents	CDI equivalents
10	10	1	0	2	2
10	10	0	1	2	2
10	10	1	1	2	2
10	10	1	2	2	2
10	10	0	2	1	1

Table 1. Table of reagents for trial coupling reactions.

The optimum of these reactions proved to be two equivalents of TEA with two equivalents of T3P. ^{1}H NMR analysis of the crude reaction mixture showed that coupling with T3P cleanly gave the product. This then was chosen to be the coupling reagent of choice with rhodamine B and the linker.

3.1.3 Water-Based Reagent Coupling

Rhodamine B was dissolved in a solution of dry DCM and a T3P solution (50% in DMF) was added along with two equivalents of TEA and a catalytic amount DMAP at 0 ^{O}C. This mixture was stirred for ten minutes before addition of 6-aminohexanol in DCM. The mixture was allowed to warm to room temperature over 48 hours. After washing with water twice, the organic phase was evaporated to a residue then analysed by ^{1}H NMR spectroscopy, which showed that only starting material had been returned.

3.1.4 Succinimide Intermediary Compound

Coupling reactions with rhodamine B then proceeded by the attempted to synthesis of a hydroxysuccinimide active ester intermediate compound. The reaction method followed a standard procedure where DCC, rhodamine B and TEA were all dissolved in dry DCM, and DMAP was then added and followed by a solution of N-hydroxysuccinimide. Analysis of ^{1}H NMR after work-up with DCM and brine showed the presence of only starting material.

3.1.5 Rhodamine Acid Chloride Synthesis

The preparation of rhodamine B acyl chloride has been reported.[131] Following this literature

procedure, rhodamine B in dichloroethane (DCE) was treated with phosphorous oxychloride ($POCl_3$)

and the mixture refluxed for 2h (Scheme 3).
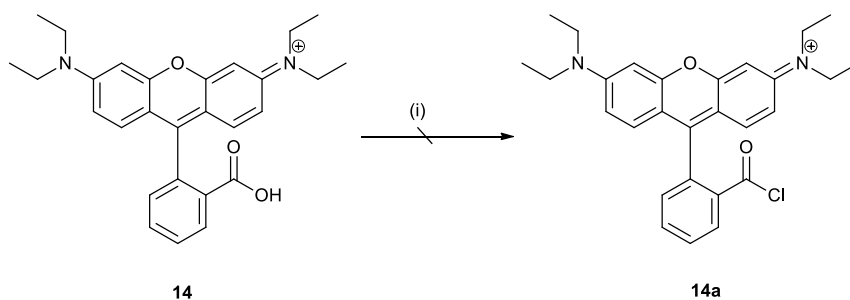
Scheme 3. Attempted rhodamine B acyl chloride synthesis. (i), $POCl_3$, DCE, reflux, 10h.

Monitoring the reaction by TLC did not suggest that any formation of the product occurred, even

after eight further hours. The ^1H NMR spectrum showed only starting material so it was concluded

that any product that formed during the reaction either isn't stable and the chloride is instantly

substituted, or that product is unable to be formed due to formation of a closed form lactone

rhodamine.

3.1.6 Benzotriazole Coupling

Having explored simple activation methods without success, a further exploration of benzotriazole

coupling reagents was made. Many of these reagents are expensive but have been shown to be

effective in difficult coupling reactions.[132]

O-(Benzotriazol-1-yl) N,N,N',N'-tetramethyluronium hexafluorophosphate (HBTU), is a popular

coupling reagent in solid phase peptide synthesis and it was explored in coupling rhodamine B to 6-

aminohexanol.[133]
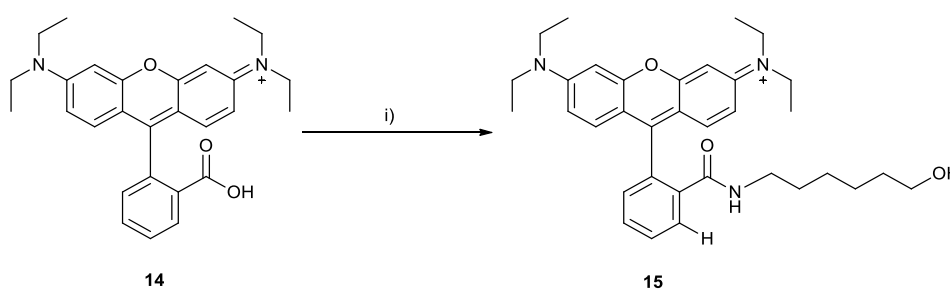
Scheme 4. Rhodamine B coupling, (i). HBTU, TEA, 6-aminohexanol dry DCM, 0 °C, 24h.

Rhodamine B was treated with 2 equivalents of TEA, 2 equivalents of HBTU and 1.1 equivalents of 6-

aminohexanol in dry DCM at 0 °C for 24 h. Aqueous work-up and partitioning with DCM, gave a 3:1

mixture of starting material and product. Chromatography proved difficult (Section 3.1.8), however

amide **15** was afforded in 26% yield (Scheme 4), and the identity confirmed by [1]H. A shift in the [1]H

NMR spectrum of the 3 position H, *ortho* to the newly formed amide bond, from 8.3 ppm to 7.9 ppm

was found to be indicative that the coupling had occurred. A shift in the triplet (2.6 ppm up to 3.1

ppm) of the CH_2 next to the NH also indicates that a new moiety had been formed. The presence of

the peaks associated with 6-aminohexanol suggested a reaction between the two had occurred as

the amine-alcohol was normally lost during work-up due to its solubility in water.

3.1.7 Protected Rhodamine Linker

Problems encountered during purification caused by the polarity of the rho-linker product were addressed by examining the synthesis of a silyl protected amino alcohol coupled to rhodamine. It was anticipated that it would reduce the polarity of the product.

Tert-butyldiphenyl silyl **39** (TBDPS) and *tert*-butyldimethyl silyl **40** (TBDPS) ethers were prepared from 6-aminohexanol and a corresponding silyl chloride, the protected alcohols were afforded in a low but un-optimised yield of 9.8% and 12.7% respectively (Scheme 5).
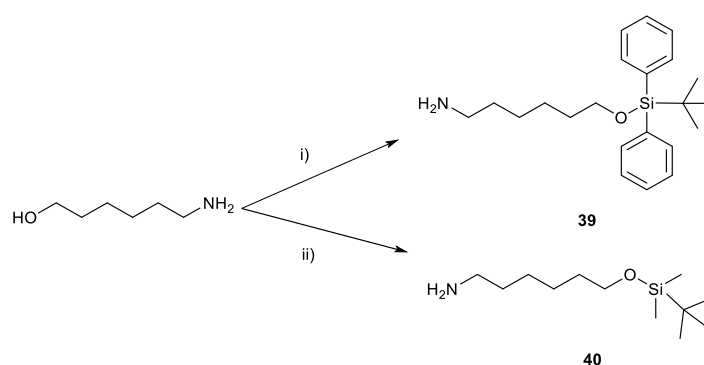
Scheme 5. Synthesis of protected 6-aminohexanol. (i). TEA, DMF, TBDPSiCl, 72 h, r.t. (ii). TEA, DMF, TBDMSiCl, 72 h, r.t.

Subsequent coupling of the TBDPS ether **39** was investigated with rhodamine B using HBTU in TEA and dry DCM at 0°C. ^{1}H NMR of the crude product mixture after work-up gave a difficult to interpret mess of peaks. Column chromatography afforded two main fractions the first contained only the silyl protected linker and the second only rhodamine B starting material. Coupling of TBDMS ether **40** did, however, yield protected rho-linker product **41** (13%) under similar conditions. This compound was purified by column using chromatography using DCM and 2% TEA on silica, the second pale yellow fraction was found to contain the product (Scheme 6).

14   **41**
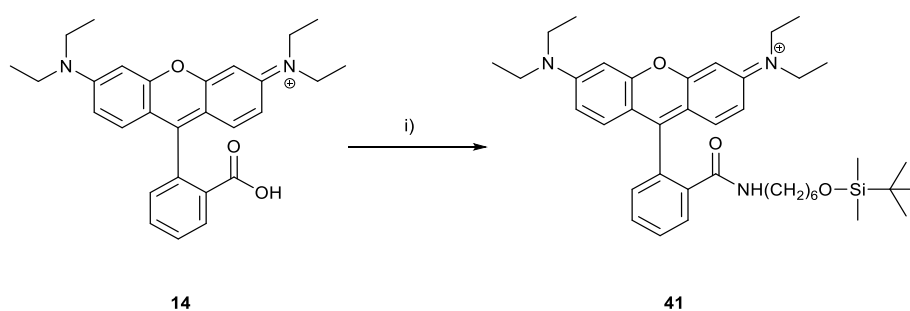
Scheme 6. Rhodamine B coupled to a protected silyl ether linker. (i). **52**, HBTU, TEA, dry DCM, 0 °C, 24 h.

The low yield of **41**, accompanied by a large amount of starting material rhodamine and protected linker led the investigation to optimise purification conditions for the synthesis of the higher yielding rhodamine linker **15.**

3.1.8 Purification of Rhodamine B Species

Rhodamine can exist as two tautomers,[134] and is in equilibrium between a closed lactone and a zwitterionic open form. When protonated, the molecule prefers an open cationic form (Scheme 7). One of the major differences between the forms is deactivation of the closed form by internal conversion.[135] This deactivation reduces the fluorescent properties of rhodamine, leaving it colourless and weakly fluorescent. [136] The cationic and zwitterionic forms exhibit minimal differences when comparing extinction coefficient (ε) and quantum yield (ϕ) with only a slight reduction in these properties for the zwitterion. There is however a hypsochromic shift and change in the fluorescence

and absorption maxima due to the inductive effect on the central carbon of the xanthene.

Fluorescent properties for rhodamine B is displayed below, (Scheme 7).

Cationic Form	Zwitterionic Form	Lactone Form
λ ex/ em (EtOH) = 553/ 572	λ ex/ em (EtOH) = 543/ 563	λ ex/ em (Et$_2$O) = 553/ 572
ε = 1.17	ε = 1.11	ε = 0.16
τ = 2.41	τ = 2.88	τ = 5.80
ϕ =0.53	ϕ =0.70	ϕ =0.02
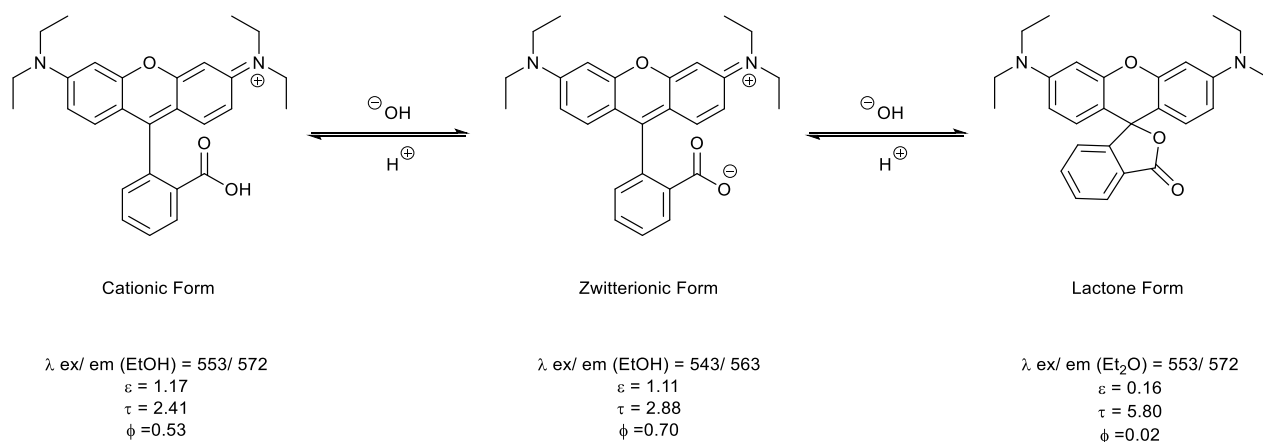
Scheme 7. Interconversion of rhodamine B forms.[137,138]

Controlling tautomeric equilibrium of rhodamine dyes can be used in applications including ion

sensors, (Section 1.3) such as with the peroxide probe. In addition to the pH dependence, the

tautomeric equilibrium can be shifted by changing temperature or with application of UV light

(Scheme 8). Increasing the temperature causes the molecule to close, giving the non-fluorescent

state which can also be colourless depending on the particular rhodamine. Exposure to UV light will

open the rhodamine into the cationic form, and the colour and fluorescent properties will return.[139]

These temperature dependent form changes can also occur for substituted amides resulting in a

lactam.[133]
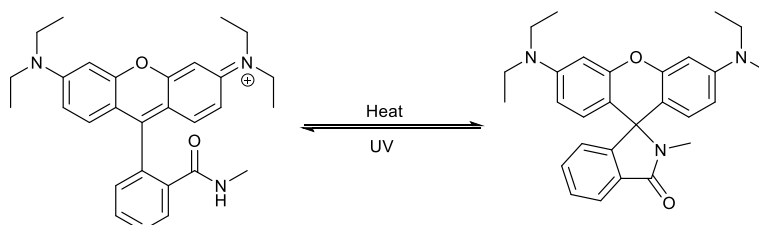
Scheme 8. Spirolactam /zwitterion equilibrium.

The major difficulty in the purification of rhodamine linkers such as **15**, was that the products and starting material move poorly on silica and overlap, smearing. This made purification of often incomplete reactions very difficult.

Many efforts were made to refine the process including a wide variety of solvent mixes, and use of reverse phase silica. All attempts led to poor separation and low purified yield. However, by exploiting the property of lactone ring closure under basic conditions, it was found that 2% TEA in 2:1 acetone and toluene caused the closed form of the product to elute more quickly and without extensive trailing, due to a decrease in polarity (Figure 34). Warming the compound in the solvent mix gently until very pale prior to loading on the column, and using warm glassware and solvent throughout also aided the purification as well.
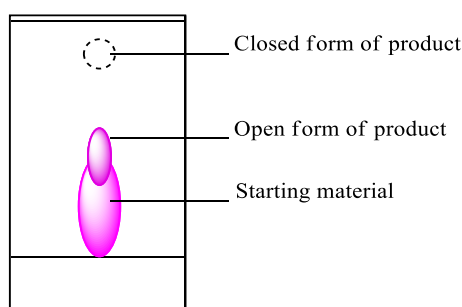
Figure 34. Illustration of TLC plate monitoring purification of rhodamine linker rho-alkyl **15**.

3.1.9 Synthesis of Amide Glycol Rhodamines

In order to examine how linker properties might change overall probe efficacy the synthesis of three other RhoB-linker systems was carried out using the HBTU coupling protocol. Treatment of Rhodamine B with triglycine, 2-(2-aminoethoxy) ethanol, or 2-(2-[2-aminoethoxy]ethoxy) ethanol (Figure 13), under similar conditions to the 6-aminohexanol coupling, gave derivatives **16** and **17** respectively. After work-up, chromatography via the improved method described above, yielded the shorter glycol rho-PEG short **16** in 35% yield and the longer glycol rho-PEG long **17** in 67% yield (Scheme 9).
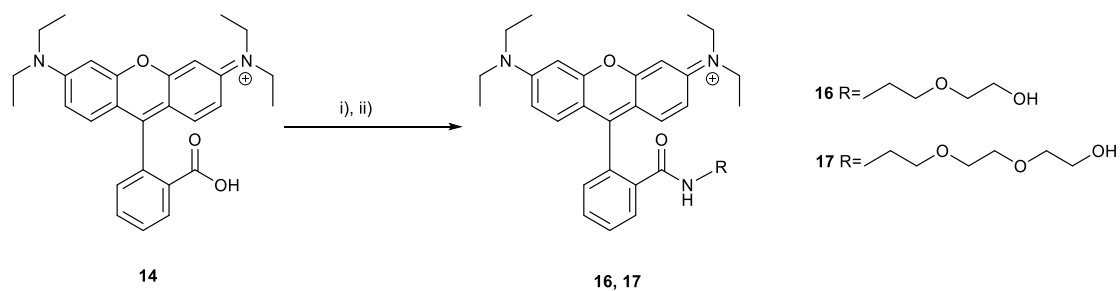
Scheme 9. Synthesis of rhodamine B glycol with (i). HBTU, TEA, dry DCM, 0 °C, 24 h, 2-(2-aminoethoxy)ethanol and (ii). BTU, TEA, dry DCM, 0 °C, 24 h, 2-(2-[2-aminoethoxy]ethoxy)ethanol.

The reaction of triglycine hydrochloride with rhodamine B was also investigated (Scheme 10).

However similar reaction conditions could not couple triglycine with rhodamine B via HBTU. Analysis of the crude compound by ^{1}H NMR after washing with water and brine returned only a mixture of starting materials, with no shifts in the 3 position H peak of the rhodamine, nor a shift in the CH_2 of the triglycine amine. Analysis of the TLC plate showed only the presence of starting material spots, and was considered as further evidence to the product not being formed.
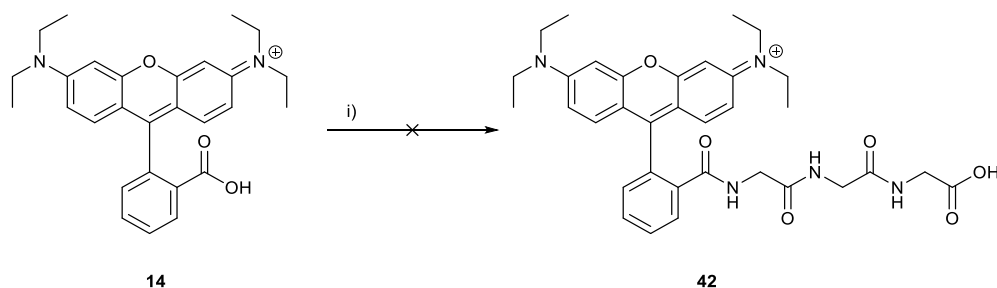
Scheme 10. Reaction of rhodamine B with triglycine, (i). HBTU, TEA, triglycine hydrochloride, dry DCM, 0 °C, 24h.

3.2 Synthesis of Saligenin Phosphate Probe

3.2.1 Synthesis of Organophosphates

With rhodamine B coupling to linker in progress, the synthesis of PSP was investigated (Scheme 11). PSP had previously been prepared from 2-hydroxybenzyl alcohol and phenyl phosphodichloridate in a one pot reaction. This was repeated and achieved in a moderate to good yield (70%).[140]
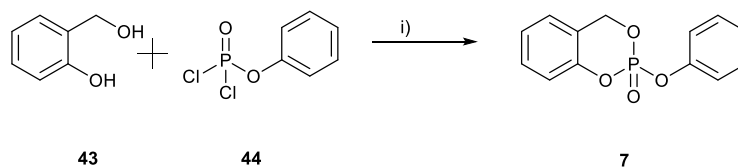
Scheme 11. Synthesis of PSP i) THF, Et$_3$N, 0 ^{o}C – RT, 4h

The structure of the organophosphate probes all featured a saligenin phosphate centre, analogous to SCOTP.[38] The synthesis of the intermediate structure can be achieved in one step from commercially available compounds (Scheme 12).

Treatment of hydroxybenzyl alcohol with POCl$_3$ and triethylamine gave saligenin chlorophosphate **45** in 95% yield after filtration from precipitated triethylamine hydrochloride. The ^{31}P NMR displayed a single peak at -5.38 ppm, which was anticipated. This compound was unstable in the air and could not be stored without decomposition. Further steps that incorporate this reagent relied on freshly prepared product.
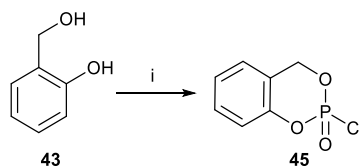
Scheme 12. i) saligenin, POCl$_3$, TEA, dry DCM, -78 ^{o}C, 1h.

3.2.2 Synthesis of Dansyl Probe

Future experimentation required a stock of the previously synthesised dansyl probe **10**. The synthetic route designed by Smida *et al* was investigated to this end.[67]

Synthesis commenced by addition of dansyl chloride to 6-aminohexanol (Scheme 13). These were added to dry DCM at 0 °C, and stirred at room temperature for 4 h. The reaction went to completion to yield compound **46** cleanly in 92% yield.

This dansyl-linker **46** was then dissolved in dry DCM and cooled to -78 °C. A solution of saligenin chlorophosphate **45** was added dropwise. The mixture was allowed to warm to room temperature for 24 hours before work-up with toluene and column chromatography to give the dansyl probe (DSP), **10** in 22% yield as an orange oil (Scheme 13).
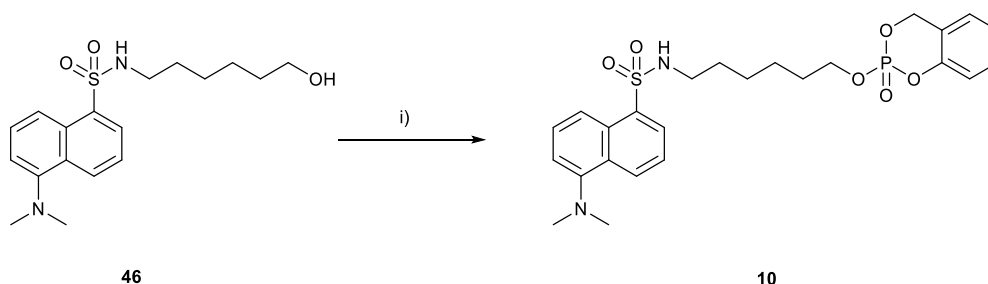
Scheme 13. Synthesis of DSP-**10**, (i). TEA, **45**, dry DCM, -78 °C, 24 h.

3.2.3 Rhodamine Probe Synthesis

With the synthesis of DSP-**10** completed, PSP probe **18** was prepared by the same two-step process in which a reactive chlorophosphate was isolated, then further reacted with an alcohol (Scheme 14).

Freshly prepared saligenin chlorophosphate **45** was then reacted with rhodamine amidohexanol **15**. The dropwise addition of saligenin chlorophosphate **45** in dry DCM to a solution of **15**, and triethylamine at 0 °C, was left to stir for 24 hours. Upon completion of the reaction, work-up proceeded with washes with water and brine, and extraction with DCM. The ^{1}H NMR spectrum of the crude mixture showed peaks that did not belong to either of the starting materials, and a ^{31}P NMR spectrum, with a single peak at − 9.06 ppm highlighting that the reaction had formed a fully

oxidised phosphate. The compound was purified by column chromatography according to the previously optimised technique of warming the crude residue in a solution of 2% TEA and 2:1 mixture of acetone in toluene until pale. Purification was achieved by column chromatography eluting with the same solvent system, collecting the first colourless fraction to give rho-alkyl PSP **18** in 34% yield. CH_2OP and POCH_2R hydrogen peaks showed the expected ABX pattern for the diastereotopic hydrogens, due to three bonds coupling to the phosphorous stereogenic centre and the P=O bond giving rise to a tetrahedral structure (Figure 35).
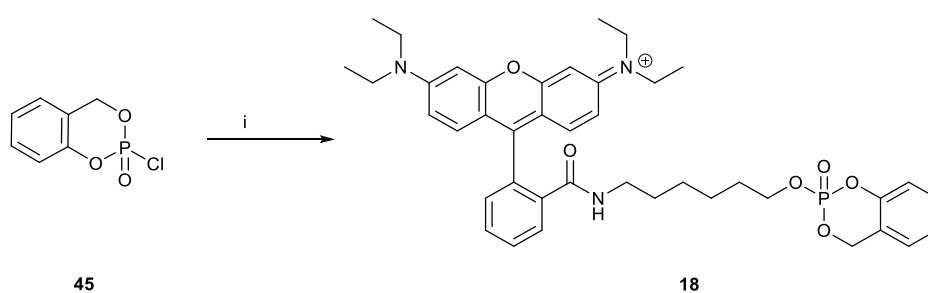
Scheme 14. Synthesis of rho-alkyl SP **18**, (i). TEA, **45**, dry DCM, -78 ^{o}C, 24 h.
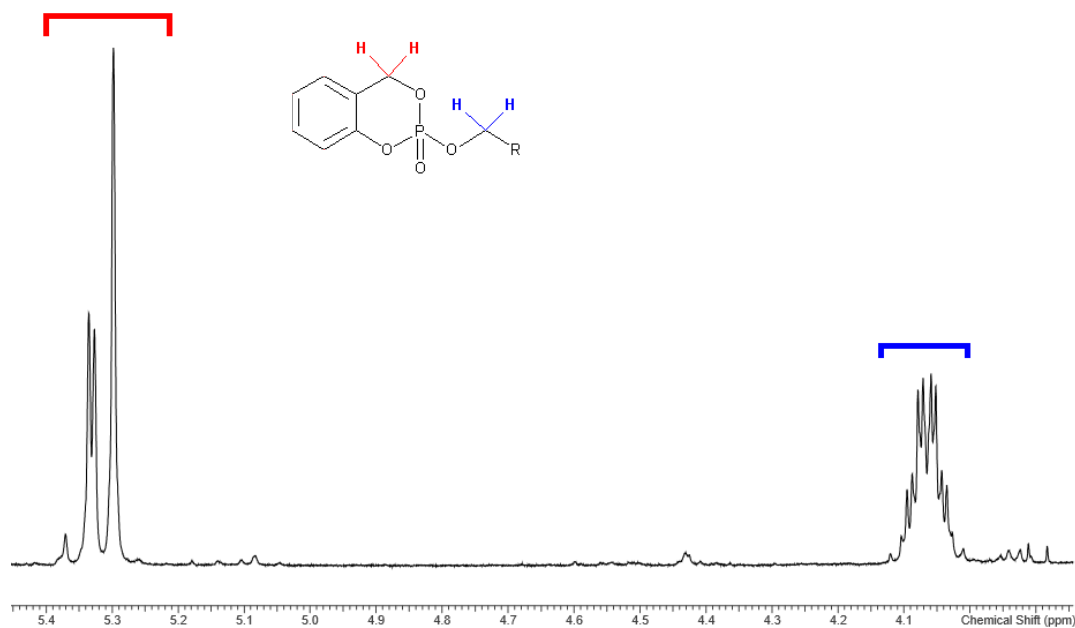
Figure 35. Zoomed in spectrum of rho-alkyl SP **18**, highlighting the multiplet caused by the CH_2 of the alkyl chain in blue; and the CH_2 of the saligenin ABX splitting pattern in red.

3.2.4 Conversion of Hydroxyphosphate

The unpurified material from the formation of **45** decomposes rapidly into saligenin

hydroxyphosphate **47**, and it was therefore carried onto the next reaction directly. Indeed, the

crystalline hydroxyphosphate **47** could be isolated cleanly, and the conversion of this material to the

chloride when needed for further synthesis was investigated (Scheme 15). Treatment of phosphate

47 with oxalyl chloride and 10% DMF did not proceed cleanly enough to give the chlorinated product

without needing further purification. In the interest of efficiency, the preparation of fresh saligenin

chlorophosphate was more viable. [141]
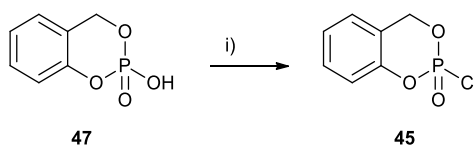
Scheme 15. Conversion of the saligenin hydrogen phosphate to the chloride, (i). Oxalyl chloride, 10% DMF, DCM, r.t., 3h

3.2.5 Synthesis of Rhodamine Glycol Probes

The successful synthetic approach was then applied to the preparation of a PSP probe featuring rhodamine glycol linkers **16** and **17**, coupled to saligenin phosphate. This would achieve three probes each with varying properties.

Freshly prepared saligenin chlorophosphate solution was added dropwise to a solution of rhodamine linker and triethylamine at 0 °C. After 24 hours the mixtures were worked-up with DCM and brine. Both were purified by column chromatography following the optimised route mentioned previously. This afforded rho-PEG short SP **48** and rho-PEG long SP **49** in 30% and 28% yield, respectively (Scheme 16).
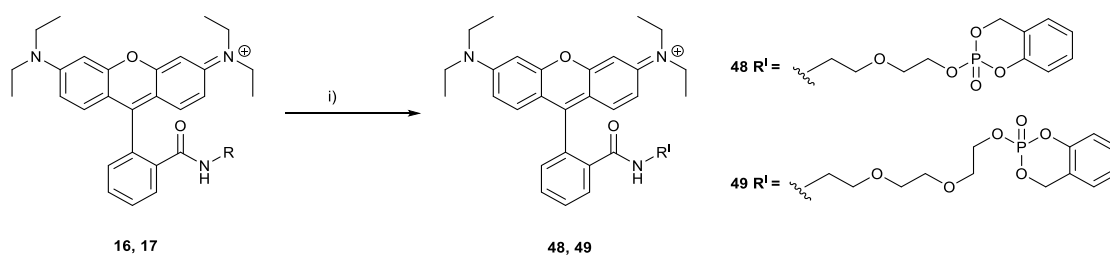
Scheme 16. Synthesis of rho-PEG short SP **48**, and rho-PEG long SP **49**, (i). TEA, **45**, dry DCM, -78 °C, 24 h.

With these three fluorescent PSP probes synthesised, the fluorescent characterisation of excitation and emission wavelength were measured. The tests were performed under conditions chosen to mimic the biological environment. Initial measurements were made in water at a concentration of 100 μM to ensure they could be used.

A comparison was also made with the dansyl probe DSP-**10** at an excitation of 324 nm.

3.2.6 Fluorimetry of Probes

The FLA5000 laser scanner from Fujifilm, has a green light laser measuring in the region of 532 nm. When the SDS-PAGE gels containing cell lysates, treated with the probe were visualised, this was the laser employed. This excitation wavelength should be selective for the rhodamine fluorophore, whereas auto fluorescence (ca. 270 – 400 nm), from the cell lysates was avoided.

The results of this experiment shows that the peak absorbance and therefore the optimum frequency to excite the probes is 560 – 578 nm. Interestingly the probe rho-alkyl SP **18** and the probe rho-PEG long SP **49,** absorb a much greater amount of light between 480 and 578 nm than the probe rho-PEG short SP **48**.
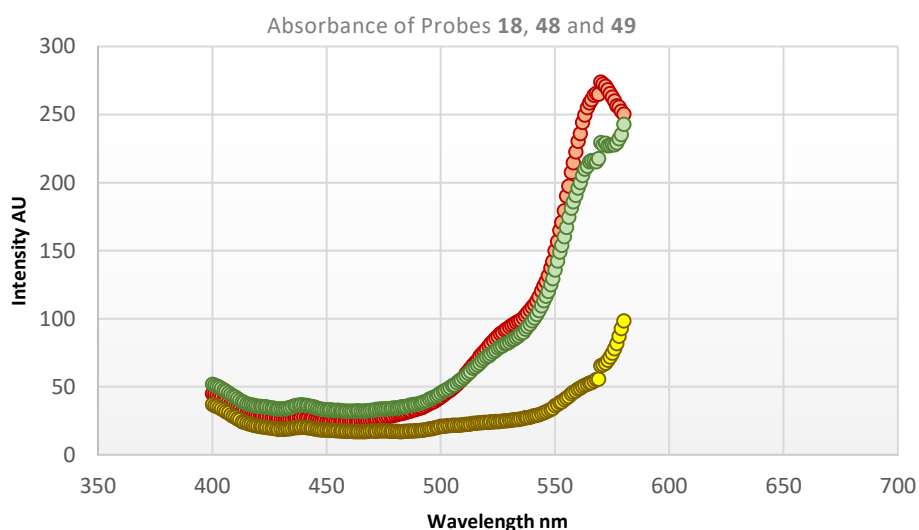
Figure 36. Absorption of the rhodamine B PSP probes. Red is rho-alkyl SP **18**, Green is rho-PEG long SP **49**, Yellow is rho-PEG short SP **48**. Fluorescence measurements were made using a 1 cm^3 fluorimetry cuvette; with a 100 µM solution of each probe dissolved in distilled water, pH of 7.5, the solutions were excited from 400 nm up to 580 nm by the fluorimeter. The emission strength in arbitrary units (AU) was recorded at 600 nm (n=3).

The results shown in Figure 36 reveal that rho-alkyl SP **18** absorbs the greatest amount of light around 575 nm, with the slope falling off towards 700 nm. This means that under green light of 532 nm, the probe will steadily fluoresce from the yellow to red region of the spectrum appearing orange. Rho-PEG short SP **48**, absorbs less light and was expected to fluoresce significantly less than the other two linkers. This difference in absorption may be due to some radiationless exchange of

energy between the rhodamine B and the organophosphate. This exchange of energy and drop in

fluorescence could be occurring in all three probes. However, the effect may be more pronounced in

the shortest of the linkers due to the closer proximity of the organophosphate and rhodamine B.

Exciting the probes at 532 nm and measuring the fluorescence emission indicates how bright the

probes will be under green light on the gels. This will also give some indication of the detection limits

that may be expected from the probe (Figure 37).
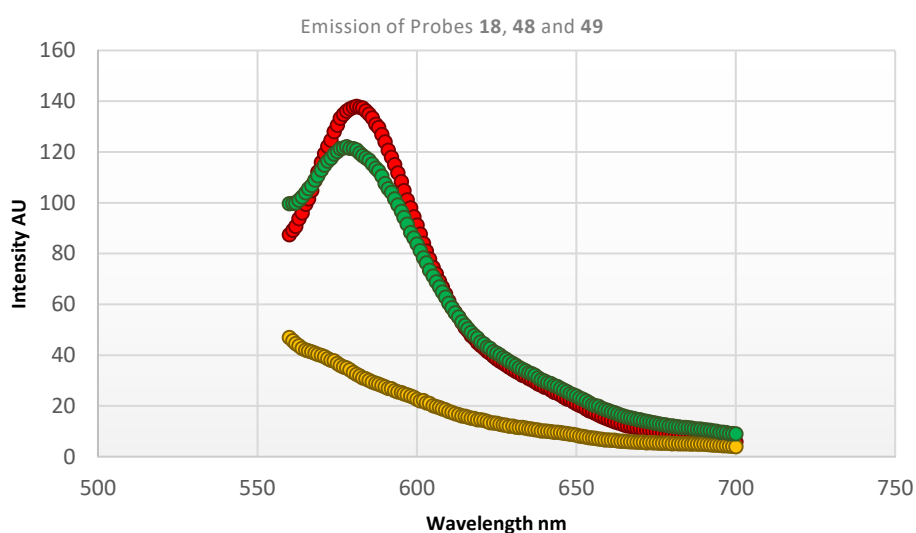
Figure 37. Emission spectrum of the rhodamine probes. Red is rho-alkyl SP **18**, Green is rho-PEG long SP **49**, Yellow is rho-PEG short SP **48.** Fluorescence measurements were made using a 1 cm^3 fluorimetry cuvette; with a 100 μM solution of each probe dissolved in distilled water, pH of 7.5, the solutions were excited at 532 nm and the emission strength recorded in AU over a wavelength of 560 to 700 nm (n=3).

Comparison of the three probes **18**, **48** and **49**, with the fluorescent behaviour of compounds **15**, **16**

and **17** the rhodamine-linker precursors, shows the effect that adding the saligenin phosphate

moiety has on the level of fluorescence (Figures 38, 39 and 40). With rho-alkyl SP **18** and its

precursor rho-alkyl **15**, we can see that the saligenin phosphate increases the amount of energy

absorbed, but emitted energy, once excited at 532 nm, remains about the same.
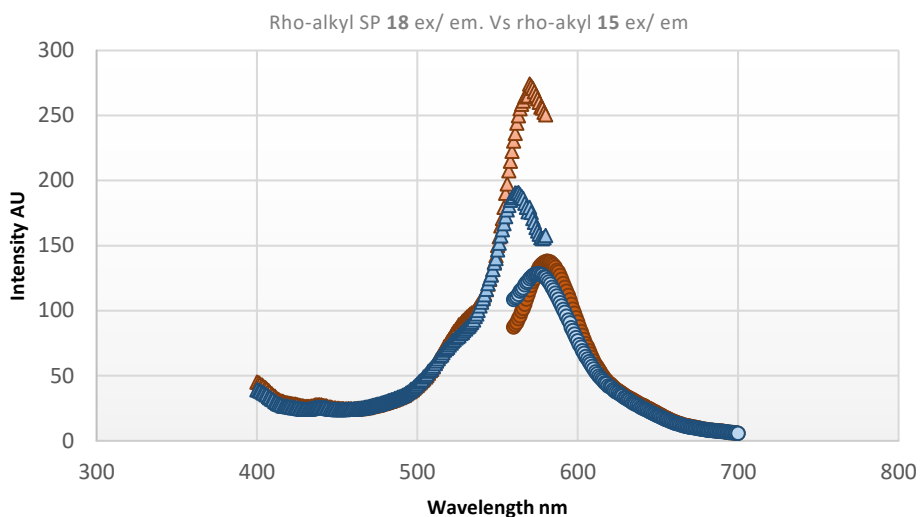
Figure 38. Emission (circles) and excitation (triangles) spectrum for rho-alkyl SP **18** in red, and precursor rho-alkyl **15** shown in blue. Fluorescence measurements were made using a 1 cm³ fluorimetry cuvette; with a 100 µM solution of each probe dissolved in distilled water, pH of 7.5 (n=3).

Probe rho-PEG short SP **48** was seven times less fluorescent with the addition of the organophosphate compared to its precursor rho-PEG short **16** (Figure 39). It is clear that with addition of saligenin phosphate the brightness of the rhodamine B is reduced. This same effect was not observed with rho-alkyl SP **18**. This influence is likely caused by the distance from the organophosphate to the rhodamine. The average bond lengths have been calculated from crystallography data, [142] and the data gives average lengths of 6-aminohexanol as 12.1 Å, 2-(2-aminoethoxy) ethanol as 8.8 Å and the longer glycol as 13.2 Å. This data confirms that rho-PEG short SP **48**, is the shortest probe compared to the other two.

Rho-PEG short SP **48** ex/ em. Vs rho-PEG short **16**
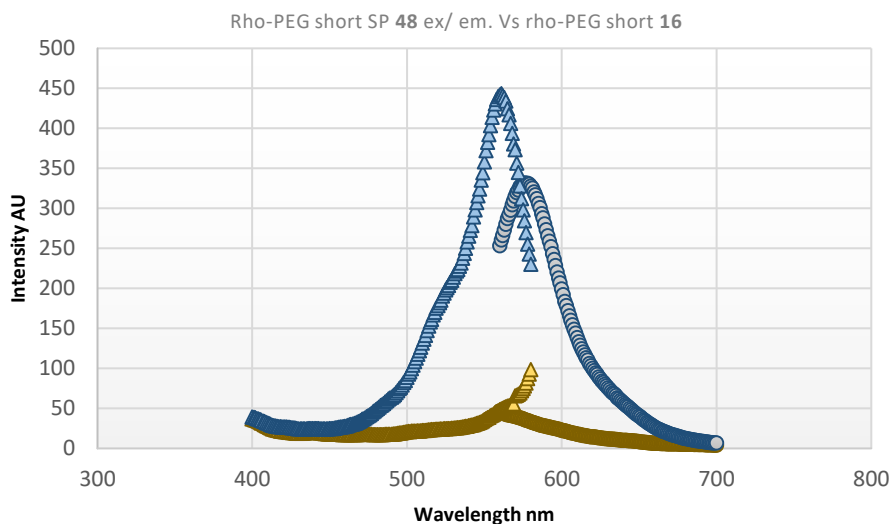
Figure 39. Emission (circles) and excitation (triangles) spectrum for rho-PEG short SP **48** in yellow, and precursor rho-PEG short **16** in blue. Fluorescence measurements were made using a 1 cm^3 fluorimetry cuvette; with a 100 µM solution of each probe dissolved in distilled water, pH of 7.5 (n=3).

It was expected then, that the difference in fluorescence between the long chain PEG linker (rho-PEG long **17**), and the subsequent probe (rho-PEG long SP **49**), would be less. It can be seen from the graph (Figure 40) that there was less of a drop in fluorescence. This is interesting when compared to the first probe and its linker, where there was no drop in emitted light, but there was still less than half the original emitted output at 532 nm.

Rho-PEG long SP **49** ex/ em. Vs rho-PEG long **17**
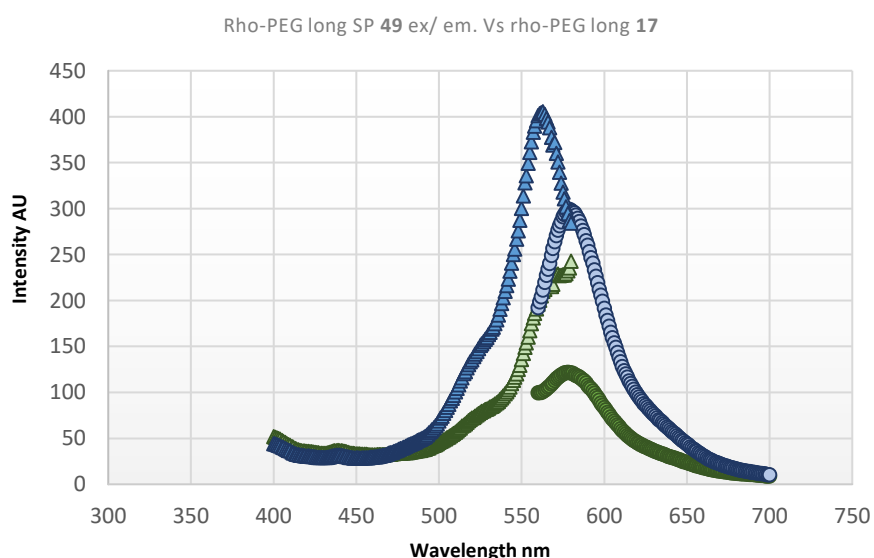
Figure 40. Emission (circles) and excitation (triangles) spectrum for rho-PEG long SP **49** in green, and precursor rho-PEG short **17** in blue. Fluorescence measurements were made using a 1 cm^3 fluorimetry cuvette; with a 100 µM solution of each probe dissolved in distilled water, pH of 7.5 (n=3).

There could be several reasons for the difference in intensity of fluorescence between the final probes, rhodamine B and the intermediate compounds. The initial difference between the three linkers is likely to do with solvent effects in interaction with the alkyl and the glycol chains. The glycol chains are miscible in water and the alkyl chain has a predicted solubility of ca. 2.65 mol/L.[143] It was apparent from the graphs that PEG linkers rho-PEG short **16** and rho-PEG long **17** are at least twice as bright as the alkyl chain rho-alkyl **15**. The effect of solubility may not be very prominent as there was only a small difference in fluorescence between the alkyl and PEG probes rho-alkyl SP **18** and rho-PEG long SP **49**, highlighting that addition of organophosphate was causing a more noticeable effect. In terms of overall efficiency it is also worth noting that the two glycol probes are likely to be more bioavailable in cell tissue cultures due to the higher solubility.

3.2.7 Investigation into Fluorescence Drop

Due to the drop in emitted light between the glycol probes and their fluorophore linker precursors, the addition of saligenin phosphate must cause a change in the fluorescent properties of the probe. The absorbance of PSP **7** was next measured by UV-vis. The measurement was made to address the possibility that the PSP absorbs any of the radiation at 532 nm, or if there was an occurrence of Förster resonant energy transfer (FRET) where the absorbed energy of the rhodamine B is nonradiatively transferred to the PSP via some type of dipole-dipole overlap.[144] Secondly, there could also be a quenching problem in which PSP can fluoresce out of phase with the rhodamine, but with the same wavelength, diminishing the strength of the fluorescence emitted by rhodamine B.

FRET is characterised by a fluorescence behaviour where an excited donor fluorophore transfers its energy to a non-excited acceptor fluorophore.[145] One example of this occurring intramolecularly with a rhodamine B fluorophore, is with a Cu^{2+} probe designed by Guan *et al*, (Figure 41).[146] This probe has an inactivated closed-rhodamine system, connected to coumarin.[147] Coumarin absorbs at 410 nm, and without the presence of copper ions, blue light is emitted at 480 nm. When Cu^{2+} is detected the rhodamine opens up, and the absorbed energy by the coumarin is transferred to the

rhodamine, then emitting that energy at 580 nm. The amount of light emitted by the two fluorophores is directly proportional to the concentration of Cu^{2+} and, as this can be measured at two wavelengths, 480 nm and 510 nm making this a very sensitive probe. Defined as a ratiometric probe, this technique can withstand environmental pressures that can so often interfere with probe sensitivity.[148]
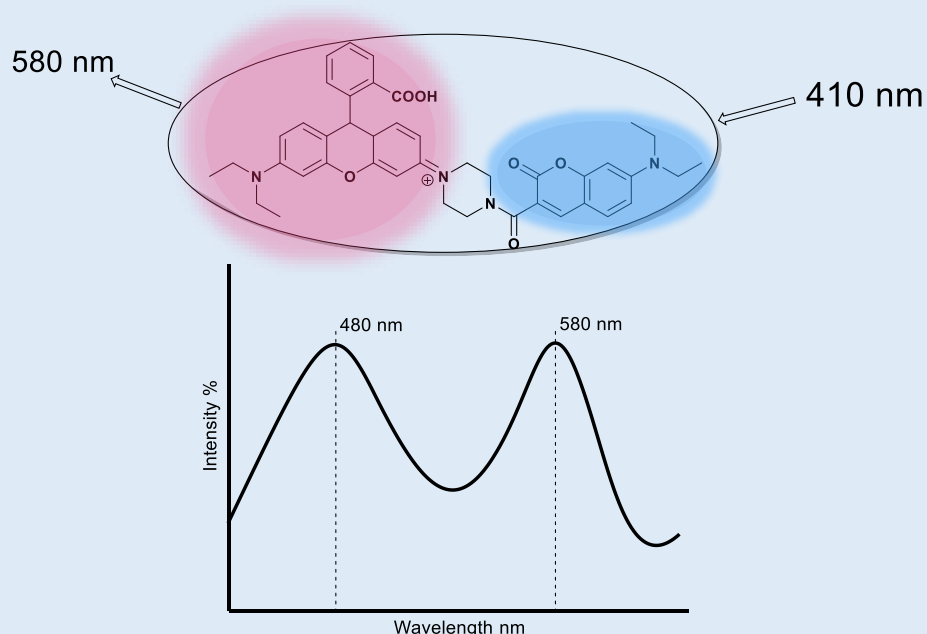
Figure 41. Förster resonance energy transfer, of two fluorophores shown as a conjugate spectrum of rhodamine B and coumarin. Excitation at 410 nm causes coumarin to fluoresce at 480 nm. In the presence of Cu^{2+} which this probe is sensitive for, the energy transfers to rhodamine B causing it to fluoresce at 580 nm.

The first question of whether intermolecular FRET occurs in the current study of rho-PSP probes could be answered easily by a graphical comparison at different concentrations of the probes in water. The shape of the graph would change to illustrate a loss in intensity of light at shorter wavelengths, and an increase in intensity at longer wavelengths as concentration increases. This corresponds to more energy being transferred from rhodamine B to saligenin phosphate of another molecule without loss, as the proximity of the dipole-dipole of the molecules increases at growing concentrations. This energy should have then been emitted by the organophosphate. If any resonant energy transfer is occurring, then it was predicted that the peak at 570 nm will lower, and an increase in intensity further towards the red shifted region will appear, indicating FRET.

The results from increasing and decreasing the concentration of probe dissolved in water provided no evidence of FRET occurring. Further evidence to this fact was that there was no change in shape of emission seen in the graphs between the precursor rho-linker emission at 532 nm and the completed probe. This was true for all three pairs of linker and probe, so it is unlikely to be a nonradiative transfer of energy as seen in FRET.

The second investigation was a simple UV-vis experiment. A reading of PSP was performed to see which wavelengths the compound absorbs, this would confirm whether the organophosphate is absorbing any of the excitation radiation from the sauce or emission radiation from fluorophore. This should have further clarified whether intramolecular FRET was possible or not.

A 10 µM solution of PSP dissolved in water was added into a cuvette and the methodology set out in 5.2.6 was followed. The results of this test show that there was considerable interference in absorbance at 200 nm up to 300 nm, and then clear absorbance up to 350 nm followed by a sharp decline after this point (Figure 42). There was very little absorbance then across the visible spectrum and into the beginning of the infrared spectrum. It is unlikely that the very low levels of absorbance between 400 and 600 nm offer much in the way of reducing the effectiveness of rhodamine B as a fluorophore.

This result led onto testing whether the pH has a any effect on the brightness of these probes.
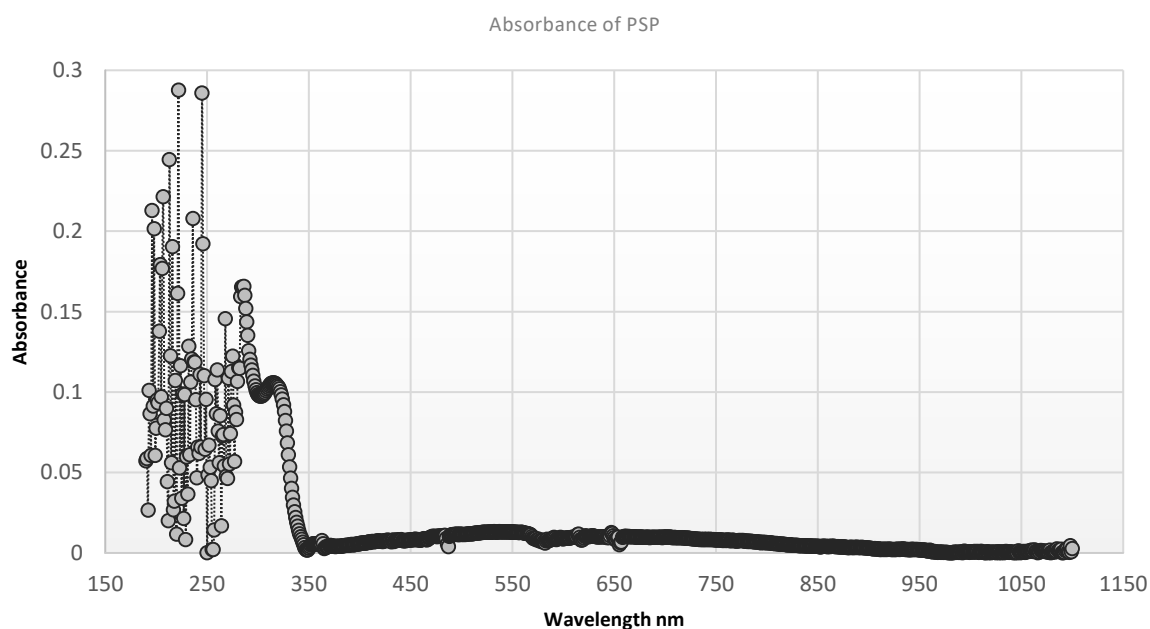
Figure 42. UV absorption of PSP in water, at room temperature. Measurements were made using a 1 cm^3 UV-VIS cuvette; with a 10 µM solution of PSP dissolved in distilled water, pH of 7.5 (n=3).

Rhodamine B is sensitive to pH, and it can aggregate into dimers and trimers depending on temperature, solvent environment, and other factors that can affect π-π interactions.[149] This aggregation can cause spectroscopic changes to photostability and efficiency, including fluorescence quenching, if the solvent is suitably hydrophobic and aggregation is high.

An experiment was performed comparing the fluorescence emissions of each probe at four different pH. Assuming water is at pH 7.5 it was expected that the fluorescence would increase in acidic

conditions and decrease in alkaline, corresponding to the open and closed forms of the fluorophore (Scheme 7).

Solutions were made up in centrifuge tubes, each containing 100 µM of each probe and then the pH was adjusted to the desired range with either 1M HCl or 1M NaOH. The various pH values were measured with a pH meter and the replicant solutions were found to be uniform at each pH. They were then added to a cuvette and excited at 532 nm in the fluorimeter according to the standard technique (Figures 43 -45).

The results confirmed the hypothesis; the more acidic environment the more light was emitted (Figure 43), whilst increasing alkalinity encourages closing of the rhodamine reducing the output.

Effect of pH on rho-alkyl SP **18** emission
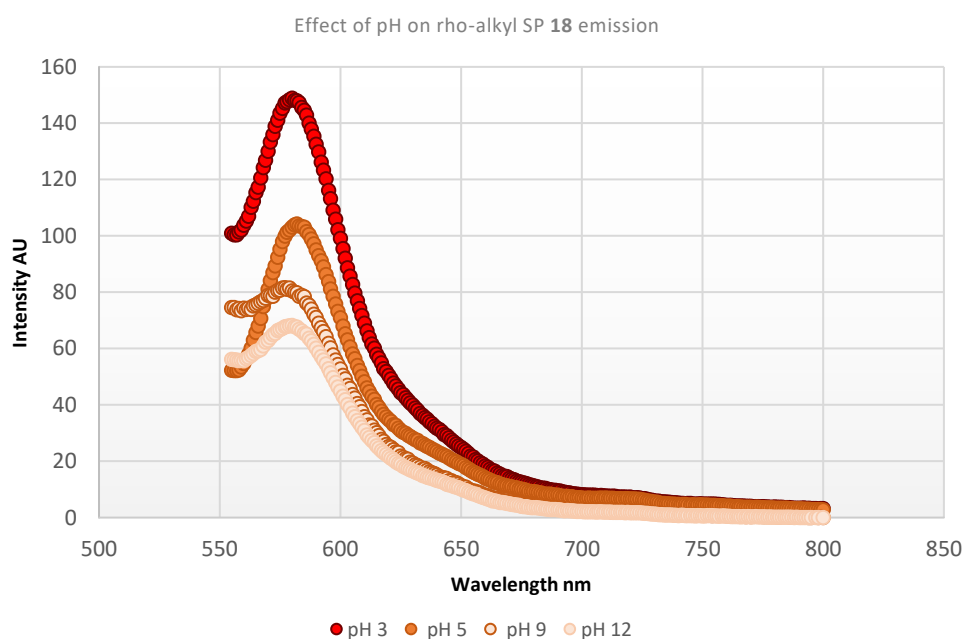
Figure 43. Fluorescence emission of rho-alkyl SP **18**, at 532 nm at four different pH. Fluorescence measurements were made using a 1 cm^3 fluorimetry cuvette; with a 100 µM solution of each probe dissolved in distilled water and made to desired pH with: 1M NaOH, 1M HCl and 1M EtCOOH (n=3).

The shape of the graph flattens as the alkalinity increases. In the case of rho-PEG short SP **48** the absorbance maxima shifts from 580 nm down to 555 nm (Figure 44).

Effect of pH on rho-PEG short **48** emission

○ pH 3　○ pH 5　○ pH 9　○ pH 12
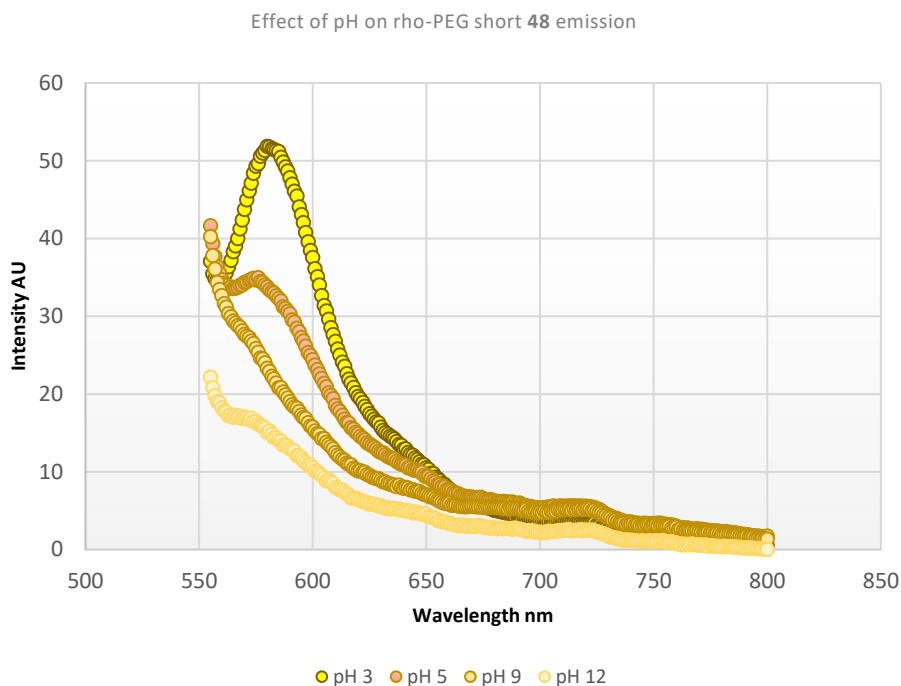
Figure 44. Fluorescence emission of rho-PEG short SP **48**, at 532 nm at four different pH. Fluorescence measurements were made using a 1 cm^3 fluorimetry cuvette; with a 100 µM solution of each probe dissolved in distilled water and made to desired pH with: 1M NaOH, 1M HCl and 1M EtCOOH (n=3).

Interestingly, the range of maximum emission for the rho-alkyl SP **18** probe is about 75 nm. This is the difference between the highest fluorescent output at pH 3 and a pH of 12. This value demonstrates the behaviour of the probes sensitivity to pH. The range of maximum emission points for the two glycol probes, rho-PEG short SP **48** and rho-PEG long SP **49** was equivalent to half the brightness of the probe in the most acidic environment (Figure 45). This indicated that the probe solutions must exist in an equilibrium between open and closed states of the rhodamine.

Effect of pH on rho-PEG long SP **49** emission
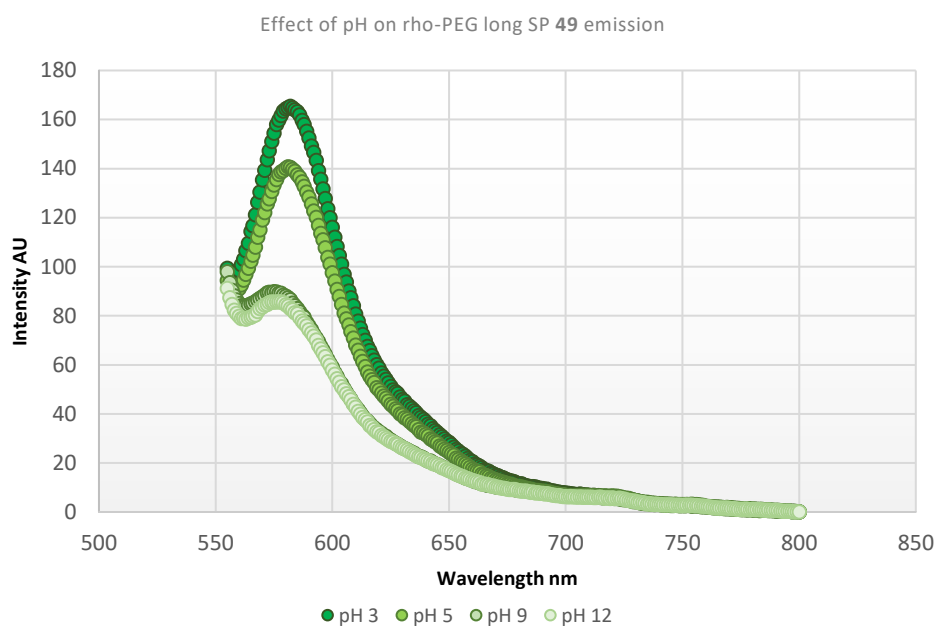
Figure 45. Fluorescence emission of rho-PEG long SP **49**, at 532 nm at four different pH. Fluorescence measurements were made using a 1 cm^3 fluorimetry cuvette; with a 100 µM solution of each probe dissolved in distilled water and made to desired pH with: 1M NaOH, 1M HCl and 1M EtCOOH (n=3).

The fact that there was still fluorescence at 555 nm decreasing to 800 nm in a solution of pH12 (light green curve), would direct thoughts to the theory that these rhodamine B probes are not overly sensitive to comparatively subtle pH changes. Rhodamine analogues used in pH sensitive probes can almost completely lose fluorescence in alkaline conditions, and brightly fluoresce in slightly acidic conditions. This led the investigation onto comparing the rhodamine probes with the previously synthesised dansyl probe, and also a comparison with the rhodamine B starting material.

Rhodamine B was dissolved in water in a variety of concentrations, starting at 100 µM and decreasing to 100 nM. The dansyl probe, DSP-**10** was also dissolved in water at a concentration of 100 µM. These solutions were poured into a cuvette and scanned on the fluorimeter following our standard technique.

The results of this test are shown below, plotted with the three probes for direct comparison (Figure 46). DSP-**10** was excited at 324 nm, this is a blue light laser that is used to visualise gels containing lysates incubated with this probe. 324 nm is close to the optimum point to excite dansyl at 338 nm.[150] DSP-**10** was approximately the same brightness as the rhodamine probes. This is problematic,

80

as the extinction coefficient (ε) of the dansyl group is very low compared to rhodamine B, 4,300 cm-1/M[80] vs 106,000 cm-1/M.[151] Rhodamine B was selected for this high ε and photostability as a replacement for the dansyl amide probe. The rhodamine B peak is much larger and therefore brighter than any other peak featured. The large drop in fluorescence must be due to the addition of the linker.
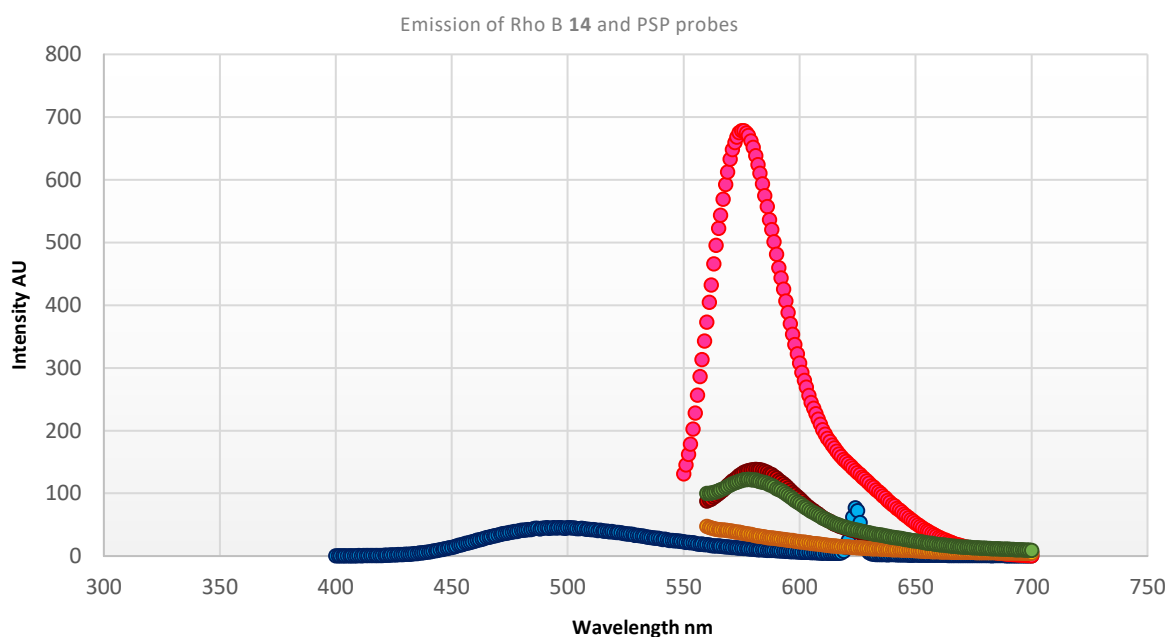
Figure 46. Fluorescence of 100 µM of the three rhodamine probes and 100 nM of rhodamine B (shown in pink) at 532 nm compared with 100 µM of DSP-**10** (shown in blue) at 324 nm. Rho-alkyl SP **18** is shown in red, rho-PEG short SP **48** is shown in yellow, and rho-PEG long SP **49** is shown in green. All measurements made at pH of 7.5 in a solution of distilled water, and added to a 1 cm^3 fluorimetry cuvette (n=3).

The equilibrium position between the ring closed and open forms of the rhodamine group is not easily discerned from ^{1}H NMR spectra. However the ^{13}C spectra allow identification of the major tautomer.

Analysis of the ^{13}C NMR spectrum of **18**, **48** and **49**, show the major form in CDCl$_3$ is the closed form. Diagnostic peaks at ca. 64 and at 153 ppm distinguish the two forms. The peak at 64 ppm arises due to the quaternary 9 position carbon being fully saturated, whereas the peak at ca. 153 ppm represents the open form sp^2 hybridised carbon. In **18**, **48** and **49**, no ^{13}C peaks at 153 ppm were found but peaks at 64 ppm were seen.

The investigation into the effects of pH indicates that the open and closed forms of the compound remain in equilibrium. Driving the fluorescence of the open forms with a chelating ion can increase the intensity of fluorescence, such that increasing temperature will not shift the compound to close, but will increase the intensity further.[152]

Furthermore, a relative preference for ring closure of the 2-amido substituted Rhodamine derivatives, in comparison to the parent carboxylate containing Rhodamine, has also been reported, with sources stating that the lactam form is quite stable in polar solvents and will remain colourless.[153]

These observations are consistent with the diminished fluorescence response found in this work, where the linker derivatives, rho-alkyl **15**, rho-PEG short **16** and rho-PEG long **17**, and the PSP probes rho-alkyl SP **18**, rho-PEG short SP **48** and rho-PEG long SP **49** are significantly less bright compared to rhodamine B.

The origins of a thermodynamic preference for the closed lactam over the corresponding lactone is not immediately obvious and, in collaboration with the Cross Group, calculations were performed to investigate the origin of this thermodynamic preference. [154] It has been established that the equilibrium between the fluorescent ring open cation and the inactive cyclised form is pH dependent, with acidic conditions favouring the ring open, fluorescent cation. Therefore, it is simplest to compare the relative thermodynamic positions of the equilibria at the same pH; within the narrow physiological pH range that these probes are expected to function, the open form is most likely the cation and the ring closed form a neutral lactone or lactam (Scheme 17). Considerations regarding the different acidities of the N*H* and O*H* groups can be neatly side stepped by calculating the relative energies of the ring open cations and the corresponding lactone or lactam species; although these calculations do not provide an absolute value for the change in Gibbs energy for each ring closure, the thermodynamic preference for each reaction can be compared since the energetic contribution of hydroxide and water will be the same in both cases. To further simplify calculations

the, perhaps significant, effect of solvent was ignored in this preliminary study but it was hoped that any basis of an intrinsic bias might still be revealed.
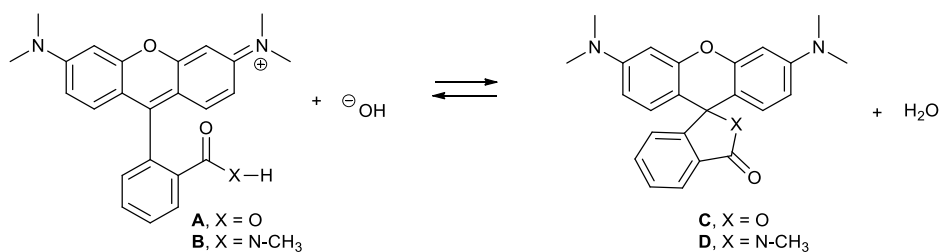
Scheme 17. Tautomeric Equilibrium of Rhodamine Derivatives at Physiological pH.

Density Functional Theory at the ωB97xD/6-31G(d,p) level was used to compute the gas phase, minimum energy conformers of the model N-methyl rhodamine derivatives in both the cationic ring open forms **A/B** and ring closed neutral forms **C/D**; optimised structures are presented in Figure 47. The relative thermodynamic disposition for ring closure was calculated from the difference in free energy for each ring open cation and its ring closed form, as shown in Eq. 1. This calculation revealed that ring closure of the 2-amido derivative **B** is 9.6 kcal/mol more exergonic than ring closure of the carboxylic acid **A**, a preference that is in agreement with the experimental observation.

$$\Delta\Delta G = \Delta G(\text{lactone}) - \Delta G(\text{lactam}) = (G_A - G_C) - (G_B - G_D) \qquad \textit{(Eq. 1)}$$

Close inspection of the optimised structures provided a rationale for this relative preference. In the ring open cation **A**, the carboxylic acid group is fully conjugated with the phenyl ring (ArC-C=O dihedral angle is 0°). In contrast, the amide cation **B** suffers a steric interaction between the carbonyl oxygen atom and the phenyl ring system, which is alleviated by a twisting of the ArC-C=O bond (dihedral angle is *ca.* 27°) and results in a loss of conjugation stabilisation; the conjugation of the carbonyl group with the phenyl ring is restored in the ring closed lactam **D**.
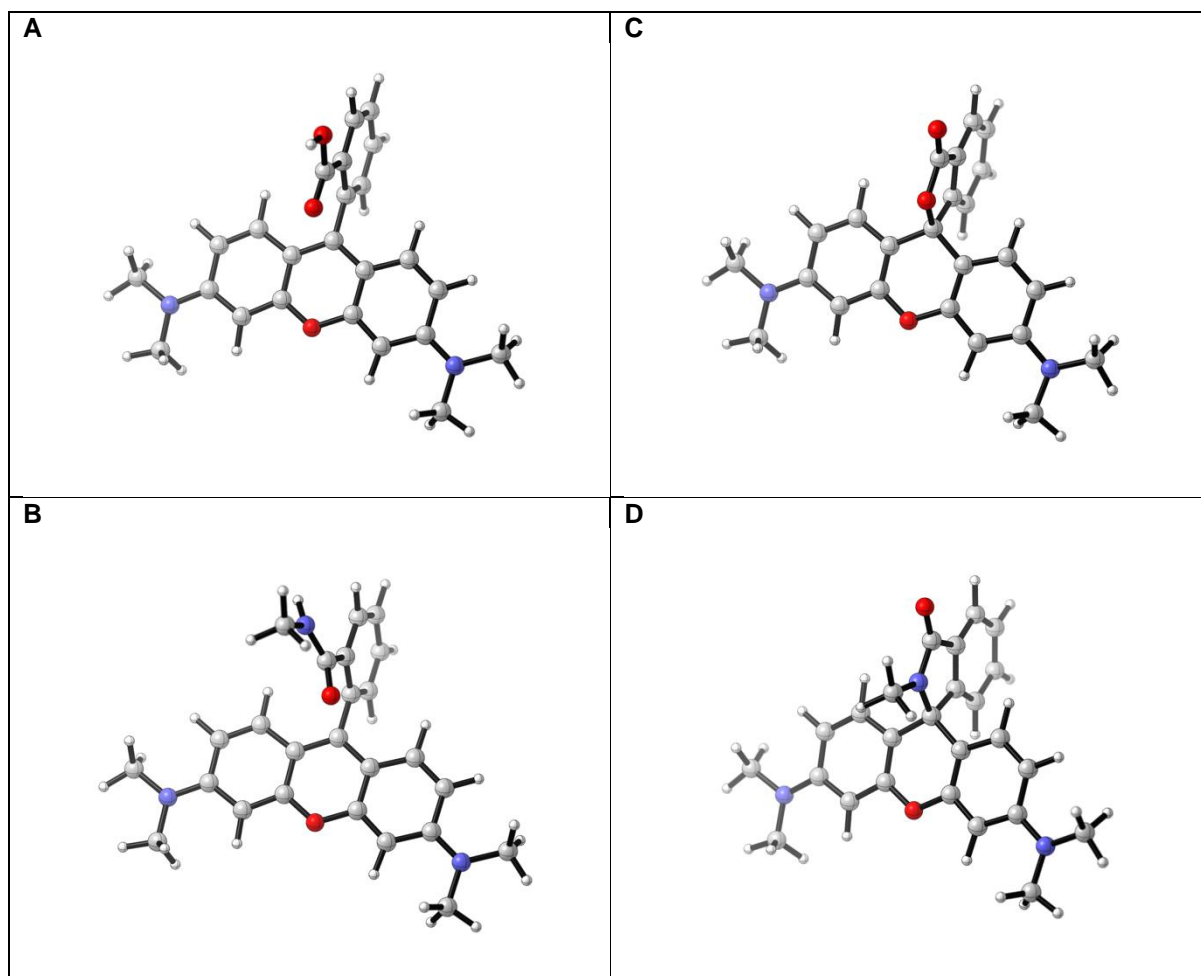
Figure 47. Computed structures for the lowest energy conformers of the ring open cations **A** and **B**, and the ring closed molecules **C** and **D**. Structures were optimised and energies calculated at the ωB97xD/6-31G(d,p) level of theory.

A survey of X-ray crystal structure data revealed a single example of a ring open amide structure which also shows a significant ArC-C=O out of plane twist while a structure similar to the calculated carboxylate shows only minor deviation from the plane. The conformations observed in these structures may be controlled by crystal packing as well as the steric requirements of the carboxylate and amide groups but does provide support for the calculated conformational preferences. X-ray data was obtained from a substructure search of the The Cambridge Structural Database (Figure 48).[155]
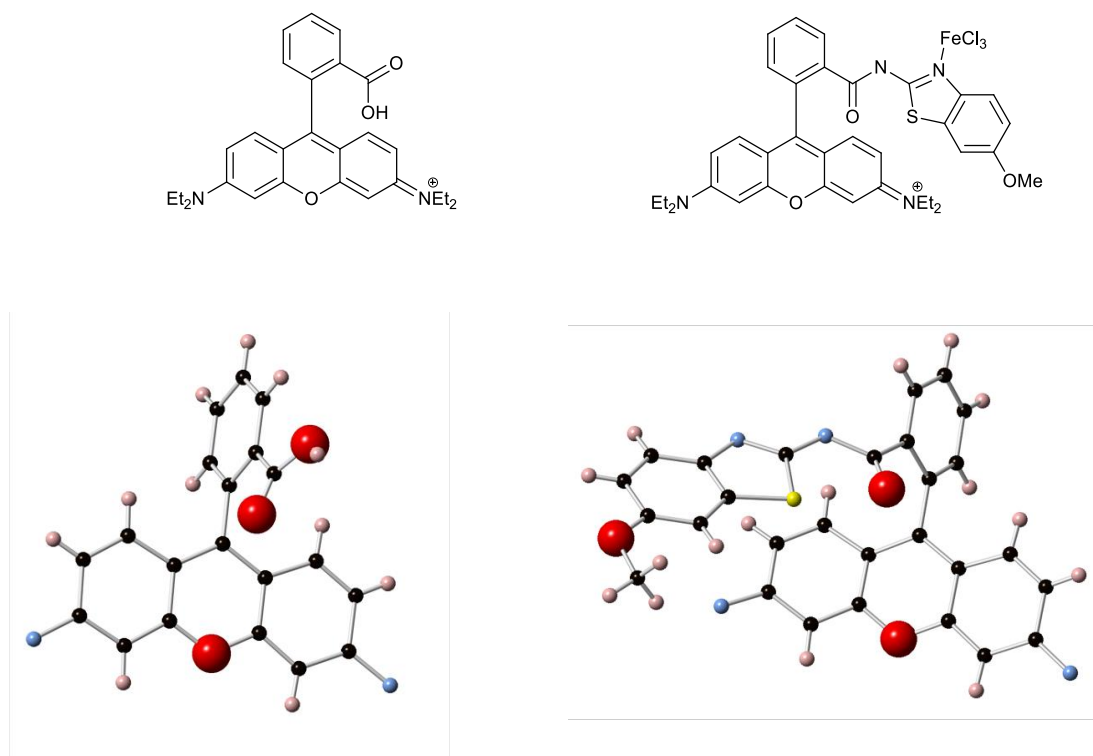
Figure 48. X-ray Crystal structure of Rhodamine carboxylic acid ring open cation (CDS entry ADIGEB) and Rhodamine amide analogue in ring open form (CSD entry SETCEA01) illustrating out of plane C=O in the amide (ethyl and FeCl₃ groups omitted for clarity).

Studies show that probes have been designed with rhodamine but feature a component that blocks the lactam ring formation via alkylation of the amide nitrogen. Cincotta *et al* patented this technique with methylation, but others have expanded on it.[156] Nguyen *et al* used a novel piperazine moiety coupled to the 2 position on the aryl ring of rhodamine B.[157] Incorporation of a lactam blocking moiety should return the probe to equivalent fluorescent strength to rhodamine B.

With the spectroscopic data gathered, the probes biological efficacy was then investigated.

3.2.8 Biological Viability of Probes

The biological effects of the three rhodamine probes on cell viability as an approximate measure of OP toxicity was investigated. It is known from preliminary work that PSP is cytotoxic to cardiomyoblasts from as little as 12 µM when incubated for 4 hours. This effect can be quantified with two assays: a metabolic assay featuring MTT (3-[4,5-dimethylthiazol-2-yl]-2,5 diphenyl tetrazolium bromide),[158] and a cell viability assay measuring lactate dehydrogenase activity (LDH).[159]

MTT Assay

The MTT assay was first described by Mosmann *et al.* This colourimetric assay measures the reduction of the yellow tetrazolium salt to insoluble purple formazan salt by mitochondrial dehydrogenases such as succinate dehydrogenase. This technique is commonly used to determine the remaining mitochondrial metabolic activity in living cells, allowing an accurate quantitative assay of living cells in a study.[160]

Living cells produce the succinate dehydrogenase enzyme and therefore the amount of formazan produced is proportional to living cells and their viability (Figure 49). The formazan is a bright purple colour so results are obtained with a colourimeter measuring at 570 nm.
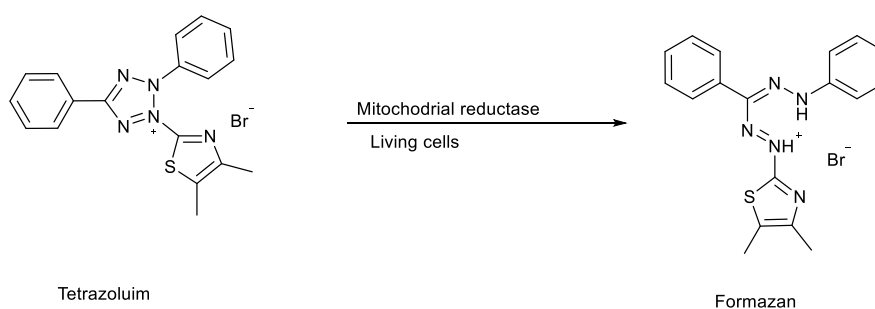
Figure 49. Reduction of MTT to Formazan

LDH Assay

The lactate dehydrogenase (LDH) assay is another way of measuring viability of cells albeit indirectly, and is often performed alongside MTT. LDH is an enzyme which is released by dying and damaged cells into the culture medium, this cell death is caused mainly by necrosis, as cell membranes do not rupture during apoptosis. The activity of LDH is therefore an indicator of cell death, the measurement which can be used to evaluate the cytotoxicity of molecular compounds such as drugs or toxins, or even other environmental factors.[161]

There is a two-step reaction that activates the reduction of NAD^+ to NADH and H^+ by oxidation of lactate to pyruvate. A diaphorase enzyme then reduces a tetrazolium salt to brightly coloured

formazan salt using NADH and H$^+$ for the second step (Figure 50). The coloured product is then measured at 480 nm using a colourimeter. The intensity of the colour is proportional to the amount of damaged tissue or dead cells that are present. This assay is a useful indicator of chronic or acute tissue damage and can be used to help diagnose and monitor a heart attacks.[162]
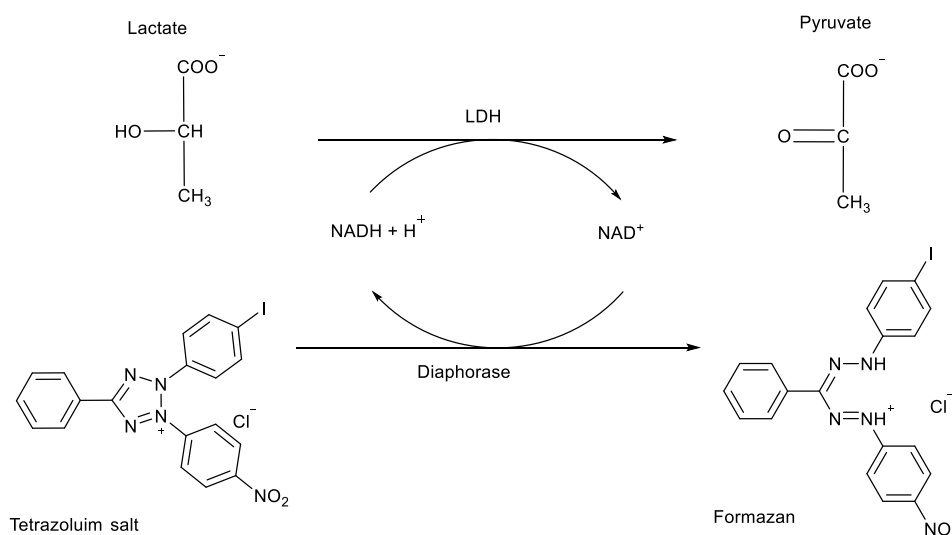
Figure 50. Mechanism of LDH assay

Rhodamine B is known to show toxicity within certain tissues, so this fluorophore was investigated along with the intermediate compounds rho-alkyl **15**, rho-PEG short **16** and rho-PEG long **17**.[163] The rationale for testing rhodamine B is to ensure observed toxicity is induced by the OP moiety and not just the rhodamine B component. This would impact the results, and control assays featuring rhodamine B, and the precursors would need to be performed. Ideally assaying these compounds would show minimal toxicity compared to the organophosphate probes.

It was assumed that if the toxicity of the rhodamine B probes could only differ slightly from the parent compound PSP, the probes would interact in a similar way with the protein targets of interest. If this was to be the case, no toxicity would indicate very little or no interaction by the probe with the organophosphate targets, and would invalidate the design of the probe.

As mentioned previously, the focus of this study is on interactions with cardiac tissue. To this end, mitotic H9c2 cells can be differentiated so that the cardiomyocyte phenotype is expressed. This process elongates the cell structure into multinucleated myotubes with recognizable actin filaments and binds the cells together tightly resembling muscle tissue fibre. This normally occurs fully after 7 days in foetal bovine serum (FBS) suppressed medium with increased retinoic acid levels of 10 nM.[64]

MTT

Rhodamine B, linkers **15**, **16** and **17**, probes: rho-alkyl SP **18**, rho-PEG short SP **48**, and rho-PEG long SP **49**, had each been subjected to 4-hour and 24-hour tests as a treatment measuring cell toxicity for short and long exposures. In the MTT tests a 24-well plate was seeded with 15,000 cells per well and differentiation was induced over 7 days in the cells. After the 7 days, the differentiation process was completed, and the cell culture medium was changed to fresh medium containing a concentration of one of the compounds for treatment. Four of the wells were left (as a control) with only fresh medium added, the other twenty wells were split into five groups of four with each treatment occupying four wells per plate.

The plates undergoing the short 4-hour time point were incubated for 3 hours before addition of the tetrazolium salt and further incubation for 1 hour. For the 24-hour time point, the plates were incubated at 37.5°C for 23 hours before having the tetrazolium salt added. Following this final hour, the medium was removed and replaced with DMSO, the solvent dissolves the insoluble formazan crystals precipitated by the cells, giving colourless, pink and purple coloured solutions dependent on the concentration of formazan. Finally, the contents of each well were transferred to a well on a 96 well-plate to be scanned at 570 nm in a colourimeter. The absorbance reading recorded is proportional to the number of cells surviving the treatment and so reflects the cell viability and an assessment of the treatment toxicity can be made.

LDH

Just as with the MTT tests, LDH tests were performed at two time points, 4 hours and 24 hours. Cells were prepared in a 96-well plate which was seeded with 5000 cells per well, and left for seven days during which, the cells had differentiated expressing the cardiomyocyte phenotype. Each treatment was then added to columns of wells on the plate as well as a column of wells containing fresh media as a control. This technique then proceeded as outlined in section 5.3.6.

The lowest concentrations measured in each test was 6.25 µM of each compound. The highest concentration tested was 100 µM. Probe concentration of over 100 µM could not be evaluated due to low solubility and saturation of the solution in water causing the probes to aggregate.

MTT and LDH Test Results

4-hour tests

The results of a 4-hour MTT test featuring a treatment of rhodamine B at varying concentrations showed very little toxicity (Figure 51). The only slightly significant result was at 100 µM where 25% of the cells are no longer metabolically viable.

The three precursor linkers all showed some toxicity at 6.25 µM, except for rho-PEG short **16** where only a little toxicity was seen at 12.5 µM and no toxicity was seen at all at 6.25 µM. Linker rho-PEG long **17** was the most toxic out of the three. The differences in bioavailability, and in solubility, of the three linkers is likely responsible.

The three organophosphate probes showed toxicity at concentrations of 12.5 µM and 6.25 µM for rho-alkyl SP **18**, and rho-PEG long SP **49**. However, the significance shown by t-test is low, and overall the toxicity between the precursor linkers and the organophosphate probes was similar, with the OPs showing more relevant toxicity at low concentrations. Rho-PEG long SP **49** is illustrating statistically significant toxicity at 6.25 µM until 25 µM where there is a consistent level of maximum toxicity.

Probe rho-alkyl SP **18** showed some toxicity from 6.25 µM, yet without the statistical significance of rho-PEG long SP **49**, and yet rho-PEG short SP **48** was significant after 25 µM.

The 4-hour LDH viability assay also indicated the low toxicity of rhodamine B as shown in the MTT assay. With only some non-significant increase in LDH of about ten percent measured at a rhodamine concentration of 100 µM (Figure 52). Compounds rho-PEG short **16** and rho-PEG long **17** have caused a large release of LDH at 100 µM and some not statistically significant toxicity at 50 µM. Both glycol precursor compounds exhibited higher toxicity than the linker rho-alkyl **15**.

The three organophosphate probes show some cytotoxicity at concentrations of 6.25 – 25 µM between them and the precursors comparatively. There was an increase in toxicity up to concentrations of 100 µM for all three probes. The probe rho-PEG long **49** has caused the largest amount of LDH to be released. Only a small statistically significant increase in LDH had been monitored in these probes, yet the inactivity of the precursors over a short period is promising.
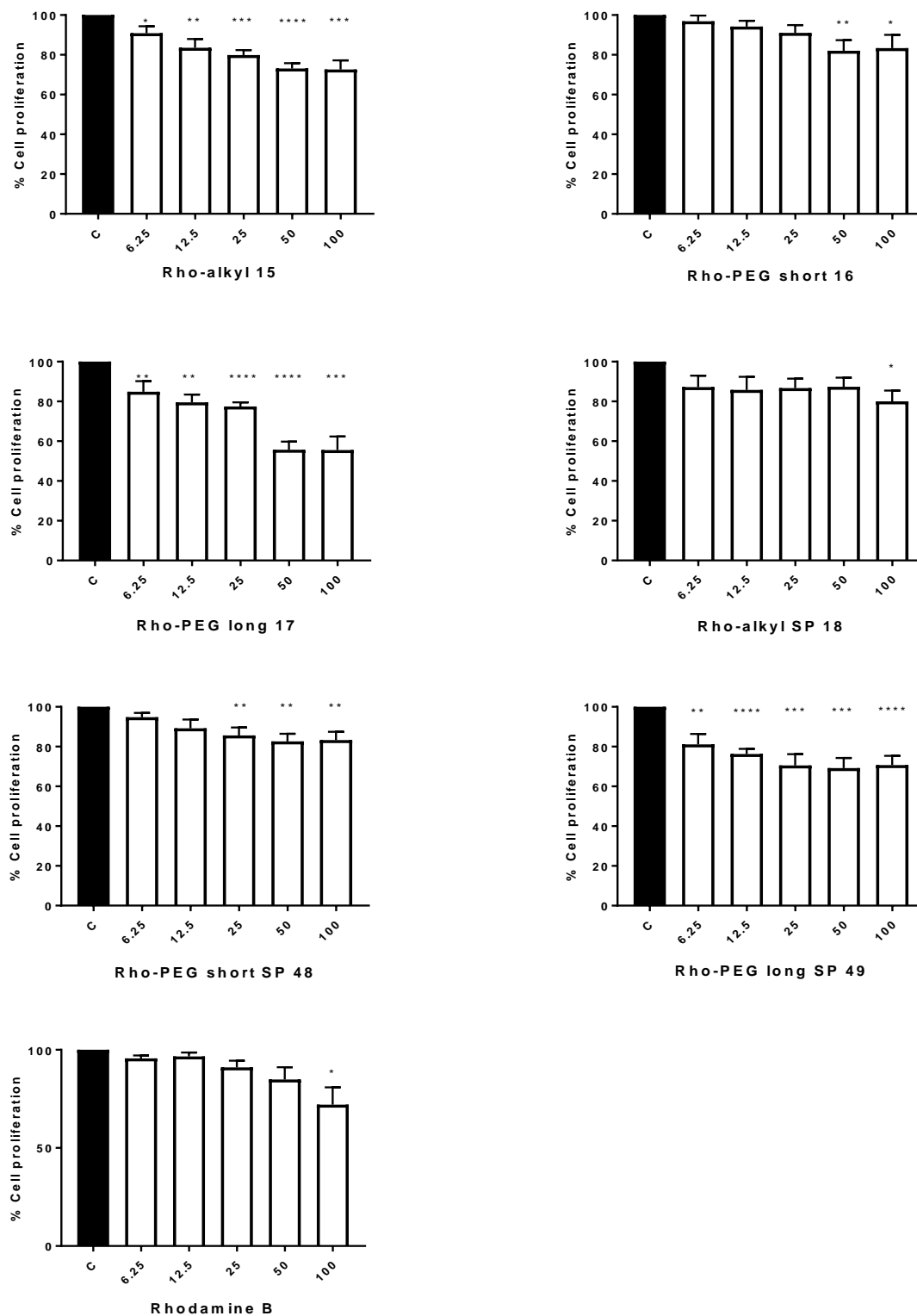
Figure 51. 4-hour MTT tests, of; Rhodamine B, three precursor linkers: rho-alkyl **15**, rho-PEG short **16**, rho-PEG long **17**. Three organophosphate probes: rho-alkyl SP **18**, rho-PEG short SP **48**, rho-PEG long SP **49**. Data is expressed as a mean percentage of reduced MTT or LDH concentration measured colourimetrically relative to the control values where untreated wells represent 100%. The "*" represent the results of a t-test comparing significance (p) against the control response. *$p<0.05$, **$p<0.01$, ***$p<0.005$, ****$p<0.001$ the lower the value the more significant i.e. the larger the average difference between the two data sets, (n = 4, control data normalised to 100%).

91

Figure 52. 4-hour LDH tests of; Rhodamine B, three precursor linkers: rho-alkyl **15**, rho-PEG short **16**, rho-PEG long **17**. Three organophosphate probes: rho-alkyl SP **18**, rho-PEG short SP **48**, rho-PEG long SP **49**. Data is expressed as a mean percentage of reduced MTT or LDH concentration measured colourimetrically relative to the control values where untreated wells represent 100%. The "*" represent the results of a t-test comparing significance (p) against the control response. *p<0.05, **p<0.01, ***p<0.005, ****p<0.001 the lower the value the more significant i.e. the larger the average difference between the two data sets, (n = 6, control data normalised to 100%).

92

24-hour tests

The results of the 24-hour MTT tests demonstrated that rhodamine B and the three precursor linkers display a small level of toxicity (Figure 53). Rhodamine B is effectively non-toxic below 25 µM but reaches over 50% cell death at 100 µM concentration. Comparatively, all three linkers began to inhibit cell metabolism at 25 µM with rho-alkyl linker **15** causing the most cell death at each concentration of treatment. Rho-PEG long **17** showed less signs of toxicity in the 24-hour time course which contrasts the 4-hour MTT tests. All three linkers are more toxic than rhodamine B at 100 µM. This increased toxicity may be due to higher bioavailability of the more lipophilic linkers or an increase in the amount of ring closed, perhaps more toxic, rhodamine.

The three organophosphate probes all exhibited toxicity in the 24-hour MTT tests. Rho-alkyl SP **18** and rho-PEG long SP **49** exhibited a pronounced increase in toxicity from the precursor linkers, rho-alkyl **15** and rho-PEG long **17**. Rho-PEG long SP **49** started showing signs of toxicity at 6.25 µM concentration, and at 12.5 µM inhibition of cell metabolism had increased to 50%, however, as concentration continues to increase the toxic effect reached a plateau. Rho-PEG short **48**, shows some minimal toxicity at 25 µM, but overall a decrease in toxicity above this concentration when compared to precursor rho-PEG short **16**. The probe still retained some toxicity and only loses about 15% effectiveness at 100 µM concentration comparatively between the two.

The results of the 24-hour LDH test compliment that which has been shown in the 24-hour MTT tests (Figure 54). All three linker precursor compounds exhibited more toxicity than rhodamine B which after 24-hour treatment was still largely inactive. All three showed some small level toxicity at 6.25 µM concentration, with significant toxicity at 100 µM. Rho-alkyl **15** indicated the highest amount of toxicity at 25, 50 and 100 µM. Whereas, rho-PEG short **16** had a higher average toxicity at 100 µM than rho-PEG long **17,** this was in contrast with the results of the 4-hour LDH tests. Rho-PEG long **17** having the highest toxic effect on average is still in keeping with the previous assay results. However, due to the amount of statistical error associated with the various concentrations of these two

treatments, the results are not significant. The trend still supports the hypothesis that the linker chains are increasing toxicity of the compounds compared to rhodamine B, where no significant toxicity at any concentration was seen by the 24h LDH tests.

The results of 24-hour LDH test also showed a small drop in toxicity between the precursors and the final probes. Rho-PEG short SP **48** was only significantly toxic at a concentration of 100 µM, rho-alkyl SP **18** also showed a decrease in toxicity compared with its precursor linker, and is apparently only cytotoxic at 50 µM and above. Probe rho-PEG long SP **49** is toxic at 12.5 µM and above but overall has a drop of 20% toxic effectiveness at 100 µM whence compared with its precursor rho-PEG long **17**. It is worth noting that toxicity found in the LDH assays is due to necrotic cell death however, not apoptotic, so it is expected that high concentrations would produce LDH release, and low doses may still be effective as an enzymatic inhibitor, but that is not seen via this type of assay.
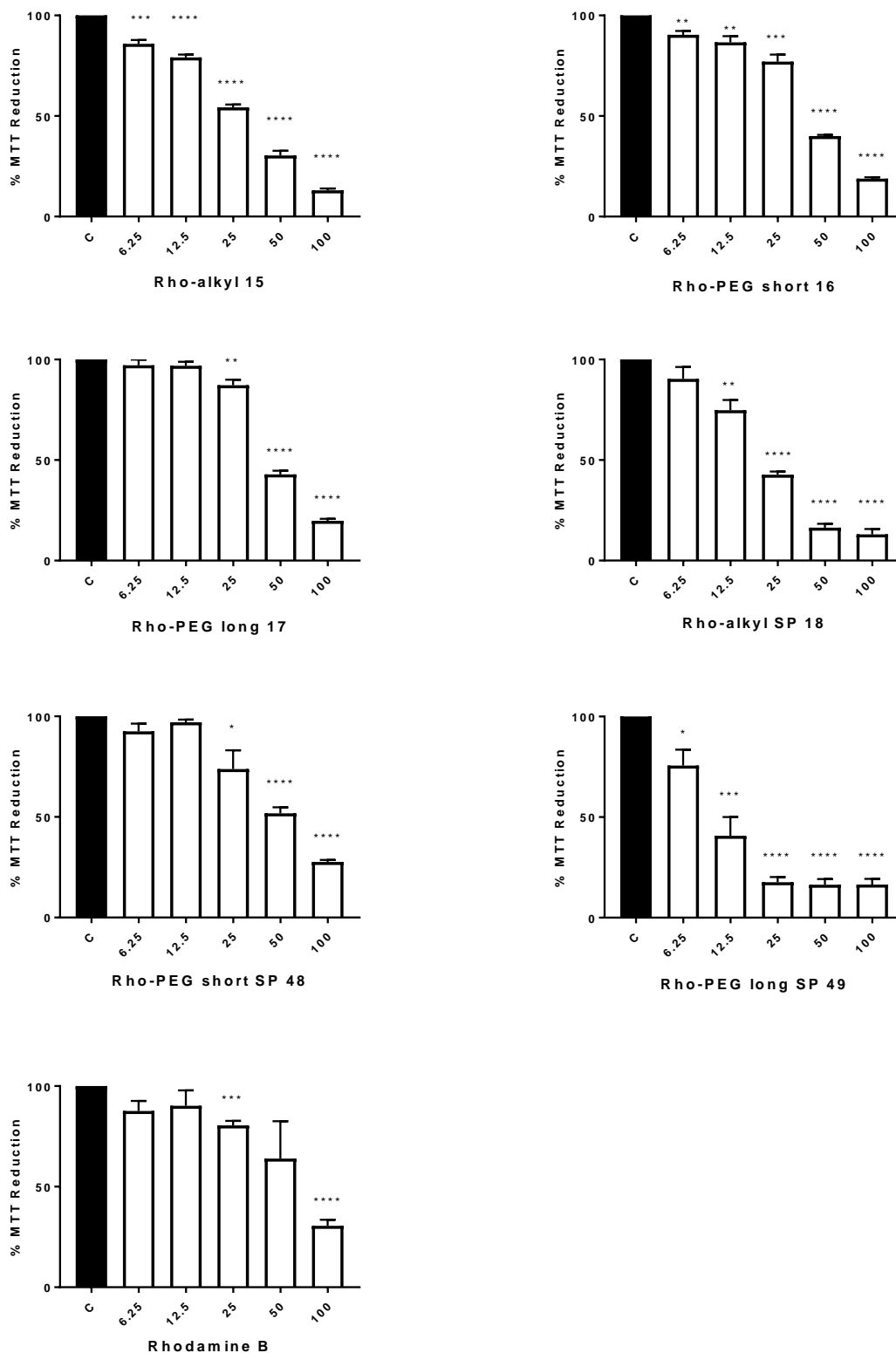
Figure 53. 24-hour MTT tests of; Rhodamine B, three precursor linkers: rho-alkyl **15**, rho-PEG short **16**, rho-PEG long **17**. Three organophosphate probes: rho-alkyl SP **18**, rho-PEG short SP **48**, rho-PEG long SP **49**. Data is expressed as a mean percentage of reduced MTT or LDH concentration measured colourimetrically relative to the control values where untreated wells represent 100%. The "*" represent the results of a t-test comparing significance (p) against the control response. *p<0.05, **p<0.01, ***p<0.005, ****p<0.001 the lower the value the more significant i.e. the larger the average difference between the two data sets, (n = 4, control data normalised to 100%).

Figure 54. 24-hour LDH tests of; Rhodamine B, three precursor linkers: rho-alkyl **15**, rho-PEG short **16**, rho-PEG long **17**. Three organophosphate probes: rho-alkyl SP **18**, rho-PEG short SP **48**, rho-PEG long SP **49**. Data is expressed as a mean percentage of reduced MTT or LDH concentration measured colourimetrically relative to the control values where untreated wells represent 100%. The "*" represent the results of a t-test comparing significance (p) against the control response. *p<0.05, **p<0.01, ***p<0.005, ****p<0.001 the lower the value the more significant i.e. the larger the average difference between the two data sets, (n = 6, control data normalised to 100%).

The IC_{50} and EC_{50} values of all seven compounds on H9c2 cells has been be calculated, and is displayed in below (Table 2).

Compound	IC_{50} (µM) MTT				EC_{50} (µM) LDH			
	4h	SD	24h	SD	4h	SD	24h	SD
Rhodamine B	>100	-	>100	-	>100	-	>100	-
Rho-alkyl **15**	12	± 0.16	98	± 0.58	13	± 0.07	18	± 0.25
Rho-PEG short **16**	41	± 0.16	56	± 0.08	51	± 0.13	38	± 0.19
Rho-PEG long **17**	39	± 0.39	52	± 0.04	71	± 0.28	33	± 0.17
Rho-alkyl SP **18**	44	± 0.15	29	± 0.07	95	± 0.13	37	± 0.18
Rho-PEG short SP **48**	10	± 0.09	67	± 0.27	24	± 0.03	36	± 0.23
Rho-PEG long SP **49**	11	± 0.19	12	± 0.08	50	± 0.07	12	± 0.12

Table 2. Calculations of mean IC_{50} (µM), determined from each assay. SD of the mean for each log, n=4 for the MTT and n=6 for LDH calculations.

The values shown in this table illustrate that rhodamine B has no effect under 100 µM. The data for the assays with treatment of rhodamine B with H9c2 cells was such that an IC_{50} and EC_{50} values could not be determined within the scope of the assays. These high values have addressed the concerns that rhodamine B may be too toxic a fluorophore to use.

In general, the organophosphate probes exhibited more toxicity than the precursor linkers seen in MTT tests. At the more clinically relevant concentration of 6.25 µM, the probes exhibited toxicity and over 24-hours this inhibition is likely due to apoptotic pathways being activated. At concentrations as high as 100 µM, inhibition of metabolism could be due to a necrotic cell death. It is interesting to note that in 24-hour assays the organophosphate probe rho-PEG long SP **49** exhibited more toxicity than with the corresponding linker rho-PEG long **17**.

In the LDH tests the results indicate that in general concentrations over 25 µM are toxic, and that the precursor linkers exhibit greater toxicity then the probes. This is indicative of cellular necrosis. For the rho-alkyl SP **18** probe, the toxicity has dropped with the addition of the PSP as measured by the LDH tests. This may be related to its ability to induce apoptosis in this cell line; apoptotic pathways are not easily highlighted in an LDH assay.[66]

However, the two glycol probes show a different pattern, rho-PEG short SP **48** was more toxic in the 4-hour LDH test then the precursor without the organophosphate, although this was not the case with the 24-hour LDH test where the opposite occurred. Probe rho-PEG long SP **49** demonstrated an increase in EC_{50} in all four tests between it and its linker.

The conclusion of this study in cell viability with the OP probes is that they are a worthwhile tool for cell culture assays, and inhibit cell metabolism at concentrations between 6.25 – 25 µM. Also at these concentrations only a small amount of LDH was released. Probe rho-PEG long SP **49** is the most potent of the probes on average and likely has a higher bioavailability than rho-alkyl SP **18** and rho-PEG short SP **48**. This was the only probe that exhibited a high toxicity at a concentration of >25 µM, and was more toxic over all the tests than its precursor linker rho-PEG long **17**.

This led the investigation onto gel electrophoresis studies. A test of the probes in the experiments they are designed to function in will prove the efficacy of each one.

3.2.9 Protein Binding with Protease

The three rhodamine organophosphate probes, were then tested for their ability to fluoresce in a polyacrylamide gel once bound to a peptide fragment. To reliably measure which probe was the most suitable in SDS-PAGE, a purified protein known to be an organophosphate target was used.

SDS-PAGE was explored by exposure of each probe to protease chymotrypsin, followed by incubation and then by running on an SDS-PAGE gel, afforded three gels in which effectiveness of probe binding and fluorescence had been be qualified. These experiments were performed by first incubating 25 µg of chymotrypsin protein with three concentrations (25, 50 and 100 µM) of each probe on ice for 15 minutes. 20 µl of each probe/ protein solution was pipetted into its corresponding well on a 10% acrylamide, 1.5 mm gel cast, as described in experimental section 5.3.7. The loaded gel was then electrophoresed, and upon completion the gel was then visualised on a 532 nm Fujifilm FLA5000 green light laser (Figure 55). Interestingly 100 µM of rho-PEG long SP **49** seems to be the brightest compound of the three probes, but when compared to the whole protein

fractions more of rho-alkyl SP **18** seems to have bound, the chymotrypsin did not fluoresce at this wavelength, meaning autofluorescence is avoided (not shown).
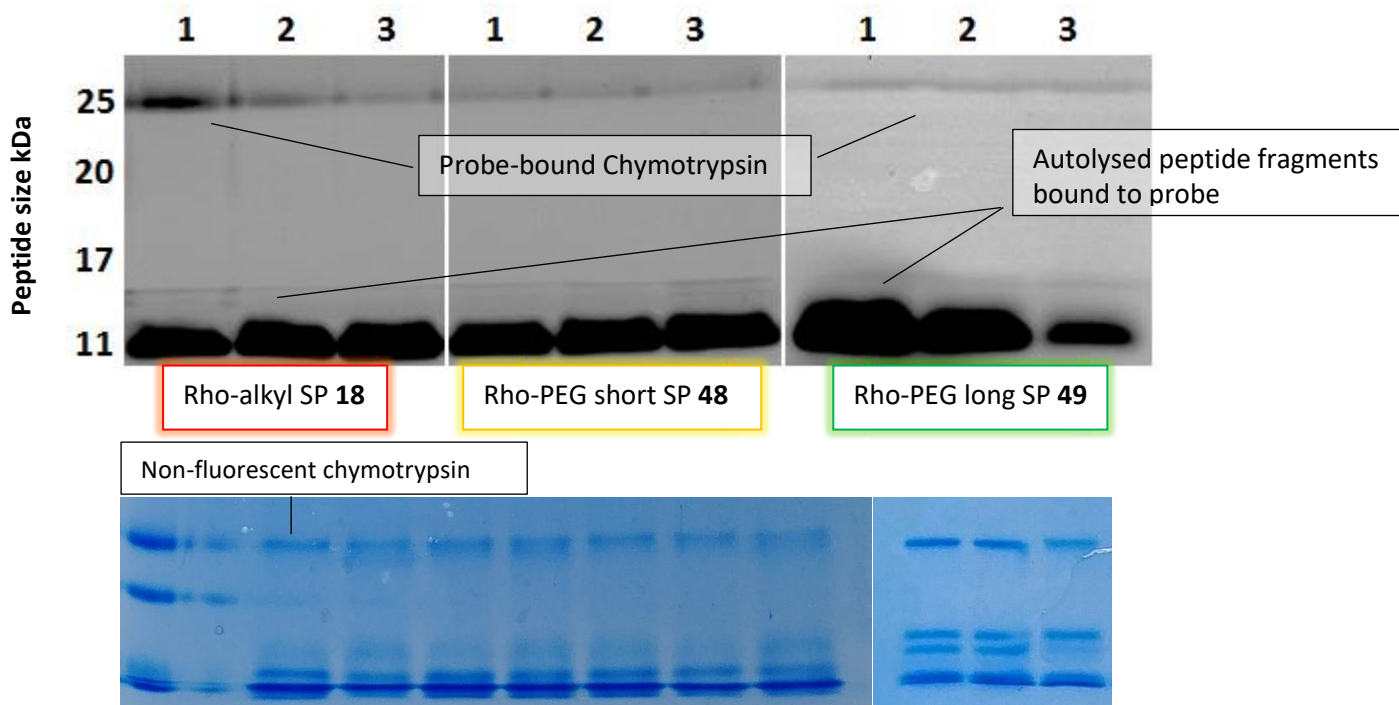
Figure 55. Probes rho-alkyl SP **18**, rho-PEG short SP **48** and rho-PEG long **49** at concentrations of 100, 50 and 25 µM in lanes 1, 2 and 3 respectively, with 10 µg of chymotrypsin, top bands are 25 kDa, with bottom bands at 11 kDa smaller peptide fraction due to self-digestion of the chymotrypsin. Coomassie gel with ladder and lane 0 containing 10 µg chymotrypsin (n=1).

3.2.10 Probe Binding with Organophosphate Targets: Neuropathy Target Esterase and Transglutaminase 2

With results obtained from exposure of chymotrypsin to the probes, a suitable experiment on interesting protein targets for organophosphates was then explored. Neuropathy target esterase (NTE), as previously mentioned is the target of organophosphates causing OPIDN, and determining whether this probe is sensitive to it within cardiac myocytes is of keen interest.[59] Transglutaminase 2 (TG2), is one interesting protein target for both the study of organophosphate interactions,[164] and cardioprotection.[165] Its cardioprotective properties are not yet well understood, but studies have shown an involvement with ATP mediation, and TG2 can be activated by protein kinases (PKC).[166]

To continue with testing of the capabilities of the rhodamine organophosphate probes, TG2 and NTE proteins were chosen as targets. TRIS-buffered solutions of NTE and TG2 were incubated on ice with a 100 μM solution of rho-alkyl SP **18**.

The results of this gel when visualised firstly on a blue laser at 412 nm then secondly under green side lamps indicated that both proteins bind with probe rho-alkyl SP **18** (Figure 56). The weight of the fragments that the two proteins can be found at are; 22 kDa for NTE, and 80 kDa for TG2 respectively. The blue laser interestingly also highlighted the background fluorescence of the proteins, as well as impurities and other protein fragments from the initial substrate these recombinants were taken from. Under green light this fluorescence disappears resulting in true emission from the probe.

The results demonstrated that fluorescent bands can be seen at the expected locations on the gel, suggesting that the probe has bound to its target protein. In order to determine how well the probe binds to TG2 particularly, a second experiment that included a TG2 competition assay, where, rho-alkyl SP **18**, PSP and an irreversible TG2 inhibitor called ZDON (Benzyloxycarbonyl-(6-Diazo-5-oxonorleucinyl)-L-Valinyl-L-Prolinyl-L-Leucinmethylester)[167], compete for binding space with TG2. The assay had three solutions all incubated with TG2: 1) 25 μM probe rho-alkyl SP **18** with TG2 control, 2) 25 μM rho-alkyl SP **18**, with 25 μM PSP, 3) 25 μM rho-alkyl SP **18**, with 25 μg of ZDON. These were buffered and boiled as mentioned previously and added to a well in each corresponding lane. On this gel, repetition of NTE binding with a lower concentration of rho-alkyl SP **18** was also attempted.

The results of this experiment showed that when visualised on a green light laser (C), the band at 80 kDa in lane 1 is clearly darker than the matching bands in lanes 2 and 3. This would indicate that the probe is competitively binding at the same active sites on TG2 as non-fluorescent PSP and ZDON.

412 nm   532 nm

Lanes 6 and 7 of this experiment show, albeit very faintly, a band at 22 kDa illustrating the binding of rho-alkyl SP **18** to the established organophosphate target NTE.
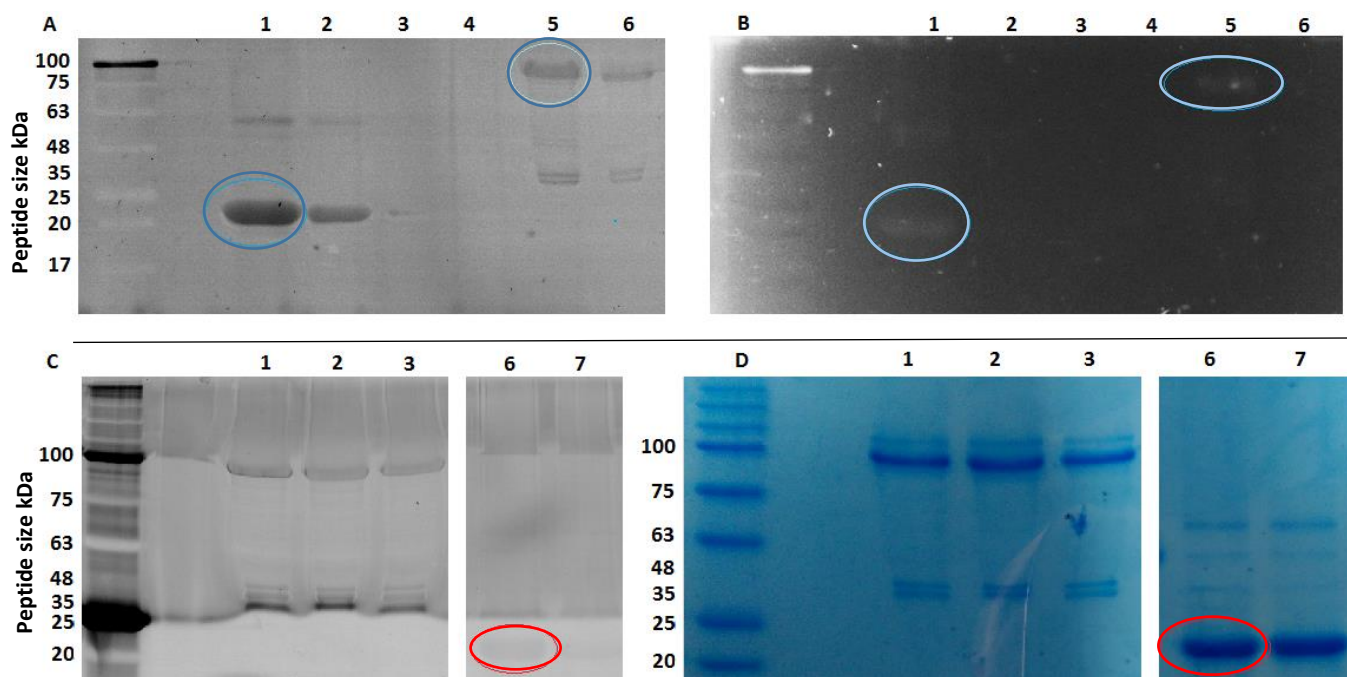
Figure 56. SDS-PAGE of organophosphate targets; gel 1 (A and B), NTE and TG2, gel 2 (C and D), competition assay of TG2 and repeat of NTE. A) Blue light gel scanned by laser. Lane 1 contains 10 μg NTE with 100 μM of rho-alkyl SP **18**. Lane 2 10 μg NTE control without probe. Lane 5, 10 μg TG2 with 100 μM of rho-alkyl SP **18**. Lane 6, 10 μg TG2 control. B) Green light isolating the rhodamine probe rho-alkyl SP **18** binding with protein targets. C) Lane 1, green light measurement of probe rho-alkyl SP **18**, in 100 μM with 10 μg TG2. Lane 2, rho-alkyl SP **18** with 10 μg TG2 and PSP. Lane 3, rho-alkyl SP **18** with 10 μg TG2 and 25 μg ZDON. Lane 6, 10 μg NTE with 25 μM of probe rho-alkyl SP **18**. Lane 7, NTE control 10 μg. D) Coomassie staining of gel (C) (n=1 for each).

Despite the effective brightness having not much improved on the dansyl PSP probe (DSP-**10**), the selectivity of these three probes still proved to be an advantage over DSP-**10** due to the absorbance/ emission located in the green region of the visible spectrum. Tyrosine and tryptophan residues fluoresce and can be seen up to the blue region of visible light. The rhodamine probes can effectively label protein with a fluorescent response highlighting bands without showing background autofluorescence.

3.2.11 2-Dimensional Gel Electrophoresis Studies

One of the challenges that approaches proteomics is the study of the relative abundances of proteins present within the proteome, and reproducibly fractionate these tissues to elucidate both a qualitative and quantitative measure of the protein complexes.[168] Gel electrophoresis performed across a charge dependent scale, isoelectric point (pI), for protein mixtures will separate them across a small gel strip dubbed isoelectric focusing gel (IEF).[169] This gel can then be loaded onto a conventional SDS-PAGE gel, ready to be separated by protein mass. The result are isolated protein

clusters found as spots on the gel. With a fluorescent probe added to the mix prior to isoelectric focussing, should provide fluorescently labelled spots on a gel.

The problem of background autofluorescence is of particular importance with analysing albumin depleted blood plasma protein which show notably high levels of autofluorescence. In a preliminary labelling experiment using DSP-**10**, it was seen that autofluorescence hides any targeted fluorescent bands from the dansylated organophosphate treatment.

Factor 13 is a transglutaminase enzyme that is responsible for cross-linking fibrin.[170] There is currently interest in organophosphates in targeting transglutaminases; a preliminary study using probe rho-alkyl SP **18** was carried out with the Hargreaves' group. The hypothesis was that using green light side lamps of the FLA-4000 gel doc or the green laser and 532 nm filter of the FLA-5000 will reveal any binding of blood serum proteins to the rhodamine probe, after incubating depleted blood plasma serum with rho-alkyl SP **18** and performing 2D-gel electrophoresis.

In collaboration with the Hargreaves' group, blood plasma serum was depleted of albumin following a known technique.[171] This was then incubated with rho-alkyl SP **18** on ice for 30 minutes then in an incubator at 37 °C for a further 30 minutes. After that, the general protocol for 2D gel electrophoresis was carried out (Figure 57, (A) and (B)).

Several clusters of proteins became visible due to the treatment, and there were no fluorescent proteins found on the control gels untreated with rho-alkyl SP **18**. However, these gels need repeating several times until consistent results illustrate the same patterns, it is a positive sign that the probe behaves as intended. The Hargreaves group currently pursues this work with the intention of processing 2D-gel spots and preparing for mass spec analysis to determine the identity of the proteins.

Within the remit of the current study of organophosphate interaction with mitochondria, a 2D experiment was also performed on a mitochondrial sample extracted from rat liver. Probe rho-PEG

long SP **49**, was incubated at a concentration of 100 µM with 80 µg of mitochondria extract in a buffered solution on ice. After 15 minutes of incubation, the sample then underwent the 2D-gel electrophoresis protocol. (See Experimental 5.3.9 for details).

Visualisation of the gel occurred using a 532 nm laser and a large – if faint – cluster of spots appeared around pI 4 – 6 and between 75 and 43 kDa. Staining with coomassie blue revealed all the protein clusters located in the gel (Figure 57, (C) and (D)).

Revealing protein spots under green light signifies probe binding with proteins associated with mitochondria. These gels still need repeating before the identity of the spots can effectively be determined. These spots can be picked out of the gels and digested, and prepared for analysis by mass spectrometry.
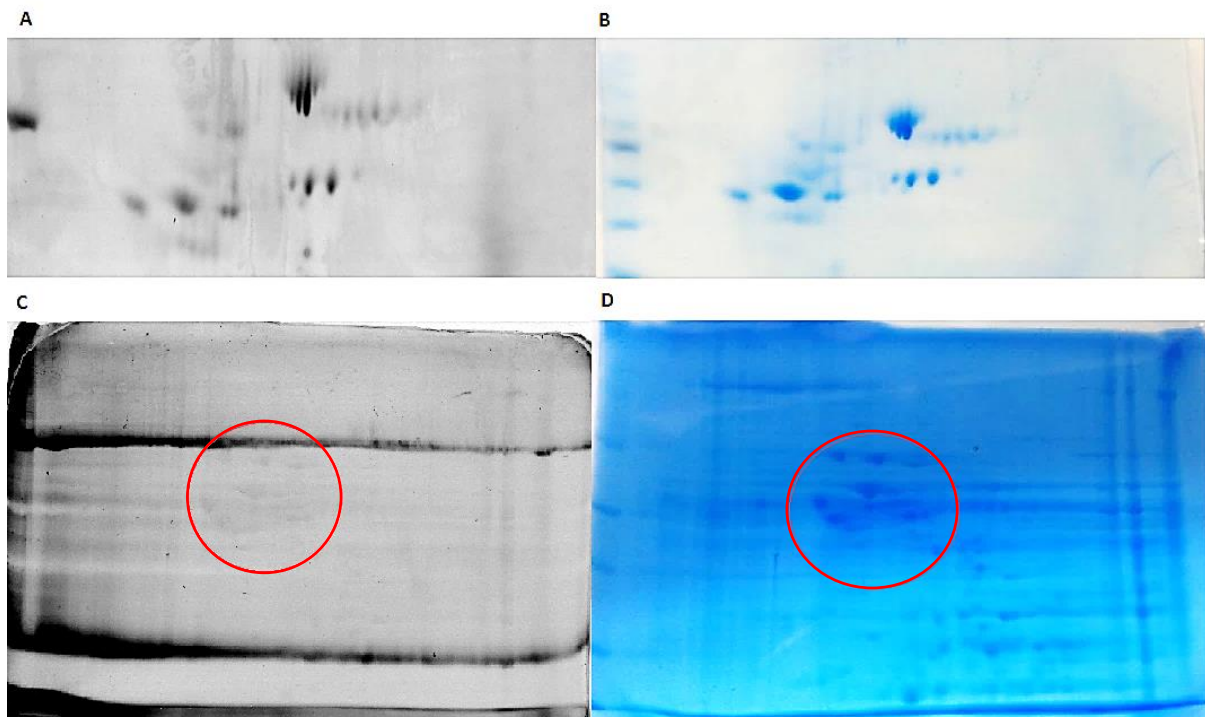
Figure 57. 2D SDS-PAGE gels. (A) Protein spots of 80 µg depleted serum albumin sample being revealed by 100 µM of probe rho-alkyl SP **18** after incubation, visualised on a green light laser at 532 nm. (B) Staining of the same gel by coomassie blue staining highlighting protein clusters (n=2). (C) 100 µM of probe rho-PEG long SP **49** bound to 80 µg of protein targets associated with mitochondria, visualised at 532 nm. (D) Coomassie stained gel of mitochondria and rho-PEG long SP **49,** highlighting many protein clusters (n=3).

The results of these gels are far from conclusive regarding probe efficacy. One fear is that the probes willingness to bind to a wide variety of free protein residues could yield it ineffective at revealing less abundant protein targets. However, as a test for the practicality of rhodamine as a fluorophore in labelling, it is appropriate for the task of 2D gels.

A final test of the probes efficacy was with a protease activity assay. Many enzyme activity assays are a part of the toolkit of biological analysis for proteomic studies. The performance of the probes within an activity assay can be measured colourimetrically by the inhibition of proteases.

3.2.12 Activity Assays

Proteases such as trypsin and chymotrypsin are a recognised organophosphate targets.[48] The binding of all three rhodamine B probes to chymotrypsin in the gel electrophoresis studies prove that there is still an affinity for the modified organophosphates to proteases (Figure 55).

One assay that could be used to determine the efficacy of not only trypsin protease inhibition, but the probes suitability for an array of colourimetric assays, was a trypsin activity assay that utilises a protein complex containing a fluorescent substrate.[172] Benzyl-L-arginine 4-nitroaniline hydrochloride (BAPNA), contains p-nitroaniline and is fluorescent at 415 nm, trypsin cleaves the amide bond between this and an arginine residue.

Incubating an organophosphate of different concentrations with trypsin on ice for fifteen minutes prior to addition of BAPNA should inhibit the action of trypsin cleavage on the substrate, resulting in a low reading of fluorescence on a plate reader.

A concentration of 25 µg/ ml of trypsin was chosen as the optimum concentration to be used to measure the rate of cleavage, determined via calibration trials (Figure 58). This trypsin solution was mixed with triplicates of six different probe concentrations and incubated on ice for fifteen minutes before the BAPNA solution was added as detailed in section 5.3.16. Readings were taken every minute for fifteen minutes.
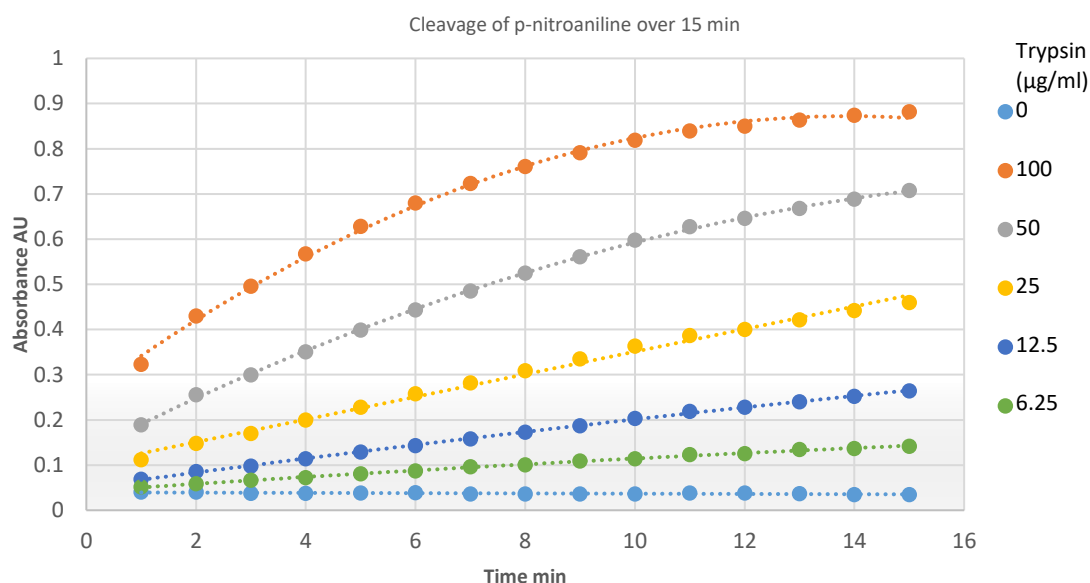
Figure 58. Action of trypsin cleavage on a solution of BAPNA substrate (1% (w/v) 10 µl/well), to cleave p-nitroaniline, at five different protease concentrations and a control solution lacking trypsin. The absorbance reading in arbitrary units (AU) measured at 415 nm on a standard plate reader, (n=3).

The results of the inhibitory action of the probe rho-alkyl SP **18** on trypsin show that the higher concentration of the probe, the higher the fluorescence (Figure 59). This is counter to the hypothesis that the higher the concentration of the probe, the more inhibition of trypsin, therefore, a lower fluorescence is exhibited. It is likely that the rhodamine B fluorophore interfered with the colourimeter reading. At high concentrations of the probe, fluorescence emitted by rhodamine B increased the absorbance reading at 415 nm. That was, until the concentration dropped below 12.5 µM of rho-alkyl SP **18**, this indicated that the measurement of fluorescence was not truly proportional to p-nitroaniline. The selectivity of the two fluorophores (rhodamine and nitroaniline) is not great enough to distinguish the two at concentrations over 12.5 µM.

Cleavage of p-nitroaniline inhibited with rho-alkyl SP **18** over 15min
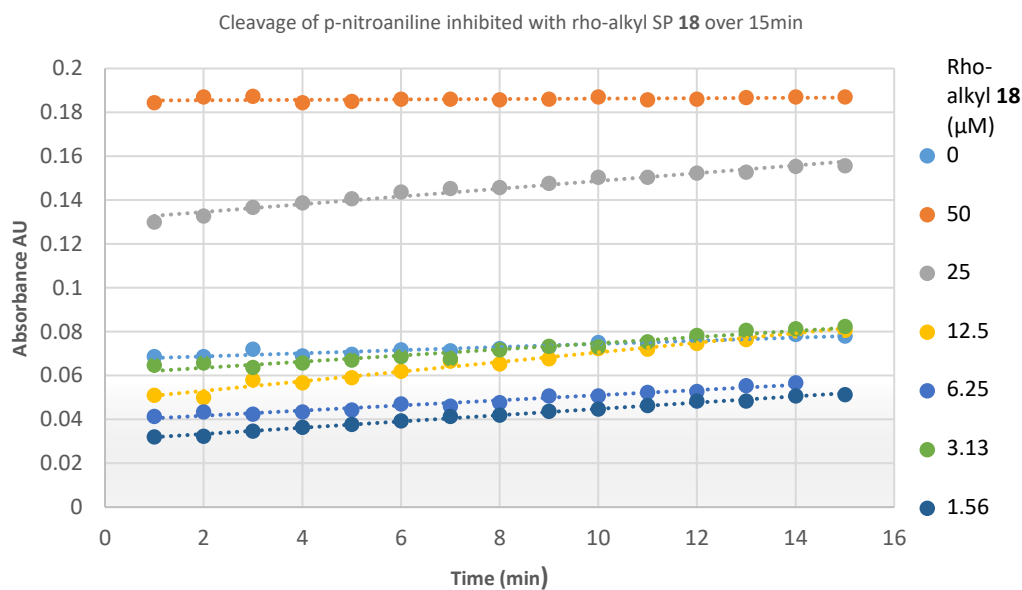
Figure 59. Action of trypsin cleavage on a solution of BAPNA substrate (1% (w/v) 10 µl/well), to cleave p-nitroaniline inhibited the presence of probe rho-alkyl SP **18** at six concentrations, absorbance measured in arbitrary units at 415 nm, (n=3).

Although this experiment is unreliable, calculating the gradient of each linear trend line for every concentration would have given the rate of substrate cleavage, and an overall trend for the inhibitory action of the probe could be seen. The rate units are in absorbance per minute at 415 nm and when plotted against concentration in µM gives an inhibition curve. Although, rhodamine B fluorescence increases absorbance results, invalidating the accuracy of measuring p-nitroaniline, the steepness of line still gave some information as to the trend in inhibition, albeit with a level of error.

Processing the gradients and plotting on a graph displayed that the control, with its absence of organophosphate, has an activity of 0.01 Abs /min, the activity of the following concentrations all drop below 5 $\times 10^{-3}$ Abs /min even when a concentration as little as 1.56 µM of inhibitor was added (Figure 60).
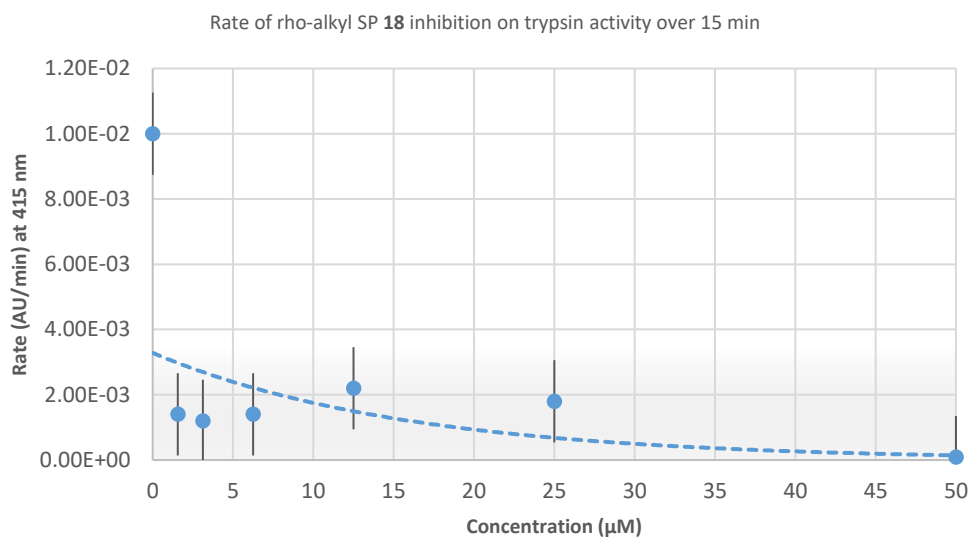
Figure 60. Mean rate of inhibition of probe rho-alkyl SP **18** vs concentration of probe in µM, error in SD.

This experiment was repeated for all three rhodamine B probes and using DSP-**10**. The results were plotted on a graph as absorbance against time, the gradient of each set of results was then plotted against concentration on one graph (Figure 61). The results of these calculations indicate that the organophosphate probes does inhibit trypsin activity. Probe rho-PEG short SP **48** had the least amount of inhibition, but compared to the control this was very high inhibitory effect vs trypsin cleavage.

The probes did not seem appropriate for any quantitative measure of inhibition in a colourimetric assay. As a qualitative measure of inhibition or trends in results the probes may be appropriate.
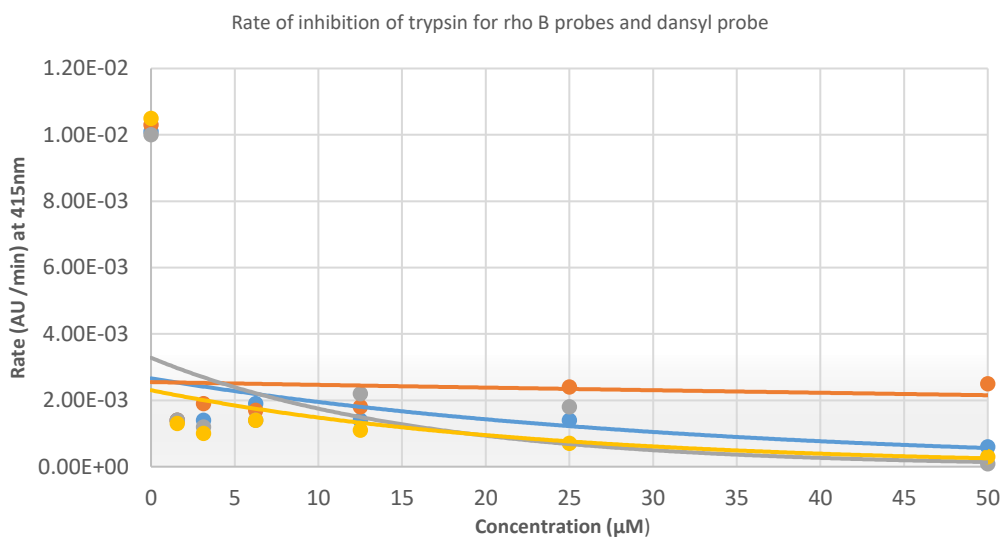
Figure 61. Mean rate of absorbance measured at 514 nm per minute of BAPNA cleaved vs concentration of organophosphate probe, error bars not shown for clarity. DSP-**10** is shown in yellow, rho-alkyl SP **18** in grey, rho-PEG short **48** in orange, and rho-PEG long SP **49** is illustrated in blue.

Following the investigations into biological efficacy of the rhodamine B organophosphate probes,

the two other families of fluorophores, BODIPYs and pyrenes were then explored.

3.3 Synthesis of BODIPY Probe

3.3.1 Background

As determined by fluorimetry studies, rhodamine B is ineffective with maintaining the bright

fluorescent properties of the open form, once an amide is incorporated on the 2 position. The best

choice of fluorophore in this system would be one that shares the red-shifted excitation /emission

properties, and high extinction coefficient (ε) and quantum yield (ϕ). A class of compounds known as

4,4-Difluoro-4-bora-3a,4a-diaza-s-indacene (BODIPY), have a high ε and ϕ, maintain their sharp

banded fluorescence in a variety of pH's and polarities, and are stable to different physiological

conditions.[173] Given their superior properties, the preparation of these fluorophores was then

explored.

Three asymmetric BODIPY analogues were the focus of this study (Figure 62). BODIPY FL –known for

its spectral similarity to fluorescein, BODIPY TMR – similar to tetramethyl-rhodamine, and BODIPY

558/568 are all commercially available, but due to expense, *de novo* synthesis was pursued. Each of

these BODIPY's possessed a carboxylate terminal side chain which was the site for coupling to a

linker. Coupling would have been achieved ideally, via an amide bond, as previously made with

rhodamine B.
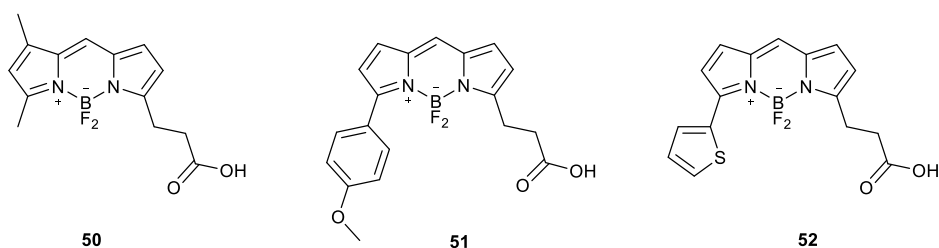
Figure 62. Structures of three BODIPY analogues; BODIPY FL **50**, BODIPY TMR **51**, and BODIPY 558/568 **52**.

BODIPY FL is a green shifted fluorophore, with an overall neutral charge that aids practical

measurements of biological systems where cellular charge is highly sensitive. It is a bright

fluorescent green, equivalent with fluorescein and exhibits a high extinction coefficient and

quantum yield of ε = 80000 and ϕ = 0.97.[174]

For future applications it would also be desirable to achieve a large stokes shift in excitation and

emission in the orange/ red region. Two bright, red-shifted BODIPY analogues that met the criteria

were; BODIPY TMR and BODIPY 558-568, (Figure 62).

BODIPY TMR gets its name from its spectral similarity to tetramethylrhodamine (TAMRA). They both

have the same excitation and emission wavelengths ex. 553 nm and em. 576 nm. [175] The BODIPY

TMR absorbance is 542 nm, emission of 574 nm and an ε of 60,000. The higher quantum yield of

BODIPY TMR, ϕ = 0.95 gives it an advantage over rhodamine's yield of ϕ = 0.68. Its use biologically, is

effective due to its overall positive charge and fatty properties, meaning it permeates membranes

effectively. [176]

BODIPY 558/568 has been used in biological testing in experiments that looked into endothelial

lipase activity. It was used for its bright red-shifted emission and for the fatty properties it has when

bought at high expense with a dodecyl linker connected.[177] BODIPY 558/568 has an extinction

coefficient of 97000 and a quantum yield of ϕ = 0.8. This confirms that both BODIPY's are brighter

dyes than the previously used dansyl amide (extinction coefficient of ca. 4300, quantum yield 0.66).

The synthesis consists of using the previously prepared pyrrole-2-ethyl propanoate, and a pyrrole

thiophene prepared from a synthetic route based on Dale *et al* synthesis of BODIPY 630.[178]

The synthesis of asymmetric BODIPY is generally made by coupling two pyrrole moieties and *in situ*

insertion of the boron centre. The synthesis that was proposed is set out below (Schemes 18 and

19).[175,179]
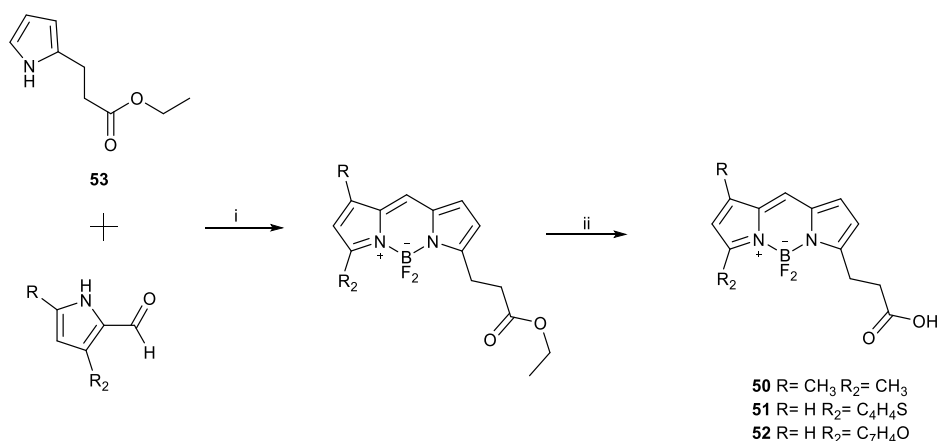
Scheme 18. Synthesis of BODIPY, (i). BF$_3$.ethereate, POCl$_3$, DIEA, DCM, (ii). THF, 33% HCl, water, 48h.

Following preparation of the BODIPY carboxylic acid analogue, just as with the rhodamine B

methodology, linker coupling reactions followed by saligenin chlorophosphate addition, would

finalise synthesis of the probe (Scheme 19).
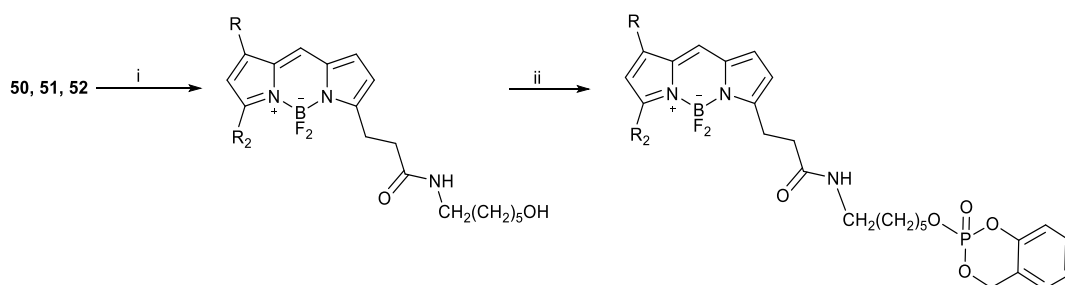
Scheme 19. (i). 6-aminohexanol, DCC, TEA, DCM, (ii). TEA, saligenin chlorophosphate, DCM.

3.3.2 Synthesis of Pyrrole-2-ethyl Propanoate

The synthesis of all three BODIPY analogues started with pyrrole-2-propan ethanoate **53**. The pyrrole

analogue was synthesised by Wittig reaction with pyrrole carboxaldehyde and

triethylphosphonoacetate. 1.1 equivalents of n-BuLi was added to the phosphonoacetate at -78°C,

then pyrrole carboxaldehyde was added and stirred at 0°C for 2h before being allowed to warm to

room temperature and left overnight. After work-up and evaporation the acrylate **55** was yielded as

a yellow oil.

A reduction of the conjugated double bond in methanol with hydrogen at atmospheric pressure on palladium and activated charcoal then followed. After 2 days at room temperature the dark oily ester was isolated in a yield of 78%, and with an acceptable level of purity (Scheme 20).[180]
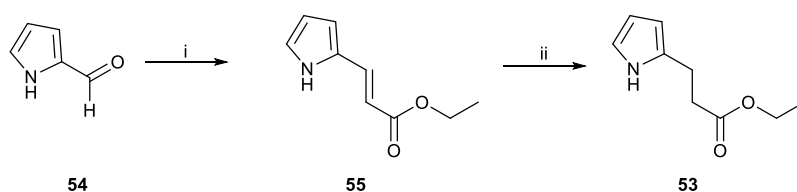
Scheme 20. (i). n-BuLi, triethylphosphonoacetate, DCM, (ii). H_2, Pd/cat, Methanol, 72 h.

This experimental work synthesised the first half of a BODIPY structure. This half was expected to be coupled to a linker following deprotection of the ethyl ester, after formation of the BODIPY core structure.

3.3.3 Carbonylation of Pyrrole

Synthesis of 5-carboxy-2,4-dimethylpyrrole commenced with carbonylation of 2,4-dimethyl pyrrole giving compound **57** (Scheme 21). This proceeded via addition of $POCl_3$ into DMF at 0 °C, then 2,4-dimethylpyrrole was added and the mixture refluxed. A solution of NaOAc in water was added and the mixture refluxed again for 30 minutes further. Work-up and column chromatography with ethyl acetate gave the product in a good yield of 70%.
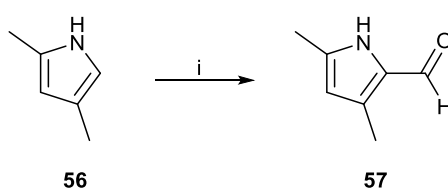
Scheme 21. (i). $POCl_3$, NaOAc, DMF, DCE, 0°C, reflux, H_2O

3.3.4 Formation of BODIPY FL

The next step was to couple both pyrrole halves to form BODIPY FL **50** (Scheme 22).

Coupling of these two compounds with POCl₃ then addition of the BF₂ centre in a two-step one pot reaction gave the BODIPY core structure. Hydrolysis of the ester group yielded BODIPY FL.
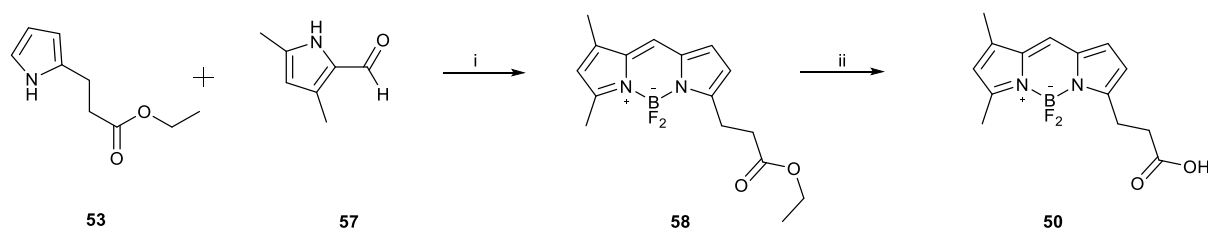
Scheme 22. (i). BF₃.ethereate, POCl₃, DIEA, DCM, (ii). THF, 33% HCl, water, 48h

One equivalent of each half was added with POCl₃ and cooled to 0 °C. The solution turned dark and was left reacting for 2 h. Following this, BF₃.OEt₂ and DIPEA was then introduced into the mixture and addition of the BF₂ centre was complete. The solution fumes on addition of boron trifluoride and turned a dark green. Column chromatography with DCM gave a 52% yield of red crystals.

The acid hydrolysis of the ester was then performed. BODIPY **58** was added to THF, water and HCl. After stirring for a few days this compound was worked up and purification occured on silica with DCM and a 0-5% methanol gradient with a yield of 34%.

Both the initial coupling reaction to give the BODIPY core structure and the ester hydrolysis were low yielding (52% and 34%), so the synthesis was repeated several times to build up enough material to attempt to couple the 6-aminohexanol linker.

3.3.5 Synthesis of 2,4-Dimethyl Pyrrole Dimer

Interestingly, the first eluted fractions in the BODIPY ester purification fluoresced bright green and after analysis it was found to be a 2,4-dimethyl pyrrole dimer **60**, in a yield corresponding to 7% of the crude weight. ^{1}H NMR matched the data from previously synthesised sources (Scheme 23).[181]
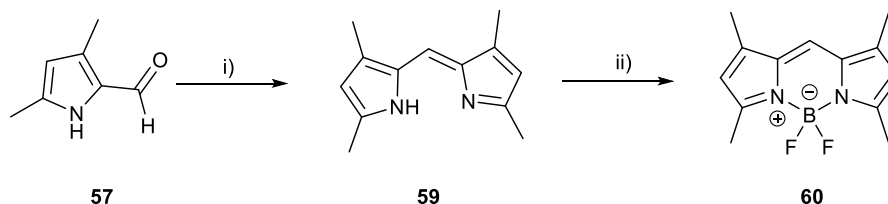
Scheme 23. Synthesis of symmetrical BODIPY dimer, (i). POCl$_3$, CH$_2$Cl$_2$, 25°C, 12h. (ii). BF$_3$.OEt$_2$, Et$_3$N, CH$_2$Cl$_2$, 25°C, 12h.

The by product is plausibly derived from formation of an imidoyl chloride from one pyrrole carboxaldehyde. Which is then attacked by a second pyrrole carboxaldehyde. Elimination of the chloride via formation of carbon monoxide yielded the dipyrromethenium cation which the gives the pyrrole dimer **59** (Figure 63).
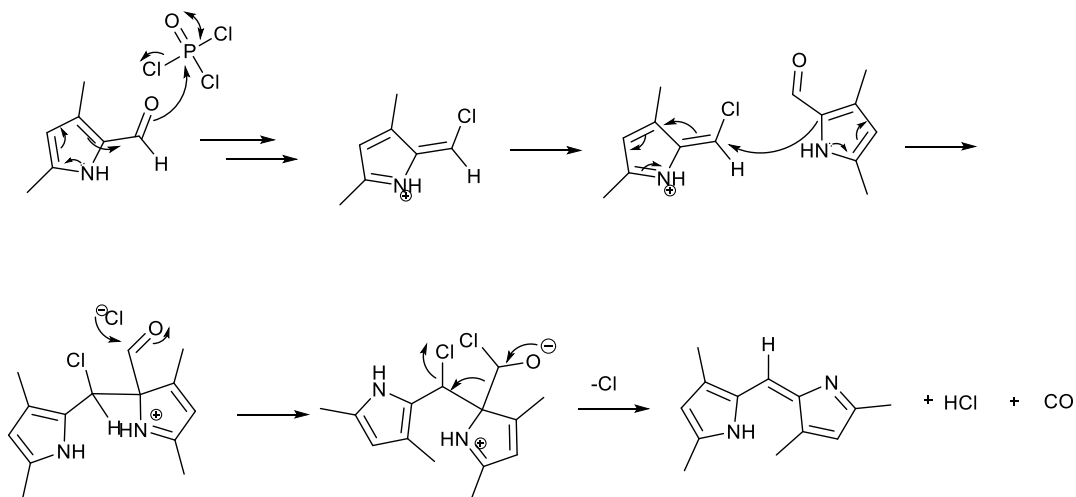
Figure 63. Proposed mechanism for dimerization of pyrrole.

The dimer **60** may be explored in future work, to investigate the possibility of attaching a linker to the 4 position of the BODIPY. However, for more BODIPY FL to be made on a larger scale commercial 2,4-dimethyl pyrrole is expensive, so synthesis was examined.

3.3.6 Synthesis of 3,5-Dimethyl Pyrrole

The literature synthesis of this pyrrole proceeded via oxidative condensation of amino keto acid **61** and ethyl acetate **62** (Scheme 24).[182]
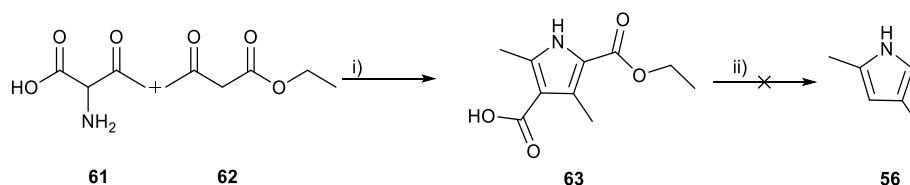
Scheme 24. Knorr pyrrole synthesis for 2,4-dimethylpyrrole.[183] (i). NaNO$_2$, AcOH, Zn, 3 h, 0 °C (ii) KOH, H$_2$O, 1 h, reflux.

Closely following the literature procedure resulted in a poor yield due to the difficulty in controlling the reaction temperature when adding the zinc. The intermediate **63** once formed was also extremely sensitive to both air and light, this called for the reaction and work-up to progress in the dark. These factors meant that the intermediate was not synthesised in high yield or purity (40%), due to the tendency to decompose rapidly. The decarboxylation step only gave minor amounts of the dimethyl pyrrole which was lost during column purification. It was decided that further pursuit of this compound was uneconomic.

The difficulties with this synthesis led the investigation to examine optimisation of the low yielding steps in BODIPY synthesis; primarily the hydrolysis of the ester group.

3.3.7 Ester Hydrolysis of BODIPYs

Synthetically, ester hydrolysis of the BODIPY was limited to acid catalysed hydrolysis, since strongly basic conditions and nucleophilic reagents lead to decomposition of the BODIPY core structure.

Under the literature conditions used, hydrochloric acid in THF, it was observed that n-chlorobutanol was produced as a side product, which could not be removed by column chromatography (Scheme 25).
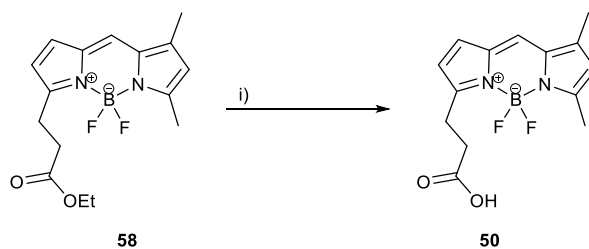
Scheme 25. Reaction for acid catalysed hydrolysis of ethylester BODIPY FL. (i). Acid, miscible solvent mix, e.g. dioxane, THF.

In order to avoid this side reaction a range of different concentrations of acids in dioxane was trialled, as dioxane is generally considered to be more stable in acidic conditions; sulphuric, hydrochloric, and polyphosphoric acids were used. Treatment of BODIPY ester **58** in dioxane with either of the acids 30% in a solution with water at room temperature for 48 hours gave BODIPY acid **50**.

All acids successfully hydrolysed the ester group, though none of the reactions progressed cleanly, or in a high conversion. Subsequent purifications of the reaction mixture led to decomposition. None of the dioxane reactions offered any improvement over the original THF mix, with 30% HCl in water and optimisation of the reaction remains unresolved.

3.3.8 Optimisation of Purification Conditions

The purification of the hydrolysis reaction mixture was then explored. Standard conditions for elution of this polar dye was to elute from silica with DCM/ MeOH mixture. It was discovered that the fluorophores decompose on contact with methanol as the boron centre can undergo substitution reactions.[184] Groves *et al* reported the synthesis of a BODIPY with a dimethoxy boron centre, with unsubstituted pyrroles but the reaction did not progress without being heated in the presence of NaOMe. [185] The products of that reaction were highly unstable and decomposed rapidly.

During column purification, the eluting solvent was a 1% mix of methanol in DCM, and it is believed that methanol in this mix contributed to the low yielding purifications and the decomposition of compounds.

116

Solvent studies were then performed, to get the same solubility and polarity required for effective

elution of the BODIPY acid. The following solvent mixes were tested (Table 3).

Solvents	Ratio	Results
DCM /acetone	1:1	Poor separation
DCM /THF	1:1	Smeary separation
Ethyl acetate /acetonitrile	9:1	Good separation on TLC, poor solubility inhibits higher scale
DCM /acetonitrile	9:1	Good separation
THF /acetonitrile	9:1	Good separation but smeary
DCM /acetonitrile	1:1	Good separation, too much dead space

Table 3. Table showing results of solvent analysis on column chromatography.

A 9:1 mix of DCM in acetonitrile was then chosen as the optimised solvent mix for eluting the

BODIPY acids in the following reactions. With the purification conditions refined, enough BODIPY FL

could be brought through to coupling experiments. Note that these experiments were done on a

small scale as the reactions leading up were still low yielding. Synthesis then progressed onto

coupling attempts of BODIPY FL with 6-aminohexanol.

3.3.9 Coupling of BODIPY FL with 6-Aminohexanol
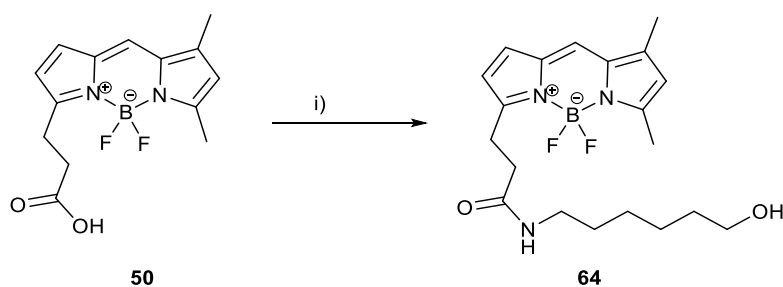
Scheme 26. Amide coupling reaction with BODIPY FL. (i) Coupling agent, TEA, 6-aminohexanol.

Despite difficulties with the efficient preparation of BODIPY FL acid **50,** coupling attempts to the

amino linker commenced. Several coupling methods were examined without success. Treatment of

acid **50** to isobutylchloroformate and base to generate a putative mixed anhydride, followed by

addition of 6-aminohexanol afforded a complex mixture. Traditional peptide coupling using N,N'-

dicyclohexylcarbodiimide (DCC) with catalytic DMAP added to BODIPY FL and TEA. Followed by 6-

aminohexanol gave a messy spectrum of ^{1}H NMR peaks. Chromatography of the mixture did not afford the amide (Scheme 26). Close examination of the ^{1}H NMR showed the BODIPY peaks accompanied with three distinctive multiplets at 1.50, 1.65 and 1.84 ppm, these were thought to belong to DCC. This means that either DCC elutes at the same fraction as the BODIPY, or it has not been substituted by the amide.

3.3.10 Coupling of BODIPY FL N-Hydroxysuccinimide

BODIPY dyes activated as a hydroxysuccinimide are commercially available at high cost, (BODIPY **66**). The synthesis of this activated compound was examined using DCC, N-hydroxysuccinimide and catalytic DMAP (Scheme 27). This ^{1}H NMR spectrum of the crude reaction mixture suggested that only a trace amount of hydroxysuccinamide ester was formed.

50   Trace **66**
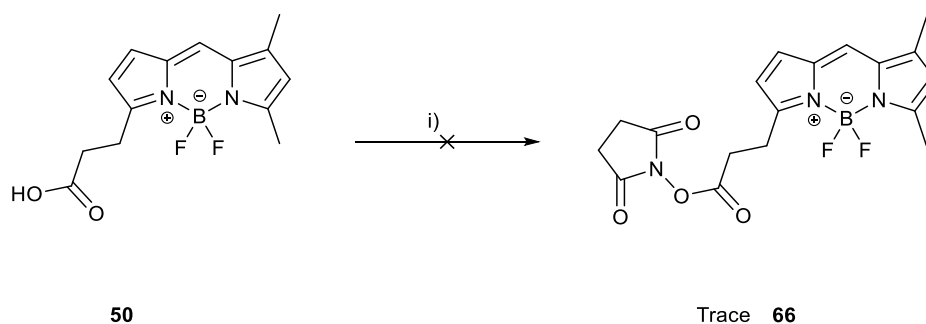
Scheme 27. (i). DCC, DMAP, N-hydroxysuccinimide, TEA, CH_2Cl_2, 24h.

3.3.11 Coupling with T3P and CDI

Coupling of BODIPY FL to 6-aminohexanol using T3P and CDI was also examined. Treatment of BODIPY FL acid **50** with TEA, and either T3P 50% in ethyl acetate, or CDI followed by addition of 6-aminohexanol returned only the starting material.

3.3.12 Synthesis of BOIDPY TMR and BODIPY 558-568

Since the functionalisation of BODIPY FL was proving problematic and time consuming, the preparation of two other BODIPY dyes was examined, in the hope that the steps to final compound

would be more successful. It was envisaged that BODIPY TMR **51** and BODIPY 558/568 **52** might also be more stable to purification, and result in higher yields of product.

The synthetic methodology of fabricating these two BODIPY, used the pyrrole propanoate right hand side pyrrole, to be converted to the acid for coupling reactions. The other pyrrole was synthesised from a starting acyl chloride forming an amide on addition with allyl amine. A pericyclic rearrangement formed the pyrrole, then carbonylation of the pyrrole followed this, as seen with 2,4-dimethylpyrrole synthesis.[175]

Synthesis of red-shifted BODIPY **51** and **52** started with the respective acyl chloride for each final compound, 4-methoxybenzoyl chloride **68**, or 2-thiophenecarbonyl chloride **69**. Allylamine and pyridine were added at 0 °C to the mixtures in dry DCM. Following aqueous work-up, the concentrated residues could be purified by addition of hexane. The product made an immiscible layer underneath, which with gentle heating turned the hexane layers cloudy with reaction impurities and the oil at the bottom could be extracted via pipette.

The crude isolates extracted this way required no further purification and gave yields of 72% for allyl amide **69**, and 57% for compound **70** (Scheme 28).
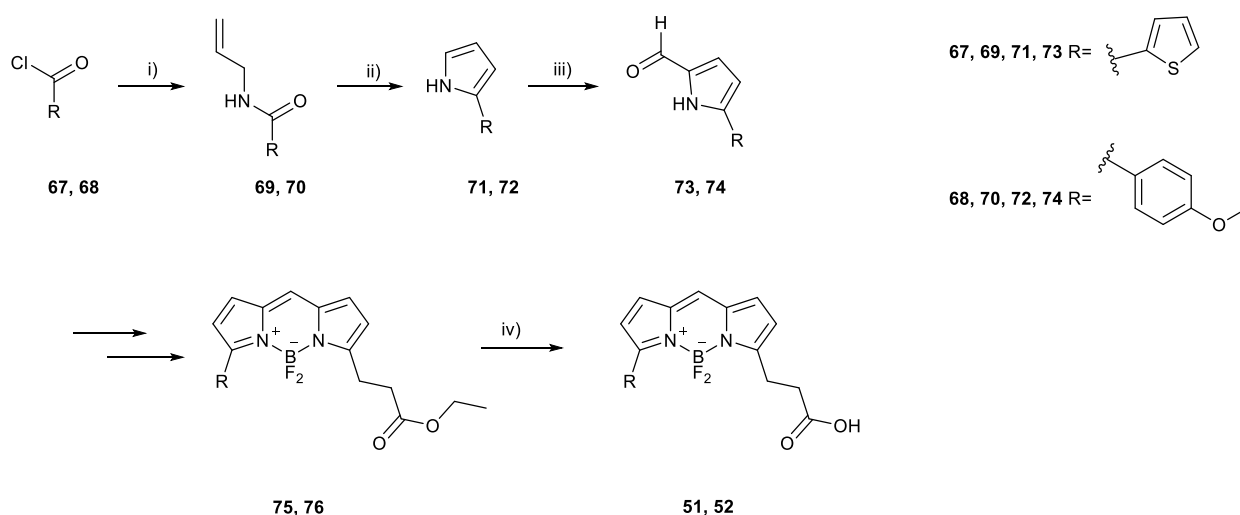
Scheme 28. (i). Allyl amine, dry DCM, pyridine, 0°C, 4h. (ii). Phosgene, cat. DMF, Toluene, -78°C, 12h, K^+ t-BuO, THF, 0°C, 1h. (iii). $POCL_3$, DCE, reflux, 1h, NaOAc, reflux, 1h. (iv). 30% HCl, dioxane, H_2O, 48 h.

Allyl amides were then converted to imidoyl chloride intermediates followed by base promoted ring closing rearrangement. Imidoyl chlorides were formed from phosgene and the amides **69** and **70** at - 78 °C in toluene and catalytic DMF over 12 hours. The solvent was then removed and the mixture dissolved in THF, cooled to 0 °C and three equivalents of sodium *tert*-butoxide were then added. The rearrangement was then left for 30 minutes.

After work-up, these products needed to be purified immediately by column chromatography and due to the instability, the electron rich pyrroles were used in the next reaction straight away. The yields of the pyrroles were 61% for the paramethoxybenzyl pyrrole **71**, and 69% for thiophene pyrrole **72**.

The substituted pyrroles were carbonylated by treatment with freshly prepared Vilsmeier reagent in a similar fashion to the dimethyl pyrrole in section 3.3.3. The paramethoxybenzyl pyrrole-2-carboxaldehyde **73**, as a yellow oil in 66% yield after column chromatography. The thiophene pyrrole **74**, was obtained as yellow diamond shaped crystals in 30% yield after chromatography.

 (Chloromethylene)dimethyliminium chloride is the intermediate iminium cation formed from DMF and $POCl_3$. Known as Vilsmeier reagent,[186] it can be bought cheaply with the idea of increasing the reaction yield of the carbonylation step. Two equivalents of the reagent were added to DCE and refluxed with the pyrrole, before being cooled and the water sodium acetate mix then being added brought up to reflux again. After work up and purification the yield was ca. 40%. This was less than the yield following the original technique, so further use of this reagent was abandoned.

Pyrrole **53** was used as one half of the BODIPY core structure. The coupling of the two halves together and adding the boron difluoride centre, commenced as in section 3.3.4 (Scheme 22). The yields were 39% and 28% after purification with DCM and acetonitrile for the ethyl ester protected derivatives of BODIPY TMR **75** and BODIPY 558/568 **76**.

Deprotection in dioxane, hydrochloric acid and column chromatography yielded the two red

BODIPY's, 28% for BODIPY TMR **51** and 36% for BODIPY 558/568 **52**. The low yields of the ester

hydrolysis were comparable to BODIPY FL, and the synthesis of these two red-shifted BODIPY were

no more efficient in time or yields, than synthesis of BODIPY FL. Coupling reactions were to be

attempted with the purified BODIPY acids.

3.3.13 Coupling of BODIPY TMR and 558/568 with Linker

Coupling of BODIPYs **51** and **52** to 6-aminohexanol were explored. None of the other previously

trialled coupling compounds gave the desired amide in reactions with BODIPY 558/568 **52**. T3P and

HBTU resulted in an impenetrable mess of peaks when analysed by ^{1}H NMR. This was the case even

after extensive efforts to purify the mixture by column chromatography and clean product could not

be obtained. CDI returned starting materials for both BODIPY TMR **51** and BODIPY 558/568 **52**. HBTU

with BODIPY TMR **51**, as with the reaction with BODIPY 558/568 **52**, gave a spectrum from which it

was too difficult to determine the outcome.

In one experiment coupling of BODIPY TMR **51** was achieved, using T3P 50% DMF, TEA, dry DCM.

The scale was small, and the yield also very low (10%). ^{1}H NMR indicated formation of product **77**

(Figure 64). The multiplet of peaks associated with the 8 central CH_2 were present at 1.1 – 1.5 ppm.

The terminal CH_2 associated with NHC=O and OH were also present indicating the presence of bound

6-aminohexanol.
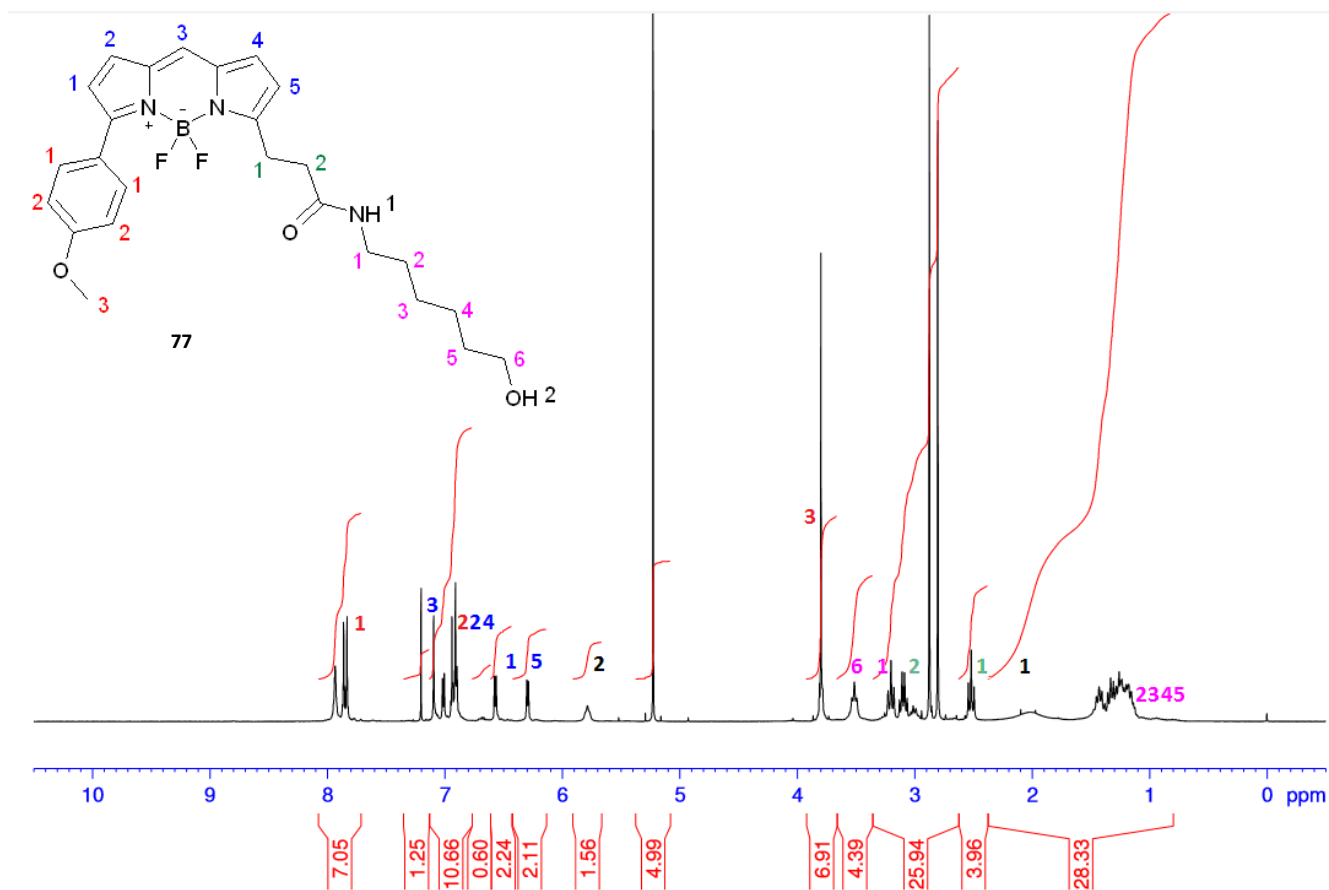
Figure 64. Product **77** of coupling 6-aminohexanol to BODIPY TMR **51** via T3P in DMF. Coloured numbers refers to hydrogen environments around the molecule, and the corresponding peaks in the spectrum.

Due to the difficulties with synthetically low yields, and difficulties with purification of asymmetrical BODIPYs, the research was not pursued further. A third fluorophore was explored; one that was cheaply commercially available.

3.4 Pyrene Probe

Schofield *et al* developed a photoreactive fluorescent probe incorporating a red-shifted analogue of pyrene **78**. They used a photon mediated aryl azide that irreversibly transformed into a nitrene[187] moiety as part of the photoaffinity probe, and a sulphonamide selectivity function known to target human carbonic anhydrase II (HCA II) (Figure 65).[188] Incubation with the HCA II followed by irradiation and gel purification gave a bright red fluorescent band in the expected region under UV. MALDI-TOF mass spectrometry then proceeded to yield the thee proteins containing the modified protein residue that was expected.

78
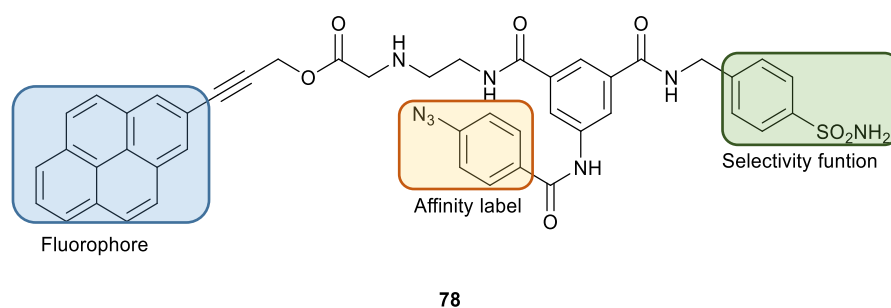
Figure 65. Structure of HCA II probe utilising arylazide photoaffinity probe, and pyrene fluorophore.

As the use of pyrene as fluorophore has already shown success in these experiments, the fluorophore was therefore deemed appropiate for use in this study on myocardial cells.

3.4.1 Background

To further understand the properties of fluorescence within our system and to continue probing for organophosphate targets, two new probes featuring alkyl chains of different lengths connected to pyrene will be synthesised. Studies into this class of fluorophore hope to shed light on the fluorescence reducing issues found with the rhodamine equivalents and their interaction with organophosphates. Although rhodamine quenching is currently attributed to being in an equilibrium between open and closed states, if the pyrene fluorophores emission is significantly reduced, then forms of resonance energy transfer may still be occurring. It is also expected that the synthetic stability issues found with BODIPY's will not be prevalent with pyrene compounds.

Pyrene and its analogues can be bought for little expense; it is relatively bright with an extinction coefficient of $\varepsilon = 54000$ and a quantum yield of $\phi = 0.32$ in cyclohexane.[189] Pyrene butanol, and pyrene butyric acid are the starting compounds of interest and excite and emit at 341 nm and 376 nm in methanol respectively (Figure 66).[190]
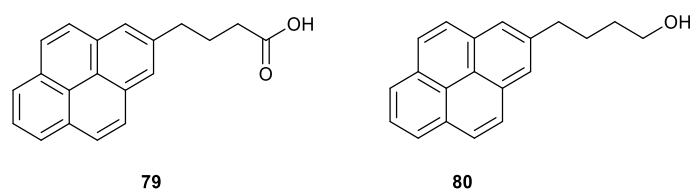
Figure 66. Structure of pyrene butyric acid **79**, and 1-pyrene butanol **80**.

3.4.2 Coupling of Pyrene to a Linker

The first strategy employed was to determine if pyrene butanol **80** could be extended with 8-chloro-1-octanol (Scheme 29), the alcohol end being used to complete the phosphate centre of the organophosphate probe. This was attempted with the presence of sodium hydride in DMF with 15-crown-5 added, and heated to 80 $^{\circ}$C for 12 h.
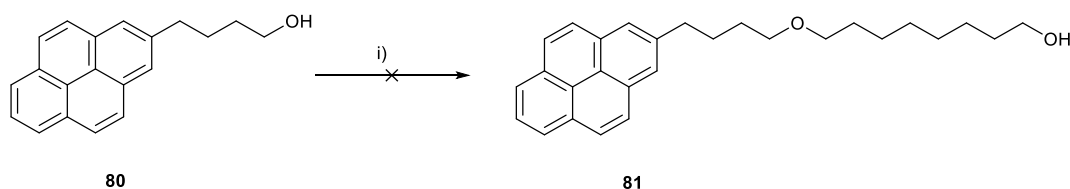
Scheme 29. (i) 8-chloro-1-octanol, 2x NaH, dry DMF, 15-crown-5, heat.

After work-up with LiCl to remove DMF, and extraction with ethyl acetate, crude ^{1}H NMR was performed. This indicated that unreacted pyrene butanol was returned.

The second attempt was to create a tosylate intermediary compound which would then be displaced by the alcohol yielding a hexanol ester. The 6-hydroxyhexanoic acid, TsCl, and TEA were placed into CH$_3$CN with some catalytic DMAP and cooled to -5 $^{\circ}$C for 30 minutes. Following this, the pyrene butanol in CH$_3$CN was added by syringe and the flask was warmed to room temperature and left for 2 h (Scheme 30).

124
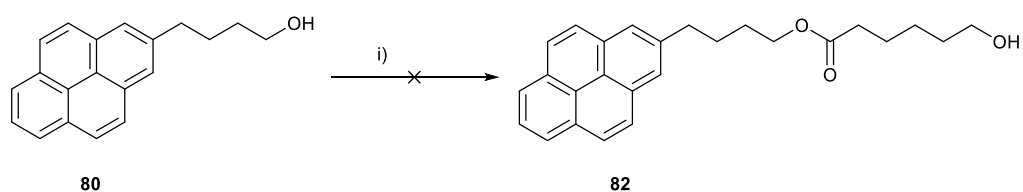
Scheme 30. (i) 6-hydroxyhexanoic acid, TsCl, DMAP, TEA, CH3CN, -5oC, then add pyrene butanol and warm at 25oC 2h.

After work-up, the crude ^{1}H NMR looked promising however, purification with ethyl acetate yielded two fractions; one fraction seemed to suggest that the tosyl group adds to the butanol chain of the pyrene. This was assumed as the spectrum between 7.6 - 8.2 ppm became a mess of peaks with a large integral comparatively to CH$_2$ of the alkyl chain. The methyl group associated with the tosyl is a distinctive singlet peak at 2.33. The second fraction returned only starting pyrene butanol.

Due to the difficulty of synthesising a long pyrene PSP probe using an alcohol moiety, pyrene butyric acid **79** was used as the starting analogue and utilising the same methodology for synthesising the rhodamine linker analogues, a mixture of HBTU and TEA in dry DCM was employed (Scheme 31).
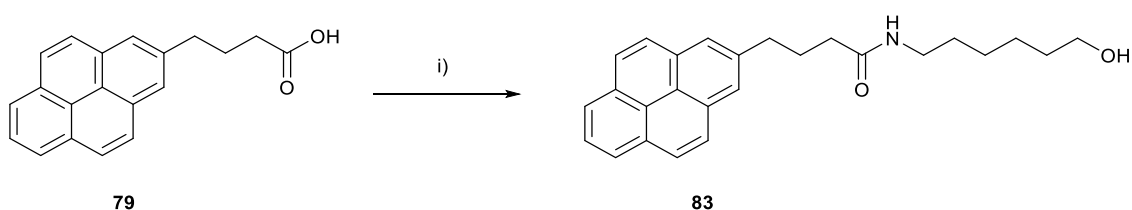
Scheme 31. Synthesis of 6-hydroxyhexyl pyrenebutamide using (i). HBTU, 2xTEA, 6-aminohexanol, dry DCM, at 0 °C, 12h.

After work-up and column chromatography the fraction containing the fluorescent pyr-alkyl **83** which was collected and characterised by ^{1}H NMR, ^{13}C NMR, MS, IR, MP and fluorimetry. The product was a pale yellow crystalline solid with 78% a yield.

3.4.3 Synthesis of Long Pyrene Organophosphate Probe

With the synthesis of the pyrene butamide linker pyr-alkyl **83** completed, synthesis then moved to

the formation of a pyrene organophosphate probe (Scheme 32). This was achieved in the same

fashion as with the rhodamine organophosphate probes in section 3.2.3. A cooled solution (-78 °C)

of pyr-alkyl **83** with TEA had freshly prepared saligenin chlorophosphate **45** solution added dropwise

and left to warm up over 12 h. After work-up crude ^{1}H NMR showed the presence of the

characteristic ABX splitting pattern at 5.24 and 5.72 ppm. Following column chromatography a yield

of 42% was given for pyr-alkyl SP **84**, ^{31}P gave a single peak at -8.79 illustrating a fully oxidised

phosphate centre.
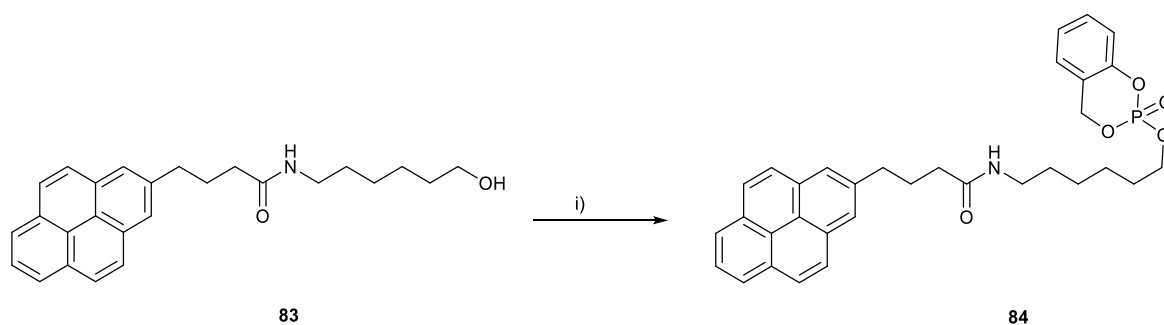
Scheme 32. Synthesis of 6-saligeninphosphatehexyl pyrenebutamide. (i). PSPCl, 2x TEA, dry DCM, -78°C, 12h.

3.4.4 Synthesis of Short Pyrene OP Probe

Creating a short PSP probe was simply a matter of mixing pyrene butanol with TEA and adding

freshly prepared saligenin chlorophosphate **44**, dissolved in dry DCM dropwise at -78 °C and allowed

to warm to room temperature over 12 h (Scheme 33). Work-up and column chromatography with

ethyl acetate then yielded probe pyr-SP **85** 24% product as a yellow oil, with characterisation made

by ^{1}H NMR, ^{13}C NMR, ^{31}P NMR, MS, IR, and fluorimetry.
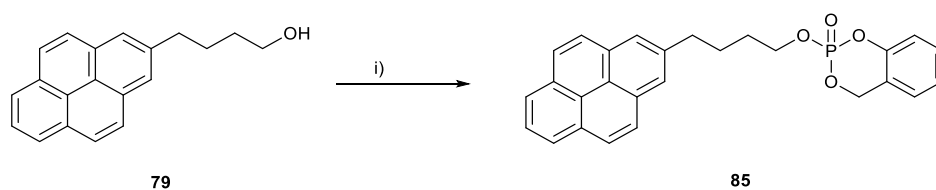
Scheme 33. Synthesis of 4-saligeninphosphatebutyl pyrene. (i). PSPCl, 2x TEA, dry DCM, -0°C, 12h.

3.4.5 Fluorimetry of Pyrene Probes

The absorbance and emissions were measured following the technique described in experimental

section 5.2.5. Firstly, the absorbance of pyrene butanol **79** starting material was measured. The

second highest peak of absorbance was at 326 nm. This was the chosen excitation frequency used

for the rest of the fluorescence measurements on the two pyrene organophosphate probes pyr-alkyl

SP **84** and pyr-SP **85**. This was to avoid saturation of the detector without having to adjust the

emission and excitation slits width between the analogues. The slit width for both emission and

excitation measurements was set to 5 nm, with a scan rate of 600 nm /min.

The results of both excitation and emission measurements showed a drop in both absorbed and emitted light with the addition of saligenin phosphate **44** (Figure 67). The starting material was in a concentration of 100 nM, whereas the probes were 100 times more concentrated at 10 µM. The probe pyr-alkyl SP **84** featuring the furthest distance between the organophosphate and pyrene, was brighter than the short butanol probe pyr-SP **84**, though this was only true up to 468 nm.

This led to the most interesting effect observed, which was the red-shifted peak found for these probes; a large emission of light in the red region of the spectrum. This, compared to the starting material pyr-butanol **79** shows that the 350 – 425 nm region dropped significantly.

The short probe pyr-SP **85** emitted slightly more in this red shifted region than probe pyr-alkyl SP **84**. This effect was due to aggregation of the probes in water. At high concentrations pyrene forms aggregates where π-π interactions between the rings of delocalised electrons can exchange energy.[191] The aggregate energy exchange results in a wavelength red-shift for the emission energy, increasing the intensity of emission.

The effect has been used in the design of composite materials with spectral properties and biological sensors. One example of this is with the peptide nucleic acid probes (PNA).[192] Pyrene units are introduced synthetically on to a PNA strand. These strands are complimentary to a specific gene, for example a mutated cystic fibrosis transmembrane conductance regulator (CFTR) gene. When hydrogen bonding to a specific matching base pair occurs, the pyrene units overlap and red-shifting can be measured by fluorescence.
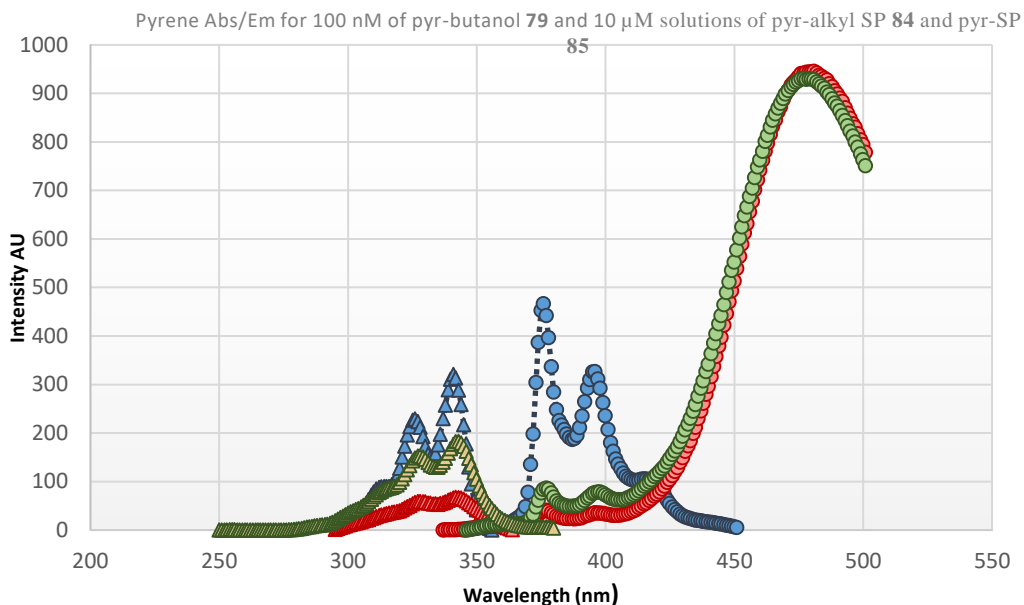
Figure 67. Fluorimetry graph displaying the absorbance (triangles) of 100 nM of pyr-butanol **79** (shown in blue), 10 µM of probes pyr-alkyl SP **84** (shown in green) and pyr-SP **85** (shown in red), and the emission (circles) of light for each compound at 326 nm. Fluorescence measurements were made using a 1 cm^3 fluorimetry cuvette (n=3); with each probe dissolved in distilled water, pH of 7.5.

The next fluorimetry experiment set out to explore how concentration effected the aggregation of the pyrene probes in water. Three concentrations of each probe were investigated: 100 nM, 1 µM and 10 µM, whilst irradiating at 326 nm.
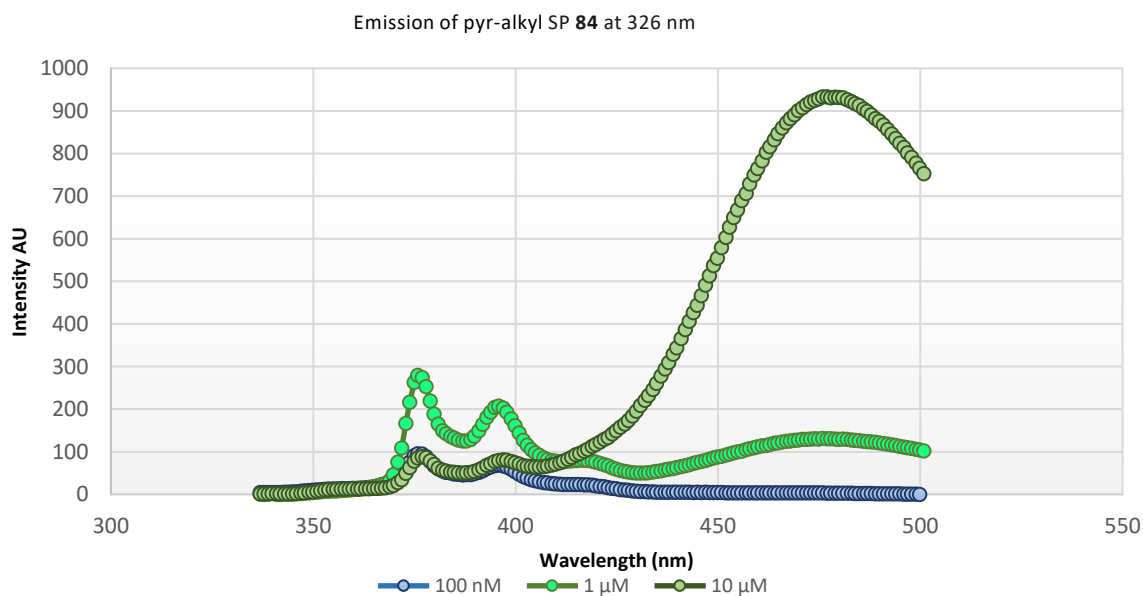
Figure 68. The effect of concentration of pyrene probe pyr-alkyl SP **84** on red-shifted emission. Fluorescence measurements were made using a 1 cm^3 fluorimetry cuvette (n=3); with each probe dissolved in distilled water, pH of 7.5.

The emission spectra of probe pyr-alkyl SP **84**, illustrates that 100 nM is too low a concentration for red-shifting to occur for this probe in water (Figure 68). At 1 µM red shifting starts to occur, but between 350 – 425 nm the curve shape still resembles the starting material, pyr-butanol **79**. At 10 µM red shifting becomes the dominant wavelength for fluorescence emission, and a large amount of light is released.

This experiment was repeated for the pyrene probe pyr-SP **85** (Figure 69). This probe seemed more sensitive to π-π stacking and aggregation. Like pyr-alkyl SP **84**, no red-shifting could be observed at the low concentration of 100 nM. At 1 µM the peak of emission was at 475 nm, not at 375 nm as found with the starting pyr-butanol **79** and 1 µM of probe pyr-alkyl SP **84**. There was very little emission that was not in the red shifted region at 10 µM, indicating that pyr-SP **85** either aggregated more readily, or the increase in red-shifting could have been due to a closer intramolecular-distance between the pyrene rings, so more energy could be shared between the molecules in the aggregate.
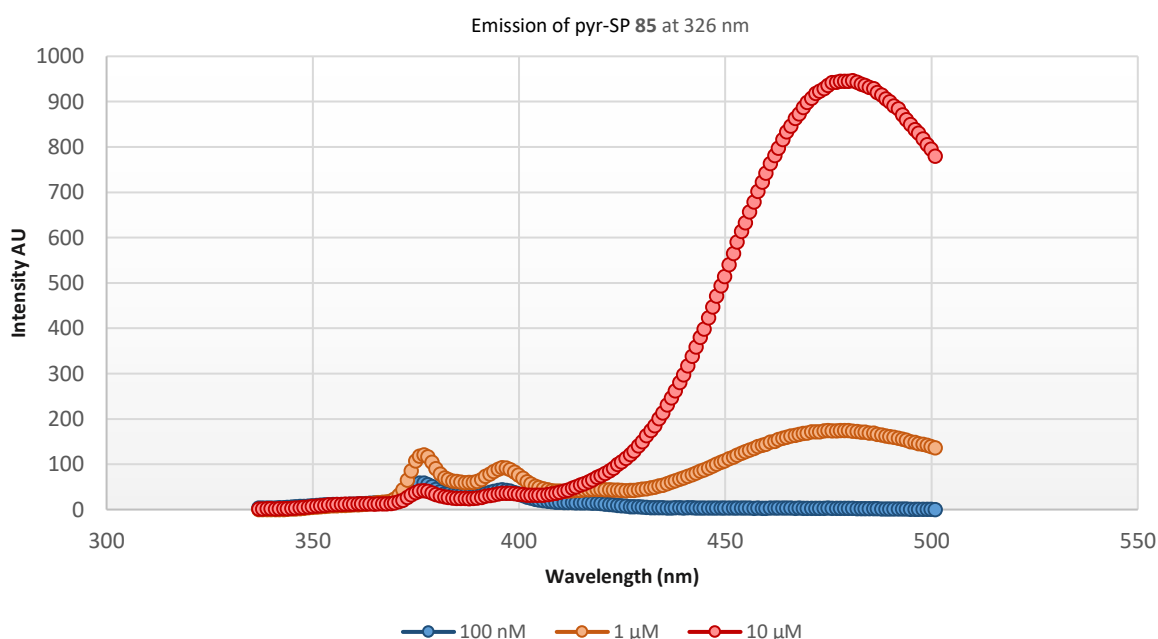
Figure 69. The effect of concentration of pyrene probe pyr-SP **85** on red-shifted emission. Fluorescence measurements were made using a 1 cm^3 fluorimetry cuvette (n=3); with each probe dissolved in distilled water, pH of 7.5.

Whether the effect of red-shifting organophosphate probes will be useful in gel electrophoresis studies or not remains to be seen. The scale of aggregation in an enzyme or receptor found within a cardiomyocyte cell lysate or mitochondrial lysate is likely to be minimal depending on the location of the binding residue.

An experiment to determine whether red-shifting occurs with a known fluorescent amino acid was explored. One such residue has been discussed previously and is commonly found to be inducing background autofluorescence, tyrosine. It was thought that the spectral properties of this residue could be mitigated, or even that the presence of tyrosine could enhance the red-shifting and probe emission through π stacking, this could have been a useful property to exploit.

Mixing different concentrations of tyrosine with the pyrene solution in water could encourage probe aggregation incorporating the tyrosine. If aggregation occurs with π stacking any spectral change can be measured by the fluorimeter.

Initially two control spectra were measured, 1 and 10 µM of tyrosine, and 1 µM of the pyr-alkyl SP **84** (Figure 70). These results showed that at 315 nm the tyrosine peak emission was at 355 nm. This emission steadily declines to 500 nm, and there was very little difference between 1 µM and 10 µM of tyrosine solutions which would suggest little spectral change due to π stacking with itself.

Following this experiment, four different concentrations of tyrosine were mixed with a 1 µM solution of pyr-alkyl SP **84**. This is the concentration that did not present any red-shifting from aggregation, so any shifting that occurred, would be noticeable.

At 377 nm pyr-alkyl SP **84** had an intensity of 57, yet with 10 µM of tyrosine added the intensity of this peak increased to 63; even at 5 µM the intensity increased to 62. The amount of red-shifting that occurred decreased as the concentration of tyrosine increased.

 It was concluded that tyrosine inhibited the red-shifting effects of pyrene aggregates, and that the emission within its non-π-stacking region increased very slightly. Energy was likely being transferred

to the tyrosine via hydrophobic interactions or photoinduced electron transfer (PET), which leads to complete fluorescence quenching.

Many kinase sensors use fluorescence quenching mechanisms, phosphorylation by the kinase on residues can mediate fluorescence. Tyrosine is known to quench fluorophores by π-π stacking interactions and PET; the phosphorylation of the OH on the aryl side chain can restore fluorescence.[193] The phosphate size and charge disrupts the interactions of tyrosine and fluorophore; one study reports a significant increase in fluorescence using a tyrosine kinase.[194]
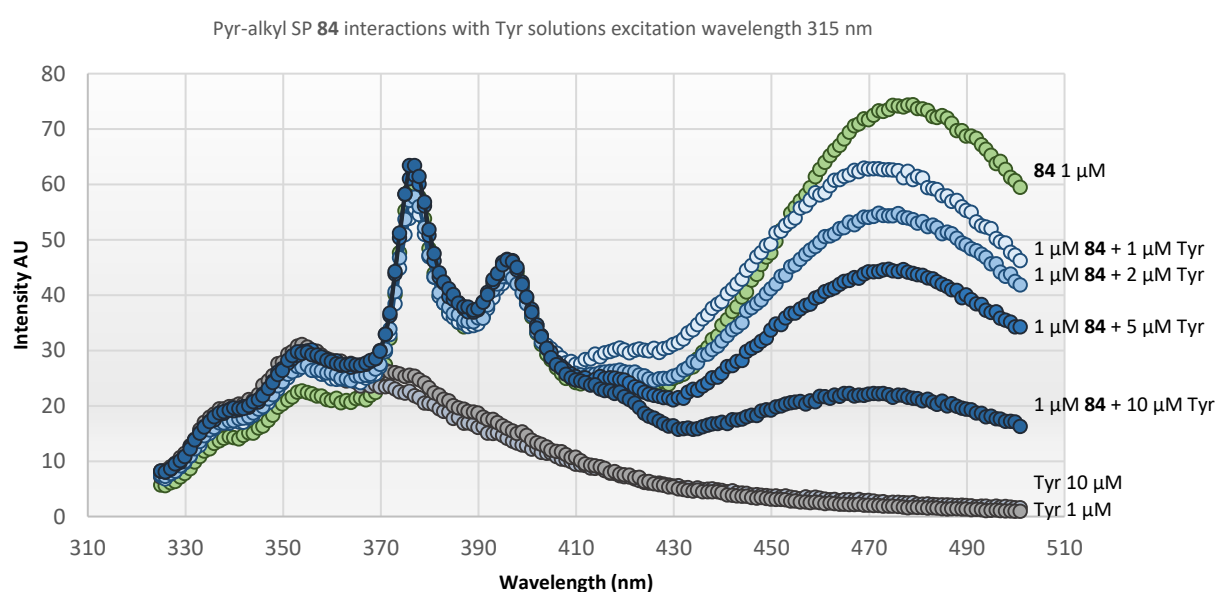
Figure 70. The spectral effect of tyrosine (Tyr) concentration on 1 μM of pyrene probe pyr-alkyl SP **84** at 315 nm. Positive control of 1 μM pyr-alkyl SP **84** in green, 1 μM of Tyr in light grey, 10 μM of Tyr in dark grey. Light blue to dark blue represents 1 μM of both Tyr and pyr-alkyl SP **84**, then 2 μM of Tyr with 1 μM probe, then 5 μM Tyr and 1 μM pyr-alkyl SP **84** and finally 10 μM Tyr 1 μM pyr-alkyl SP **84** in dark blue. Fluorescence measurements were made using a 1 cm³ fluorimetry cuvette (n=3); with each probe dissolved in distilled water, pH of 7.5.

The Lawrence group demonstrated the increase in fluorescence over 4-fold when the tyrosine inhibiting pyrene was phosphorylated by a kinase.[195] However, González-Vera *et al* claims that pyrene is an inappropriate fluorophore for the development of a sensor kit due to its short excitation and emission wavelengths, and the fluorescent interference that cellular components such as organelles and lysates can cause.[196] These effects may moderate the effectiveness of any pyrene based probes.

3.4.6 Gel-Electrophoresis Studies of Pyrene Probes

Notwithstanding the potential shortcomings of the pyrene probes, organophosphate binding to protease chymotrypsin in gel electrophoresis was explored. The Pyrene organophosphate probes were compared against rhodamine probe rho-PEG long SP **49** and DSP-**10**.

The fluorescent bands found in this gel suggests that the control, PSP with chymotrypsin, was slightly visible on the blue laser light due to autofluorescence (Figure 71). The shorter pyrene probe pyr-SP **85** seemed to be brighter at all concentrations than the lanes containing pyr-alkyl SP **84**. Although, lane 6 contained the lowest concentration of pyr-alkyl SP **84** (25 μM), and was still clearly visible. The proposed reasoning for why the difference in brightness was so apparent here could be the binding efficiency of short pyr-SP **85**. Its small size and length may have given it more access to residues on chymotrypsin, so more binds to the protein. Whereas, pyr-alkyl SP **84** would have impeded access to residues according to its length, and therefore less of the probe binds.
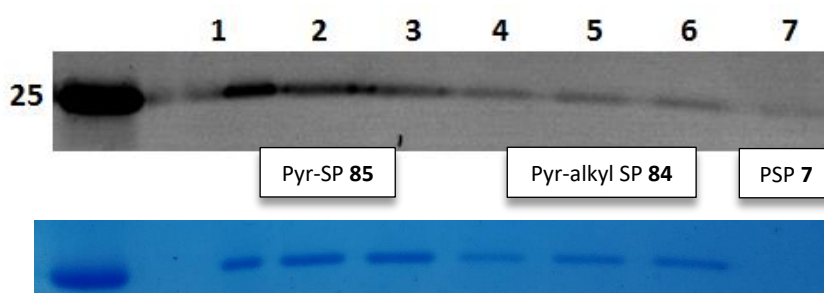
Figure 71. Pyrene probes bound to 20 μg chymotrypsin, incubated on ice for fifteen minutes with three concentrations of both pyrene probes. After reduction with Laemmli buffer, 10 μl is loaded into each well, the gel was visualised after running at 412 nm (n=1). Lane 1, 100 μM of pyr-SP **85**. Lane 2, 50 μM and lane 3, contains 25 μM of pyr-SP **85**. Lane 4, contains 100 μM, lane 5, 50 μM, and lane 6, 25 μM of pyr-alkyl SP **84** respectively. Lane 7, 100 μM PSP with chymotrypsin control. Coomassie staining of gel with lane 7 protein missing.

This led to a second gel electrophoresis experiment directly comparing rho-PEG long SP **49** and DSP-**10** using the same method as in the last gel, but comparing the two pyrene probes to long glycol chain featuring rhodamine and dansyl. The visualisation of these two gels occurred on a UV-transilluminator. This excitation was chosen so the dansyl could be seen fluorescing optimally and UV-transilluminators are common place in the majority of bioscience research labs. The results of this experiment indicated the practical brightness in standard conditions for the three families of probe.

The rhodamine B probe rho-PEG long SP **49** was determined to be the second brightest compared to DSP-**10**. This was to be expected as the excitation frequency was about 312 nm, closer to the wide excitation range of dansyl of 300 – 400 nm which is not optimal for pyrene probes pyr-alkyl SP **84** and pyr-SP **85.** These probes were very faint comparatively, since the narrow excitation wavelength that pyrene responds to is 310 – 350 nm. Another explanation could be that the pyrene probes did not bind as efficiently to chymotrypsin as the other two probes. A way of measuring excess probes unbound to protein would need to be performed to consider this.
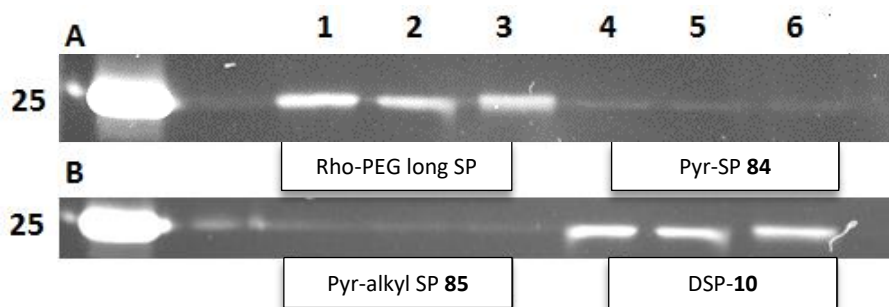
Figure 72. Pyrene probes compared with rho-PEG long SP **49**, and DSP-**10**. (A), probe rho-PEG long SP **49** of three concentrations, 100, 50 and 25 μM in lanes 1, 2 and 3. Probe pyr-SP **85** of the same three concentrations in lanes 4, 5 and 6. (B), probe DSP-**10** of three concentrations, 100, 50 and 25 μM in lanes 1, 2 and 3. Probe pyr-alkyl SP **84** of the same three concentrations in lanes 4, 5 and 6, (n=1).

The results of probe performance in SDS-PAGE experiments led onto a final experiment for the pyrene probe, where a solution containing 100 μM of pyr-alkyl SP **84**, was incubated with 80 μg of mitochondrial lysate in extract buffer on ice. Following the same technique as found in previous 2D-gel electrophoresis studies, the gel displayed in Figure 73 was obtained. Fluorescently labelled

protein clusters could be seen, these are awaiting de-staining and mass spectrometry analysis to determine the bound protein target identity.
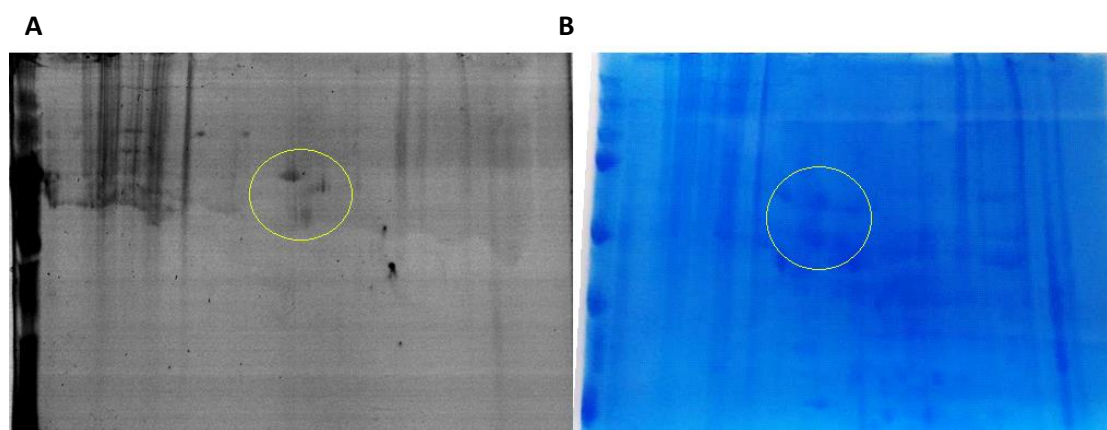
Figure 73. 2D SDS-PAGE gel displaying: A) long pyrene probe pyr-alkyl SP **84** labelled to mitochondrial proteins in 2D-gel study and, B) Gel staining by coomassie blue, revealing all proteins present in the gel (n=1).

This 2D gel suggested that the tagging efficiency of these probes was not compromised. However, enough information on fluorophore and probe behaviour means research into pyrenes has reached an end, and a new system featuring organophosphates will need to be designed with further optimisations.

3.5 Synthesis of Bright Rhodamine Analogues

3.5.1 Background

The pursuit of fluorophores with desirable properties for these probes beyond maintaining biological effectiveness are good solubility and high brightness at low concentrations. The rhodamine skeleton lends itself to modifications and optimisations.

The focus of this current study returned to literature analysis of analogues with the rhodamine core structure. Rhodamines as previously mentioned are highly varied and continue to be utilised for a wide variety of purposes. Since it has been discovered that using an amide on rhodamine B in the 2 position causes the fluorescence to decrease in the organophosphate probes, it would be viable to try other analogues of rhodamine that will have high extinction coefficients. Also desirable would be useful absorption and emission properties, and ideally are more favoured to exist in the open form

and have a higher fluorescence yield than current use of rhodamine B, which prefers to form a closed lactam ring.

Two other rhodamine core structures that were explored are rhodamine 101 and rhodamine Q. Preliminary work already suggested a water solubility issue with the probes. The rhodamine analogues being synthesised needed to have a useful level of water solubility. Rhodamine Q is the core structure for a few patented dyes currently on the market including Atto Rho 14,[197] NVOC$_2$-5-carboxy-Rhodamine Q a metabolic label for cellular DNA,[198] as well as other analogues found in DNA sequencing kits.[199]

A synthetic methodology for a sulphonated rhodamine Q starts from the inexpensive 7-Hydroxy-3,4-dihydro-2(1H)-quinolinone. The final step of sulphonation increases water solubility, and allows high concentrations (>100 µM) to be tested (Scheme 34).[200]
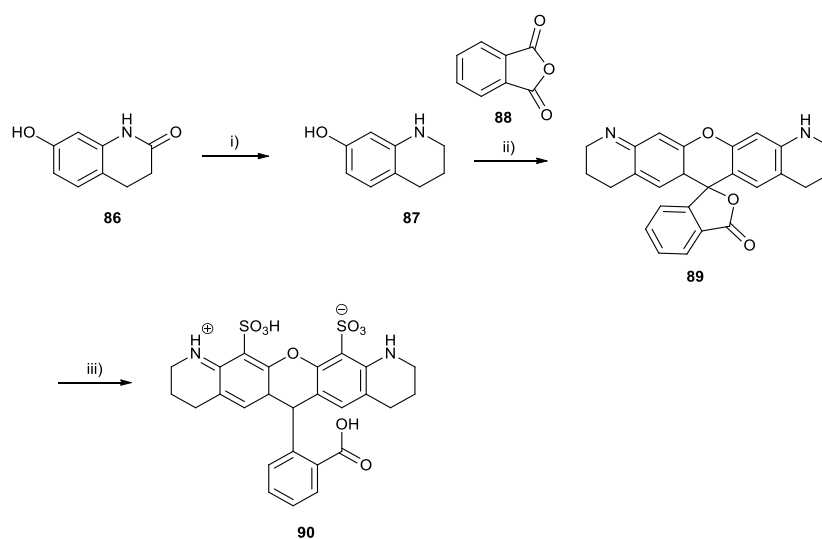
Scheme 34. Synthesis of highly water soluble sulphonated rhodamine Q. (i). BH3.THF, THF, reflux, 24h (ii). 7-Hydroxy-1,2,3,4-tetrahydroquinoline, phthalic anhydride, 85% H$_3$PO$_4$, 150 °C (iii). 30% SO$_3$ in H$_2$SO$_4$, 0 °C, 12h.

3.5.2 Synthesis of 7-Hydroxy-1,2,3,4-tetrahydroquinoline

The first step explored in the synthesis was creating the amino phenol **87**. The reaction was performed by 24 h reflux of compound **86** with borane THF, then with the solvent removed, was worked-up and analysed by ^{1}H NMR returned starting material. This indicated that no reduction had occurred. It was likely that the borane used was no longer functional.

As the reduction with borane THF did not afford the desired amine the experiment was repeated but with a different boron-centred reducing agent, borane dimethylsulphide.[201] The desired product was achieved after refluxing the reactants for 6 hours followed by a further reflux with methanol for 30 minutes. Work-up with the addition of a methanol wash and column chromatography in DCM gave the amino alcohol **87** as a green oil with a 55% yield.

3.5.3 Synthesis of Rhodamine Q

Compounds **87** and **88** were then mixed and heated to 150 °C for 3 h, 85% H_3PO_4 was then added and the mixture was refluxed for a further 3 h. There was a noticeable colour change however, from colourless to a deep red. This indicated that product **89** had been formed. Crude ^{1}H NMR gave an unclear spectrum with some peaks indicating a trace product, this could not be isolated after column chromatography however.

A second synthetic route was then explored. Using an O_2 atmosphere, aminophenol **87** and phthalic anhydride **88** were dissolved in a mix of trifluoroethanol and water in a 4:1 ratio; followed by heating at 80 °C for 12 hours.[202] After analysing the crude ^{1}H NMR the spectra looked promising, displaying the key peaks documented by the literature. The product, if any had formed, could not be retrieved from the silica during column chromatography.

Continued efforts to purify this crude with silica have not been fruitful. Using a 2:1 mix of acetone and toluene, and even treating with base prior to purification to close any formed rhodamine in the hope that it may run off the silica first, the compound was still lost.

Further exploration into the synthesis of rhodamine Q was abandoned. The next additional rhodamine fluorophores to be explored, 5 and 6-carboxy-X-rhodamine, now become the focus of synthesis (Figure 74). These are analogues of rhodamine 101.

3.5.4 Synthesis of 5 /6-Carboxy-X-rhodamine

Rhodamine 101 has excitation and emission wavelengths of 560 nm and 589 nm in methanol, and is used in many biological imaging experiments. Two synthetically simple analogues of interest exist, 5-X-carboxy-rhodamine, and 6-X-carboxy-rhodamine. Both patented for many applications including cosmetics,[203] assay kits,[204] and temperature sensors[205] and both analogues feature a carboxylic acid substituted on the phenyl ring, in either the 5 or 6 position.

6-carboxy-X-rhodamine
91

5-carboxy-X-rhodamine
92
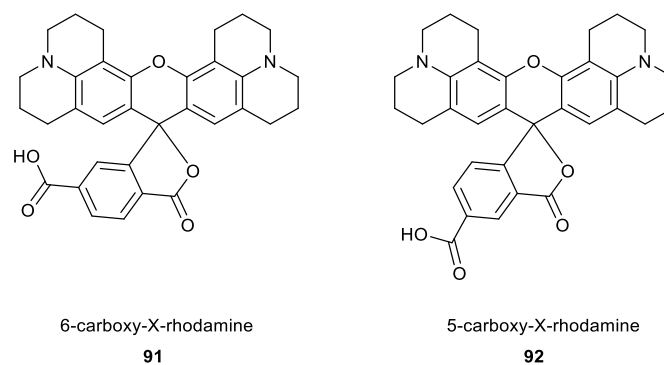
Figure 74. Structures of both carboxy-X-rhodamine derivatives.

These two fluorophores both have a dicarboxy substituted phenyl ring. Synthetically bioconjugation is more readily achieved with the secondary carboxylic acid. The issue of the position of the equilibrium between open and closed forms should be dealt with by using the free carboxy group for amide coupling. It is energetically more stable to be open and with an overall neutral charge in aqueous solution.[134]

The synthesis of 5-carboxy-X-rhodamine and 6-carboxy-X-rhodamine commenced with 8-hydroxyjulolidine and trimellitic anhydride both dissolved in a mix of 4:1 TFE and water in an O_2 atmosphere. The mixture turned from a pale orange to a dark red after 4 hours. Analysis of the

crude ^{1}H NMR gave a promising spread of peaks. Column chromatography with acetone, toluene and TEA, returned only starting material however.
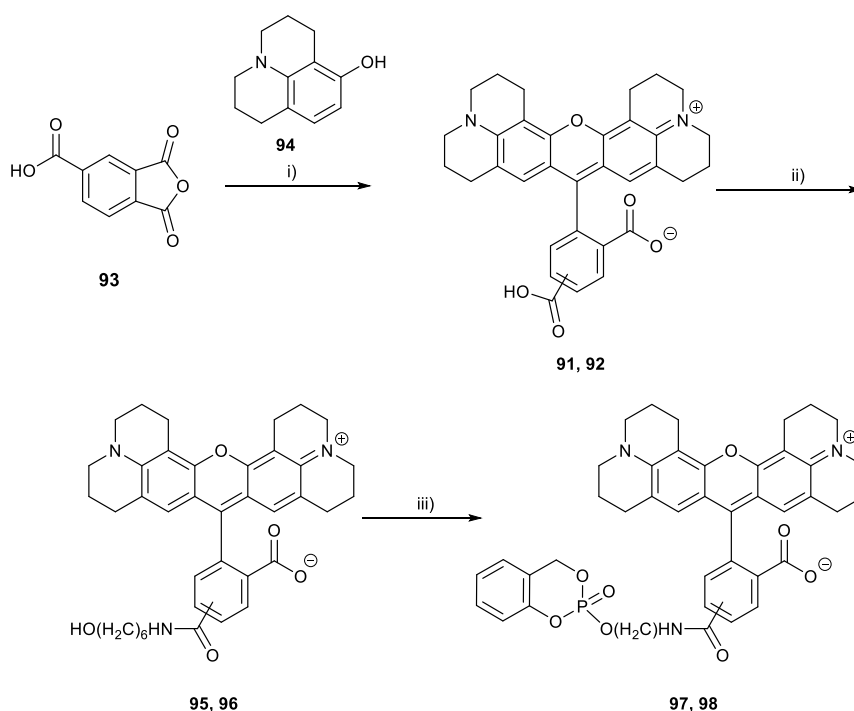
Scheme 35. Synthesis of 5 and 6-carboxy-X-rhodamine OP probes. (i). TFE, H_2O, O_2, 80 $^{\circ}$C, 12h. (ii). HBTU, TEA, dry DCM, 0 $^{\circ}$C, 12h. (iii). PSCl, TEA, dry DCM, -78 $^{\circ}$C, 12h.

Another synthesis for carboxy-X-rhodamine was then tried. This Scheme 35 was adapted from Uddin *et al* method where refluxing the starting components in butanoic acid and 2M H_2SO_4 for 12 hours produced the compound. [206]

In the following method however, butanoic acid was replaced with ethanoic acid. The crude ^{1}H NMR again looked promising, though only starting materials were returned from the column.

The reagents were optimised further as it was noticed that a grey precipitate was forming with addition of the 2M H_2SO_4. This was found to be a salt of the hydroxyjulolidine and the method was changed to incorporate two drops of concentrated HCl instead. The reaction was also modified to occur in a mix of dioxane and ethanoic acid. After work-up the crude once again showed peaks that were in the expected positions.

However, the product from the column retrieved was the wrong colour, a blue green residue instead of the expected purple crystals. ^{1}H NMR suggested that only half of the 8-hydroxyjulolidine had coupled with the trimellitic anhydride in a 44% yield. The reaction was tried again with this intermediate product, and more equivalents of 8-hydroxyjulolidine, this time the reaction going to completion with the formation of a dark red crude mix. Purification in a MeOH DCM gradient gave two purple coloured fractions, the 5-carboxy-X-rhodamine **91** 218 mg 34% and the 6-carboxy-X-rhodamine **92** had a dried weight of 155 mg which is a 24% yield.

3.6 Conclusions to the Organophosphate Studies

Three rhodamine B organophosphate probes have been synthesised and tested; rho-alkyl SP **18**, rho-PEG short SP **48** and rho-PEG long SP **49.** The emission of light when fluoresced at 532 nm was greatly diminished from that of rhodamine B starting material. It is suggested that a closed lactam ring is more thermodynamically and sterically favoured in water than the fluorescent amide open form. Evidence of the closed lactam form existing has been proposed with data illustrated in Figures 47 and 48. Analysis of the ^{13}C NMR spectrum with HMQC and HMBC experiments seems to suggest that the closed form quaternary carbon in position 9 of the xanthene ring can be seen with a distinguishable peak of *ca.* 64.9 ppm.

Investigations into the biological interactions of all three probes, exhibited toxicity on differentiated H9c2 cardiomyocytes at a clinically relevant toxicity of 6.25 µM over 24 hours, illustrating the bioactivity of the probes. The LDH assays concluded that high doses of treatments are necrotic however, and low concentrations are largely inactive, this is demonstrated in the calculations of the IC$_{50}$ (Table 2). The precursor linkers rho-alkyl **15**, rho-PEG short **16** and rho-PEG long **17**, in general had a higher toxicity than the organophosphate probes at concentrations over 25 µM, however, rhodamine B demonstrated a negligible toxicity over both 4 hours and 24 hours.

Gel electrophoresis tests determined that the probes bind to protein residues found on chymotrypsin, NTE and TG2 (Figures 55 and 56), highlighting that there are interactions between

organophosphates and TG2. The problem of autofluorescence was also circumvented by use of these probes, visualising at 532 nm was useful in deciphering the protein spots found in 2D gel electrophoresis. Mass spectrometry of the protein clusters looking for organophosphate target proteins, are waiting to be performed. Completion of the studies of factor XIII and mitochondria with the probes will bring to light novel target proteins that may play a role in OPIDN and general organophosphate toxicity (Figures 57 and 73).

Attempts to synthesise organophosphate probes that do not suffer from the quenching, that rhodamine amides experience, led the investigation onto BODIPYs and pyrenes. Work with the BODIPY fluorophores is inconclusive due to the synthesis and functionalisation revealing a rhapsody of problems.

Further work will investigate synthesis of pyrroles featuring terminal alcohol chains that organophosphates can be extended on. The outcome of the pyrene studies is the synthesis of two novel probes, pyr-alkyl SP **84**, and pyr-SP **85**. These both bind to chymotrypsin, and have bound to novel organophosphate protein targets found in mitochondria. Although, the brightness of this family of fluorophores, and the excitation wavelength is far from optimum for what is required in this study.

Ultimately this work will continue to seek to identify proteins targets found via probe binding in 2D gel electrophoresis tests. Synthesis of brighter organophosphate probes is also still being explored. One methodology could be to stop the closing of rhodamine amide via the incorporation of a piperazine ring coupled to the 2 position of the aryl ring, forming an amide that is unable to close.

4. Diazoxide

4.1 Previous Work

Alongside the work with organophosphates, research into the cardioprotective mechanisms of diazoxide **19** was explored (Figure 76).

Previous work invested by Garner group *et al* in this field, was aimed at the synthesis of fluorescent tags using diazoxide as a protein bait. The biological study of cardioprotective properties of analogues of diazoxide was made in collaboration with Dr Manuel Galiñanes, Department of Cardiac Surgery, Area University Hospital Vall d'Hebron Pg, Spain. Ten analogues were synthesised with the following structures (Figure 75):
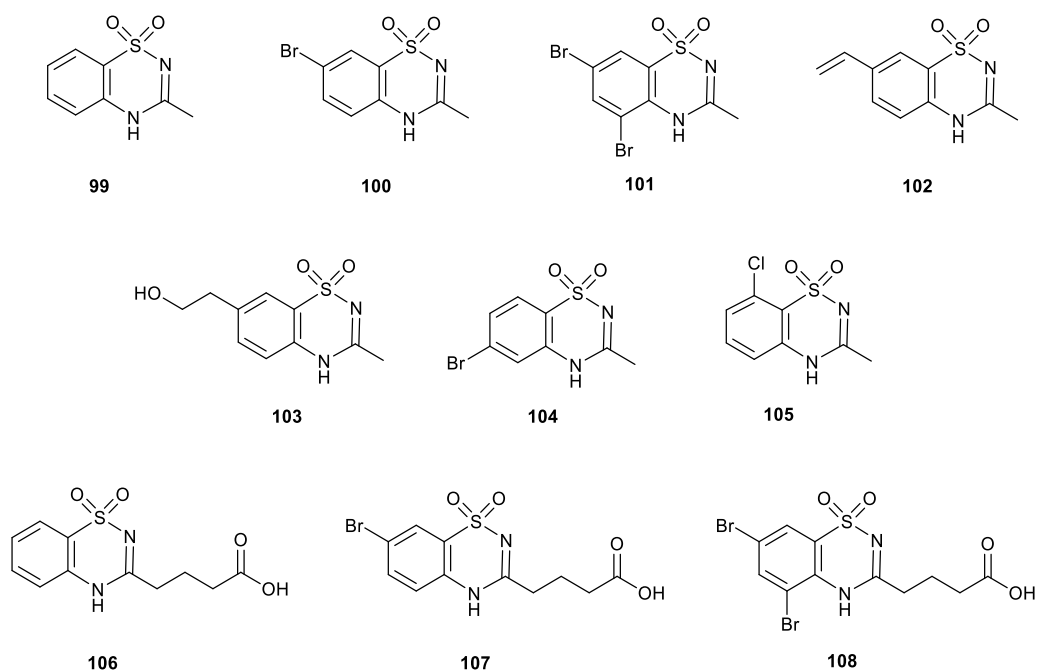
Figure 75. Garner group diazoxide analogues synthesised at Nottingham Trent University by Fathi Smida.[67]

The cardioprotective activity of the analogues was assessed by incubation with myocardial slices from the human right atrial appendage, in ischaemia/reperfusion experiments and the viability of the treated tissue was determined as described in the literatures.[207,208]

It was concluded that all the analogues displayed a varying level of physiological activity. Substituting positions 5 and 7 with two bromines biologically inactivated compound **108**. Analogues **105** and **106** both show significant cardioprotection, and when compared with analogues where the 3 position is methylated the results had indicated that side chain extension is not detrimental to activity. These results in general are in concordance with the suggested pattern of behaviour indicated by Topliss *et al.* although, no compounds for direct comparison are available.[110,111]

The results of the tests performed previously formed the basis for diazoxide probe design, having an active analogue specific for cardiac cells, and not brain or pancreatic tissue for example.

109
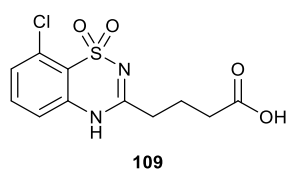
Figure 76. Bioactive diazoxide analogue designed by Garner group.[67]

With the information from the previously mentioned SAR studies, analogue D-**109** was synthesised. This has a similar core structure as the parent compounds **105** and **106**, with the chlorine group in position 8 and a butanoic acid side chain in the 3 position. This, by no means was the optimum structure for potency, as previously mentioned in the SAR studies, having the chlorine at position 7 and a trifluoromethyl at position 6 would have been ideal. For ease of synthesis, however, some compromises were made and this analogue should still have retained some activity. The butanoic side chain was added to allow coupling to the linker and the rest of the proteomic tool.

Diazoxide probe DZX-**110** was previously synthesised by this research group (Figure 77). This featured diazoxide analogue of D-**109** that was coupled to a 6-aminohexanol linker, with a dansyl sulphonamide fluorescent component and a benzophenone photoaffinity label.
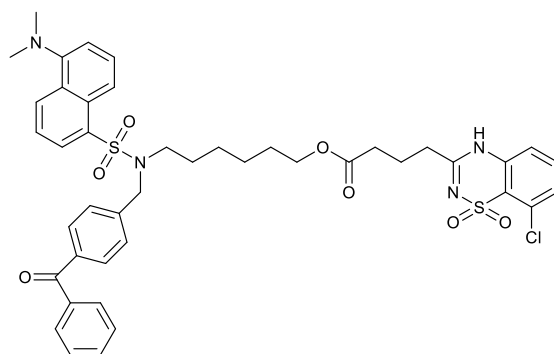
110

Figure 77. Photoreactive diazoxide probe DZX-**110**.

Incubation of the probe with mitochondrial extract, irradiation at 360 nm for 30 minutes prior to

running the samples in an SDS-PAGE gel electrophoresis study, also showed some fluorescent bands

around 25 kDa (Figure 78).
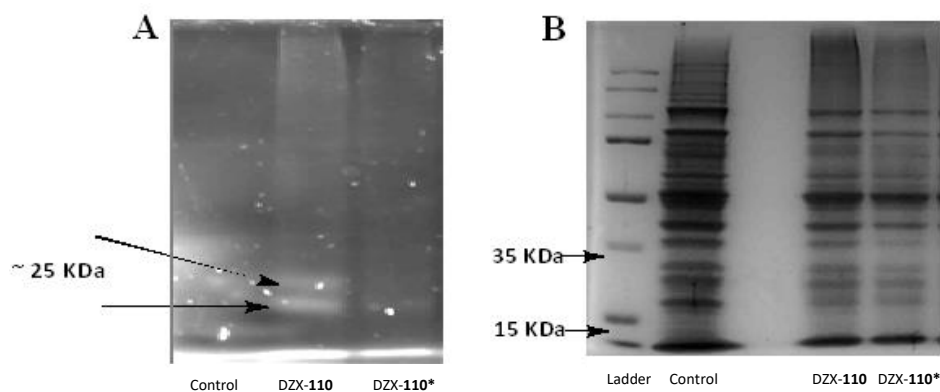
Figure 78. Previous work by Smida *et al.* illustrating DZX-**110** labelling. A). SDS-PAGE gel showing fluorescent bands from the incubation of diazoxide probe DZX-**110**, centrifuged sample prior to irradiation DZX-**110***, and low background fluorescence from the control of **110**. B). The gel after staining with coomassie blue, the pigment showing all the protein bands.

These previous experiments highlighted some of the efficacy of the probe. It was necessary to

discovering whether probe DZX-**110** was an effective cardioprotective agent in and of itself

compared to the parent compound and analogue D-**109.** Assuming the probe was still biologically

effective, it would interact with the mitochondrial proteins and the study moved onto to investigate

this.

The identity of the proteins can be found after the photoreactive component of the probe

irreversibly binds with them and 2-dimensional gel electrophoresis is performed alongside mass

144

spectrometry. Mitochondrial proteins found will include the components for the mitoK$_{ATP}$ channel, and (if the probe is selective enough), the presence of the probe bound to these proteins will add to the body of information regarding what sub units these channels contain and whether DZX targets these channels.

4.1.1 Confocal Imaging of Diazoxide Probe

Confocal imaging is a powerful tool in the field of microscopy that utilises tuneable lasers to pinpoint a single plain on a sample to image. This allows for 3 dimensional cross sections of a cell to be viewed, as well as various fluorescent components to excite with high selectivity.

The probe DZX-**110** was incubated with cells 1 hour prior to irradiation on chamber slides which had been cultured with 5000 H9c2 cells per well, 7 days before the experiment began. This enabled the myocytes to be serum starved, causing differentiation and expression of cardiomyocytes properties.[62,65] The wells had the treated culture aspirated and fresh medium added before being exposed for a minute to UV light from a transilluminator to bind the probe to the protein targets in the cell. The slides were washed with phosphate buffer solution, and then counter stained with cell dye known as 4,6-diamidino-2-phenylindole (DAPI). The slides are transferred to the confocal microscope and visualised with a UV laser at 312 nm, and a violet laser at 405 nm (Figure 79).
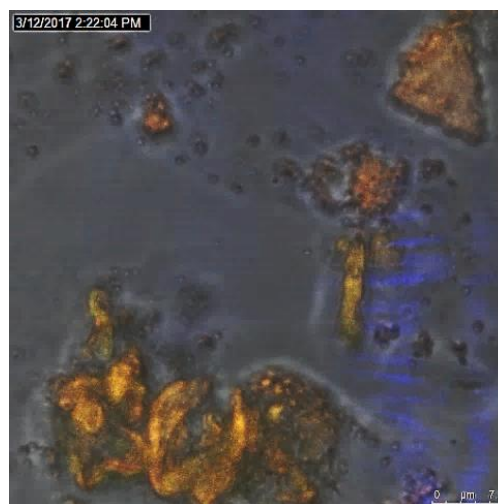
Figure 79. Confocal image of H9c2 cardiomyocyte cells fluorescing yellow with staining from the diazoxide probe and DAPI counterstain for nuclear visualisation (blue) of H9c2 cells. Scale bar = 75 μm, and 20x magnification (n=1).

The DAPI fluoresced at 405 nm and allowed the cell nucleus to be clearly seen, as it became bound to adenine-thymine rich regions in DNA.[209] The diazoxide probe emitted light at ca. 500 nm. What can be seen in this image is that the diazoxide probe had entered the cells, which was proven by visualising down the z-axis (not shown). The resolution of the camera and the brightness of the dansyl fluorophore are limiting factors in visualising the mitochondrion, so a large concentration of DZX-**110 (**100 μM), had to be used. Therefore, determination of where the probe targeted primarily (sarcolemma or mitochondria) was not possible. The high concentration may have caused the benzophenone to bind to nearby protein residues, not specifically the diazoxide targeted ones.

With the knowledge of probe binding to mitochondrial proteins determined by previous work, the probe can visibly be seen in the cell from the confocal experimentation. Cell viability assays of diazoxide analogue **109** and DZX-**110** were next investigated.

4.1.2 Cell Viability Assays of Diazoxide Probe

The viability of cells was measured by lactate dehydrogenase release and the metabolic reduction of MTT by living cells. When in the presence of ischaemic insult such as hydrogen peroxide (H_2O_2) the cardioprotective capabilities could be explored. The assay used hydrogen peroxide as the insult because it mimicked ischemia and reperfusion injury chemically.[210] Some preliminary studies showed that the solubility of the dansylated diazoxide probe in water was limited to 100 μM; above this concentration the solution would saturate and precipitation of probe aggregates would occur.

In initial MTT and LDH tests, the 800 μM concentration of H_2O_2 gave poor results with the scale of cell death being at a point where comparison of analogues was difficult. Better results were found with lower concentration of 600 μmol H_2O_2.
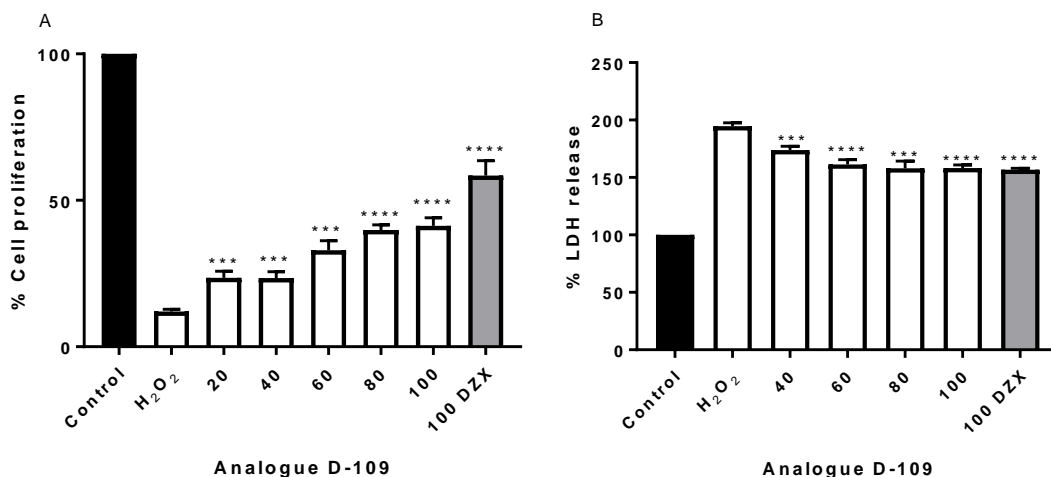
Figure 80. A). MTT test using treatment of diazoxide (DZX) **19** and analogue D-**109**. Effect of 1-hour pretreatment of each in μM, and 2 hour treatment of 600 μM H_2O_2 (MTT 15,000cell /well H9c2 n = 6, control normalised to 100%) B). LDH test results. Effect of 1h pretreatment with parent DZX **19**, and analogue D-**109**, and 2-hour treatment of 600 μM H_2O_2 (LDH 5000 cells/well n = 6, control normalised to 100%). The "*" represent the results of an ANOVA t-test comparing significance (p) against the control H_2O_2 response. *$p<0.05$, **$p<0.01$, ***$p<0.005$, ****$p<0.001$. For the MTT tests, cardiomyocytes were seeded at 15,000 cells per well in 24-well plates. LDH tests were seeded with 5000 in 96-well plates.

The results illustrated in Figure 80 show significant activity of analogue D-**109**. Although there was a decrease in activity between the parent DZX (**19**) and the active analogue D-**109**, this was further confirmation to the trend in activity of **105** and **106** reported by Galiñanes *et al*.

LDH and MTT tests were then explored with the complete diazoxide probe DZX-**110**. The tests were performed via the same method as above. Confirmation of cardioprotective activity of DZX-**110** can be seen by the comparison of the control insult via hydrogen peroxide and the residual activity of treated cells (Figure 81).

The results of the MTT tests show a significant increase in the metabolism of the cells demonstrating a trend in viability when damage from H_2O_2 occurs. At the 20 μM concentration of DZX-**110** treatment the amount of MTT reduced improves by ca. 10% compared with the H_2O_2 control. The LDH tests are not displaying the same trend. Cells are not protected against necrotic damage through H_2O_2 use. However, statistically significant cardioprotection is only seen at 80 μM and 100 μM. Further tests to determine exact efficacy include decreasing the amount of O_2 in the atmosphere inducing hypoxia in the cells, where intracellular ROS would be generated.[211]

147
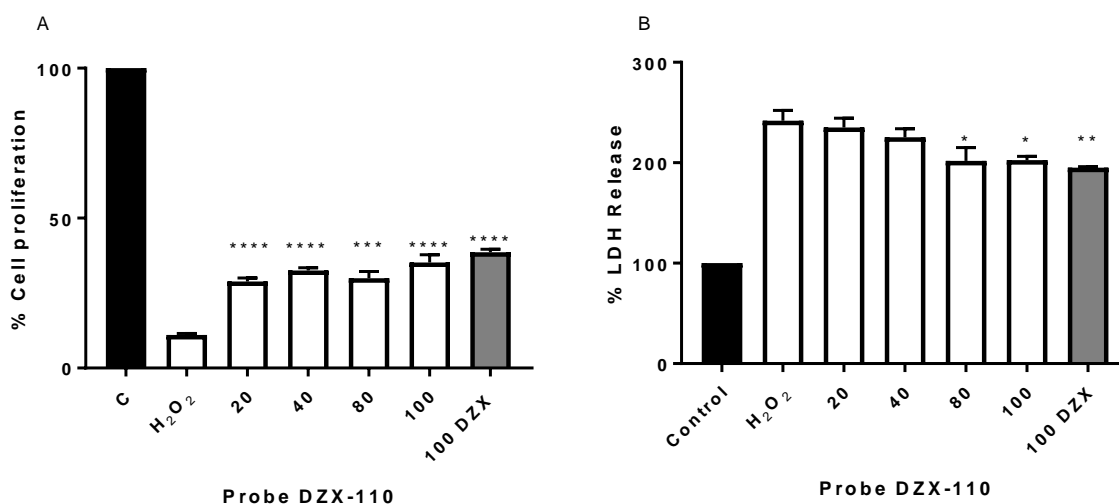
Figure 81. Effects of DZX-**110** on MTT reduction and LDH release and 100 µM of parent DZX **19**. A). MTT test using 1-hour pretreatment DZX-**110** in µmol, and 2-hour treatment of 600 µM H_2O_2 (MTT 15,000cell /well H9c2 n=6 control normalised to 100%) B). LDH test results. Effect of 1h pretreatment with DZX-**110**, and 2-hour treatment of 600 µM H_2O_2 (LDH 5000 cells /well n = 6, control normalised to 100%). The "*" represent the results of a t-test comparing significance (p) against the control H_2O_2 response. *$p<0.05$, **$p<0.01$, ***$p<0.005$, ****$p<0.001$.

Interestingly, the protective qualities of the complete probe DZX-**110** were less than compound D-**109**. This could be due to less of the active analogue being solubilised around the target protein, as it is already known that solubility of this compound is an issue, and there is a large increase in size (302 vs 829 Da).

Nevertheless, the probe should have been appropriate for the function of targeting the elusive K_{ATP} channel subunits, leading the investigation onto 2D gel electrophoresis tests.

4.1.3 2D-Gel Electrophoresis Studies

The mitochondrial extracts used for 2-dimensional SDS PAGE gel electrophoresis experiments on organophosphates were used again for the DZX-**110** tests. This assay involved incubation of a DZX-**110** solution with the extract followed by centrifugation and irradiation. At this stage the benzophenone photoreactive component would covalently bind to free residues around the site(s) where the probe is located. Visualisation of the gels under 412 nm of blue light revealed spots where protein clusters containing the probe were likely to be found.

The spots revealed by the probe could have been very dense clusters of proteins which were auto-fluorescing at this wave length. However, this was unlikely, as other protein spots would have shown up. It had to be assumed that these spots were mitochondrial proteins bound to benzophenone after being targeted by DZX-**110**. (Figure 82).
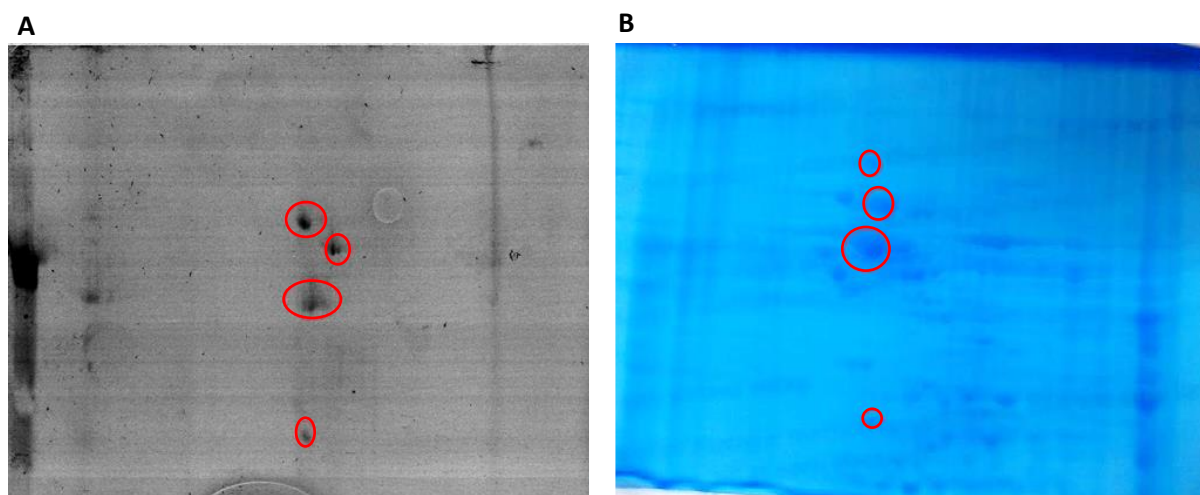
Figure 82. Gel displaying bound protein spots found via diazoxide probe DZX-110 with mitochondria. Probe DZX-**110** is incubated on ice with the extract in TRIS buffer. After 10 minutes they are transferred to a glass bottomed 384 well plate to be irradiated at 360 nm for 10 minutes. The samples were added to acetone at 0 °C to precipitate the protein and wash off excess solution, this is dissolved in solubilisation buffer and continued the 2D-gel protocol outlined in 5.3.9. The gels were visualised at 412 nm using a blue light laser (n=3).

These spots are undergoing analysis by mass spectrometry by the John van Geest Cancer Research Centre to determine the identity of the proteins. Currently 228 peptide fragments with the increased mass associated with DZX-**110** have been isolated from one protein spot and seven of the most confident results are displayed, (Table 4). The identities of the proteins that these peptides originate from, measured via comparisons with databases, have not revealed any known proteins.

Peptide residues (+DZX-**110**)	Tag length	ALC
KC(+828.24)ELLDYVGLDTTK	14	81
T(+828.24)PVLEVDLAAFDK	13	81
L(+828.24)LPALNVTLTDFAAGK	16	81
N(+828.24)PQDYESEEQLEHR	14	76
K(+828.24)YEDHLSGPVR	11	76
T(+828.24)LPKRGNKVYVR	12	75
T(+828.24)WLFFYSR	8	75

Table 4. Table of peptide fragments modified by DZX-**110**, average local confidence (ALC) is a percentage given for *de novo* analysis relating to the percentage of correctly sequencing a peptide.

4.2 Synthesis of a Brighter, More Selective Diazoxide Probe

The results of the confocal visualisation and the gel electrophoresis studies highlighted the weaknesses of the probe's use of the dansyl fluorophore. Brightness at low concentrations and background autofluorescence are issues that can be circumvented by exciting bright photostable probes that respond at green – red-shifted wavelengths. A fluorophore which has a higher extinction coefficient than dansyl (ε = 4000) would increase the sensitivity of the probe, allowing for less populous protein units to be detected.

The families of rhodamine, pyrene, and BODIPY have all been presented throughout this project. Each has a higher extinction coefficient than dansyl amide, and each would be more selective. There are problems with these choices however. The BODIPY family of fluorophores are not appropriate for investigation, due to difficulty with synthesis. Pyrenes have a narrow excitation and emission wavelength and an easily inhibited fluorescence due to aromatic amino acid residues. This would judge the synthesis of such a probe no better than the current tool.

Rhodamines were explored and the issue of lactam closing can be circumvented by positioning the benzophenone photo affinity probe on the tertiary amide, as in probe DZX-**110**. Rhodamine B has high extinction coefficients and quantum yields, (ε =106,000, ϕ =0.95), and with rho-PSP probes used in SDS-PAGE gels, the severely fluorescently-diminished rhodamine organophosphate probes were brighter than the dansyl and pyrene probes. Adding to this rationale, being selective to green /yellow light considers the background fluorescence is insignificant.

4.2.1 Synthesis of Diazoxide Analogue D-109

Fabrication commenced with synthesis of active analogue D-**109**. Which was achieved via a known procedure in four-steps starting with 1,2-dichloro-3-nitrobenzene **111**.[83] Benzyl thiol was generated *in situ* from refluxing benzyl chloride, thiourea, ethanol, water and catalytic ammonia, followed by addition of potassium hydroxide and refluxed with dichloronitrobenzene **111** for 2 hours. Upon cooling the precipitated 2-(benzylsulfanyl)-1-chloro-3-nitrobenzene **112** was collected as a yellow solid with a 77% yield (Scheme 36).
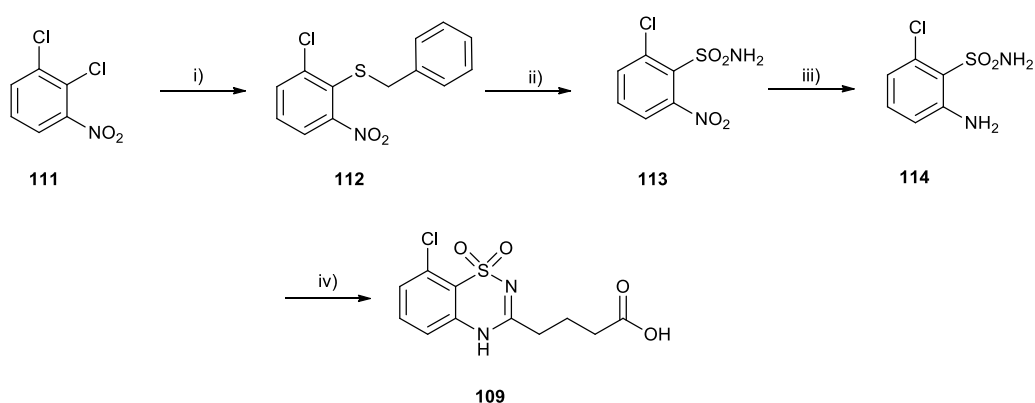
Scheme 36. Synthesis of analogue D-**109**. (i). Benzyl chloride, thiourea, 1,2-chloro-3-nitrobenzene, NH_3, CH_3CH_2OH, H_2O reflux, 3h, KOH, CH_3CH_2OH, H_2O, reflux, 2h (ii). Cl_2, HCl, $KMnO_4$, CH_3COOH, H_2O, rt, 30 min, dioxane, $NH_3.H_2O$, NaOH, HCl (iii). NH_4Cl, iron powder, EtOH, H_2O, reflux, 45 min. (iv). Glutaric acid monomethyl ester chloride, dioxane, rt, 1 h, NaOH, 1 h, HCl.

The second step involved the generation of chlorine gas from reacting HCl on potassium permanganate and bubbling this through a solution of 2-(benzylsulfanyl)-1-chloro-3-nitrobenzene in acetic acid and water at room temperature for 30 minutes. This was then extracted with diethyl ether, and concentrated under reduced pressure. The resulting orange oil was then dissolved in dioxane and aqueous ammonia. A precipitate formed which was dissolved with NaOH. The mixture was treated with charcoal and filtered, and a precipitate was reformed using HCl. Product **113** was then filtered and collected in a 28% yield.

After the formation of the sulphonamine **113**, it was dissolved in hot ethanol and water mix with ammonium chloride and iron powder, then refluxed for 45 minutes. After work-up, addition of hexane caused the precipitate to form a brown powder of product **114** with a 50% yield.

2-Amino-6-chlorobenzenesulfonamide was dissolved in dioxane, and glutaric acid monomethyl ester chloride was added and the mixture stirred for 1 hour. Following this, the mix was concentrated and dissolved in 3% sodium hydroxide solution and stirred for 1 hour further. HCl was then added until a precipitate formed. It was left overnight for more to form. The product was then filtered and washed in ether to yield diazoxide D-**109** with 42% yield. The ^{1}H NMR data is consistent with data from the previously synthesised material.[67]

4.2.2 Rhodamine Diazoxide Probe

The next step in synthesis of a rhodamine B diazoxide probe was deciding which linker was to be used to connect the fluorophore to the benzophenone photoaffinity label and D-**109**. It was envisaged that a tertiary amide would be the simplest and most efficient method of joining the three components (Scheme 37). To this end, rho-alkyl **15**, rho-PEG short **16** and rho-PEG long **17** were all considered.

Rho-alkyl **15**, rho-PEG short **16**, and rho-PEG long **17** were dissolved in DMF at -78 $^{\circ}$C, with potassium carbonate, in three separate reactions. 4-Bromomethyl benzophenone was then added dropwise and the mixture turned from pale pink to a black colour. This was then left for 12 hours to warm steadily to room temperature. Crude ^{1}H NMR showed a mess of peaks, and column chromatography returned only starting material.

This reaction was then repeated at 0 $^{\circ}$C with sodium ethoxide to see if the reaction between the amide and the 4-bromomethyl benzophenone could be encouraged. This resulted in a mess of peaks that had no discernibly identifiable CH_2 shifts between 3.5 and 4.5 ppm as an expected marker for the success of this reaction. Column chromatography returned starting rhodamine linker.

A third set of conditions were trialled, using NaH as the base and refluxing in toluene and DMF. The mixture turned from a pale pink colour to a yellow with addition of the 4-bromomethyl benzophenone. This then disappeared and the mix turned colourless. It was assumed that the

rhodamine was completely closing into its spirolactam form, hence the loss of colour. Only starting materials were returned after column chromatography.
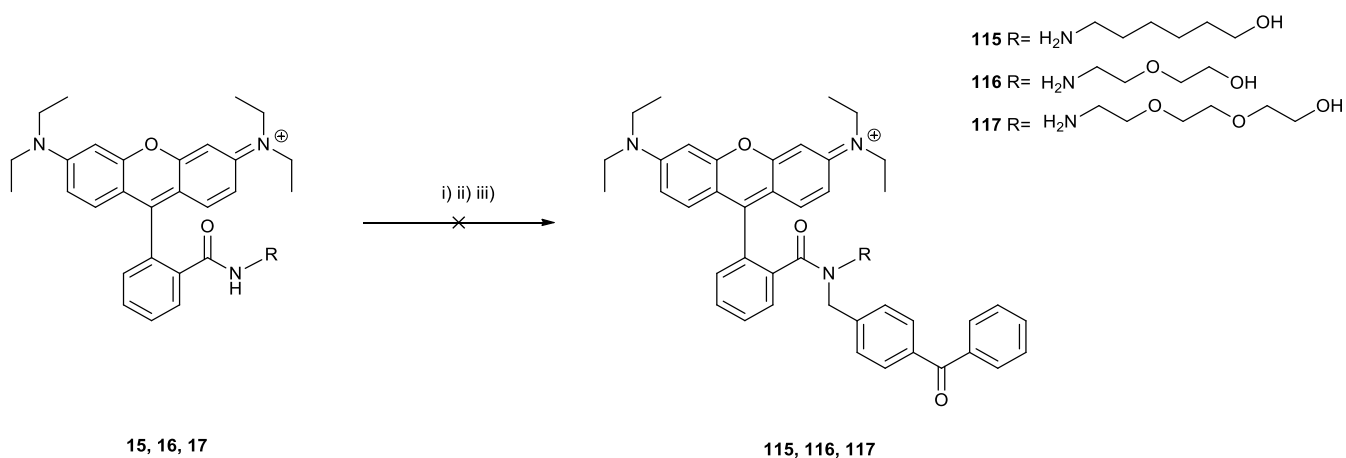
Scheme 37. The coupling of rhodamine B linkers **15**, **16** and **17** with 4-bromomethyl benzophenone. (i). K$_2$CO$_3$, dry DMF, -78°C, 12 h. (ii). NaOEt, dry DMF, 0°C, 12 h. (iii) NaH, Toluene/DMF, reflux, 6 h.

This led to synthesis of benzophenone coupled linkers **118** and **119**, which began with 6-aminohexanol, and TBDMS protected linker **40**. Using DMF at -78°C and potassium carbonate, both products were achieved after column chromatography with ethyl acetate in yields of 23% for **118** 54% for **119**.

These two products would then be coupled to rhodamine B. HBTU was employed for this end due to the success with previous rhodamine compounds. Reaction Scheme 38 was planned to synthesise the final diazoxide probe. Regrettably, the tertiary amide was not formed from this reaction. DIPEA was trialled instead of TEA and starting materials were returned.
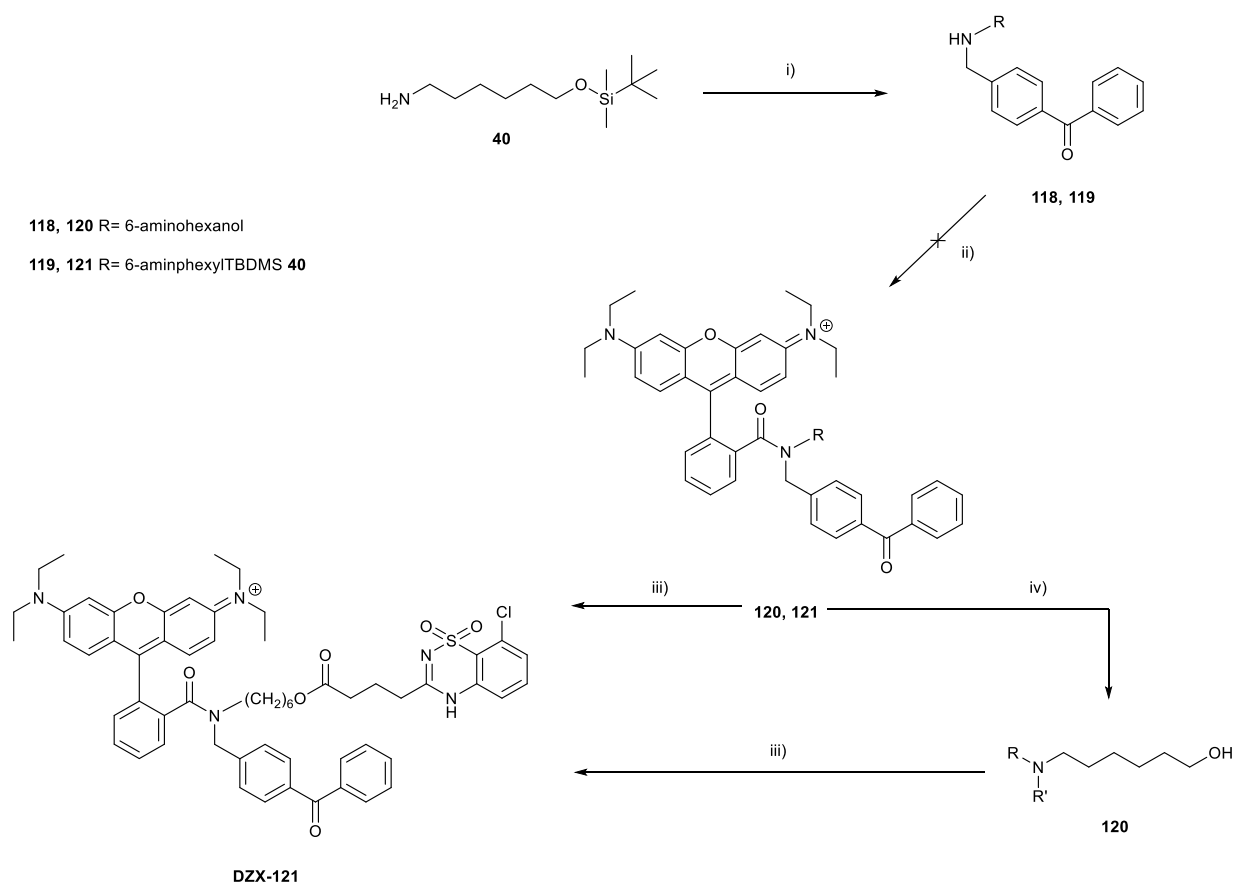
Scheme 38. Synthesis of diazoxide probe with rhodamine B. (i). K_2CO_3, DMF, -78 °C, 12 h. (ii). HBTU, rhodamine B, TEA, DCM, 0 °C, 12 h. (iii). TsCl, TEA, DMAP, 0 °C, 25 °C 12 h. (iv). TBAF, DCM, 25 °C.

The failure of this coupling experiment led to the conclusion that creating a tertiary amide at this point of substitution on a rhodamine fluorophore is unlikely due to the bulk of the methylbenzophenone. Benzyl groups are the largest groups found bound to a tertiary amide in this fashion on a rhodamine fluorophore.[212] The benzyl group acts as a blocking group for formation of the spirolactam ring, and the quenching of fluorescence. It was hoped that the benzophenone group would achieve the same effect.

Attention then turned to rhodamine analogues with substitution in other positions about the benzene ring. The rhodamine 5 /6-carboxy-X-rhodamine had a free acid on either the 5 or 6 position of the aryl ring. Successful synthesis of 6-carboxy-X-rhodamine led us to explore whether a probe could be made with the linker already connected. The goal was to use trimellitic anhydride **93** or the trimelitic chloride **122** and methylbenzophenone aminohexanol **118**, to synthesise the amide **123**.

This then could be reacted with 8-hydroxyjulolidine to yield the rhodamine connected with affinity

label and probe as in Scheme 39.

Coupling the trimellitic chloride **122** was attempted by mixing **118** and TEA in dry DCM at 0 °C. The

chloride was then added dropwise and an evolution of gas was given off. Crude ^{1}H NMR gave an

unclear spectrum, which even after purification gave indiscernible compounds. The next two

attempts were with trimellitic anhydride **93** and coupling agents HBTU and T3P. ^{1}H NMR spectra of

both crude products showed an array of peaks associated with **118** but with a mess of peaks around

7 – 8 ppm. Attempts at returning purified product **123** from crude residues failed. One suggestion as

to why the product did not form is that the trimellitic anhydride decomposed in the aqueous layer.
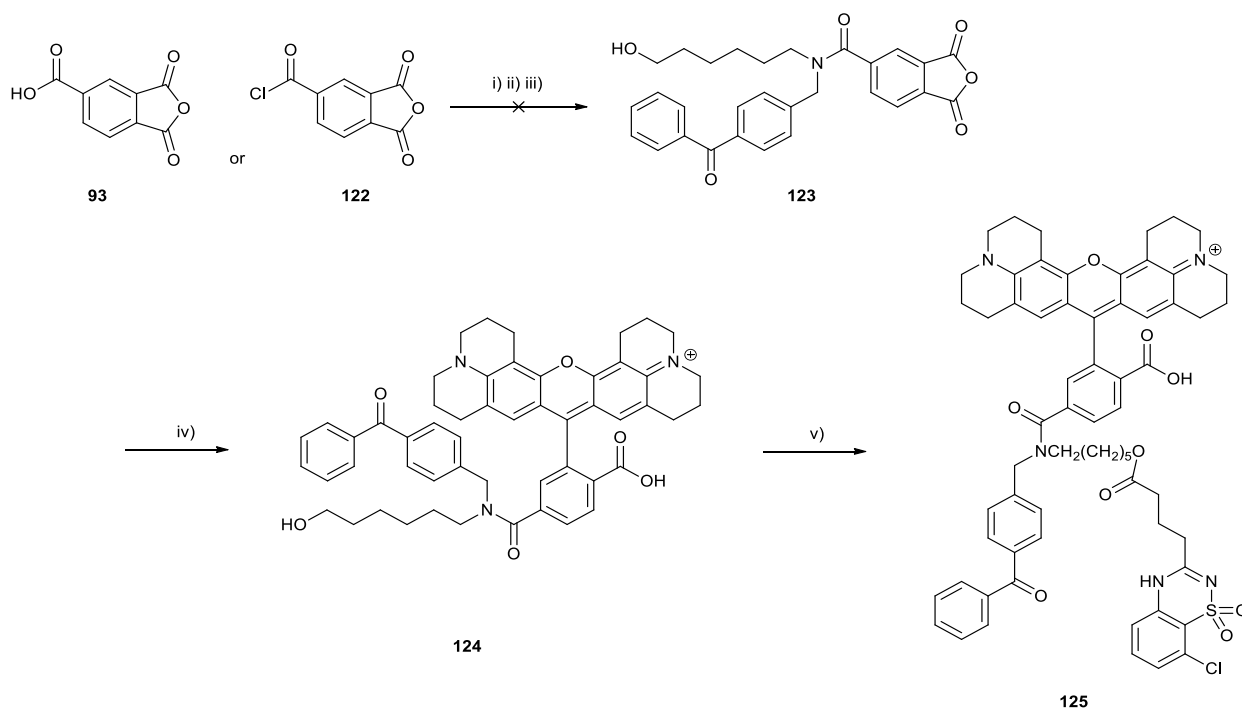
Scheme 39. Proposed synthetic route for 5 /6-carboxy-X-rhodamine diazoxide probe **125**. (i). **122**, **118,** TEA, dry DCM, 0 °C. (ii). **93**, **118,** HBTU, TEA, dry DCM 0 °C, 24 h. (iii). **93**, **118**, T3P, TEA, dry DCM, EtOAc, 0 °C, 24 h. (iv). 8-hydroxyjulolidine, MeCOOH, dioxane, conc. HCl, reflux, 24 h. (v). TsCl, TEA, DMAP, 0 °C, 25 °C 12 h.

With compound **123** unable to be synthesised, the attention turned to a final methodology of

achieving a rhodamine diazoxide probe.

4.2.3 Sulphorhodamine B Probe via Click Chemistry

With synthesis of a tertiary amide starting from rhodamine B proving difficult, a new scheme was

formed relying on 1,2-cycloaddition to an azide to form a di-substituted cyclotriazide ring.

This would couple together the rhodamine B fluorophore with either a protected linker, that would

be deprotected and then coupled to a photoaffinity label and the selectivity function, or a linker with

some of or all the functionality already present.

In order to explore this methodology, two components needed to be fabricated. The synthesis of a

terminal alkyne connected to benzophenone was investigated as the first component to the click

chemistry (Scheme 40). TBDMS protected secondary amine **119** was dissolved in DMF and cooled to

-78 °C. Potassium carbonate and then propargyl bromide was added. After work-up, crude ^{1}H NMR

illustrated the formation of the product. This however, has yet to be purified by column

chromatography.

119   **126**
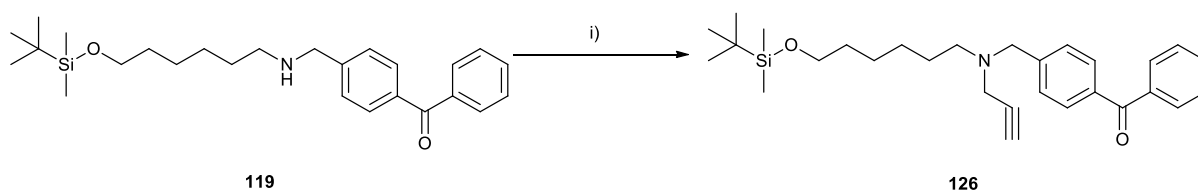
Scheme 40. Synthesis of propargyl benzophenone TBDMS-protected amino hexanol. (i). K_2CO_3, propargyl bromide, DMF, -78°C, 6 h.

The second component for click chemistry would deliver the azide moiety. Sulphorhodamine B **127**

could be bought commercially with little expense and contained a sulphonyl chloride substituent on

the lower ring of the rhodamine. A substitution reaction with propanol azide in the presence of base

would give one half of the click compound (Scheme 41).[213]

This was potentially achieved by mixing sulphorhodamine B chloride **127** with 1-bromo-3-

propanolazide in dry DCM at 0 °C for 4 h. Workup in DCM gave a crude compound with a promising

^{1}H NMR spectra. Column chromatography returned a mixture of products. It is believed that the

desired product is in the mixture, but future purification steps need refining to isolate the product

128 before click reactions can be explored, and probe **129** can be realised.
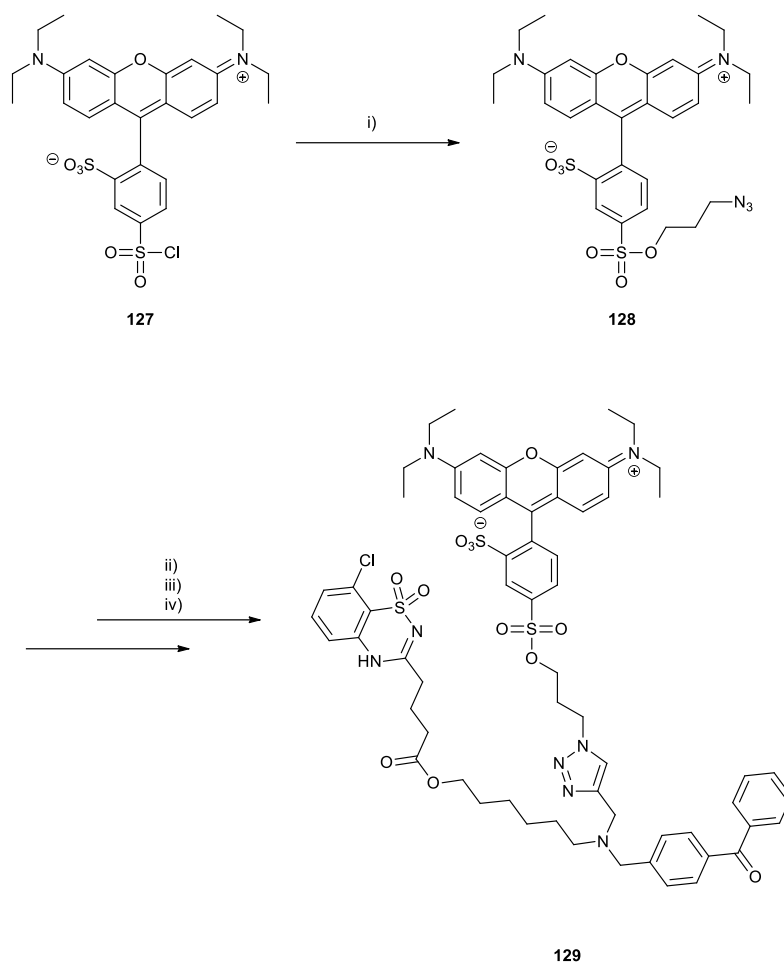
Scheme 41. Synthesis of a sulphorhodamine B diazoxide probe utilising click chemistry. (i). 1-bromo-3-propanolazide, dry DCM, TEA, 0°C, 4 h. (ii). **123**, CuI, H_2O, THF, heat, 24 h (iii). TBAF, dry DCM, 25°C, 4 h. (iv). TsCl, TEA, DMAP, 0°C, 25°C 12 h.

4.3 Conclusions of Diazoxide Studies

Diazoxide analogue D-**109** has been shown to protect cells from H_2O_2 insult through maintaining

metabolism at 20 µM in MTT tests, and the cells are protected from necrosis at 40 µM as seen in

LDH tests. These results illustrated a potential cardioprotective quality, as the tests were performed

in conditions mimicking ischaemia with insult coming from H_2O_2. When D-**109** was incorporated into

DZX-**110** with the dansyl fluorophore and benzophenone photo affinity barb, the protective

properties were retained and could be seen at concentrations of 20 µM in MTT and 80 µM in LDH

assays (Figures 80, and 81).

When DZX-**110** was incubated with differentiated H9c2 cardiomyocytes at a concentration of 100 μM, and exposed to UV light, the probe bound to proteins inside the cells. Visualisation of this relied on confocal microscopy (Figure 81). At a large concentration of 100 μM, DZX-**110** is not specifically selective, and the benzophenone barb is likely binding to residues of proteins in close proximity. A brighter probe, in a lower concentration, imaged on a higher resolution confocal microscope, could reveal mitochondria fluorescing with the probes bound to the inner membrane. A suitable counter stain dye utilised in competition with DZX-**110** would further confirm selectivity for mitochondria.

2-Dimensional gel electrophoresis studies on mitochondrial extracts incubated with DZX-**110**, highlighted fluorescent proteins under 412 nm blue light laser. These clusters of fluorescent proteins indicated that probe DZX-**110** had bound to the residues. These spots have been processed and are awaiting analysis by mass spectrometry. Preliminary analysis of one cluster of proteins had revealed tagged peptides. These have not been identified as of yet, but this work is ongoing.

The synthesis of a brighter rhodamine based diazoxide probe that incorporated a tertiary amide – a moiety that forces the rhodamine to retain its open form, and therefore fluorescence, was met with difficulties. It was apparent from literature that the largest group successfully added to a rhodamine secondary amide was a phenyl.[209] The attempts to synthesise an anhydride precursor **123** to rhodamine that incorporated a 5 /6 position tertiary amide with the 6-aminohexanol linker and benzophenone did not yield the desired product. Reaction stability of the trimellitic anhydride in basic or aqueous conditions was theorised to be the problem.

To this end, the formation of rhodamine diazoxide probe **129** was planned. This integrated attractive click chemistry into the synthesis, by coupling the linker tertiary amide **126** to sulforhodamine propanyl azide **128**. This chemistry needs to be further explored, as the current study was drawing to a close. Completion of synthesis of a brighter diazoxide probe leads into further mitochondrial protein fishing, and identification of target proteins.

5. Experimental Techniques

5.1 Synthetic Reference

5.1.1 3,5-Dimethyl-1H-pyrrole-2-carboxaldehyde 57
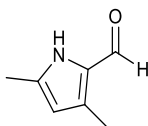
Phosphorous oxychloride (1.88 g, 1.15 ml, 12.26 mmol) was added to DMF (0.9 g, 0.95 ml, 12.31 mmol) over 20 minutes at 0 °C. The mixture was left to stir for 15 minutes at room temperature before being diluted with DCM (5 ml) and then cooled to 0 °C. A solution of 2,4-dimethylpyrrole (1.0 g, 10.51 mmol) in DCM (5 ml) was then added drop wise. The mixture was refluxed for 30 minutes and cooled to room temperature followed by the addition of sodium acetate (8.30 g) in water (20 ml). The reaction was refluxed for a further 30 minutes. The cooled mixture was then separated and the aqueous layer, extracted with diethyl ether (3 x 50 ml) and the organic layers were combined and dried with magnesium sulphate. Removal of the solvent *in vacuo* gave a brown oil. Purification by chromatography (silica, ethyl acetate) gave brown crystals, 0.08 g, (11%); IR (ATR, cm^{-1}): 3235 (N-H), 1617 (C=O); δ_H (400 MHz, CDCl$_3$): 2.27 (s, 3H, *CH$_3$*), 2.29 (s, 3H, *CH$_3$*), 5.78 (s, 1H, *pyrrole-H*), 9.38 (s, 1H, *CHO*), 12.28 (br.s 1H, *NH*). Data consistent with the literature values.[214]

5.1.2 4-Methoxy-N-(prop-2-en-1-yl)benzamide 70
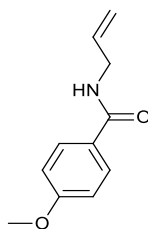
To dry DCM (25 ml), *p*-anisoyl chloride (8 ml, 59.12 mmol) and TEA (16.7 ml, 120 mmol) were mixed and cooled to 0 °C. A solution of allyl amine (4.50 ml, 60 mmol) and) in DCM 100 ml was then added dropwise to the amine solution. The reaction was then left to stir for 4 hours at RT. Water (75 ml) was added and the phases were then separated. Organic phase was then washed with a 1M HCl (100 ml) solution and brine (100 ml). The mixture was then dried over MgSO$_4$, filtered and concentrated resulting in a pale-yellow oil, 8.11 g, (71%).

δ_H (CDCl$_3$, 400MHz): 3.77 (s, 3H, *OCH$_3$*), 4.05 (tt, 2H, *J*= (5.7, 1.5) x3, CH$_2$), 5.19 (dq, 1H, *J*= 10.3, 1.4, C=C), 5.28 (q, 1H, *J*= 1.6 x3, C=C), 5.92 (ddt, 1H, *J*= 17.1, 10.4, 5.6, 5.6, 1.1, C=C), 7.05 -7.08 (m, 2H, Ar-*H*-OCH$_3$), 7.46 -7.54 (m, 2H, Ar-*H*-amide), 8.00 (s, 1H, N*H*); Data is consistent with literature data.[215]

5.1.3 2-(4-Methoxyphenyl)-1H-pyrrole 72
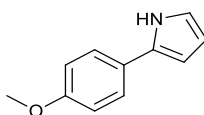
Compound **70** (2.10 g, 11.0 mmol) was placed into a dry RBF, purged with nitrogen and put in an ice bath. Phosgene (20% in toluene, 1.2 ml, 10.4 mmol) was injected into the system, and 8 drops of dry DMF added, then the reaction was then to left stir over night. The toluene was removed *in vacuo* and the residue dissolved in dry THF (40 ml). Potassium *tert*-butoxide (2.59 g, 38 mmol) was dissolved in dry DMF (20 ml), and cooled to 0 °C and this mixture was added dropwise to the butoxide solution, and the reaction was then left to stir for 30 minutes at 0 °C and was then poured over 60 ml of ice water, and separated. The aqueous phase was extracted using diethyl ether (3 x 60 ml). The combined organic phases were then washed with water (2 x 60 ml) and brine (60 ml). The organic phase was then dried over $MgSO_4$ and concentrated to give a mustard yellow powder. Yield 1.10 g, (61%). δ_H (CDCl$_3$, 300MHz): 3.81 (s, 3H, *OCH$_3$*), 6.27 (q, 1H, *J*= 2.7 x3, *CH^2 pyrrole*), 6.39 -6.41 (m, 1H, *CH^3 pyrrole*), 6.80 -6.82 (m, 1H, *CH^4 pyrrole*), 6.88 -6.92 (m, 2H, Ar-*H*-OCH$_3$), 7.38 -7.48 (m, 2H, Ar-*H*-pyrrole), 8.33 (br.s, 1H, *NH*). Data consistent with the literature values.[216]

5.1.4 2-Formyl-5-(4-methoxyphenyl)-pyrrole 74
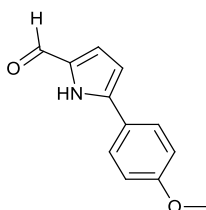
POCl$_3$ (0.6 ml, 6.68 mmol) was added dropwise to dry DMF at 0 °C, and the solution was stirred for 15 minutes at room temperature. Dry DCM (40 ml) and compound **72** (1.0 g, 5.76 mmol) was then added dropwise, at 0 °C. The reaction then refluxed for 30 minutes, before being cooled to room temperature and NaOAc (4.55 g, 33.48 mmol) in water (40 ml) was added. This mixture was then refluxed for a further 30 minutes. The organic phase was then separated, and the aqueous phase was extracted using diethyl ether (3 x 100 ml). The combined organic phases were washed with water (2 x 100 ml) and saturated Na$_2$CO$_3$ solution (1 x 100 ml), and then dried over Na$_2$SO$_4$. The resulting green powder required no further purification and was carried forward. (0.76 g, 65%); δ$_H$ (CDCl$_3$, 300MHz): 3.78 (s, 3H, *OCH$_3$*), 6.47 (d, 1H, *J*= 3.9, *CH^4 pyrrole*), 6.83 -6.91 (m, 2H, Ar-*H*-OCH$_3$), 6.94 (d, 1H, *J*= 3.9, C*H^3 pyrrole*), 7.47-7.52 (m, 2H, Ar-*H*-pyrrole), 9.40 (br.s, 1H, C*H*O), 9.52 (s, 1H, *NH*); Data consistent with the literature values.[217]

5.1.5 Pyrrole-2-(ethyl)propenoate 52
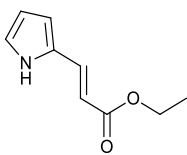
Dry THF (150 ml) was added to triethyl phosphonoacetate (13.25 ml, 67 mmol) and n-BuLi

(1.6 M in hexanes, 45.93 ml, 73 mmol) at -78 °C. The reaction was then stirred for 5

minutes before warming to 0 °C, where it stirred for a further 40 minutes. Pyrrole-2-

carboxaldehyde (6.35 g, 67 mmol) was added, and stirred for 2 hours at 0 °C, then

warmed to room temperature over 12 hours. This was concentrated *in vacuo* and the

remaining residue was portioned between water (150 ml) and ethyl acetate (150 ml). The

aqueous phase was extracted (3 x 150 ml EtOAc) and the combined organic phases were

then washed with water (2 x 200 ml) and brine (1 x 200 ml). This was dried over $MgSO_4$

and concentrated. The resulting oil was purified by column chromatography (Silica, 70: 30

cyclohexane: diethyl ether). The desired compound resulted as an off-white powder, 3.80

g (34%). δ_H (CDCl$_3$, 300MHz): 1.30 (t, 3H, *J*= 7.1 x2, *CH$_3$*), 4.22 (q, 2H, *J*= 7.1 x3, CH$_2$), 5.95

(m, 1H, C=C), 5.99 (m, 1H, C=C), 6.25 -6.27 (m, 1H, Ar*H^3*), 6.53 -6.57 (m, 1H, Ar*H^4*), 6.90 -

6.92 (m, 1H, Ar*H^5*), 8.86 (br.s, 1H, *NH*); Data consistent with the literature values.[218]

5.1.6 Pyrrole-2-(ethyl)propanoate 53
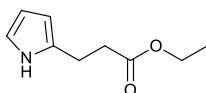
Compound **52** (2.0 g, 12.12 mmol) was dissolved in methanol (40 ml), and to this palladium on activated charcoal catalyst was added in good amounts. Hydrogen balloons were then fitted to the system for consumption and the reaction was left to run for 48 hours. A celite column was packed (3 cm celite) and wetted with methanol, and the product was pushed through with nitrogen. The resulting dark yellow oil required no further purifying and yielded 1.86 g, (78%). δ_H (CDCl$_3$, 300MHz): 1.30 (t, 3H, *J*= 7.1 x2, *CH$_3$*), 2.67 (t, 2H, *J*= 6.6 x2, C*H$_2$*COO), 2.94 (t, 2H, *J*= 6.4 x2, C*H$_2$* pyrrole), 4.17 (q, 2H, *J*= 7.1 x3, C*H$_2$*CH$_3$), 5.94 -5.97 (m, 1H, C*H^3*), 6.13 (q, 1H, *J*= 2.8 x3, C*H^4*), 6.68 -6.70 (m, 1H, C*H^5*), 8.65 (br.s, 1H, *NH*); Data consistent with the literature values.[175]

5.1.7 2-Thiophene-allyl Amide 69
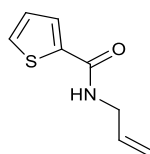
Thiophene acyl chloride (3.0 g, 2.19 ml, 20.19 mmol) was added dropwise to a mixture of allyl amine (1.16 g, 1.45 ml, 18.17 mmol) in dry DCM (15 ml) at 0 °C. Pyridine then followed (1.45 ml, 18.17 mmol), and the reaction was left to stir for 4 hours at room temperature. The reaction was diluted with DCM (50 ml) and then separated with the addition of water and the organic phase was washed with water (3 x 50 ml), brine (50 ml), and the aqueous phase extracted with DCM (3 x 50 ml). The organics were then dried over MgSO$_4$ and the mixture was concentrated to give an off white solid yielding 1.59 g, (57.2 %); δ_H (CDCl$_3$, 300 MHz): 3.95- 3.99 (m, 2H, *CH$_2$*), 5.03- 5.19 (m, 2H, *CH$_2$*), 5.77 -5.90 (m, 1H, *CH*), 6.99 (dd, 1H, *J*= 4.9, 3.7 C*H^3*), 7.40 (dd, 1H, *J*= 4.9, 1.1, C*H^4*), 7.68 (dd, 1H, *J*= 3.7, 1.1, C*H^5*); δ_C (100 MHz, CDCl$_3$): 42.3 (CH$_2$), 116.9 (=CH$_2$), 128.4, 129.9, 131.2, (3 x ArCH), 134.0 (CH=), 137.5 (C), 161.7 (C=O). Data consistent with the literature values.[177]

5.1.8 2-(2-Thienyl)-pyrrole 71
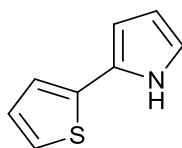
N-2-propenyl-2-thiophenecarboxamide **69** (1.5 g, 9.79 mmol) was dissolved in phosgene

solution (20% in toluene, 4.36 ml), 5 drops of anhydrous DMF were added, and the

solution was stirred at room temperature for 16 hours before being concentrated to give

a pale-yellow liquid. This was then dissolved in dry THF (4 ml), and added drop wise to a

solution of sodium *tert*-butoxide (2.00 g, 29.4 mmol) dissolved in dry DMF (14 ml). The

reaction was stirred at 0 $^{\circ}$C for 10 minutes and the poured into ice water (50 ml). The

reaction was extracted with diethyl ether (3 x 50 ml), dried with MgSO$_4$ then concentrated

to a residue, and after purification through flash column chromatography (silica, DCM) 1.0

g (68%) of brown crystals were yielded. These crystals were used immediately as the

product rapidly decomposes. δ_H (CDCl$_3$, 300 MHz): 6.23 -6.26 (m, 1H, CH^4 *pyrrole*), 6.40 -

6.42 (m, 1H, CH^3 *pyrrole*), 6.79 -6.81 (m, 1H, CH^5 *pyrrole*), 6.99 -7.01 (m, 1H, CH^3 *thienyl*),

7.04 -7.06 (m, 1H, CH^4 *thienyl*), 7.13 (dd, 1H, *J*= 5.0, 1.2, 1.2, CH^5 *thienyl*), 8.80 (br.s, 1H,

NH); Data consistent with the literature values.[177]

5.1.9 2-Foryml-5-(2-thienyl)-pyrrole 73
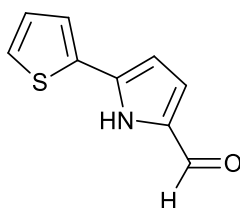
Phosphorus oxychloride (1.13 g, 0.69 ml, 7.32 mmol) was added drop wise to dry DMF

(0.54 g, 0.56 ml, 7.32 mmol) at 0 $^{\circ}$C, then warmed to room temperature over 15 minutes.

The reaction was again cooled to 0 $^{\circ}$C and dry DCE (13 ml) was added followed by a

solution of thiophene pyrrole **72** (1.0 g, 6.7 mmol) in dry DCE (33 ml) drop wise. This

mixture was refluxed for 1 hour, and upon cooling a solution of sodium acetate (5.0 g,

12.3 mmol) in water (13 ml) was added. The reaction was refluxed for a further hour. The

organic layer was washed with water (3 x 50 ml), brine (50 ml) and collected, and the

aqueous layer extracted with DCM (3 x 100 ml). The combined organics were and dried

with MgSO$_4$. The desired product was recrystallized using hexane to give gold crystals.

Yield 0.39 g, (30%); δ_H (CDCl$_3$, 300 MHz): 6.52 (d, 1H, *J*= 3.9, C*H^3 pyrrole*), 7.03 (d, 1H, *J*=

3.8, C*H^4* pyrrole), 7.11 (dd, 1H, *J*= 5.1, 3.6, C*H^3 thienyl*) 7.54 (dd, 1H, *J*= 5.1, 1.2, C*H^4*

thienyl), 7.68 (m, 1H, *J*= 3.6, 1.1, C*H^5* thienyl), 9.45 (s, 1H, C*H*O), 12.50 (br.s, 1H, N*H*); δ_C

(100 MHz, CDCl$_3$): 114.1 (CH pyrrole), 130.0 (CH pyrrole), 131.3, 131.9, 133.4 (3 x CH

thienyl) 138.5, 139.0, 139.3, (3 x C3) 183.8 (C=O). Data consistent with the literature

values. [214]

5.1.10 BODIPY TMR Ethyl Ester 76
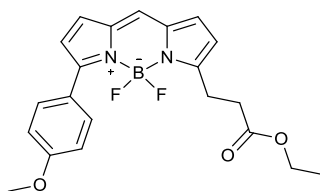
Compound **74** (300 mg, 1.49 mmol) and Compound **53** (231 mg, 1.49 mmol) were placed in a dry RBF with dry DCM (50 ml). $POCl_3$ (0.15 ml, 1.64 mmol) was mixed with dry DCM (5 ml) in a second RBF and the $POCl_3$ solution was added to the pyrrole solution dropwise at 0 °C, and left to stir for 30 minutes. The reaction warmed to room temperature and stirred for 2 hours. The solution was then cooled to 0 °C, and BF_3 diethyl etherate (0.74 ml, 6 mmol) and DIEA (1.09 ml, 6.3 mmol) was added, and the reaction was stirred overnight. To this 50 ml of DCM was added, the mixture separated, and the organic phase was washed with water (3 x 50 ml) and brine (1 x 100 ml). The aqueous phase was then extracted using DCM (50 ml) and the combined organic phases were dried over $MgSO_4$ and concentrated. The residue was purified by flash column chromatography (DCM), yielding 230 mg, (39%). δ_H (CDCl$_3$, 400MHz): 1.23 (m, 6H, CH_3), 2.65 (t, 2H, J= 7.4, CH_2), 3.22 (t, 2H, J= 7.7, CH_2), 3.76 (m, 3H, OCH_3), 4.15 (m, 2H, COOCH_2), 6.24 (d, 1H, J= 4.1, CH^3 pyrrole), 6.54 (d, 1H, J= 4.4, CH^7 pyrrole), 6.91 (d, 2H, J= 9.6, Ar-H-OCH$_3$), 6.97 (d, 1H, J= 4.4, CH^4), 7.44, (dd, 1H, J= 5.7, 3.3, CH^6 pyrrole) 7.62 (dd, 1H, J= 5.7, 3.2, CH^5 pyrrole), 7.86 (d, 2H, J= 8.0, Ar-H-pyrrole); Data consistent with the literature values.[175]

5.1.11 BODIPY 558/568 Ethyl Ester 75
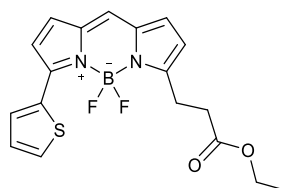
Compound **73** (200 mg, 1.20 mmol) and compound **53** (230 mg, 1.32 mmol) were dissolved in dry DCM (50 ml). POCl$_3$ (200 mg, 0.12 ml, 1.32 mmol) in DCM (2 ml) was added at 0 ^{o}C. The mixture was stirred for 30 minutes at 0 ^{o}C then at room temperature for 2 hours. The solution was cooled to 0 ^{o}C, and boron trifluoride etherate (0.69 g, 0.6 ml, 4.82 mmol) and DIEA (0.65 g, 0.88 ml, 5.04 mmol) were added. After stirring for 12 hours at room temperature, DCM (50 ml) was then added as well as water (100 ml) and the mixture was separated, washed with water (3 x 50 ml) and brine (100 ml), the aqueous later was extracted with DCM (2 x 50 ml) and the combined organic layers were dried (MgSO$_4$) and concentrated *in vacuo*. The crude product was purified by flash chromatography (silica, DCM) to give the resulting product as a red oil yielding 0.13 g, (28%); δ_H (CDCl$_3$, 400 MHz): 1.23 (m, 3H, *CH$_3$,*), 2.86 (t, 2H, *CH$_2$*, J= 7.55 Hz), 3.38 (t, 2H, *CH$_2$*, J= 7.38), 4.14 (q, 2H, *CH$_2$*), 6.39 (d, 1H, *J*= 4.12, C*H^7 pyrrole*), 6.81 (d, 1H, J= 4, *CH^3 pyrrole*), 6.99, (d, 1H, J= 4.35, C*H^6 pyrrole*), 7.04 (d, 1H, J= 4.35, C*H^4 pyrrole*), 7.13 (m, 1H, *CH^5 pyrrole*), 7.19 (dd, 1H, J= 4.97, 3.95 *CH^4 thienyl*), 7.50 (d, 1H, J= 4.48, C*H^3 thienyl*), 8.14 (d, 1H*,* J= 3.56, C*H^5 thienyl*); Data consistent with the literature values.[177]

5.1.12 BODIPY FL Ethyl Ester 58
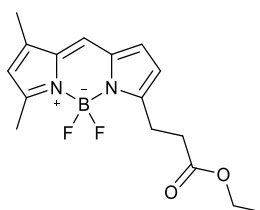
Compound **56** (200 mg, 1.20 mmol) and 3,5-dimethyl-1H-pyrrole-2-carboxaldehyde **74** (160 mg, 1.3 mmol) was dissolved in dry DCM (50 ml). POCl$_3$ (200 mg, 0.12 ml, 1.32 mmol) in DCM (2 ml) was added at 0 ^{o}C, the mixture was stirred for 30 minutes at 0 ^{O}C then at room temperature for 2 hours. Boron trifluoride etherate (0.69 g, 0.6 ml, 4.82 mmol) and DIEA (0.65 g, 0.88 ml, 5.04 mmol) were added at 0 ^{o}C and after 12 hours the mixture had warmed to room temperature. DCM (100 ml) was added and the mixture was washed with water (3 x 100 ml) then brine, (100 ml). The aqueous later was extracted with DCM (2 x 50 ml) and the combined organic layers were dried (MgSO$_4$) and concentrated *in vacuo*. The crude product was purified by flash chromatography (silica, DCM) to give the resulting product as red crystals, yielding 141 mg, (52%). δ_H (400 MHz, CDCl$_3$): 1.17 (t, 3H, *J*= 7.1, CH$_3$), 2.16 (s, 3H, C*H$_3$ pyrrole*), 2.48 (s, 3H, C*H$_3$ pyrrole*), 2.69 (t, 2H, *J*= 7.7, C*H$_2$ pyrrole*), 3.21 (t, 2H J=7.5, *CH$_2$*COO), 4.04 (m, 2H, *CH$_2$*), 6.01 (s, 1H, *CH^3*), 6.17 (d, 1H, *J*= 3.9, *CH^7*), 6.77 (d, 1H, *J*= 3.7, *CH^6*), 6.99 (s, 1H, *CH^5*); Data consistent with the literature values.[158]

5.1.13 BODIPY FL 50
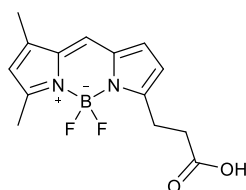
Compound **58** (500 mg, 1.60 mmol) was dissolved in THF (30 ml) and conc. HCl (37%, 10

ml) was added with water (30 ml). The reaction was left to stir for 48 hours and then DCM

(100 ml) was added, and the organic phase was separated then washed with water (2 x

100 ml) and brine (1 x 200 ml). The aqueous phase was then extracted using DCM (3 x 100

ml). The combined organic phases were dried over MgSO$_4$ then concentrated under

vacuum. The product was purified by flash column chromatography (silica, DCM, 2%

MeOH) yielding a red powder 160 mg, (34%). δ_H (400 MHz, CDCl$_3$): 2.18 (s, 3H, *CH$_3$*), 2.47

(s, 3H, *CH$_3$*), 2.76 (t, 2H, *J*= 7.5, C*H$_2$ pyrrole*), 3.23 (t, 2H *J*= 7.5, *CH$_2$*COOH), 6.05 (s, 1H, *CH^3*),

6.22 (d, 1H, *J*= 3.9, *CH^7*), 6.81 (d, 1H, *J*= 3.7, *CH^6*), 7.02 (s, 1H, *CH^5*); δ_F (376 MHz, CDCl$_3$): -

145.26 (q, *J$_{B-F}$* 33.2). Data consistent with the literature values.[158]

5.1.14 BODIPY 558/568 52
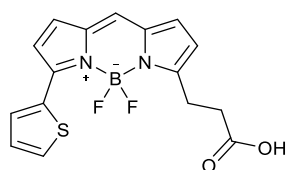
Compound **75** (550 mg, 1.38 mmol) was dissolved in THF (30 ml) and conc. HCl (37%, 10 ml) was added with water (30 ml). The reaction was left to stir for 48 hours then DCM (100 ml) was added, and the organic phase was separated and washed with water (2 x 100 ml) and brine (1 x 100 ml). The aqueous phase was then extracted using DCM (3 x 100 ml). The concentrated crude residue was purified by flash column chromatography (silica, DCM 2% MeOH) yielding the resulting product as purple crystals 170 mg, (35%); δ_H (CDCl$_3$, 400 MHz): 2.85 (t, 2H, J= 7.5, CH_2 *pyrrole*), 3.38 (t, 2H, J= 7.5, *CH$_2$*COOH), 6.39 (d, 1H, *J= 4.1, CH^7 pyrrole*), 6.79 (d, 1H, *J= 4.3, CH^3 pyrrole*), 6.96, (d, 1H, J= 4.1, CH^6 *pyrrole*), 7.02 (d, 1H, J= 4.1, CH^4 *pyrrole*), 7.11 (m, 1H, *CH^5 pyrrole*), 7.19 (dd, 1H, J= 4.9, 3.9, *CH^4 thienyl*), 7.50 (dd, 1H, J= 5.1, 0.9, CH^3 *thienyl*), 8.14 (d, 1H, J= 3.8, CH^5 *thienyl*); Data consistent with the literature values.[177]

5.1.15 BODIPY TMR 51
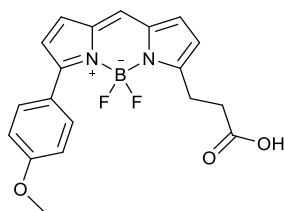
Compound **76** (550 mg, 1.38 mmol) was dissolved into THF (30 ml). To this conc. HCl (37%, 10 ml) was added with water (30 ml) and the reaction was left to stir. After 48 hours, DCM (100 ml) was added, and the organic phase was separated. This was washed with water (2 x 100 ml) and brine (1 x 200 ml), and the aqueous phase was then extracted using DCM (3 x 100 ml). The organics were concentrated and purified by column chromatography (silica, DCM 2% MeOH) yielding 80 mg, (28.84%). δ_H (CDCl$_3$, 400MHz): 2.74 (t, 2H, J= 7.4, CH_2 *pyrrole*), 3.29 (t, 2H, J= 7.5, CH_2COOH), 3.86 (s, 3H, OCH_3), 6.35 (d, 1H, J= 4.1, CH^3 *pyrrole*), 6.63 (d, 1H, J= 4.4, CH^7 *pyrrole*), 6.94 (d, 1H, J= 4.1, CH^4 *pyrrole*), 6.99 (m, 2H, Ar-*H*-pyrrole), 7.06 (d, 1H, J= 4.0, CH^6 *pyrrole*), 7.13 (m, 1H, CH^5 *pyrrole*), 7.93 (m, 2H, Ar-*H*-OCH$_3$); Data consistent with the literature values.[175]

5.1.16 (6-Hydroxyhexyl)carbamoyl BODIPY TMR 77
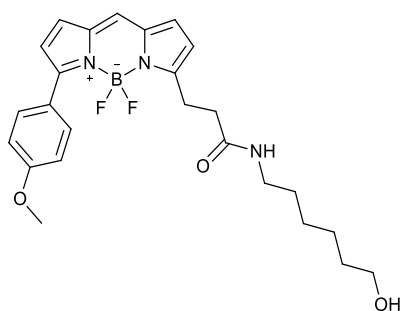
In an RBF, BODIPY TMR (100 mg, 0.27 mmol) was placed, and dry DCM (20 ml) was added.

T3P solution (0.2 ml, 50% in DMF, 0.54 mmol) was added along with TEA (0.1 ml), and 6-

aminohexan-1-ol (31 mg, 0.26 mmol). This was left stirring at room temperature for 12h

and then separated with water (20 ml), and the organic phase was washed with water (2 x

20 ml), brine (50 ml) and extracted with DCM (2 x 20 ml). The compound was put through

a plug of silica and several fractions collected. The first fractions contained the desired

product with 20 mg yield (20%). δ_H (CDCl$_3$ 300MHz): 1.15 -1.45 (m, 8H, CH$_2$), 2.49 (t, 2H, $J=$

6, CH$_2$ pyrrole), 3.09 (t, 2H, $J=$ 6, CH$_2$NH), 3.18 (t, 2H, $J=$ 6, CH$_2$CO), 3.51 (t, 2H, $J=$ CH$_2$OH),

3.80 (s, 3H, OCH$_3$), 5.80 (s, 1H, NH), 6.29 (d, 1H, $J=$ 3, CH^3 pyrrole), 6.56 (d, 1H, $J=$ 6 CH^7

pyrrole), 6.90 (d, 1H, CH^4 pyrrole), 6.93 (d, 2H, $J=$ 9, Ar-H-pyrrole), 7.02 (d, 1H, $J=$ 3, CH^6

pyrrole), 7.10 (d, 1H, $J=$ 3, CH^5 pyrrole), 7.84 (d, 2H, $J=$ 9, Ar-H-OCH$_3$).

5.1.17 Saligenin Chlorophosphinine-2-oxide 45
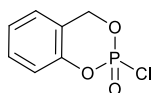
2-Hydroxybenzyl alcohol (1.00 g, 8.05 mmol) and TEA (2.50 ml, 2.15 mmol) in dry DCM (200 ml), had a solution of POCl$_3$ (0.83 ml, 8.83 mmol) in dry DCM (4 ml) added dropwise at -78 °C. The mixture was stirred for 45 minutes, allowed to warm to room temperature and then concentrated under a vacuum. Dry toluene (30 ml) was added and the mixture stood in a fridge for 1 hour and then filtered, the solvent was removed *in vacuo.* The product was dried to obtain the desired compound **45** (1.50 g, 91%) which can be brought forward with no further purification. δ_H (400 MHz, CDCl$_3$): 5.50- 5.59 (m, 2H, *CH$_2$*), 7.08 (d, 1H, J= 8.2, Ar*H^1*), 7.18 (d, 1H, J= 7.2, Ar*H^4*), 7.25 (t, 1H, J= 7.4, Ar*H^2*), 7.38 (t, 1H, J= 7.8 Ar*H^3*); δ_P (162 MHz, CDCl$_3$): (s, -5.38 ppm). Data consistent with the literature values.[219]

5.1.18 Phenyl Saligenin Phosphate 7
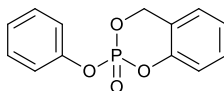
Phenyl phosphorodichloridate (1 g, 4.73 mmol), 2-hydroxybenzyl alcohol (0.5 g, 4.02 mmol) and TEA (2 ml, 26 mmol) were placed into a RBF and dissolved in dry THF (50 ml) then stirred at 0 °C for 30 minutes. Refluxing for 12 hours then followed, and the reaction solution was then diluted with water (50 ml) and extracted with $CHCl_3$ (3 x 50 ml). The combined organic layers were dried over $MgSO_4$ and concentrated in vacuo. This gave the product in a yield of 70% (700 mg). δ_H (400 MHz, $CDCl_3$): 5.40-5.47 (m, 2H, CH_2), 7.11-7.21 (m, 9H, Ar-H); δ_P ($CDCl_3$, 162 MHz): -15.08 ppm. Data consistent with the literature values.[220]

5.1.19 2-Hydroxy-dioxaphosphinine-2-oxide 47
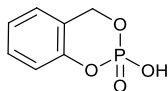
After formation of compound **45** (7.33 mmol), water (2 ml) is added to the RBF and the mixture is left overnight. All the solvent is removed and the compound recrystalised from chloroform to leave a white amorphous solid, 1.00 g (73%). δ_H (400 MHz, CDCl$_3$): 5.37-5.40 (d, 2H, J= 13.5 CH_2), 7.03 (d, 1H, J= 8.2, ArH^1), 7.12 (m, 1H, ArH^4), 7.21 (m, 1H, ArH^2), 7.33 (t, 1H, J= 7.83, ArH^3), 9.71 (s, 1H, OH); δ_C (100 MHz, CDCl$_3$): 67.9 (J_{PC}= 6, CH$_2$), 118.3 (J_{PC}= 9, CH^1), 118.4 (J_{PC}= 9.5, CH^4), 123.9 (CH^2), 125.8 (J$_{PC}$ = 77, CH^3), 129.5 (J_{PC}= 49, C^6), 150.5 (J_{PC}= 6, CO^5); δ_P (162 MHz, CDCl$_3$): (s, -8.62ppm).

5.1.20 (6-Hydroxyhexyl)carbamoyl Rhodamine B 15
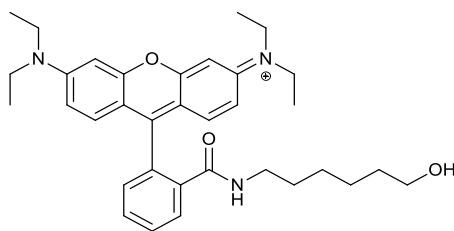
Rhodamine B 1 g (2.08 mmol), and HBTU 0.79 g (2.08 mmol) was dissolved in dry DCM (250 ml) and TEA 2 ml (26 mmol) then followed. 365 mg (3.12 mmol) of 6-aminohexan-1-ol dissolved in dry DCM (10 ml) is then injected into the system. The reaction was left stirring for 12 hours after this work-up proceeded by washing with water (2 x 100 ml), brine (100 ml) and then extracted with DCM (3 x 100 ml). After drying with magnesium sulphate and filtering, the resulting solution was then purified on silica with 49% acetone, 50% toluene and 1% TEA returning the product 300 mg (26.6 %). IR (ATR, cm^{-1}): 3352 (OH), 2970, 2929, 2862 (CH, rhodamine), 1665 (C=O, amide), 1613 (C=C) 1513 (NH bending); δ_H (400 MHz, CDCl$_3$): 1.16 (m, 18H, 12CH_3, 6CH_2), 1.35 (m, 2H, CH_2), 3.11 (t, 2H, J= 6.8 CH_2NH), 3.34 (q, 8H, *J*= 6.9 N(CH_2)$_2$), 3.52 (t, 2H, J= 6.6 CH_2OH), 6.27 (d, 2H, *J*= xanthene*H*^{4,5}), 6.48 (m, 4H, xanthene*H*^{1,2,7,8}), 7.07 (m, 1H, Ar*H*^{6}), 7.40 -7.44 (m, 2H, Ar*H*^{4,5}), 7.88 -7.97 (m, 1H, Ar*H*^{3}); δ_C (100 MHz, CDCl$_3$): 12.5 (CH$_3$ xanthene), 24.7 (CH$_2$), 26.3 (CH$_2$), 27.9 (CH$_2$), 32.3 (CH$_2$), 39.9 (CH$_2$NH), 44.3 (CH$_2$ xanthene), 62.6 (CH$_2$OH), 64.7 (C9 lactam), 97.5 (4/ 5 xanthene), 105.7 (2/ 7 xanthene), 107.8 (8a/ 9a xanthene), 122.4 (Ar 3), 123.5 (Ar 6), 128.7 (Ar 4), 128.8 (Ar 2), 131.9 (Ar 1), 132.3 (Ar 5), 148.5 (3/ 6 xanthene), 153.1 (4a/ 5a xanthene), 153.3 (1/ 8 xanthene), 167.8 (C=O); HRMS (NSI) (m/z), [M+H] calcd, for C$_{34}$H$_{44}$N$_3$O$_3^+$ 542.3377 found 542.3364.

5.1.23 (6-TBDMShydroxyhexyl)carbamoyl Rhodamine B 41
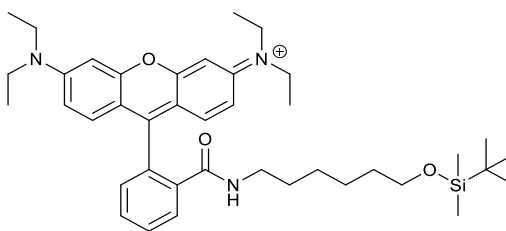
Rhodamine B (305 mg, 0.7 mmol), compound **15** (160 mg, 0.7 mmol) and HBTU (262 mg, 0.7 mmol) were dissolved in dry DCM (100 ml), cooled to 0 °C and 1 ml (13 mmol) of TEA then followed. The reaction warmed to room temperature and left for the next 24 hours. Work-up then followed by washes with water (2 x 100 ml), brine (100 ml) and extracted with DCM (2 x 100 ml). Column chromatography with 98 % DCM and 2 % TEA yielded 61 mg of a clear pink oil (13 %).

IR (ATR, cm^{-1}): 2950, 2929, 2856 (rhodamine), 1689 (amide), 1614, 1513 (NH bending), 1467 1219 (xanthene) 1256 (Si-CH$_3$), 1092 (Si-O-C(CH$_3$)) δ_H (400 MHz, CDCl$_3$): 0.04 (m, 6H, CH_2Si), 0.87 (m, 9H, SiC(CH_3)) 1.08- 1.16 (m, 18H, 12CH_3, 6CH_2), 1.33 (m, 2H, CH_2), 3.09 (t, 2H, J= 7.3, CH_2NH), 3.34 (q, 8H, J= 7.0, N(CH_2)$_2$) 3.48 (t, 2H, J= 6.6, CH_2O), 6.26 (dd, 2H, J= 8.9, 2.6, xanthene$H^{4,5}$), 6.38- 6.44 (m, 4H, xanthene$H^{1,2,7,8}$), 7.06 (m, 1H, ArH^6), 7.42 (m, 2H, Ar$H^{4,5}$), 7.89 (m, 1H, ArH^3); δ_C (100 MHz, CDCl$_3$): -5.3 (CH$_3$Si), 12.5 (CH$_3$ xanthene), 25.3 (CH$_2$), 25.9 (CH$_3$), 26.9 (CH$_2$), 28.1 (CH$_2$), 32.6 (CH$_2$), 40.3 (CH$_2$NH), 44.3 (CH$_2$ xanthene), 63.2 (CH$_2$O), 64.7 (C9 lactam), 97.5 (4/ 5 xanthene), 105.9 (2/7 xanthene), 107.8 (8a/ 9a xanthene), 122.6 (Ar 3), 123.6 (Ar 6), 127.8 (Ar 4), 128.9 (Ar 2), 131.5 (Ar 1), 132.0 (Ar 5), 148.6 (3/ 6 xanthene), 153.2 (4a/ 5a xanthene), 153.5 (1/ 8 xanthene), 167.9 (C=O); HRMS (NSI) (m/z), [M+H] calcd, for C$_{40}$H$_{58}$N$_3$O$_3$Si$^+$ 656.4242 found 656.4230.

5.1.24 (6-Saligeninhexyl)carbamoyl Rhodamine B Phosphate 18
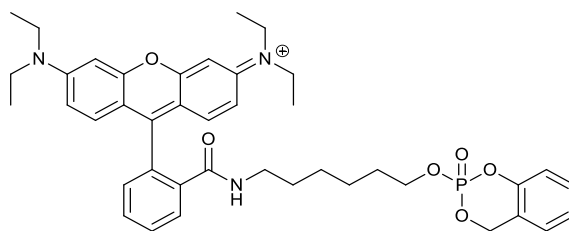
To a stirring solution of rhodamine amidohexanol **15** (260 mg 0.44 mmol), and TEA (1 ml, 13 mmol) in dry DCM (250 ml) at 0 °C, saligenin chlorophosphate **45** (270 mg, 1.32 mmol) dissolved in dry DCM (10 ml) was added dropwise. This was then left to stir for 24 hours. Upon completion, work-up proceeded with washes of water (2 x 100 ml) and brine (100 ml), extraction with DCM (3 x 100 ml). The purified pink oil compound was achieved by chromatography on silica with toluene: acetone: TEA (1:1.9:0.1) and yielded with 34% (106 mg). IR (ATR, cm^{-1}): 2970, 2934, 2929 (CH, rhodamine), 1682 (C=O, amide), 1613 (C=C) 1513 (NH bending), 1017, 932 (P=O); δ_H (400 MHz, CDCl$_3$): 1.06 -1.08 (m, 6H, CH_2), 1.16 (t, 12H, J= 7.0, CH_3), 1.52 (m, 2H, CH_2), 3.05 (t, 2H, J= 6.9, CH_2NH), 3.33 (q, 8H, J= 6.9, CH_2), 4.03- 4.10 (m, 2H, CH_2OP), 5.29- 5.33 (m, 2H, CH_2OP), 6.26 (dd, 2H, J= 8.8, 2.5, xanthene $H^{4,5}$), 6.37 -6.42 (m, 4H, xanthene $H^{1,2,7,8}$), 7.01 -7.12 (m, 4H, ArH^6), 7.29 (m, 1H, OPArH), 7.41- 7.48 (m, 3H, Ar$H^{4,5}$), 7.89 (m, 1H, ArH^3); δ_C (100 MHz, CDCl$_3$): 12.5 (CH$_3$ xanthene), 24.7 (CH$_2$), 26.3 (CH$_2$), 27.8 (CH$_2$), 29.7 (CH$_2$, J_{AC}= 7), 40.0 (CH$_2$NH), 44.3 (CH$_2$ xanthene), 64.7 (C9 lactam), 68.4 (CH$_2$O, J_{AC}= 5), 68.8 (CH$_2$O, J_{AC}= 6), 97.5 (4/ 5 xanthene), 105.8 (2/ 7 xanthene), 107.8 (8a/ 9a xanthene), 118.6 (CH^1, J_{AC}= 10), 122.6 (Ar 3), 123.7 (Ar 6), 124.0 (CH^2), 125.2 (CH^3, J_{AC}=) , 127.9 (Ar 4), 128.9 (Ar 2), 129.6 (C^6), 131.5 (Ar 1), 132.1 (Ar 5), 148.6 (3/ 6 xanthene), 153.3 (4a/ 5a xanthene), 153.4 (1/ 8 xanthene), 167.9 (C=O): δ_P (162 MHz, CDCl$_3$): (s, -8.90ppm); HRMS (NSI) (m/z), [M+H] calcd, for C$_{41}$H$_{49}$N$_3$O$_6$P$^+$ 710.3353 found 710.3343.

5.1.25 (2-(2-Hydroxyethoxy)ethyl)carbamoyl) Rhodamine B 16
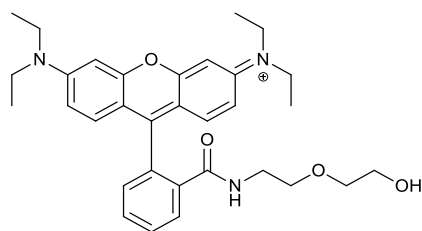
Rhodamine B (1 g, 2.08 mmol), was added to a RBF with HBTU (0.79 g, 2.08 mmol) in dry DCM (250 ml), 2 ml (26 mmol) of TEA then follows. 2-(2-Aminoethoxy) ethanol (309 mg 2.08 mmol) dissolved in dry DCM (10 ml) is then injected into the system and the reaction left for 12 hours. Water (100 ml) was then added and the phases separated. The organic phase was washed with water (2 x 100 ml), and brine (100 ml), and the aqueous phases were extracted with DCM (3 x 100 ml). After drying with $MgSO_4$ and filtering, the resulting solution is purified with silica column chromatography with 49% acetone, 50% toluene and 1% TEA. The yield returned is 384 mg (35 %).

IR (ATR, cm^{-1}): 3374 (OH), 2967, 2924, 2870 (CH, rhodamine), 1686 (C=O, amide), 1613 (C=C) 1513 (NH bending), 1116 (C-O); δ_H (400 MHz, CDCl$_3$): 1.16 (t, 12H, J= 7.1, CH_3), 3.18 (t, 2H, J= 6.1, CH_2NH), 3.32-3.36 (m, 12H, CH_2), 3.58 (t, 2H, J= 4.5, CH_2OH), 6.26 (dd, 2H, J= 8.9, 2.4, xanthene $H^{4,5}$), 6.37 -6.46 (m, 4H, xanthene $H^{1,2,7,8}$), 7.05 -7.09 (m, 2H, ArH^3), 7.41- 7.45 (m, 2H, Ar$H^{4,5}$), 7.89 (m, 1H, ArH^6); δ_C (100 MHz, CDCl$_3$): 12.6 (CH$_3$ xanthene), 39.8 (CH$_2$NH), 44.4 (CH$_2$ xanthene), 47.0 (CH$_2$OH), 61.6 (CH$_2$O), 65.1 (C9 lactam), 72.1 (CH$_2$OH), 97.7 (4/ 5 xanthene), 105.4 (2/ 7 xanthene), 108.1 (8a/ 9a xanthene) 122.8 (Ar 3), 123.8 (Ar 6), 128.1 (Ar 4), 128.9 (Ar 2), 131.0 (Ar 1) 132.6 (Ar 5), 148.8 (3/ 6 xanthene), 153.3 (1/ 8 xanthene), 153.7 (4a/ 5a xanthene), 168.7 (C=O); HRMS (NSI) (m/z), [M+H] calcd, for C$_{32}$H$_{40}$N$_3$O$_4{}^+$ 530.3013 found 530.2999.

5.1.26 (2-(2-Saligeninethoxy)ethyl)carbamoyl) Rhodamine B 48
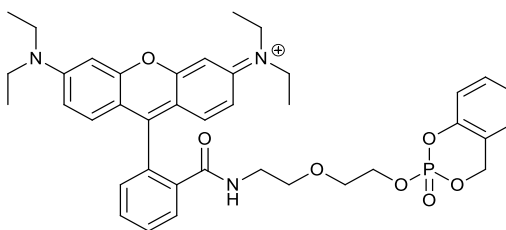
Compound **16** (384 mg, 0.72 mmol) was mixed in dry conditions with TEA (2 ml, 26 mmol), and dry DCM (250 ml). This synthesis follows the same technique as 5.1.24, with saligenin chlorophosphate being added dropwise (444 mg, 2.17 mmol). Work-up proceeded by the standard technique (2 x H_2O, 1 x brine) and extracted with DCM. Acetone, toluene and TEA column yielded a very pale pink oil of about 151 mg (30%). IR (ATR, cm^{-1}): 2970, 2925, 2871 (CH, rhodamine), 1686 (C=O, amide), 1613 (C=C), 1513 (NH bending), 1116 (C-O), 1018, 935 (P=O); δ_H (400 MHz, $CDCl_3$): 1.14 (t, 12H, J= 7.0, CH_3), 3.12 (t, 2H, J= 7.0, CH_2NH), 3.19-3.37 (m, 12H, CH_2), 4.10 (m, 2H, CH_2OP), 5.18- 5.39 (m, 2H, CH_2OP), 6.22 (ddd, 2H, J= 17.7, 8.9, 2.5, xanthene $H^{4,5}$), 6.33 -6.41 (m, 4H, xanthene $H^{1,2,7,8}$), 6.95- 7.05 (m, 3H, ArH^3, OPC$H^{1,2}$), 7.14- 7.26 (m, 2H, OPC$H^{3,4}$), 7.40- 7.44 (m, 2H, Ar$H^{4,5}$), 7.87 (m, 1H, ArH^6); δ_C (100 MHz, $CDCl_3$): 12.5 (CH_3 xanthene), 39.1 (CH_2NH), 44.3 (CH_2 xanthene), 64.3 (C9 lactam), 67.5 (CH_2OP, J_{PC}= 5), 68.5 (CH_2O, J_{PC}= 8), 69.03 (CH_2OP, J_{PC}= 6), 97.5 (4/ 5 xanthene), 105.3 (2/ 7 xanthene), 107.9 (8a/ 9a xanthene), 118.6 (CH^1, J_{PC}= 9), 120.5 (CH^4, J_{PC}= 10), 122.6 (Ar 3), 123.7(CH^2), 123.9 (Ar 6), 125.2 (CH^3), 127.9 (Ar 4), 128.8 (Ar 2), 129.4 (C^6), 130.7 (Ar 1), 132.3 (Ar 5), 148.6 (3/ 6 xanthene), 150.1 (J_{PC}= 6, CO^5), 153.2 (1/ 8 xanthene), 153.7 (4a/ 5a xanthene), 168.2 (C CONH). δ_P (162 MHz, $CDCl_3$): (s, -9.01ppm); HRMS (NSI) (m/z), [M+H] calcd, for $C_{39}H_{45}N_3O_7P^+$ 698.2990 found 698.2987.

5.1.27 (2-(2-(2-Hydroxyethoxy)ethoxy)ethyl)carbamoyl) Rhodamine B 17
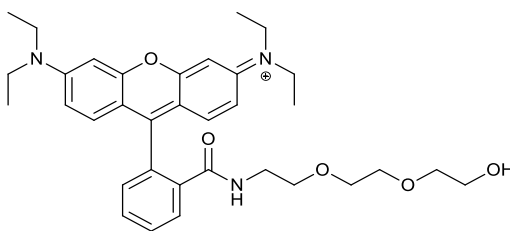
Rhodamine B (1 g, 2.08 mmol), was added to a RBF with HBTU (0.79 g, 2.08 mmol), and dissolved in dry DCM (250 ml). TEA (2 ml, 26 mmol) was added and a solution of 2-[2-(2-aminoethoxy) ethoxy] ethanol (309 mg, 2.70 mmol) dissolved in dry DCM (10 ml) was also injected into the system. The reaction was left for 12 hours before the phases were separated on addition of water (100 ml). Washes followed with water (2 x 100 ml), brine (100 ml) and then extraction with DCM (3 x 100 ml). After drying with MgSO$_4$ and filtering, the resulting residue is purified via silica column chromatography with 49% acetone, 50% toluene and 1% TEA and returned the product 800 mg (67%).

IR (ATR, cm^{-1}): 3362 (OH), 2969, 2926, 2871 (CH, rhodamine), 1685 (C=O, amide), 1613 (C=C) 1513 (NH bending), 1116 (C-O); δ_H (400 MHz, CDCl$_3$): 1.14-1.16 (t, 12H, J= 7.03, CH$_3$), 3.15 (t, 2H, J= 7.1, CH_2NH), 3.28- 3.39 (m, 8H, CH_2), 3.48- 3.52 (m, 8H, CH_2), 3.69-3.73 (t, 2H, CH_2OH), 6.24 (dd, 2H, J= 8.8, 2.1, xanthene $H^{4,5}$), 6.31- 6.42 (m, 4H, xanthene $H^{1,2,7,8}$), 7.01- 7.06 (m, 1H, ArH^3), 7.37-7.42 (m, 2H, Ar$H^{4,5}$), 7.85-7.88 (m, 1H, ArH^6) ; δ_C (100 MHz, CDCl$_3$): 12.6 (CH$_3$ xanthene), 39.1 (CH$_2$NH), 44.4 (CH$_2$ xanthene), 61.8 (CH$_2$OH), 64.9 (C9 lactam), 67.8 (CH$_2$O), 70.0 (CH$_2$O), 70.4 (CH$_2$O), 72.5 (CH$_2$O), 97.8 (4/ 5 xanthene), 105.8 (2/ 7 xanthene), 108.1 (8a/ 9a xanthene) 122.8 (Ar 3), 123.8 (Ar 6), 128.0 (Ar 2), 128.9 (Ar 4), 131.0 (Ar 1) 132.4 (Ar 5), 148.8 (3/ 6 xanthene), 153.3 (1/ 8 xanthene), 153.7 (4a, 5a xanthene), 168.4 (C=O); HRMS (NSI) (m/z), [M+H] calcd, for C$_{34}$H$_{44}$N$_3$O$_5^+$ 574.3275 found 574.3267.

5.1.28 (2-(2-(2-Saligeninethoxy)ethoxy)ethyl)carbamoyl Rhodamine B 49
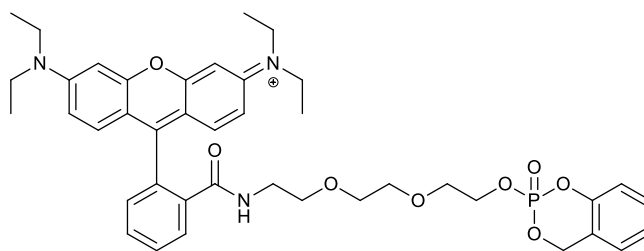
Compound **17** (300 mg, 0.52 mmol) was dissolved in dry DCM (250 ml), with TEA (1 ml, 13 mmol) also being added. Saligenin chlorophosphite solution **45** was added dropwise (80 mg, 0.40 mmol) in dry DCM (10 ml) at -78 °C. The organic phase was washed with water (2 x 50 ml), and brine (50 ml) and then extracted with DCM (3 x 50 ml). After drying, the compound was purified through a column of silica, 50% acetone in toluene, yielding 80 mg (27%). IR (ATR, cm^{-1}): 2970, 2925, 2871 (CH, rhodamine), 1686 (C=O, amide), 1613 (C=C) 1514 (NH bending), 1116 (C-O),), 1019, 934 (P=O); δ_H (400 MHz, CDCl$_3$): 1.15 (t, 12H, $J=$ 6.9, CH_3), 3.15 (t, 2H, $J=$ 7.3, CH_2NH), 3.31-3.51 (m, 12H, CH_2), 3.43 -3.46 (m, 2H, CH_2), 3.63 (bt, 2H, $J=$ 4.69, CH_2), 4.19- 4.34 (m, 2H CH_2OP), 5.21-5.44 (m, 2H, CH_2OP), 6.26 (bt, 2H, $J=$ 8.9, 2.5, xanthene $H^{4,5}$), 6.37- 6.44 (m, 4H, xanthene $H^{1,2,7,8}$), 6.99- 7.09 (m, 4H, ArH^3, OPC$H^{1,2,3}$), 7.24- 7.30 (m, 1H, OPCH^3), 7.40- 7.44 (m, 2H, Ar$H^{4,5}$), 7.87- 7.89 (m, 1H, ArH^6) ; δ_C (100 MHz, CDCl$_3$): 12.5 (CH$_3$ xanthene), 39.1 (CH$_2$NH), 44.2 (CH$_2$ xanthene), 64.7 (C9 lactam), 67.3 (CH$_2$OP, $J_{AC}=$ 6), 67.7 (CH$_2$O), 68.6 (CH$_2$OP, $J_{AC}=$ 7), 69.6 (CH$_2$O), 69.8 (CH$_2$O), 70.3 (CH$_2$O), 97.6 (4/ 5 xanthene), 105.4 (2/ 7 xanthene), 107.9 (8a/ 9a xanthene), 118.5 (CH^1, $J_{AC}=$ 8), 120.4 (CH^4, $J_{PC}=$ 9), 122.5 (Ar 3), 123.7 (Ar 6), 124.0 (CH^2), 125.2 (CH^3, $J_{AC}=$ 3), 127.8 (1/ 8 xanthene), 128.6 (Ar 2), 128.9 (Ar 4), 129.4 (C^6), 130.8 (Ar 1) 132.3 (Ar 5), 148.6 (3/ 6 xanthene), 149.9 (CO^5, $J_{PC}=$ 9), 153.1 (4a/ 5a xanthene), 153.6 (1/ 8 xanthene), 168.1 (C=O); δ_P (162 MHz, CDCl$_3$): (s, -9.02ppm); HRMS (NSI) (m/z), [M+H] calcd, for C$_{41}$H$_{49}$N$_3$O$_8$P$^+$ 742.3252 found 742.3246.

5.1.29 1,2,3,4-Tetrahydroquinolin-7-ol 87
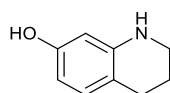
7-Hydroxy-3,4-dihydro-2-quinolinone (200 mg, 1.2 mmol), was dissolved in THF (20 ml),

borane dimethylsulfide (9.8 ml, 2M in THF, 19.6 mmol) was then added and heated to

reflux for 30 minutes. After this methanolic HCl (20 ml) was added and refluxed for a

further 30 minutes. The solvent was evaporated, and residue washed with MeOH (3 x 10

ml) to remove boric acid. Work-up then proceeded by dissolving the crude green oil in

DCM (20 ml), water washes (2 x 20 ml) and brine (20 ml). Column chromatography with

3:1 hexane and ethyl acetate yielded 100 mg (55%) of a clear oil.

δ_H (400 MHz, CDCl$_3$): 1.69 (m, 2H, CH_2), 2.46 (t, 2H, J= 6.35, CH_2NH), 3.09 (t, 2H, J=

5.49, CH_2Ar), 5.42 (br.s, 2H, OH, NH), 5.92 (m, 1H, ArH^5), 5.99 (d, 1H, J= 2.4, ArH^6),

6.5 (d, 1H, J= 7.76, ArH^8); Data consistent with the literature values. [143]

5.1.30 (6-Hydroxyhexyl)-4-(pyren-2-yl)butanamide 83
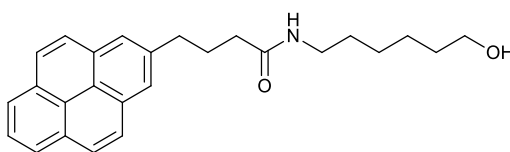
Pyrene butyric acid (200 mg, 0.7 mmol) was added to a RBF with HBTU (263 mg, 0.7 mmol) and 6-aminohexanol (164 mg, 1.4 mmol), in dry DCM (200 ml). The reaction was cooled to 0 °C and TEA (2 ml, 26 mmol) was then added and the mixture allowed to stir for 12 hours, warming to room temperature. Work-up followed with water (2 x 100 ml) and brine (100 ml), and extraction with ethyl acetate (3 x 100 ml). Column purification with ethyl acetate resulted in 210 mg (78.12 %) yield of a clear, pale orange waxy, crystalline solid. M.p. 143 -145 °C. IR (ATR, cm^{-1}): 3379 (CH aromatic), 3308 (OH), 3040 (NH), 2931 (CH alkane), 1638 (C=O), 1537 (C=C aromatic); δ_H (400 MHz, CDCl$_3$): 1.24 -1.39 (m, 4H, CH_2), 1.42 -1.56 (m, 4H, CH_2), 2.19 -2.26 (m, 4H, CH_2), 3.22 (q, 2H, J= 6.8 x3, CH_2NH), 3.40 (t, 2H, J= 7.3, CH_2CO), 3.60 (t, 2H, J= 6.6, CH_2OH), 5.36 (br.s, 1H, NH), 7.86 (d, 1H, J= 7.8, ArH), 7.97 -8.03 (m, 3H ArH), 8.10 -8.12 (m, 2H, ArH), 8.17 (dd, 2H, J= 8.0, 2.29, ArH), 8.30 (d, 1H, J= 8.0, ArH); δ_C (CDCl$_3$ 100 MHz): 25.3, 26.5, 27.5, 29.7, 32.9, 32.6, 32.8 (CH$_2$CO), 36.1 (CH$_2$ pyrene), 39.4 (CH$_2$NH), 62.8 (CH$_2$OH), 123.4 (C3a^1), 124.8 (C5a^1), 124.9 (C3), 125.0 (C6), 125.1 (C8), 125.2 (C2), 125.9 (C7), 126.7 (C4), 127.4 (C5), 127.5 (C9), 128.8 (C10), 129.9 (C3a), 130.9 (C5a), 131.4 (C8a), 134.5 (C10a), 135.8 (C1), 172.6 (CO); HRMS (NSI) (m/z), [M+H] calcd, for C$_{26}$H$_{30}$NO$_2^+$ 388.2271 found 388.2269.

5.1.31 (6-Saligeninhexyl)-4-(pyren-2-yl)butanamide Phosphate 84
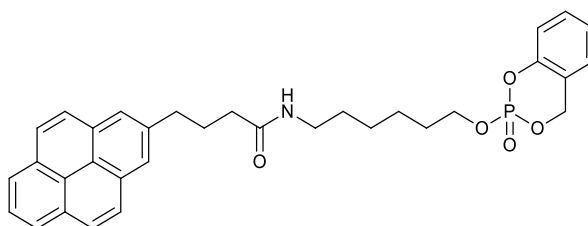
(6-hydroxyhexyl)-4-(pyren-2-yl)butanamide **83** (200 mg, 0.51 mmol) is dissolved in THF

and dry DCM (1:3) and cooled to -78 °C. Then TEA (2 ml, 26 mmol) was added followed by

the dropwise addition of saligenin chlorophosphate **45** (350 mg, 1.71 mmol). The product

was yielded after work-up with water, brine and extraction with DCM, proceeded by

column chromatography with ethyl acetate. The resulting pale orange oil weighed 120 mg

(42%). IR (ATR, cm^{-1}): 3314 (CH aromatic), 3308 (OH), 3040 (NH), 2931 (CH alkane), 1644

(C=O), 1542 (C=C aromatic) 1289 (P=O), 1014 (POC), 932 (P=O); δ_H (400 MHz, CDCl$_3$): 1.23 -

1.42 (m, 6H, CH_2), 1.59 -1.64 (m, 2H, CH_2), 2.15 -2.25 (m, 4H, CH_2), 3.15 (q, 2H, J= 6.8 x3,

CH_2NH), 3.34 (t, 2H, J= 7.3 x2, CH_2CO), 4.12 (m, 2H, CH_2OP), 5.24 -5.27 (m$_{ABX}$, 2H, POCH_2),

5.73 (br.s, 1H, NH), 6.97 -7.01 (m, 2H, ArH), 7.05 (td, 1H, J= 7.5, 0.9, ArH^4), 7.25 (m, 1H,

ArH^5), 7.81 (d, 1H, J= 7.78, pyrene), 7.94 -7.99 (m, 3H, pyrene), 8.06 (m, 2H, ArH^3), 8.13 (d,

2H, J= 7.78, pyrene), 8.28 (d, 1H, J= 9.15, pyrene);

δ_C (CDCl$_3$ 100 MHz): 24.8, 26.1, 27.6, 29.4, 30.1 (CH$_2$, J_{PC}= 7) 32.8 (CH$_2$CO), 36.1 (CH$_2$), 39.2

(CH$_2$NH), 68.6 (CH$_2$OP, J_{PC}= 8), 68.7 (POCH$_2$, J_{PC}= 6), 118.7 (CH^1, J_{PC}= 8), 120.7 (CH^4, 10),

123.5 (C3a^1), 124.2 (C5a^1), 124.8 (CH^2 J_{PC}= 4), 124.9 (C3), 125.0 (C6), 125.1 (C8), 125.3 (C2),

125.9 (C7), 126.7 (C4), 127.4 (C5), 127.5 (C9), 128.8 (C10), 129.8 (C^6), 129.9 (C3a), 130.9

(C5a), 131.5 (C8a), 136.1 (C1), 150.2 (CO^5, J_{PC}= 6.7), 172.8 (CO);

δ_P (CDCl$_3$, 162 MHz): -8.79 ppm; HRMS (NSI) (m/z), [M+H] calcd, for C$_{33}$H$_{35}$NO$_5$P$^+$ 556.2247

found 556.2235.

5.1.32 2-(4-(Pyren-2-yl)butoxy)saligenin Phosphate 85
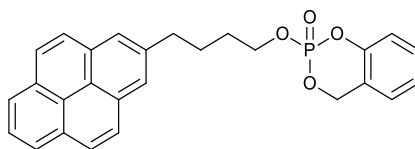
Pyrene butanol (200 mg, 0.73 mmol), was dissolved in dry DCM (200 ml), and (1 ml, 13 mmol) TEA. At 0 °C, saligenin chlorophosphate **45** was added (300 mg, 1.46 mmol). After warming to room temperature over 12 hours, water (100 ml) was added and the phases separated then the organic phase is washed with water (2 x 100 ml) and brine (100 ml). Extraction of the aqueous fraction with ethyl acetate (3 x 100 ml), drying with MgSO$_4$ and filtering gives the yellow crude oil. This is purified with ethyl acetate on a silica column giving a pale-yellow oil, 76 mg (24%). IR (ATR, cm^{-1}): 3673 (CH aromatic), 2936 (CH alkane), 1457 (C=C aromatic), 1294 (P=O), 1016 (POC), 932 (P=O); δ_H (400 MHz, CDCl$_3$): 1.84 -1.88 (m, 4H, CH_2), 3.33 (t, 2H, J= 7.2, CH_2NH), 4.27 (m, 2H, CH_2OP), 5.21 -5.29 (m, 2H, POCH_2), 6.91 -7.03 (m, 2H, ArH), 7.17 -7.26 (m, 1H ArH), 7.79 (d, 2H, J= 7.8, pyrene), 7.97 -8.21 (m, 7H, pyrene); δ_C (CDCl$_3$ 100 MHz): 27.6 (CH$_2$), 30.2 (CH$_2$, J$_{PC}$ =6), 32.9 (CH$_2$pyrene), 68.6 (POCH$_2$, J$_{PC}$= 7), 68.8 (CH$_2$OP, J$_{PC}$= 6), 118.8 (CH^1, J$_{PC}$ =8), 120.6 (CH, J$_{PC}$ =10), 123.3 (C3a^1), 124.2 (CH^2), 124.8 (C5a^1), 124.9 (C3), 125.0 (C6), 125.1 (C2), 125.3 (CH^3), 125.9 (C7), 126.8 (C4), 127.3 (C5), 127.4 (C9), 127.6 (C10), 128.6 (C^6 J$_{PC}$ =5), 129.7 (C3a), 129.9 (C5a), 130.9 (C8a), 131.5 (C10a), 136.1 (C1), 150.2 (CO^5, J$_{PC}$ =7), 187.4 (C=O); δ_P (CDCl$_3$, 162 MHz): -8.76 ppm; HRMS (NSI) (m/z), [M+H] calcd, for C$_{27}$H$_{24}$NO$_4$P$^+$ 443.1407 found 443.1399.

5.1.31 6-Hydroxyhexylamino-4-benzophenone 118
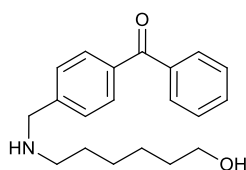
6-Aminohexan-1-ol (250 mg 2.16 mmol) was dissolved in dry DMF (50 ml) and cooled to -78 °C. Into this RBF, potassium *tert*-butoxide followed (242 mg, 2.16 mmol). A solution of 4-bromomethylbenzophenone (594 mg, 2.16 mmol) was then added dropwise. The mixture turned black rapidly and was left to warm to room temperature over 6 hours. The solution was then diluted with ethyl acetate, worked-up with washes of water (6 x 100 ml), LiCl (3 x 100 ml), and brine (3 x 100 ml). The aqueous phase was extracted with ethyl acetate (3 x 100 ml), dried and concentrated. Column chromatography with 1% TEA in ethyl acetate yielded the product, 200 mg (30%). δ_H (400 MHz, CDCl$_3$): 1.26- 1.39 (m, 4H, C*H*$_2$), 1.43- 1.53 (m, 4H, C*H*$_2$), 2.57 (t, 2H, *J*= 7.2, C*H*$_2$NH), 3.55 (t, 2H, *J*= 6.5, C*H*$_2$OH), 3.79 (s, 2H, C*H*$_2$Ar), 7.35- 7.43 (m, 4H, Ar*H*), 7.49- 7.53 (dt, 1H, *J*= 7.4, 1.26, Ar*H*), 7.69- 7.73 (m, 4H, Ar*H*); δ_c (100 MHz, CDCl$_3$): 25.7, 27.1, 30.0, 32.7 (4 x CH$_2$), 49.5 (CH$_2$NH), 53.7 (CH$_2$Ar), 62.8 (CH$_2$OH), 127.9, 128.35, 130.0, 130.4, 132.4 (5 x CH), 136.3 (C, Ar-Me), 137.8, 145.4 (2 x *C*CO), 196.4 (C=O); HRMS (NSI) (m/z), [M+H] calcd, for C$_{20}$H$_{26}$NO$_2^+$ 312.1958 found 312.1959.

5.1.32 TBDMS-6-hydroxyhexylamine 40
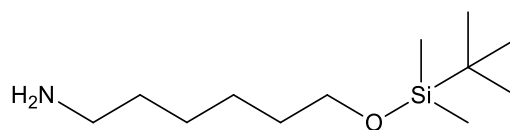
6-Aminohexanol (100 mg, 0.85 mmol) was dissolved in dry DMF (15 ml). Into it a small amount of catalytic DMAP and TBDMSiCl (150 mg, 0.99 mmol) was also added. TEA (1 ml, 13 mmol) was then injected and the reaction was left for 72 hours. Ethyl acetate was added, and the reaction mixture was washed with water (6 x 100 ml), LiCl (3 x 100 ml), and brine (3 x 100 ml). The aqueous phase was extracted with ethyl acetate (3 x 100 ml), dried and concentrated. This was purified by silica column in 1% TEA /ethyl acetate mix, yielding 100 mg (51%). δ_H (400 MHz, CDCl$_3$): 0.02 (s, 6H, (CH_3)$_2$Si), 0.86 (s, 9H, CH_3), 1.29- 1.49 (m, 8H, CH_2), 3.17 (t, 2H, J= 5.9, CH_2NH), 3.55 (t, 2H, J= 6.6, CH_2OH); Data consistent with the literature values.[221]

5.1.33 4-Methylbenzophenone-6-O-TBDMS-hexylamine 119
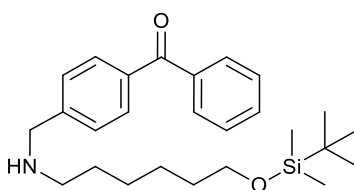
TBDMS-6-hydroxyhexylamine (500 mg, 2.1 mmol), and potassium *tert*-butoxide (360 mg, 3.2 mmol) were dissolved in dry DMF (50 ml) and cooled to -78 °C. 4-bromomethylbenzophenone (594 mg, 2.1 mmol), solution was then added dropwise and the solution turned black, then allowed to warm to room temperature over 12 hours. The solution was then diluted with ethyl acetate, worked-up with washes of water (6 x 100 ml), LiCl (3 x 100 ml), and brine (3 x 100 ml). Column chromatography with ethyl acetate and 1% TEA awarded 265 mg (30%) oily product. δ_H (400 MHz, CDCl$_3$): 0.00 (s, 6H, (CH_3)$_2$Si), 0.84 (s, 9H, CH_3), 1.25- 1.28 (m, 4H, CH_2), 1.42- 1.54 (m, 4H, CH_2), 2.61 (t, 2H, J= 7.3, CH_2NH), 3.55 (t, 2H, J= 6.3, CH_2OH), 3.85 (s, 2H, CH_2Ar), 7.38- 7.43 (m, 4H, ArH), 7.48- 7.52 (m, 1H, ArH), 7.70 (d, 4H, J= 8.3, ArH); δ_c (100 MHz, CDCl$_3$): -5.2 (CH$_3$), 25.7, 26.3 (CH$_3$) 27.1, 29.4, 32.8 (4 x CH$_2$), 49.1 (CH$_2$NH), 53.2 (CH$_2$Ar), 63.1 (CH$_2$OH), 128.3, 130.0, 130.4, 132.4 (5 x CH), 136.5 (C, Ar-Me), 137.6, 143.9 (2 x CCO), 170.3 (CCH$_3$), 196.4 (C=O).

5.1.34 TBDPS-6-hydroxyhexylamine 39
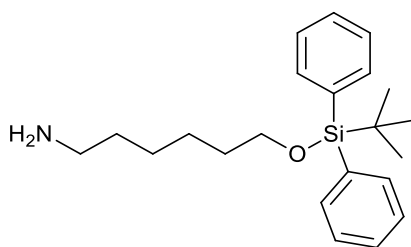
6-Aminohexanol (1 g, 8.53 mmol) of was dissolved in of dry DMF (50 ml), and a small amount of catalytic DMAP was added along with TBDPSiCl (2.35 g, 8.53 mmol). TEA was then added (2 ml, 26 mmol) and then left for 72 hours. The mixture was then diluted with ethyl acetate, worked-up with washes of water (6 x 100 ml), LiCl (3 x 100 ml), and brine (3 x 100 ml). An ethyl acetate column doped with 1% TEA achieved the purified product. 1.36 g (45%). δ_H (400 MHz, CDCl$_3$): 1.04 (s, 9H, C*H*$_3$), 1.26- 1.59 (m, 8H, C*H*$_2$), 2.67 (t, 2H, *J*= 7.2, C*H*$_2$NH), 3.55 (t, 2H, *J*= 6.5, C*H*$_2$OH), 7.35- 7.43 (m, 6H, Ar*H*^{3,4,5}), 7.65- 7.67 (m, 4H, Ar*H*^{2,4}). Data consistent with the literature values.[222]

5.1.35 N-(6-hydroxy-hexyl)-5-dimethylamino-naphthalene-1-sulfonamide 46
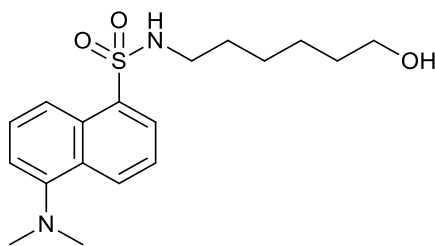
A flask was charged with dansyl chloride (1 g, 3.71 mmol), and dissolved in dry DCM (250 ml). Cooling to 0 °C proceeded the addition of DMAP (cat), and TEA (2 ml, 26 mmol). After 15 minutes, 6-aminohexanol (500 mg, 4.3 mmol) was added. The whole mixture then returned to room temperature over 4 hours. Work-up procedure consisted of washes with water (3 x 100 ml) and brine (100 ml), followed by extraction with DCM (3 x 100 ml). After drying with MgSO$_4$ and filtering, the crude residue was analysed by ^{1}H NMR and found to be of an acceptable purity for the next reaction. (1.2 g, 92%). δ_H (CDCl$_3$, 400 MHz): 1.10 -1.13 (m, 4H, CH_2), 1.30 -1.37 (m, 4H, CH_2), 2.33 (br.s, 1H, OH), 2.84 -2.89 (m, 9H, N(CH_3)$_2$), 3.46 (t, 2H, J= 6.5, CH_2OH), 5.51 (t, 1H, J= 6.1, SO$_2$NH), 7.14 (d, 1H, J= 7.3, ArH^6), 7.49 (q, 2H, J= 7.8, Ar$H^{7,8}$), 8.21 (dd, 1H, J= 7.3, 1.14, ArH^3), 8.33 (d, 1H, J= 8.7, ArH^2), 8.52 (d, 1H, J= 8.5, ArH^4); Data is consistent with previous work.[67]

5.1.36 N-(6-hydroxysaligeninposphate-hexyl)-5-dansyl-sulfonamide 10
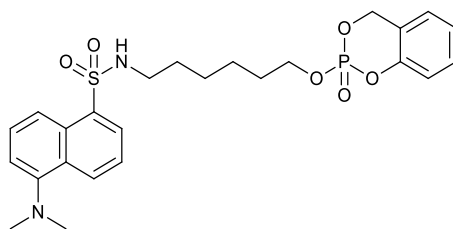
A solution of N-(6-hydroxy-hexyl)-5-dimethylamino-naphthalene-1-sulfonamide (200 mg, 0.57 mmol) in dry DCM (100 ml) was added (1 ml, 13 mmol) TEA and cooled to -78 °C. Saligenin chlorophosphite solution **45** (174 mg, 0.85 mmol) in dry DCM (10 ml) was added dropwise, this was left stirring to warm to room temperature for 24 hours. The mixture was concentrated *in vacuo*, and then dissolved in cold toluene (0 °C). This was left at 4 °C for 1 hour before being filtered and concentrated. Column chromatography on silica with ethyl acetate yielded the resultant orange oil 110 mg (22%). δ_H (400 MHz, CDCl$_3$): 1.08 (m, 4H, CH_2), 1.27 (t, 2H, J= 7.2, CH_2), 1.46 (t, 2H, J= 7.2, CH_2), 2.78 (t, 2H, J= 6.8, CH_2NH), 2.85 (s, 9H, N(CH_3)$_2$), 4.10 (m, 2H, CH_2OP), 5.34 (m, 2H, POCH_2), 6.97 (d, 1H, J= 8.2, ArH^1), 7.01- 7.07 (m, 2H, Ar$H^{2,3}$), 7.17 (d, 1H, J= 7.5, CH^6 dansyl), 7.22 -7.26 (m, 1H, ArH^4), 7.44 -7.51 (m, 2H, C$H^{7,8}$ dansyl), 8.18 (d, 1H, J= 7.3, CH^3 dansyl), 8.28 (d, 1H, J= 8.7, CH^2 dansyl), 8.48 (d, 1H, J= 8.5, CH^4 dansyl); δ_P (162 MHz, CDCl$_3$): -8.9. Data is consistent with previous work.[67]

5.1.37 Benzyl(2-chloro-6-nitrophenyl)sulfane 112

1,2-Chloro-3-nitrobenzene (10 g, 52 mmol) was dissolved in ethanol (100 ml). After 3 hours of refluxing this mixture was added to a solution of benzyl chloride (6 ml, 50 mmol), thiourea (4 g, 50 mmol), ethanol (10 ml) and water (10 ml) and some catalytic ammonia. Potassium hydroxide solution (7.0 g/ 50 ml H$_2$O) was added dropwise then refluxed for further 2 hours. The mixture was then cooled in an ice bath and the precipitate containing the 2-(benzylsulfanyl)-1-chloro-3-nitrobenzene then collected as a yellow solid with a 77% yield. This was brought forward to the next step in a crude state.

5.1.38 2-Chloro-6-nitrobenzenesulfonamide 112
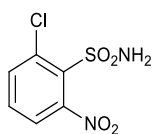
Gaseous chlorine gas was generated from HCl (10 g, 0.27 mol) dropped onto potassium

permanganate (2 g, 0.01 mmol) in a twin-necked flask. The chlorine was bubbled through a solution

of 2-(benzylsulfanyl)-1-chloro-3-nitrobenzene (600 mg, 1.8 mmol) in acetic acid (12 ml) and water (3

ml) at room temperature for 30 minutes. This was then poured onto ice (ca. 50 g), extracted with

diethyl ether, dried with MgSO$_4$ and concentrated under reduced pressure. The resulting orange oil

was then dissolved in dioxane (5 ml) and a volume of 30% solution of aqueous ammonia (10 ml) until

completely dissolved. This solution was then treated with charcoal, filtered, and using 6M HCl,

adjusted to pH 3. A precipitate then forms which was collected in a 28% yield. M.p. = 127 – 132 $^{\circ}$C

Data consistent with the literature values. [120]

5.1.39 2-Amino-6-chlorobenzenesulfonamide 114
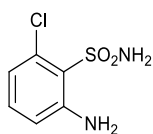
The 2-chloro-6-nitrobenzenesulfonamide **113** (100 mg, 0.42 mmol) was dissolved in 1:1 mix of hot

ethanol and water (5 ml), with ammonium chloride (80 mg, 1.5 mmol) and a spatula full of iron

powder (ca. 200 mg), and refluxed for 45 minutes. This was filtered and concentrated, then

extracted with DCM (3 x 50 ml), then dried and concentrated once more. Addition of hexane (10 ml)

causes precipitation which is collected under gravity and washed with ice cold hexane, to yield 43

mg of light brown powder with a 50% yield. δ_H (CDCl$_3$, 400 MHz): 6.72 (m, 1H, *Ar-H*), 7.06 (d, 1H, *Ar-*

H), 7.41 (m, 1H, *J*= 7.9, *Ar-H*), Data consistent with the literature values.[120]

5.1.40 4-(8-Chloro-1,1-dioxido-4H-benzo[e][1,2,4]thiadiazin-3-yl)butanoic Acid 109
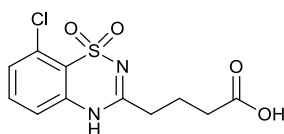
2-Amino-6-chlorobenzenesulfonamide (1 g, 4.84 mmol) was dissolved in dioxane (10 ml). Glutaric

acid monomethyl ester chloride (1.2 ml, 8.64 mmol) was then added and allowed to stir at room

temperature for 1 hour. The mixture was concentrated *in vacuo*, and dissolved in a 3% sodium

hydroxide solution (10 ml) and stirred for 1 hour further. Precipitate forms when acidified with 2 M

HCl and continues forming when it is left overnight. The product is then filtered and washed in

diethylether to yield 614 mg (42%) diazoxide **109**. M.p. 208-210 °C; δ_H (CDCl$_3$, 400 MHz): 2.01 (m, 2H,

CH$_2$) 2.42 (t, 2H, *J*= 7.2, *CH$_2$*), 2.65 (t, 2H, *J*= 7.5, *CH$_2$*), 7.24 (d, 1H, *J*= 8.2, *ArH*), 7.39 (d, 1H, *J*= 7.8,

ArH), 7.55 (t, 1H, *J*= 8, *ArH*), 11.04 (br.s, 1H, *NH*); Data is consistent with data from the previous

work.[67]

5.1.41 5 /6-Carboxy-X-rhodamine 91 /92
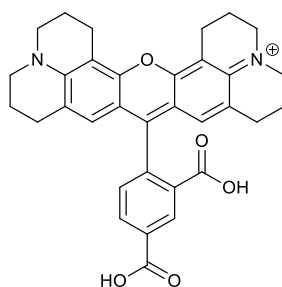
Trimellitic anhydride (230 mg, 1.2 mmol) was dissolved in ethanoic acid (20 ml). 8-hydroxyjulolidene

(450 mg, 2.4 mmol) was subsequently dissolved in dioxane (10 ml). Both solutions were added to a

RBF with 2 drops of catalytic, concentrated HCl. This was refluxed for 12 hours and the solution

turned from an orange colour to a dark red. Mixture was diluted with DCM (50 ml), followed by

washing with water (2 x 100 ml) and brine (100 ml). The resultant blue residue from drying with

MgSO$_4$ and concentrating was purified. The product of the column was then further refluxed for 6

hours with 8-hydroxyjulolidene (400 mg, 2.1 mmol), in dioxane /ethanoic acid (20 ml) with 2 more

drops of conc. HCl. After work-up by the same technique the black residue was purified by column

chromatography (DCM 1% MeOH) to yield both the 5, and 6-carboxy-X-rhodamine as dark purple

oils 155 mg (24%) yield and 218 mg (33%).

5-Carboxy-X-rhodamine δH (MeOD, 400 MHz): 1.74- 1.80 (m, 4H, CH2), 1.84- 1.88 (m, 4H, CH2), 2.35

(m, 4H, CH2) 2.57 (m, 4H, CH2), 3.16 (m, 4H, CH2), 3.26 (dt, 4H, *J*= 3.26, 1.69, CH2), 6.34 (s, 2H, CH),

7.26 (m, 1H, Ar-H), 8.08 (dd, 1H, *J*= 7.8, 1.72, *Ar-H*), 8.52 (s, 1H, *Ar-H*);

6-Carboxy-X-rhodamine δ$_H$ ((CD$_3$)$_2$CO, 400 MHz): 1.89- 1.90 (m, 4H, CH$_2$), 2.05 (m, 4H, CH$_2$), 2.65 (m,

4H, *CH$_2$*) 2.99 (m, 4H, *CH$_2$*), 3.30 (m, 4H, *CH$_2$*), 3.49 (m, 4H, CH$_2$), 6.69 (s, 2H, CH), 7.79 (s, 1H, *Ar-H*),

8.20 (d, 1H, *J*= 7.9, *Ar-H*), 8.69 (d, 1H, *J*= 6.4, *Ar-H*); Data consistent with the literature values. [156]

5.1.42 1,3,7,9-Tetramethyl BODIPY 60
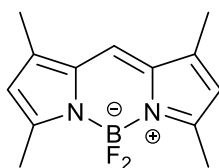
As a by-product of the synthesis of BODIPY FL ethyl ester **58** the reaction technique is the same as 5.1.12. 3-(1H-pyrrol-2-yl)propanoate (200 mg, 1.20 mmol) and 3,5-dimethyl-1H-pyrrole-2-carboxaldehyde (160 mg, 1.3 mmol) then phosphorus oxychloride (200 mg, 0.12 ml, 1.32 mmol) in DCM (2 ml) was added at 0 °C and stirred for 2 hours. Boron trifluoride etherate (0.6 ml, 4.82 mmol) and DIEA (0.88 ml, 5.04 mmol) follows and left stirring for 12 hours. After the standard work-up procedure the crude product was purified by flash chromatography (silica, DCM) to give the resulting product as bright red crystals, yielding 35 mg, (7%). δ_H (400 MHz, CDCl$_3$): 2.35 (s, 3H, CH_3), 2.65 (s, 3H, CH_3), 6.16 (s, 2H, $CH^{2,6}$), 7.06 (s, 1H, CH^4).

5.2 Synthetic Techniques

5.2.1 General Techniques

The glassware for reactions performed under anhydrous conditions was dried in an oven at ca. 100°C. When needed, nitrogen gas is introduced and the glassware allowed to cool to room temperature before addition of reagents. All needles and syringes were used either fresh out of the plastic package, or dried glass syringes and metal needles were utilised. Reagents sensitive to air and moisture were transferred via syringe. Solutions in organic solvents were concentrated on a rotary evaporator and vacuum pump.

All solvents were bought as analytical grade from either Fisher Scientific, or Sigma Aldrich and required no further purification. Solvents were kept dry in an MBraun MB SPS-800 solvent drier or distilled over $MgSO_4$ and stored on drying beads (heated overnight >100°C in oven) in a sealed bottle.

5.2.2 Column Chromatography

Column chromatography was performed using Fluorochem silica gel (60A, 40 ± 63 micron). The silica gel was mixed in solvent to a slurry then poured into a glass column. The samples were then dissolved in solution and pipetted onto the surface of the silica, or absorbed onto dry silica, dried in vacuo, then the powder poured onto the top of the slurry in column. An electric pump was then used to apply pressure.

For purification utilising warm glassware and solvents care is needed when heating flammable solvent. The mix was warmed gently on a low setting heat gun until evaporation of solvent started. Glassware only needed to be at > 50 °C, and the technique was performed in a fume hood to vent solvent vapour.

5.2.3 NMR Spectroscopy

Hydrogen, carbon, fluorine and phosphorous, (^{1}H NMR, ^{13}C NMR, ^{19}F NMR, ^{31}P NMR), NMR spectra were measured on a Jeol ECX 400 spectrometer at 400 MHz, 100 MHz, 376 MHz and 162 MHz respectively. Results of the chemical shifts corresponding to each species are reported in parts per million (ppm), and coupling constants (J) are given in Hertz (Hz). Abbreviations for the multiplicity of proton data are as follows: s = singlet, d = doublet, dd = doublet of doublets, dt = doublet of triplets, t = triplet, tt = triplet of triplets, q = quintet, m = multiplet, br = broad. Assignments were based on HMQC, COSY and HMBC experiments. Phosphorous NMR's determined with aid from Olaf Kühl Phosphorous-31 NMR spectroscopy.[223]

 Solvent peaks listed are used as a reference value:

Solvent	^{1}H NMR	^{13}C NMR
$CDCl_3$	7.27 ppm	77.00 ppm
CD_3OD	3.31 ppm	49.0 ppm
$(CD_3)_2SO$	2.50 ppm	39.5 ppm

5.2.4 Mass Spectrometry

Mass spectrometry (MS) spectra were recorded at high resolution by the EPSRC National Mass Spectrometry Service Centre, School of Medicine, Swansea University.

5.2.5 IR Spectrometry

Infrared (IR) absorption spectra were measured with a Perkin Elmer Spectrum 100 FT-IR Spectrometer using an ATR attachment, and are reported in cm^{-1}.

5.2.6 Fluorimetry

All fluorimetry experiments occurred on a Cary Eclipse 3, with a scan rate of 600 nm/min, a data interval of 1.0000 nm, and average time of 0.1000 s. PMT voltage was medium, excitation filter on auto and emission filter auto. Excitation and emission slits width was set to at 5 nm, unless otherwise stated. The machine was controlled between each reading using a sample of distilled

water. All samples were measured in triplicate in a quartz fluorimetry cuvette with a path length of 1 cm. the volume of all samples in cuvette was 3.5 cm^3.

5.2.7 UV-Vis Spectrometry

The UV absorptions and emissions were measured by using an Agilent Technologies Cary 8454 UV-Vis, at a range of wavelength from 150-1150 nm. All samples were measured in triplicate in a quartz cuvette with a path length of 1 cm.

5.2.8 Thin Layer Chromatography

Thin-layer chromatography (TLC) was carried out using silica plates in duran jars with various solvent mixes contained. The plates are UV-active and substances were detected with either short wave or long wave UV light. They are then made visible (if not already), by dipping into a container with iodine on silica, ninhydrin solution, phosphomolybdic acid (PMA) or potassium permanganate solution.

5.3 Biological Techniques

5.3.1 H9c2 Cell Culture

H9c2 (rat embryonic cardiomyoblast-derived) cells were obtained from the European Collection of Animal Cell Cultures (Porton Down, Salisbury, UK). Mitotic cells were cultured in 25 cm^2 cell culture flasks in Dulbecco's modified Eagle's Medium (DMEM) containing 10 % (v/v) foetal bovine serum (FBS), 2 mM L-glutamine, penicillin (100 U/ml) and streptomycin (100 μg/ml). These cultures were maintained in an incubator at 37°C with a controlled atmosphere of 95 % air/5 % CO_2 until 80% confluent. Cells were then detached using trypsin (0.05 % w/v)/EDTA (0.02 % w/v) in sterile phosphate buffered saline (PBS). They were distributed into n-well plates appropriate for further testing. Remaining cells then re-cultured in 25 cm^2 flasks.

5.3.2 H9c2 Cell Differentiation

Differentiation of H9c2 cells was induced by culturing the cells for 7 days in the continued presence of 10 nM retinoic acid in DMEM growth medium with 1 % (v/v) FBS. The differentiation medium was replaced every 48 h. The cells were observed to form multinucleated elongated myotubes, consistent with the structure of a cardiomyocyte.

5.3.3 Cell Lysis

After the cell culture and differentiation period as described above the cells were ready to be lysed. Cells were lysed using boiling lysis solution (300 µl 0.5 % (w/v) SDS solution in TBS (20 mM Tris base, 150 mM NaCl). To gather the cells and ensure complete lysis the surface of the T25 flasks were scraped using a scraper. Eppendorf tubes (2 ml), were then filled with the lysate and boiled for 10 min. The samples were then stored for future use at -20°C.

5.3.4 Protein Estimation

The protein content of the lysates was calculated using 2 different techniques. The first, is a modification of the Lowry method[224] by Bio-Rad called *DC* Protein assay. Samples of cell lysates (5 µl) were added to a 96 well plate, 25 µl of assay reagent A' (20 µl of reagent S and 1 ml of reagent A), and 200 µl assay reagent B were then added to the wells. The samples were incubated in the dark with gentle agitation for 30 minutes at room temperature. Then the absorbance was read at 620 nm using a standard 96 well plate reader CLARIOstar (BMG Labtech). To calculate the protein content of the samples, the results were compared to the absorbance reading with a standard curve plotted from the results of BSA standards.

The second technique employed to estimate protein concentration was the bicinchoninic acid protein assay (BCA).[225] Firstly the BCA working reagent was per the manufacturer's instructions by mixing 50 parts reagent A with 1-part reagent B (6 ml of A and 0.12 ml B). Unknown samples were diluted 1:10, 1:50 and 1:250 and loaded into a 96 well plate in triplicate. 200 µl of BCA standard working reagent was then added and in the dark at 37°C the plate was incubated. 30 minutes later

the plate was read at 570 nm and the absorbance values plotted against the standard curve. As in the Lowry method BSA standards are used for a standard curve.

5.3.5 MTT Reduction Assay

Differentiated H9c2 cells in culture were assessed for viability proportional to metabolism using the MTT assay. Addition of 15,000 cells per well of undifferentiated H9c2 cells were seeded in 24-well cell culture plates. This was incubated overnight at 37°C in complete DMEM growth medium. Cells were then induced to differentiate for several days using the differentiation method in 5.3.2. They were treated in accordance to the particular experiment being undertaken. The cell plates were incubated for 1 h in 0.5 mg/ml MTT solution in DMEM at 37°C. The medium was aspirated from each well, leaving blue, insoluble formazan crystals at the bottom of each well. 500 µl of DMSO (dimethyl sulphoxide) was added to dissolve formazan crystals. 200 µl of the resulting solution was transferred into a 96-well plate and the absorbance was read at 570 nm using a standard 96-well plate reader CLARIOstar (BMG Labtech). After subtracting the blank absorbance from each assay, the magnitude of the MTT reduction determined by the absorbance at 570 nm is proportional to cell viability.

5.3.6 Lactate Dehydrogenase Assay

LDH (lactate dehydrogenase) assay was performed using the CytoTox 96® non-radioactive cytotoxic assay kit (Promega). This kit allows LDH release to be measured via production of a coloured formazan product. The first reaction allows released LDH from cells to catalyse the formation of pyruvate and NADH from lactate and NAD+. The second reaction occurring, is the catalyses of NAD+ (from NADH) and a red coloured, formazan product (from a tetrazolium salt) by the dehydrogenase enzyme diaphorase (present in the substrate mix in kit). A standard plate reader measuring absorbance at 490 nm, shows that LDH release is proportional to the red formazan product.

H9c2 cells were cultured for 24h in complete DMEM growth medium with 5000 cells/well, in a 96 well plate. The cells were then allowed to differentiate over several days in differentiation medium

as described above. Treatment was then performed in 200 µl of complete medium with appropriate concentrations of treatment. The well plate was centrifuged to compact cellular debris and 50 µl of supernatant was then transferred to a non-sterile 96 well plate. Reconstituted assay buffer (50 µl, from kit, 10 ml assay buffer added to one bottle of substrate mix) was added to each well, then incubated in the dark for 30 min at room temperature with gentle agitation. The reaction was quenched with 50 µl of assay stop solution (1M acetic acid).

5.3.7 SDS-PAGE

A protein solution containing 75 µl of each sample suspended in 25 µl of 4x Laemmli buffer[226] is boiled for 10 min. 10% (w/v) polyacrylamide gels of 0.75 mm thickness (Resolving gel; 5.9 ml deionised water, 5ml ProtoGel® 30% acrylamide mix, 3.8ml of 1.5 M TRIS-HCL pH 8.8, 0.15ml SDS solution (10 % (w/v) sodium dodecyl sulphate in deionised water) 0.15ml APS solution (10 % (w/v) ammonium persulfate in deionised water), 1 µl/ml TEMED) were cast using a Bio-Rad Mini-Protean III system with a layer of stacking gel on top, (Stacking gel; 3.4ml deionised water, 0.83 ml ProtoGel® acrylamide mix, 0.63 ml 1.0 M TRIS-HCL pH 6.8, 0.05 SDS solution, 0.05 APS solution and 0.005ml TEMED). Loaded into the wells on the gel was 40 µg of each sample dissolved in buffer, and 5 µl of protein ladder (Precision Plus Protein™ dual standards, BioRad). Electrophoresis was then performed at 200 V for 45 min, with the gels submerged in 1x electrophoresis buffer (2.5 mM TRIS, 19.2 mM glycine, 0.01 % (w/v) SDS, pH 8.3). The migration of the proteins could be observed due to the dye movement. Once protein separation was achieved the gels were removed from the electrophoresis tank and from the glass casting frames. They were then fixed for visualisation by incubating with 20 ml of a solution of 40% (v/v) methanol, 10% (v/v) acetic acid and 50% (v/v) distilled water at room temperature for 15 minutes with gentle agitation.

5.3.8 Irradiation of Samples

Mitochondrial extracts (50 µl) were added to 49 µl of tris-buffered saline (TBS) (50 mM Tris-Cl, pH 7.6; 150 mM NaCl), and 1 µl of desired concentration of diazoxide analogue. This was incubated for

ca. 30 minutes, then divided into two 50 µl aliquots. One aliquot is then centrifuged for 14,000g/20 minutes and re-suspended in 50 µl TBS. The samples are then pipetted into an optical 384 well plate (nunc), and irradiated on a transilluminator at ca. 360 nm for 10 minutes. The samples were then added to 3.6 µl of 4x Laemmli buffer for SDS-PAGE processing.

5.3.9 2D Gel Electrophoresis

Protein samples can be identified using MALDI-TOF MS/MS with a greater level of accuracy after running samples through 2D gel electrophoresis. This separates cellular proteins by two parameters, molecular weight and isoelectric point (pH). After irradiation, the sample was re-suspended 300 µl urea lysis buffer (8 M urea, 50 mM DTT, 4 % (w/v) CHAPS, 0.2 % (v/v) Biolite® ampholytes (pH 3-10) (Biorad®), in deionised water). Acetone was then added (1800ul) to allow the protein to precipitate, this was incubated at -20 °C for 15 hours. The lysate-acetone mixture forms a visible precipitate, this was then centrifuged at 10,000 RCF for 10 minutes at 4 °C to gather the proteins into a pellet. The pellet was then covered and left to dry out for 1 h in a fume cupboard. 300 µg of protein was suspended in 120 µL rehydration buffer (pH 3-10). The 120 µl sample was transferred into an IEF focusing tray, ensuring an even spread on the bottom of the tray with the liquid making contact with both anode and cathode wires. A 7 cm 3-10 pH IGP ReadyStrip™ (Biorad) was positioned on top of the protein sample, ensuring correct orientation and full contact with the protein sample without bubbles. The samples were left for one hour so it could be absorbed into the IPG gel. Active rehydration at 50 V for 16 h then occurs using a Protean IEF Cell (Biorad). A layer of mineral oil was poured on top of the IPG strip to prevent buffer evaporation. After rehydration IEF system electrode wicks (Biorad) were inserted in-between the IPG strip and the top of the electrodes in the focusing tray, these function to remove excess salts and ensure an effective focusing. The IPG strips were focused with the following protocol, which separates the proteins in the 1st dimension; a linear voltage slope, up to 250 V was utilised for 20 min. Following this, a second linear voltage slope increasing to 4000 V was applied for 2 h. A rapid voltage slope to 4000 V for 10,000 Volt hours was then employed, before a final rapid voltage slope down to 500 V was applied to the gel for 25 h.

After focusing, the IPG strips were prepared for running in the second dimension. The IPG strips were placed in an equilibration tray and 2500 µl of equilibration buffer 1 was added for 10 min at room temperature with gentle agitation. Buffer 1 was then substituted with 2500 µl equilibration buffer 2 and incubated at room temperature for 10 min with gentle agitation.

The strips were then positioned on top of a 15 % SDS acrylamide gel. A small piece of filter paper was soaked in a mixture of 10 % protein ladder (Precision Plus Protein™ dual standards, BioRad) and 90% 4x Laemmli buffer and placed at the side of the IPG strip to allow for molecular weight comparison. The second-dimension separation was then carried out by electrophoresing the gel at 200 V for 45 min, in an electrophoresis tank containing 1 x electrophoresis buffer. The bromophenol blue present in the IPG strips allowed for visible tracking of the dye to ensure optimal separation of protein. After electrophoresis the gels were removed and washed for 5 min three times in deionised water. The gels could then be fixed and visualised.

5.3.10 Visualisation of Gels

Imaging of gels utilised three different imagers. The Syngene U:Genius3 was used for any gels requiring UV light to excite bands. Fujifilm FLA-4000 was used for green / blue LED side lamps and white light imaging. Fujifilm 5000 contains the 473 nm (blue light), 532 nm (green light) and 685 nm (red light) lasers. The gels were placed onto the sample platforms, and then scanned according to manufacturer's guidelines.

5.3.11 Extraction of Mitochondria from Rat Liver

Rat livers were harvested from freshly slaughtered rats and kept on ice until ready for fractionating. These were divided into chunks using scissors and forceps in extraction medium, (0.25M sucrose, 5 mM HEPES buffer, and 1 mM EDTA, pH 7.2) on ice and washed and drained until the extraction medium was clear. The solution was poured into a Pyrex homogenisation flask, a Teflon mortar (Potter-Elvehjem) was attached to the tissuemiser (RW20, Janke & Kunkel, IKA-Labortechnik). The machine was used in bursts to prevent prolonged or overly vigorous homogenization, as this can

damage the mitochondria. This process occurs at ca. 1,600 rpm at no warmer then 4°C to prevent

activation of proteases and phospholipases.

This solution was then transferred to a precooled centrifuge cartridge and placed into a cold

centrifuge (Beckman Avanti J-30 I) to form a nuclear pellet, the homogenate was centrifuged at 500

g for 10 minutes. The supernatant fluid was then removed from the large cellular fragments that

gathered. The supernatant was then added to a clean centrifuge tube and spun at 9400 g for 10

minutes at 4 °C.

The supernatant was then discarded and fresh extraction buffer added to the formed mitochondrial

pellet. Damaged uncoupled mitochondria break off during this process and can be lost with the

discarded supernatant as the more intact mitochondria sediment more quickly. This was centrifuged

again at 9400 g for 10 minutes at 4 °C and the supernatant discarded. This process can be repeated

until the pellet retains its creamy yellow colour and all the large red extracellular components have

been removed.

A white foamy material at the top of the centrifuge tubes was removed by wiping with a cotton bud.

This material contains lipids and can uncouple the mitochondria causing damage. When the process

of centrifugation and washing was completed the supernatant was discarded with care not to

disturb the pellet. Remaining fluid was removed with a Pasteur pipette. A glass rod was then used to

stirs the pellet into a smooth paste, trying not to introduce air into the suspension. The

mitochondrial paste was kept concentrated at -80 °C to minimise exposure to oxygen, and to retain

dormancy. A small amount of the paste was diluted and used for protein concentration estimation.

5.3.12 Visualisation of Cells by Confocal Microscopy

H9c2 cells were seeded into an 8 well BD Falcon™ CultureSlide at a density of 15,000 cells/well. The

chamber slide was incubated for 24 hours in fully supplemented DMEM growth medium.

Differentiation of the cells was then induced as described above with 7 days of culturing in serum

deficient medium. After this point the medium was aspirated and the differentiated cells adhere to

the slides and are washed 3 times with PBS solution that has been incubated at 37°C for 5 min each wash.

Fixing the cells proceeded with a 3.7 % (v/v) solution of paraformaldehyde in PBS for 15 minutes at room temperature. They were then washed three times with PBS for 5 minutes.

If antibodies are to be used to label cellular components then the cells must first be permeabilised with 0.1 % Triton X-100 in PBS. Then the cells are washed with 3 % (w/v) BSA in PBS to block non-specific binding of the antibodies, prior to overnight incubation with primary antibody. Incubation with secondary antibody after this connects the fluorophore to specific protein target.

If the cells are being labelled with a probe this can occur either of two ways:

1. For the organophosphate probes the cells were incubated with 25 µM of probe for 1 hour prior to washing and fixation.

2. For the DZX probe incubation occurs with 100 µM of probe in fully supplemented DMEM for 1 hour, prior to washing and fixation. Optimal results were then achieved by washing the cells with PBS then quickly flashing the cells with UV light for <2 seconds. Washing with PBS removes excess probe solution.

The slides are washed with PBS three times then allowed to air dry. Vectashield$^©$ mounting medium containing 4,6-diamidino-2-phenylindole (DAPI) is then applied to the slides. This is a nuclear counterstain allowing for cell visualisation. Glass cover-slips were then applied and sealed using colourless nail varnish. Visualisation was then achieved with an Olympus DP71 fluorescent microscope equipped with an argon/krypton laser.

5.3.13 De-Staining of Gel Spots and Preparation for MS

Proteins identified as being labelled with probe after 2D gel technique were picked out of the gels using a scalpel and placed in a 1 ml Eppendorf™ tube containing the dehydration solution (50 mM ammonium bicarbonate, equal volumes of deionised water and acetonitrile).

The cut-out spots were incubated for 5 min at 37 °C in the solution under gentle agitation. The supernatant was aspirated and replaced with fresh dehydration solution. Incubation at room temperature for 15 min with gentle agitation then followed and the gel spots were then dehydrated by adding 100% acetonitrile to the mixture for a further 5 minutes. The supernatant was then removed and replaced with dehydration solution for 5 minutes. The process of addition of acetonitrile followed by addition of dehydration solution and incubation was repeated three times. The gels were then rehydrated with deionised water for 5 minutes.

The gel pieces were then reduced and alkylated with the respective buffers. Reducing buffer (25 mM dithiothreitol in 25 mM $(NH_4)HCO_3$) was added and then incubated at 56^oC for 20 minutes. The gel then cools to room temperature and reducing buffer was pipetted off before the addition of the alkylating buffer (55 mM iodoacetamide in 25 mM $(NH_4)HCO_3$). Incubation of the gel spots at room temperature for 20 minutes then occurs in the dark. The alkylating before is removed, and the gel pieces washed with 20 volumes of Millipore water for 30 seconds. Final dehydration occurs with 5 minutes of dehydration solution followed by addition of 100% acetonitrile. The particles are then dried in a vacuum centrifuge.

The gel spots are then sent to the John van Gheest research centre for digestion with trypsin, preparation by ZipTip reverse phase chromatography and then spotted onto a steel mass spectrometry target plate with α-Cyano-4-hydroxycinnamic acid 5.0 mg/ml (Bruker), 50 % v/v acetonitrile, 0.1 % v/v TFA (CHCA) matrix solution.

5.3.14 Coomassie Blue Staining

Gels were fixed with 20 ml Coomassie Brilliant Blue dye (Fisher scientific) after washing with distilled water to remove any left-over running buffer. The gels were incubated with the blue dye for 12 hours, at which point the dye was removed and the gels were washed three time with distilled water. The gels were then left in water for 24 hours at room temperature so that excess dye leaches into the water. Washing a final time reveals the stained protein bands in the gel.

5.3.15 Statistical Analysis of Cell Viability Assays

Statistical analysis of the LDH and MTT assays was performed using Prism software (GraphPad 7 version 7, California, USA). Statistical significance was determined by one-way t-tests, or ANOVA for the diazoxide tests.

An unpaired parametric Students t-test, compares the two data sets for significance (control vs treatment). This was performed according to the software guidelines. The significance of the differences could further be demonstrated with comparison of a two tailed P value between two sets of data, $P < 0.05$ statistically significant, highlighted with an asterisk (*).

IC50 values (concentrations of drug producing 50% of the maximal inhibition), were derived from both LDH and MTT assays were obtained using the Prism software which assists curve fitting.

Error bars for the data sets are presented as the mean ± standard error of mean (SEM). The number of separate experiments are represented by the character n in the text.

5.3.16 Protease Activity Assays

The measurement of protease activity on a substrate of Nα-benzoyl-DL-arginine-p-nitroanilide (L-BAPNA) takes place in a 96-well plate. For the calibration curve, different concentrations of trypsin were added to a 96-well plate which was read at 415 nm as a zero point. L-BAPNA solution (10 µl) was added (0.1% (w/v) BAPNA in distilled water), and readings were taken every minute for 15 minutes.

For the inhibition assay, 25 µg of trypsin (from porcine pancreas, SigmaAldrich, UK) was incubated on ice with a trypsin inhibitor solution (TRIS buffer pH 6.8) or control solution of TRIS buffer. 100 µl of each solution was added in triplicate to a well on the plate and 10 µL of BAPNA solution was added to each well with readings being taken over a 15-minute interval.

5.4.1 Appendix 1: Computational Methods

Calculations were performed with Gaussian 09, Revision E.01.[S1] Geometry optimizations and thermal contributions to energies were computed in the gas phase with the functional wB97xD;[S2] the 6–31G(d,p) basis set was used for all atoms.[S3] Stationary points were identified as minima through analytical frequency calculations. The energies reported in the main text are Gibbs energies.

Table S1. Computed relative energies for ring open cations **A** and **B**, and the ring closed molecules **C** and **D**. Structures were optimised and energies calculated at the wB97xD/6-31G(d,p) level of theory.

	SCF energy	SCF + ZP energy	SCF + thermal energy	SCF + thermal enthalpy	SCF + thermal free energy
A	0.0	0.0	0.0	0.0	0.0
B	262.9	254.2	253.7	253.7	**254.6**
C	0.0	0.0	0.0	0.0	0.0
D	254.2	245.9	245.5	245.5	**245.0**

Computed Cartesian coordinates (Å) and energies (hartrees)

A
SCF Energy (gas phase)= –1263.039477
Zero-point correction= 0.43169300
Thermal correction to Energy= 0.45722300
Thermal correction to Enthalpy= 0.45816700
Thermal correction to Gibbs Free Energy= 0.37550800

```
C    -3.63584   -0.16168   -0.28158
C    -3.58417   -1.58468   -0.09543
C    -2.31709   -2.19793   -0.00939
C    -1.17738   -1.42741   -0.09964
C    -1.20968   -0.02255   -0.28243
C    -2.49550    0.57770   -0.36633
O    -0.00036   -2.08390   -0.00915
C     1.17689   -1.42765   -0.09963
C     1.20948   -0.02284   -0.28240
C    -0.00007    0.68499   -0.34509
C     2.31637   -2.19850   -0.00942
C     3.58361   -1.58556   -0.09545
C     3.63560   -0.16262   -0.28159
C     2.49541    0.57707   -0.36633
C     0.00023    2.15528   -0.59114
O     0.00120    3.64825    2.74016
C     0.00052    2.63918    1.86164
O    -0.00018    1.47558    2.19819
C     0.00059    3.10285    0.44512
C     0.00103    4.46446    0.13561
C     0.00110    4.88685   -1.18787
C     0.00069    3.94808   -2.21382
C     0.00024    2.58875   -1.91657
N    -4.72050   -2.31006   -0.00760
C    -6.02532   -1.66952   -0.11206
C    -4.64910   -3.75109    0.18379
N     4.71976   -2.31129   -0.00765
C     6.02474   -1.67107   -0.11198
C     4.64793   -3.75230    0.18349
H    -4.59167    0.33868   -0.35498
H    -2.19797   -3.26315    0.12823
H    -2.56140    1.65116   -0.50519
H     2.19698   -3.26369    0.12819
H     4.59150    0.33758   -0.35506
H     2.56168    1.65050   -0.50525
H     0.00130    5.18757    0.94239
H     0.00150    5.94681   -1.41598
H     0.00076    4.27060   -3.24945
H    -0.00008    1.85505   -2.71617
H    -6.17314   -0.93134    0.68285
H    -6.15407   -1.17994   -1.08295
H    -6.80044   -2.42707   -0.01393
H    -4.14136   -4.23846   -0.65592
H    -4.12149   -4.00016    1.11070
H    -5.65675   -4.15656    0.25113
```

H	6.17255	-0.93275	0.68280
H	6.79967	-2.42877	-0.01346
H	6.15383	-1.18173	-1.08294
H	4.14003	-4.23939	-0.65629
H	5.65546	-4.15810	0.25072
H	4.12029	-4.00142	1.11037
H	0.00101	3.25567	3.62418

B

SCF Energy (gas phase)= -1282.47814082
Zero-point correction= 0.47161700
Thermal correction to Energy= 0.49928300
Thermal correction to Enthalpy= 0.50022700
Thermal correction to Gibbs Free Energy= 0.41281900

C	-3.41541	-0.78176	-0.57755
C	-3.18191	-2.16778	-0.28841
C	-1.85038	-2.59118	-0.10235
C	-0.82205	-1.67599	-0.19365
C	-1.03394	-0.30451	-0.47384
C	-2.38180	0.10130	-0.66611
O	0.42608	-2.15858	-0.01087
C	1.50644	-1.35046	-0.08442
C	1.35902	0.03101	-0.36100
C	0.07209	0.56112	-0.53466
C	2.73188	-1.94723	0.12316
C	3.90568	-1.16672	0.07948
C	3.77392	0.23859	-0.18259
C	2.55232	0.80327	-0.38815
C	-0.10985	1.99382	-0.90089
C	-0.54206	2.95465	0.02569
C	-0.67813	4.28125	-0.38603
C	-0.41845	4.65001	-1.70129
C	-0.01198	3.69081	-2.62162
C	0.14708	2.36849	-2.22013
C	-0.78223	2.51920	1.44605
O	-0.19904	1.54621	1.90840
N	-1.66337	3.25729	2.16136
C	-1.97979	2.92526	3.53773
N	5.12182	-1.71968	0.28304
N	-4.21294	-3.03875	-0.20393
C	-5.58480	-2.59012	-0.39982
C	-3.95780	-4.44139	0.08726
C	6.32736	-0.90163	0.25274
C	5.23614	-3.14322	0.56273
H	-4.42386	-0.42353	-0.73316
H	-1.59701	-3.61957	0.11259
H	-2.58367	1.14271	-0.89115
H	2.75157	-3.00858	0.32606
H	4.65214	0.86906	-0.20800
H	2.47624	1.86918	-0.56981
H	-0.95306	5.04474	0.33472
H	-0.52367	5.68660	-2.00188
H	0.19051	3.96881	-3.65008
H	0.47220	1.61818	-2.93389
H	-2.23949	3.93147	1.68498
H	-2.76536	2.16524	3.60086

H	-1.08341	2.53298	4.01758
H	-2.30678	3.82507	4.06041
H	-5.87323	-1.84460	0.34854
H	-5.72887	-2.16598	-1.39900
H	-6.25543	-3.44137	-0.29918
H	-3.46942	-4.56268	1.06037
H	-4.90315	-4.97974	0.11476
H	-3.32833	-4.89841	-0.68415
H	6.46113	-0.42383	-0.72314
H	6.30711	-0.12960	1.02880
H	7.19194	-1.53702	0.43492
H	4.69997	-3.41178	1.47965
H	4.84381	-3.74230	-0.26609
H	6.28522	-3.39885	0.69784

C

SCF Energy (gas phase)= -1262.62049498
Zero-point correction= 0.41778400
Thermal correction to Energy= 0.44259600
Thermal correction to Enthalpy= 0.44354000
Thermal correction to Gibbs Free Energy= 0.36224600

C	-3.66624	-0.11245	-0.11170
C	-3.59124	-1.51489	0.06172
C	-2.31860	-2.09957	0.09651
C	-1.17674	-1.31409	-0.02721
C	-1.23998	0.06580	-0.18779
C	-2.51478	0.63778	-0.22868
O	-0.00002	-2.00174	0.03073
C	1.17671	-1.31410	-0.02719
C	1.23997	0.06578	-0.18777
C	0.00000	0.90118	-0.36069
C	2.31856	-2.09960	0.09652
C	3.59120	-1.51495	0.06172
C	3.66623	-0.11250	-0.11167
C	2.51478	0.63774	-0.22865
C	0.00001	2.13951	0.51329
O	0.00005	3.49352	-2.70458
C	0.00005	2.82527	-1.70441
O	0.00002	1.46953	-1.71578
C	0.00003	3.26417	-0.28788
C	0.00005	4.54878	0.24249
C	0.00004	4.67057	1.62683
C	0.00002	3.53103	2.44215
C	0.00001	2.25045	1.89654
N	-4.73137	-2.27873	0.20016
C	-4.61978	-3.72021	0.22863
C	-6.02841	-1.67213	-0.00891
N	4.73133	-2.27877	0.20020
C	4.61976	-3.72025	0.22880
C	6.02836	-1.67219	-0.00908
H	-4.62439	0.38801	-0.15928
H	-2.17400	-3.16470	0.21598
H	-2.60154	1.71203	-0.36415
H	2.17393	-3.16473	0.21595
H	4.62439	0.38796	-0.15921
H	2.60156	1.71200	-0.36410

```
H      0.00007    5.41327   -0.41289          H      2.17409   -3.18045    0.37385
H      0.00006    5.65397    2.08519          H      4.62884    0.33706   -0.22841
H      0.00002    3.65195    3.52096          H      2.60057    1.66356   -0.42719
H     -0.00002    1.36794    2.52809          H     -0.00113    5.40931    0.06738
H     -4.00577   -4.05151    1.07426          H     -0.00236    5.42190    2.57602
H     -5.61092   -4.15729    0.35311          H     -0.00250    3.29576    3.82423
H     -4.17825   -4.12692   -0.69271          H     -0.00141    1.11414    2.62304
H     -6.21895   -0.87854    0.72301          H      0.89309    0.27584   -2.92174
H     -6.13628   -1.24279   -1.01505          H     -0.88877    0.27392   -2.92194
H     -6.80258   -2.42894    0.12062          H      0.00081    1.65697   -3.61906
H      5.61087   -4.15731    0.35354          H     -4.14381   -4.19989   -0.53780
H      4.00558   -4.05146    1.07434          H     -4.02729   -4.03610    1.22789
H      4.17841   -4.12708   -0.69259          H     -5.60840   -4.18786    0.46269
H      6.80253   -2.42902    0.12029          H     -6.24103   -0.90363    0.67790
H      6.21905   -0.87863    0.72283          H     -6.11349   -1.33137   -1.04248
H      6.13605   -1.24282   -1.01522          H     -6.80151   -2.47900    0.11894
                                              H      6.10974   -1.33856   -1.04916
                                              H      6.24272   -0.89815    0.66764
**D**                                         H      6.80214   -2.47717    0.11901
SCF Energy (gas phase)=                       H      4.02421   -4.03861    1.22234
1282.07297745                                 H      4.14937   -4.19525   -0.54341
Zero-point correction= 0.45833200             H      5.60904   -4.18665    0.46476
Thermal correction to Energy=
0.48540600
Thermal correction to Enthalpy=
0.48635000
Thermal correction to Gibbs Free
Energy= 0.39805700

C     -3.67007   -0.15648   -0.13231
C     -3.59365   -1.54843    0.10771
C     -2.31955   -2.12242    0.20640
C     -1.17766   -1.33491    0.08783
C     -1.24254    0.03560   -0.13440
C     -2.51798    0.59519   -0.24422
O      0.00032   -2.01612    0.20626
C      1.17814   -1.33441    0.08912
C      1.24275    0.03606   -0.13325
C      0.00000    0.89221   -0.28161
C      2.32023   -2.12149    0.20884
C      3.59420   -1.54710    0.11148
C      3.67031   -0.15532   -0.12939
C      2.51808    0.59601   -0.24235
C     -0.00066    2.06499    0.68860
C     -0.00059    3.26162   -0.00935
C     -0.00119    4.48785    0.64013
C     -0.00188    4.48313    2.03145
C     -0.00195    3.27594    2.73875
C     -0.00135    2.05122    2.07507
C      0.00018    2.97133   -1.46978
O      0.00050    3.76569   -2.39447
N      0.00048    1.60391   -1.57065
C      0.00146    0.90541   -2.82890
N      4.73497   -2.31187    0.24979
N     -4.73397   -2.31373    0.24365
C     -4.61608   -3.75065    0.34800
C     -6.02795   -1.72295   -0.01881
C      6.02778   -1.72257   -0.02225
C      4.61712   -3.74942    0.34660
H     -4.62871    0.33568   -0.23152
H     -2.17331   -3.18134    0.37167
H     -2.60066    1.66280   -0.42863
```

S1.   Gaussian 09 (Revision E.01), M. J. Frisch, G. W. Trucks, H. B. Schlegel, G. E. Scuseria, M. A. Robb, J. R. Cheeseman, G. Scalmani, V. Barone, B. Mennucci, G. A. Petersson, H. Nakatsuji, M. Caricato, X. Li, H. P. Hratchian, A. F. Izmaylov, J. Bloino, G. Zheng, J. L. Sonnenberg, M. Hada, M. Ehara, K. Toyota, R. Fukuda, J. Hasegawa, M. Ishida, T. Nakajima, Y. Honda, O. Kitao, H. Nakai, T. Vreven, J. A. Montgomery, Jr., J. E. Peralta, F. Ogliaro, M. Bearpark, J. J. Heyd, E. Brothers, K. N. Kudin, V. N. Staroverov, T. Keith, R. Kobayashi, J. Normand, K. Raghavachari, A. Rendell, J. C. Burant, S. S. Iyengar, J. Tomasi, M. Cossi, N. Rega, J. M. Millam, M. Klene, J. E. Knox, J. B. Cross, V. Bakken, C. Adamo, J. Jaramillo, R. Gomperts, R. E. Stratmann, O. Yazyev, A. J. Austin, R. Cammi, C. Pomelli, J. W. Ochterski, R. L. Martin, K. Morokuma, V. G. Zakrzewski, G. A. Voth, P. Salvador, J. J. Dannenberg, S. Dapprich, A. D. Daniels, O. Farkas, J. B. Foresman, J. V. Ortiz, J. Cioslowski, and D. J. Fox, Gaussian, Inc., Wallingford CT, 2013.

S2.   J.-D. Chai and M. Head-Gordon, *Phys. Chem. Chem. Phys.*, 2008, **10**, 6615.

S3.   (a) W. J. Hehre, R. Ditchfield, and J. A. Pople, *J. Chem. Phys.*, 1972, **56**, 2257; (b) P.C. Hariharan and J. A. Pople, *Theor. Chem. Acta*, 1973, **28**, 213-222.

6.0 References

[1] J. Shaw, *Studies in History and Philosophy of Science Part C: Studies in History and Philosophy of Biological and Biomedical Sciences*, 2016, **55**, 61-69.

[2] D. Greenbaum, A. Baruch, L. Hayrapetian, Z. Darula, A. Burlingame, K.F. Medzihradszky and M. Bogyo, *Mol. Cell. Proteomics*, 2001, **1**, 60-68.

[3] E.R. Stadtman, *Free Radic. Res.*, 2006, **40**, 1250–1258.

[4] V. Checchetto, E. Teardo, L. Carraretto, L. Leanza and I. Szabo, *Biochim. Biophys. Acta, Bioenerg.,* 2016, **1857**, 1258 –1266.

[5] W. Xu, Z. Zeng, J.H. Jiang, Y.T. Chang and L. Yuan*, Angew. Chem., Int. Ed.*, 2016, **55**, 44, 13658–13699.

[6] L.V. Johnson, M.L. Walsh, and L.B. Chen, *Proc. Natl. Acad. Sci. U. S. A.*, 1980, **77**, 2, 990-994.

[7] Y. Li, Y.J. Liu, G. Lv, D.I. Zhang, L. Zhang, and D. Li, *Eur. Rev. Med. Pharmacol. Sci.*, 2014, **18**, 10, 1517-1524.

[8] B.C. Dickinson, and C.J. Chang, *J. Am. Chem. Soc.*, 2008, **130**, 30, 9638-9639.

[9] G.V. Los, L.P. Encell, M.G. McDougall, D.D. Hartzell, N. Karassina, C. Zimprich, M.G. Wood, R. Learish, R.F. Ohana, M. Urh, D. Simpson, J. Mendez, K. Zimmerman, P. Otto, G. Vidugiris, J. Zhu, A. Darzins, D.H. Klaubert, R.F. Bulleit, and K.V. Wood, *ACS Chem. Biol.*, 2008, **3**, 6, 373-382.

[10] M. Best, I. Porth, S. Hauke, F. Braun, D.P. Herten, and R. Wombacher, *Org. Biomol. Chem.*, 2016, **14**, 5606–5611.

[11] K. Fujimoto, K. Toyosato, S. Nakamura, and T. Sakamoto, *Bioorg. Med. Chem. Lett.*, 2016, **26**, 5312–5314.

[12] Z. Chen, T.B. Gibson, F. Robinson, L. Silvestro, G. Pearson, B. Xu, A. Wright, C. Vanderbilt, and M.H. Cobb, *Chem. Rev.,* 2001*,* **101**, 8, 2449–2476.

[13] J. Bain, L. Plater, M. Elliott, N. Shpiro, C.J. Hastie, H. McLauchlan, I. Klevernic, J.S. Arthur, D.R. Alessi, and P. Cohen, *Biochem. J.*, 2007, **408**, 3, 297-315.

[14] J. Li, T.S. Kaoud, J. LeVieux, B. Gilbreath, S. Moharana, K.N. Dalby, and S.M. Kerwin, *ChemBioChem*, 2013, **14**, 1, 66–71.

[15] L. Wecker, R.E. Mrak, and W.D. Dettbarn, Toxicol. Sci., 1986, 6, 1, 172– 174

[16] H. John, F. Balszuweit, K. Kehe, F. Worek, and H. Thiermann, in *Handbook of Toxicology of Chemical Warfare Agents*, ed. R. Gupta, Elsevier, Amsterdam, 2nd edn, 2012, ch. 56.

[17] Organisation for the Prohibition of Chemical Weapons, https://www.opcw.org/chemical-weapons-convention/annexes/annex-on-chemicals/schedule-1/, (accessed October 2017)

[18] British Broadcasting Corporation, http://news.bbc.co.uk/onthisday/hi/dates/stories/march/16/newsid_4304000/4304853.stm, (accessed October 2017)

[19] Live Science, http://www.livescience.com/58013-what-is-vx-nerve-agent.html, (accessed June 2017)

[20] M.I. Smith, and R.D. Lillie, *Arch. Neurol. Psychiatry*, 1931, **26**, 2, 976-992.

[21] J.P. Morgan, and T.C. Tulloss, *Ann. Intern. Med.*, 1976, **85**, 6, 804-808.

[22] C. Winder, P. Fonteyn, and J.C. Balouet, *Occup. Health Saf.*, 2002, **18**, 8, 321-338.

[23] M.R. Montgomery, G.T. Wier, F.J. Zieve, and M. W. Anders, *Clin. Toxicol.*, 1977, **11**, 4, 423-426.

[24] Lord Alec Broers, presented in part at the 1st Report of Session 2007-08, The Stationery Office, Great Britain: Parliament: House of Lords: Science and Technology Committee, December, 2007.

[25] Division on Earth and Life Studies, National Research Council, in *The Airliner Cabin Environment and the Health of Passengers and Crew*, The National Academies Press, Washington. DC, 2002.

[26] A. Gilligan, Telegraph, 21 Feb 2015, 9:35PM GMT.

[27] H. Lodish, A. Berk, S.L. Zipursky, P. Matsudaira, D. Baltimore, and J. Darnell, in *Molecular Cell Biology*, W. H. Freeman, New York, 4th edn, 2000, ch. 21.

[28] M. Jokanović, M. Kosanović, D. Brkić, and P. Vukomanović, *Clin. Neurol. Neurosurg.*, 2011, **113**, 1, 7-10.

[29] L. Karalliedde, D. Baker, and T.C. Marrs, *Toxicology Review*, 2006, **25**, 1, 1-14.

[30] Brigadier General R. Zajtchuk, *Medical Aspects of Chemical and Biological Warfare*, ed. R. Bellamy, Office of The Surgeon General Department of the Army, Washington. DC, 1997.

[31] R.J. Richardson, *Organophosphates Chemistry, Fate, and Effects: Chemistry, Fate, and Effects*, ed. J.E. Chambers, P.E. Levi, Academic Press, Cambridge, 1992.

[32] D.T. Bowden, L.A. Turley, and H.A. Shoemaker, *1930. Am. J. Public Health Nations Health*, 1930, **20**, 11, 1179-1186.

[33] K. Solbu, S. Thorud, M. Hersson, S. Øvrebø, D. G. Ellingsen, E. Lundanes, and P. Molander, *J. Chromatogr. A,* 2007, **1161**, 275-283.

[34] K. Husain, *J. Environ. Immunol. Toxicol.*, 2013, **1**, 14–21.

[35] T.J. Kropp, and R.J. Richardson, *J. Toxicol. Environ. Health*, A, 2003, **278**, 8820-8825.

[36] R.C. Gupta, *Toxicology of Organophosphate and Carbamate Compounds*, Academic Press, Cambridge, 2005.

[37] P.E. Baker, T.B. Cole, M. Cartwright, S.M. Suzuki, K.E. Thummel, Y.S. Lin, A.L. Co, A.E. Rettie, J.H. Kim, and C.E. Furlong, *Chem.-Biol. Interact.,* 2013, **203**, 1, 257-264.

[38] M. Eto, H. Ohkawa, K. Kobayashi and T. Hosoi, *Agric. Biol. Chem.*, 1968, **32**, 1056-1058.

[39] A.J. Hargreaves, M.J. Fowler, M. Sachana, J. Flaskos, M. Bountouri, I.C. Coutts, P. Glynn, W. Harris, and W.G. McLean, *Biochemical Pharmacology*, 2006, **71**, 1240–1247.

[40] J.E. Chambers and S.F. Oppenheimer, *Toxicol. Sci.*, 2004, **77**, 185-187.

[41] T.C. Tsao, Y.C. Juang, R.S. Lan, W.B. Shieh, and C.H. Lee, *Chest*, 1990, **98**, 631-636.

[42] L.G. Costa, *Clinica. Chimica. Acta.*, 2006, **366**, 1-2, 1-13.

[43] J. Barril, J. Estévez, M.A. Escudero, M.V. Céspedes, N. Níguez, M.A. Sogorb, A. Monroy, and E. Vilanova, *Chem.-Biol. Interact.*, 1999, **14**, 119–120, 541–550.

[44] R.J. Richardson, N.D. Hein, S.J. Wijeyesakere, J.K. Fink, and G.F. Makhaeva, *Chem.-Biol. Interact.*, 2013, **203**, 238–244.

[45] C. Meier, U. Muus, J. Renze, L. Naesens, E. De Clercq and J. Balzarini, *Antiviral Chem. Chemother.*, 2002, **2**, 101-114.

[46] M.H. Tarhoni, T. Lister, D.E. Ray, and W.G. Carter, *Biomarkers*, 2008, **13**, 4, 343-363.

[47] M. Jokanovic, and M. Kosanovic, *Environ. Toxicol. Pharmacol.*, 2010, **29**, 195–201.

[48] O. Lockridge, *Adv. Mol. Toxicol.*, 2013, **7**, 179-205.

[49] M.K. Johnson, *Toxicol. Appl. Pharmacol.*, 1990, **102**, 385-389.

[50] K. Pichamuthu, J. Jerobin, A. Nair, G. John, J. Kamalesh, K. Thomas, A. Jose, J.J. Fleming, A. Zachariah, S.S. David, D. Daniel, and J.V. Peter, *Clin. Toxicol.*, 2010, **48**, 8, 813-819.

[51] B. Li, I. Ricordel, L. M. Schopfer, F. Baud, B. Mégarbane, F. Nachon, P. Masson, and O. Lockridge, *Toxicol. Sci.*, 2010, **116**, 1, 23-31.

[52] M.J. vdSchans, A.G. Hulst, D. vdRiet – vOeveren, D. Noort, H.P. Benschop, and C. Dishovsky, *Chem.-Biol. Interact.*, 2013, **203**, 1, 96–102.

[53] M.S. Liyasova, L.M. Schopfer, and O. Lockridge, *Chem. Res. Toxicol.*, 2012, **25**, 1752-1761.

[54] A. Roth, I. Zellinger, M. Arad, and J. Atsmon, *Chest*, 1993, **103**, 2, 576-582.

[55] M.L. Chhabra, G.C. Sepaha, S.R. Jain, R.R. Bhag-Wat, and J.D Khandekar, *Indian J. Med. Sci.*, 1970, **24**, 424-429.

[56] R.S. Wadia, C. Sadagopan, R.B. Amin, and H.V. Sardesai, *J. Neurol., Neurosurg. Psychiatry*, 1974, **37**, 7, 841–847.

[57] N. Senanayake, and L. Karalliedde, *N. Engl. J. Med.*, 1987, **316**, 761-763.

[58] P.S. Mankad, M. Amrani, S. Rothery, N.J. Severs, and M.H. Yacoub, *Acta Physiol.*, 1997, **161**, 103–112.

[59] J.E. Casida, and G.B. Quistad, *Chem. Res. Toxicol.*, 2008, **17**, 8, 2004.

[60] A. Masoud, R. Kiran, and R. Sandhir, *Cell. Mol. Neurobiol.*, 2009, **29**, 8, 1245-1255.

[61] P. Kaur, B. Radotra, R.W. Minz, and K.D. Gill, *Neurotoxicology*, 2007, **28**, 6, 1208-1219.

[62] J. Hescheler, R. Meyer, S. Plant, D. Krautwurst, W. Rosenthal, and G. Schultz, *Circ. Res.*, 1991, **69**, 3, 1476-1487.

[63] B.W. Kimes, and B.L. Brandt, *Exp. Cell Res.*, 1976, **98**, 2, 367-381.

[64] C. Menard, S. Pupier, D. Mornet, M. Kitzmann, J. Nargeot, and P. Lory, *J. Biol. Chem.*, 1999, **274**, 41, 29063-29070.

[65] L. Hosseinzadeh, J. Behravan, F. Mosaffa, G. Bahrami, A. Bahrami, and G. Karimi, *Food Chem. Toxicol.*, 2011, **49**, 5, 1102-1109.

[66] S.G. Felemban, A.C. Garner, F.A. Smida, D.J. Boocock, A.J. Hargreaves, and J.M. Dickenson, *Chem. Res. Toxicol.*, 2015, **28**, 11, 2179–2191.

[67] F.A. Smida, PhD thesis, Nottingham Trent University, 2013.

[68] Proteopedia http://proteopedia.org/wiki/index.php/Trypsin (accessed June 2017).

[69] R.F. Chen, *Anal. Biochem.*, 1968, **25**, 412-416.

[70] J. Bramhall, *Biochemistry*, 1986, **25**, 11, 3479-3486.

[71] J.M. Menter, *Photochem. Photobiol. Sci.*, 2006, **5**, 4, 403–410.

[72] G.T. Hermanson, *Bioconjugate Techniques*, 3rd edn, 2013, ch. 10, 395-463.

[73] L.D. Lavis, *Biochemistry*, 2017, **56**, 39, 5165–5170.

[74] U. Muus, C. Kranz, T. Marquardt and C. Meier, *Eur. J. Org. Chem.*, 2004, **2004**, 6, 1228-1235.

[75] O. Lockridge, *Adv. Mol. Toxicol.*, 2013, **7**, 179-205.

[76] K. Kolmakov, C.A. Wurm, D.N.H. Meineke, F. Göttfert, V.P. Boyarskiy, V.N. Belov, and S.W. Hell, *Chem. – Eur. J.*, 2014, **20**, 146-157.

[77] N.D. Wong, *Nat. Rev. Cardiol.*, 2014, **11**, 5, 276-89.

[78] C. Peterson, *Lancet*, 2015, **385**, 9963, 117-171.

[79] The Office for National Statistics https://www.ons.gov.uk/peoplepopulationandcommunity/birthsdeathsandmarriages/deaths/bulletins/deaths registeredinenglandandwalesseriesdr/2015#ischaemic-heart-diseases-leading-cause-of-death-for-men-aged-50-to-79-in-2015 (accessed March 2017).

[80] D.J. Hausenloy, and D.M. Yellon, *Cardiovasc. Res.*, 2004, **61**, 3, 448-60.

[81] P.S. Mankad, M. Amrani, S. Rothery, N.J. Severs, and M.H. Yacoub, *Acta Physiol.*, 1997, **161**, 1, 103–112.

[82] D.J. Hausenloy, and D.M. Yellon, *Cardiovasc. Res.*, 2008, **79**, 3, 377-386.

[83] D.A. Healy, M.C. Moloney, S.M. McHugh, P.A. Grace and S.R. Walsh, *Int. J. Surg.*, 2014, **12**, 1093-1099.

[84] C.E. Murry, R.B. Jennings, and K.A. Reimer, *Circulation,* 1986, **74**, 5, 1124-1136.

[85] A. Rubino, and D. M. Yellon, *Trends Pharmacol. Sci.,* 2000, **21**, 6, 225-230.

[86] WebMD, http://www.webmd.com/drugs/2/drug-11711-9234/proglycem-oral/diazoxide-oral/details (accessed March 2017).

[87] F.M. Ashcroft, *J. Clin. Invest.*, 2005, **115**, 8, 2047-2058.

[88] J.C. Henquin, S. Charles, M. Nenquin, F. Mathot, and T. Tamagawa, *Diabetes*, 1982, **31**, 9, 776-783.

[89] P. Korge, H.M. Honda, and J.N. Weiss, *Proc. Natl. Acad. Sci. U. S. A.*, 2002, **99**, 5, 3312-3317.

[90] H.H. Patel, and G.J. Gross, *Cardiovasc. Res.*, 2001, **51**, 633–636.

[91] R. Carroll, V.A. Gant, and D.M. Yellon, *Cardiovasc. Res.,* 2001, **51**, 691–700.

[92] O. Pongs, *Physiol. Rev.*, 1992, **72**, 69-88.

[93] W.A. Catterall, *Annu. Rev. Biochem.*, 1995, **64**, 493-531.

[94] B. Hille, *Ion channels of excitable membranes*, 3rd edn, Sinauer Associates, Oxford, 2001.

[95] S.A. Goldstein, *Pharmacol. Rev.*, 2005, **57**, 4, 527-540.

[96] Y. Kubo, J.P. Adelman, D.E. Clapham, L.Y. Jan, A. Karschin, Y. Kurachi, M. Lazdunski, C.G. Nichols, S. Seino, and C.A. Vandenberg, *Pharmacol. Rev.*, 2005, **57**, 4, 509–26.

[97] A.E. Alekseev, D.M. Hodgson, A.B. Karger, S. Park, L.V. Zingman, and A. Terzic, *J. Mol. Cell. Cardiol.*, 2005, **38**, 6, 895–905.

[98] A.P. Babenko, and J. Bryan, *J. Biol. Chem.*, 2003, **278**, 43, 41577–80.

[99] S. Seino, *Annu. Rev. Physiol.*, 1999, **61**, 337-362

[100] Q. Du, S. Jovanović, A.K. Clelland, A. Sukhodub, G.R. Budas, K. Phelan, V. Murray-Tait, L. Malone, and A. Jovanović, *FASEB J.,* 2006, **20**, 8, 1131-1141.

[101] L. Aguilar-Bryan, and J. Bryan, *Endocr. Rev.*, 1999, **20**, 2, 101–135.

[102] Z. Lacza, J.A. Snipes, A.W. Miller, C. Szabo, G. Grover, and D.W. Busija, *J. Mol. Cell. Cardiol.*, 2003, **35**, 1339 –1347.

[103] H. Ardehali, Z. Chen, Y. Ko, R. Mejia-Alvarez, and E. Marban, *Proc. Natl. Acad. Sci. U. S. A.*, 2004, **101**, 32, 11880–11885.

[104] H. Ardehali, and B. O'Rourke, *J. Mol. Cell. Cardiol.*, 2005, **39**, 7-16.

[105] J. Minners, L. Lacerda, D.M. Yellon, L.H. Opie, C.J. McLeod, and M.N. Sack, *Mol. Cell. Biochem.*, 2007, **294**, 1-2, 11–18.

[106] A.K. Rines, M. Bayeva, and H. Ardehali, *Circ. Res.*, 2012, **111**, 392-393.

[107] Z. Lacza, J.A. Snipes, A.W. Miller, C. Szabo, G. Grover, and D.W. Busija, *J. Mol. Cell. Cardiol.*, 2003, **35**, 1339–1347.

[108] A.J. Kowaltowski, N.C. de Souza-Pinto, R.F. Castilho, and A.E. Vercesi, *Free Radical Biol. Med.*, 2009, **47**, 4, 333–343.

[109] A.A. Starkov, B.M. Polster, and G. Fiskum, *J. Neurochem.*, 2002, **83**, 220-228.

[110] J.G. Topliss, and M.D. Yudis, *J. Med. Chem.*, 1972, **15**, 4, 341-448.

[111] Z.W. Yang, T. Zheng, A. Zhang, B.T. Altura, and B.M. Altura, *Eur. J. Pharmacol.*, 1998, **344**, 169–181.

[112] S. Khelili, *Medicinal Chemical Research*, 2003, **12**, 457-470.

[113] P. Jimonet, F. Audiau, J.C. Aloup, M. Barreau, J.C. Blanchard, A. Bohme, A. Boireau, M. Chevé, D. Damour, A. Doble, J. Lavayre, G. Dutruc-Rosset, J.C.R. Randle, J. Rataud, J. Stutzmann and S. Mignani, *Bioorg. Med. Chem. Lett.*, 1994, **4**, 2735-2740.

[114] G.L. Collingridge, R.W. Olsen, J. Peters, and M. Spedding, *Neuropharmacology*, 2009, **56**, 1, 2–5.

[115] I.V. Chizhmakov, N.I. Kiskin, O.A. Krishtal, and A.Ya. Tsyndrenko, *Neurosci. Lett.*, 1986, **63**, 225-230.

[116] K.A. Yamada, and C.M. Tang, *J. Neurosci.*, 1993, **13**, 3904-3915

[117] P.H. Seeburg, *Trends Pharmacol. Sci.*, 1993, **14**, 8, 297-303.

[118] G. Puia, G. Losi, G. Razzini, D. Braghiroli, M. Di Bella and M. Baraldi, *Prog. Neuro-Psychopharmacol. Biol. Psychiatry*, 2000, **24**, 1007-1015.

[119] I. Zivkovic, D.M. Thomson, M. Bertolmo, D. Uzunov, M. Dibella, E. Costa, and A. Guidotti, *J. Pharmacol. Exp. Ther.*, 1994, **272**, 1, 300-309.

[120] P. Francotte, P. de Tullio, E. Goffin, and B. Pirotte, *J. Med. Chem.*, 2007, **50**, 3153-3157.

[121] P. de Tullio, A.C Servais, M. Fillet, F.Gillotin, F. Somers, P. Chiap, P. Lebrun, and B Pirotte, *J. Med. Chem.*, 2011, **54**, 8353–8361

[122] M. Dabrowski, and F.M. Ashcroft, *Diabetes*, 2002, **51**, 1896–1906.

[123] B. Pirotte, M.H. Antoine, P. de Tullio, M. Hermann, A. Herchuelz, J. Delarge, and P. Lebrun, *Biochemical Pharmacology*, 1994, **47**, 8, 1381-1386.

[124] B. Pirotte, P. de Tullio, Q.A. Nguyen, F. Somers, P. Fraikin, X. Florence, P. Wahl, J.B. Hansen and P. Lebrun, *J. Med. Chem.*, 2010, **53**, 147-154.

[125] I.I.A. Tabachnick, and A. Gulbenkian, *Ann. N. Y. Acad. Sci.*, 1968, **150**, 204-218.

[126] S. Howell, and K. Taylor, *Lancet*, 1966, **1**, 7429, 128-29.

[127] A.E. Rouho, H. Kiefer, P.E. Roeder, and S.J. Singer, *Proc. Natl. Acad. Sci. U. S. A.*, 1973, **70**, 9, 2567-2571.

[128] A. Singh, E.R. Thornton, and F.H. Westheimer, *J. Biol. Chem.*, 1962, **237**, 3006 – 3008.

[129] Y. Sadakane, and Y. Hatanaka, *Anal. Sci.*, 2006, **22**, 9, 209.

[130] J.R. Dunetz, Y. Xiang, A. Baldwin, and J. Ringling, *Org. Lett.*, 2011, **13**, 19, 5048 – 5051.

[131] M. Saleem, R. Abdullah, I.S. Hong, and K. Lee, *Korean Chem. Soc.*, 2013, **34**, 2, 389.

[132] E. Valeur, and M. Bradley, *Chem. Soc. Rev.*, 2009, **38**, 606-631.

[133] L.A. Carpino, H. Imazumi, A. El-Faham, F.J. Ferrer, C.W. Zhang, Y.S. Lee, B.M. Foxman, P. Henklein, C. Hanay, C. Mugge, H. Wenschuh, K. Klose, M. Beyermann, and M. Bienert, *Angew. Chem., Int. Ed.,* 2002, **41**, 3, 441-445.

[134] V.N. Belov, M.L. Bossi, J. Folling, V.P. Boyarskiy, and S.W. Hell, *Chem. - Eur. J.*, 2009, **15**, 41, 10762 – 10776.

[135] M. Beija, C.A.M. Afonso, and J.M.G Martinho, *Chem. Soc. Rev.*, 2009, **38**, 2410 – 2433.

[136] F. Arbeloa, T. Arbeloa, M.J. Estevez, and I. Arbeloa, *J. Phys. Chem.*, 1991, **95**, 2203 – 2208.

[137] J. Karpiuk, Z.R. Grabowski, and F.C. de Deschryver, *J. Phys. Chem.*, 1994, **98**, 3247 – 3256.

[138] U.K.A. Klein, and F.W. Hafner, *Chem. Phys. Lett.*, 1976, **43**, 141 – 145.

[139] V.N. Belov, G.Yu. Mitronova, L. Bossi, V. P. Boyarskiy, E. Hebisch, C. Geisler, K. Kolmakov, C.A. Wurm, K.I. Willig and S.W. Hell, *Chem. - Eur. J.*, 2014, **20**, 13162 – 13173.

[140] J.E. Casida, M. Eto, and R.L. Baron, *Nature*, 1961, **191**, 1396.

[141] T. Li, A. Tikad, W. Pan, and S.P. Vincent, *Org. Lett.*, 2014, **16**, 5628 – 5631.

[142] F.H. Allen, O. Kennard, D.G. Watson, L. Brammer, A.G. Orpen, and R. Taylor, *J. Chem. Soc., Perkin Transactions 2*, 1987, **0**, S1-S19.

[143] United States Environmental Protection Agency, https://comptox.epa.gov/dashboard/dsstoxdb/results?search=1-Hexanol%2C+6-amino- (accessed November 2017).

[144] V. Helms, *in Principles of Computational Cell Biology*, Wiley-VCH, Weinheim, 2008, ch. 8, 202.

[145] S. Mondal, S.K. Manna, K. Maiti, R. Maji, S.S. Ali, S. Manna, S. Mandal, R. Uddin, and A.K. Mahapatra, *Supramol. Chem.*, 2017, **29**, 8, 616 – 626.

[146] X.Y. Guan, W.Y. Lin, and W.M. Huang, *Org. Biomol. Chem.*, 2014, **12**, 3944.

[147] G. Reynolds, and K.H. Drexhage, *Opt. Commun.*, 1975 **13**, 222 – 225.

[148] A.P. Demchenko, *Exp. Oncol.*, 2012, **34**, 3, 263 – 268.

[149] I. Moreno-Villoslada, M. Jofre, V. Miranda, R. Gonzalez, T. Sotelo, S. Hess, B. Rivas, T. Shibue, and H. Nishide, *J. Phys. Chem. B*, 2006, **110**, 43, 11809 – 11812.

[150] H. Du, R.C.A. Fuh, J. Li, L.A. Corkan, and J.S. Lindsey, *Photochem. Photobiol.*, 1998, **68**, 141 – 142.

[151] Eastman Laboratory Chemicals Catalog No. 55 (1993-94), Fisher Scientific.

[152] X. Wan, H. Liu, S. Yao, T. Liu, and Y. Yao, *Macromol. Rapid Commun.*, 2014, **35**, 323–329.

[153] Z.Q. Hu, C.S. Lin, X.M. Wang, L. Ding, C.L. Cui, S.F. Liu, and H.Y. Lu, *Chem. Commun.*, 2010, **46**, 3765–3767.

[154] W.B. Cross, unpublished work.

[155] C.R. Groom, I.J. Bruno, M.P. Lightfoot, and S.C. Ward, *Acta Crystallogr., Sect. B: Struct. Sci., Cryst. Eng. Mater.*, 2016, **72**, 2, 171-179.

[156] L. Cincotta, and J. Foley, US4290955A, 1981.

[157] T. Nguyen, and M.B. Francis*, Org. Lett.*, 2003, **5**, 18, 3245–3248.

158 T. Mosmann, *J. Immunol. Methods*, 1983, **65**, 55-63.

159 T. Decker, and M.L. Lohmann-Matthes, *J. Immunol. Methods*, 1988, **115**, 61-69.

160 J.C. Stockert, A. Blázquez-Castro, M. Cañete, R.W. Horobin, and Á. Villanueva, *Acta Histochem.*, 2012, **114**, 785–796.

161 K.B. Storey, *Comp. Biochem. Physiol.*, 2016, **199**, B, 13–20.

162 M. Kemp, J. Donovan, H. Higham, and J. Hooper, *Br. J. Anaesth.*, 2004, **93,** 1, 63-73.

163 D.R. Sulistina, R. Ratnawati, and I.A. Wiyasa, *Asian Pac. J. Reprod.*, 2014, **3**, 3, 180-183.

164 W. Harris, D. Muñoz, P.L. Bonner, and A.J. Hargreaves, *Toxicol. in Vitro*, 2009, **23**, 1559-1563.

165 Z. Szondy, P.G. Mastroberadino, J. Varadi, M.G. Farrace, N. Nagy, I. Bak, I. Viti, M.R. Wieckowski, G. Mellino, R. Rizzuto, A. Tosaki, L. Fesus, and M. Piacentini, *Cell Death Differ.*, 2006, **13**, 1827–1829.

166 F.S. Vyas, A.J. Hargreaves, P.L.R. Bonner, D.J. Boocock, C. Coveney, and J.M. Dickenson, *Biochemical Pharmacology*, 2016 **107**, 41-58.

167 S.J. McConoughey, M. Basso, Z.V. Niatsetskaya, S.F. Sleiman, N.A. Smimova, B.C. Langley, L. Mahishi, A.J.L. Cooper, M.A. Antonyak, R.A. Cerione, B. Li, A. Starkov, R.K. Chaturvedi, M.F. Beal, G. Coppola, D.H. Geschwind, H. Ryu, L. Xia, S.E. Iisma, J. Pallos, R. Pasternack, M. Hils, J. Fan, L.A. Raymond, J.L. Marsh, L.M. Thompson, and R.R. Ratan, *EMBO Mol. Med.,* 2010, **2**, 9, 349–370.

168 K. Chandramouli, and P.Y. Qian, *Hum. Genomics Proteomics*, 2009, **2009**, 239204.

169 T. Rabillouda, and C. Lelong, *J. Proteomics*, 2011, **74**, 1829 – 1841.

170 I. Komáromi , Z. Bagoly, and L. Muszbek, *J. Thromb. Haemostasis*, 2011, **9**, 1, 9–20

171 Thermofisher, https://www.thermofisher.com/order/catalog/product/85160 (accessed June 2018).

172 E. von Elert, M.K. Agrawal, C. Gebauer, H. Jaensch, U. Bauer, and A. Zitt, *Comp. Biochem. Physiol., Part B*, 2004, **137**, 3, 287–296.

173 A. Loudet, and K. Burgess, *Chem. Rev.*, 2007, **107**, 11, 4891-4932.

174 Lumiprobe Life Science Solutions, https://www.lumiprobe.com/p/bodipy-fl-nhs-ester accessed 02/10/17.

175 Fluorophores.org, http://www.fluorophores.tugraz.at/substance/171 accessed 02/10/2017.

176 K. Gießler, H. Griesser, D. Göhringer, T. Sabirov, and C. Richert, *Eur. J. Org. Chem.*, 2010, **2010**, 19, 3611–3620.

177 L.J. Mitnaul, J. Tian, C. Burton, M.H. Lam, Y. Zhu, S.H. Olson, J.E. Schneeweis, P. Zuck, S. Pandit, M. Anderson, M.M. Maletic, S.T. Waddell, S.D. Wright, C.P. Sparrow, and E.G. Lund, *J. Lipid Res.*, 2007, **48**, 472-482.

178 C.L. Dale, S.J. Hill, and B. Kellam, *MedChemComm*, 2012, **3**, 333–338.

179 N. Boens, V. Leen, and W. Dehaen, *Chem. Soc. Rev.*, 2012, **41**,1130–1172.

180 E. Cuevas-Yanez, J.M. Muchowski, and R. Cruz-Almanza, *Tetrahedron*, 2004, **60**, 1505–1511.

181 L. Wu, and K. Burgess, *Chem. Commun.*, 2008, **40**, 4933-4935.

182 L. Knorr, *Ber. Dtsch. Chem. Ges.*, 1884, **17**, 2, 1635-1644.

183 G. Meng, M.L. Zheng, and M. Wang, *Org. Prep. Proced. Int.*, 2011, **43**, 3, 308-311.

184 R. Ziessel, G. Ulrich, and A. Harriman, *New J. Chem.*, 2007, **31**, 496-501.

185 B.R. Groves, S.M. Crawford, T. Lundrigan, C.F. Matta, S. Sowlati-Hashjin, and A. Thompson, *Chem. Commun.*, 2013, **49**, 816-818.

186 Sigma-Aldrich, http://www.sigmaaldrich.com/catalog/product/aldrich/280909?lang=en&region=GB (accessed November 2017).

187 C.J. Shields, D.E. Falvey, G.B. Schuster, O. Buchardt, and P.E. Nielsen, *J. Org. Chem.*, 1988, **53**, 3501.

188 P.S. Addy, B. Saha, N.D. Singh, A.K. Das, J.T. Bush, C. Lejeune, C.J. Schofield, and A. Basak, *Chem. Commun.*, 2013, **49**, 1930—1932.

189 I. Berlman, *Handbook of Fluorescence Spectra of Aromatic Molecules*, Academic Press, N.Y., 1971.

190 M. Baeumle, *BioFiles*, 2011, **6.3**, 23.

191 Y.N. Teo, and E.T. Kool, *Chem. Rev.*, 2012, **112**, 4221-4245.

192 A. Manicardi, L. Guidi, A. Ghidini, and R. Corradini, *Beilstein J. Org. Chem.*, 2014, **10**, 1495-1503.

193 H. Chen, S.S. Ahsan, M.B. Santiago-Berrios, H.D. Abruna, and W.W. Webb, *J. Am. Chem. Soc.*, 2010, **132**, 7244–7245.

194 A. Wakata, S.M. Cahill, M. Blumenstein, R.H. Gunby, S. Jockusch, A.A. Marti, B. Cimbro, C. Gambacorti-Passerini, A. Donella-Deana, L.A. Pinna, N.J. Turro, and D.S. Lawrence, *Org. Lett.*, 2008, **10**, 301–304.

195 Q. Wang, S.M. Cahill, M. Blumenstein, and D.S. Lawrence, *J. Am. Chem. Soc.*, 2006, **128**, 1808–1809.

196 J.A. Gonzalez-Vera, *Chem. Soc. Rev.*, 2012, **41**, 1652-1664.

197 ATTO-TEC, https://www.atto-tec.com/attotecshop/product_info.php?language=en&info=p62_atto-rho14.html& (accessed September 2017).

198 L.M. Wysocki, J.B. Grimm, A.N. Tkachuk, T.A. Brown, E. Betzig, and L.D. Lavis, *Angew. Chem., Int. Ed.*, 2011, **50**, 11206–11209.

199 L. Lee, M. Taing, and B. Rosemblum, from PCT Int. Appl., WO 2002036832 A2 20020510, 2002.

200 V.P. Boyarskiy, V.N. Belov, R. Medda, B. Hein, M. Bossi, and S.W. Hell, *Chem. – Eur. J.*, 2008, **14**, 1784–1792.

[201] H.C. Brown, Y.M. Choi, and S. Narasimhan, *J. Org. Chem.*, 1982, **47**, 16, 3153-3163.

[202] S.J. Dwight, and S. Levin, *Org. Lett.*, 2016, **18**, 5316–5319.

[203] L. Vidal, E. Huguet, and P. Barbarat, from PCT Int. Appl., WO 2011089571 A2 20110728, 2011.

[204] X. Zhang, Z. Liu, X. Kong, and R. Zhang, from Faming Zhuanli Shenqing, CN 102140554 A 20110803, 2011.

[205] A. Bousseksou, L. Salmon, G. Molnar, and S. Cobo, from PCT Int. Appl., WO 2011058277 A1 20110519, 2011.

[206] J. Uddin, and L.J. Marnett, *Org. Lett.*, 2008, **10**, 21, 2008.

[207] J. Linares-Palomino, M.A. Husainy, V.K. Lai, J.M. Dickenson, M. Galiñanes, *J. Physiol. (London),* 2010, **588**, 2173-2191.

[208] M.A. Husainy, J.M. Dickenson, and M. Galiñanes, *J. Surg. Res.*, 2012, **174**, 62-72.

[209] Thermofisher Scientific, https://www.thermofisher.com/uk/en/home/life-science/cell-analysis/fluorophores/dapi-stain.html (accessed November 2017).

[210] Y. Li, Y.J. Liu, G. Lv, D.I. Zhang, L. Zhang, and D. Li, *Eur. Rev. Med. Pharmacol. Sci.*, 2014, **18**, 10, 1517-1524.

[211] D. Chen, Z. Jin, J. Zhang, L. Jiang, K. Chen, X. He, Y. Song, J. Ke, and Y. Wang, *PLoS ONE*, 2016, **11**, 5, e0153587.

[212] L. Brulikova, Y. Okorochenkova, and J. Hlavac, *Org. Biomol. Chem.*, 2016, **14**, 10437–10443.

[213] H.C. Kolb, M.G. Finn, K.B. Sharpless, *Angew. Chem., Int. Ed.*, 2001, **40**, 2004-2021.

[214] E.V. Antina, G.B. Guseva, A.E. Loginova, A.S. Semeikin, and A.I. V'yugin, *Russ. J. G. Chem.,* 2010, **80**, 2374-2381.

[215] N.G. Moon, and A.M. Harned, *Tetrahedron Lett.*, 2013, 54, 2960–2963.

[216] A. Spaggiari, D. Vaccari, P. Davoli, and F. Prati, *Synthesis*, 2006, **6**, 995–998.

[217] J.E. Zweig, and T.R. Newhouse, *J. Am. Chem. Soc.*, 2017, **139**, 10956–10959.

[218] E. Cuevas-Yanez, J.M. Muchowski, and R. Cruz-Almanza, *Tetrahedron*, 2004, **60**, 7, 1505–1511.

[219] E.H. Rios Morales, J. Balzarini and C. Meier, *J. Med. Chem.,* 2012, **55**, 7245-7252.

[220] M. Kainosho, and A. Nakamura, *Tetrahedron*, 1969, **25**, 4071-4081.

[221] R.T. Pon, *Tetrahedron Lett.*, 1991, **32**, 14, 1715-1718.

[222] A. Bartoszewicz, M. Kalek, and J. Stawinski, *Tetrahedron*, 2008, **64**, 8843–8850.

[223] O. Kühl, *Phosphoros-31 NMR Spectroscopy: A Concise Introduction for the Synthetic Organic and Organometallic Chemist*, Springer-Verlag, Berlin Heidelberg, 2008.

[224] O.H. Lowry, N.J. Rosebrough, A.L. Farr, and R.J. Randall, *J. Biol. Chem.*, 1951, **193**, 1, 265–75.

[225] P.K. Smith, R.I. Krohn, G.T. Hermanson, A.K. Mallia, F.H. Gartner, M.D. Provenzano, E.K. Fujimoto, N.M. Goeke, B.J. Olson, and D.C. Klenk, *Anal. Biochem.*, 1985, **150,** 1, 76–85.

[226] U.K. Laemmli, *Nature*, 1970, **227**, 680 – 685.